frontiers | Research Topics

Recent advances of minor saponins in panax species

Edited by
Weicheng Hu, Guangbo Fu, Yunyao Jiang, Bing Chun Yan and Jae Youl Cho

Published in
Frontiers in Pharmacology

ISSN 1664-8714
ISBN 978-2-83251-580-8
DOI 10.3389/978-2-83251-580-8

About Frontiers

Frontiers is more than just an open access publisher of scholarly articles: it is a pioneering approach to the world of academia, radically improving the way scholarly research is managed. The grand vision of Frontiers is a world where all people have an equal opportunity to seek, share and generate knowledge. Frontiers provides immediate and permanent online open access to all its publications, but this alone is not enough to realize our grand goals.

Frontiers journal series

The Frontiers journal series is a multi-tier and interdisciplinary set of open-access, online journals, promising a paradigm shift from the current review, selection and dissemination processes in academic publishing. All Frontiers journals are driven by researchers for researchers; therefore, they constitute a service to the scholarly community. At the same time, the *Frontiers journal series* operates on a revolutionary invention, the tiered publishing system, initially addressing specific communities of scholars, and gradually climbing up to broader public understanding, thus serving the interests of the lay society, too.

Dedication to quality

Each Frontiers article is a landmark of the highest quality, thanks to genuinely collaborative interactions between authors and review editors, who include some of the world's best academicians. Research must be certified by peers before entering a stream of knowledge that may eventually reach the public - and shape society; therefore, Frontiers only applies the most rigorous and unbiased reviews. Frontiers revolutionizes research publishing by freely delivering the most outstanding research, evaluated with no bias from both the academic and social point of view. By applying the most advanced information technologies, Frontiers is catapulting scholarly publishing into a new generation.

What are Frontiers Research Topics?

Frontiers Research Topics are very popular trademarks of the *Frontiers journals series*: they are collections of at least ten articles, all centered on a particular subject. With their unique mix of varied contributions from Original Research to Review Articles, Frontiers Research Topics unify the most influential researchers, the latest key findings and historical advances in a hot research area.

Find out more on how to host your own Frontiers Research Topic or contribute to one as an author by contacting the Frontiers editorial office: frontiersin.org/about/contact

Recent advances of minor saponins in panax species

Topic editors

Weicheng Hu — Yangzhou University, China
Guangbo Fu — Huaian NO.1 People's Hospital Nanjing Medical University, China
Yunyao Jiang — Tsinghua University, China
Bing Chun Yan — Yangzhou University, China
Jae Youl Cho — Sungkyunkwan University, Republic of Korea

Citation

Hu, W., Fu, G., Jiang, Y., Yan, B. C., Cho, J. Y., eds. (2023). *Recent advances of minor saponins in panax species*. Lausanne: Frontiers Media SA.
doi: 10.3389/978-2-83251-580-8

Table of contents

frontiers | Frontiers in Pharmacology

ORIGINAL RESEARCH
published: 04 May 2022
doi: 10.3389/fphar.2022.878937

Network Pharmacology-Based Prediction and Verification of Ginsenoside Rh2-Induced Apoptosis of A549 Cells *via* the PI3K/Akt Pathway

Chao Song[1†], *Yue Yuan*[2†], *Jing Zhou*[1], *Ziliang He*[1], *Yeye Hu*[1], *Yuan Xie*[1], *Nan Liu*[3*], *Lei Wu*[4*] *and Ji Zhang*[1*]

[1]*Jiangsu Collaborative Innovation Center of Regional Modern Agriculture and Environmental Protection, School of Life Sciences, Huaiyin Normal University, Huaian, China,* [2]*School of Pharmaceutical Sciences, Institute for Chinese Materia Medica, Tsinghua University, Beijing, China,* [3]*Beijing Increasepharm Safety and Efficacy Co., Ltd, Beijing, China,* [4]*Institute of Applied Chemistry, Academy of Sciences, Nanchang, China*

OPEN ACCESS

Edited by:
Bing Chun Yan,
Yangzhou University, China

Reviewed by:
Rongjie Zhao,
Qiqihar Medical University, China
Sun Eun Choi,
Kangwon National University, South Korea

***Correspondence:**
Nan Liu
nanliu0304@163.com
Lei Wu
wulei858196@163.com
Ji Zhang
zhangji@hytc.edu.cn

[†]*These authors have contributed equally to this work and share first authorship*

Specialty section:
This article was submitted to Experimental Pharmacology and Drug Discovery, a section of the journal Frontiers in Pharmacology

Received: *18 February 2022*
Accepted: *20 April 2022*
Published: *04 May 2022*

Citation:
Song C, Yuan Y, Zhou J, He Z, Hu Y, Xie Y, Liu N, Wu L and Zhang J (2022) Network Pharmacology-Based Prediction and Verification of Ginsenoside Rh2-Induced Apoptosis of A549 Cells via the PI3K/Akt Pathway. Front. Pharmacol. 13:878937. doi: 10.3389/fphar.2022.878937

Ginsenoside Rh2 (G-Rh2), a rare protopanaxadiol (PPD)-type triterpene saponin, from *Panax ginseng* has anti-proliferation, anti-invasion, and anti-metastatic activity. However, the mechanisms by which G-Rh2 induces apoptosis of lung cancer cells are unclear. In the present work, a G-Rh2 target-lung cancer network was constructed and analyzed by the network pharmacology approach. A total of 91 compound-targets of G-Rh2 was obtained based on the compound-target network analysis, and 217 targets were identified for G-Rh2 against lung cancer by PPI network analysis. The 217 targets were significantly enriched in 103 GO terms with FDR <0.05 as threshold in the GO enrichment analysis. In KEGG pathway enrichment analysis, all the candidate targets were significantly enriched in 143 pathways, among of which PI3K-Akt signaling pathway was identified as one of the top enriched pathway. Besides, G-Rh2 induced apoptosis in human lung epithelial (A549) cells was verified in this work. G-Rh2 significantly inhibited the proliferation of A549 cells in a dose-dependent manner, and the apoptosis rate significantly increased from 4.4% to 78.7% using flow cytometry. Western blot analysis revealed that the phosphorylation levels of p85, PDK1, Akt and IκBα were significantly suppressed by G-Rh2. All the experimental findings were consistent with the network pharmacology results. Research findings in this work will provide potential therapeutic value for further mechanism investigations.

Keywords: ginsenoside Rh2, network pharmacology, lung cancer, A549 cells, PI3K-Akt signaling pathway

INTRODUCTION

Lung cancer is one of the most diagnosed cancers and a leading cause of cancer deaths. Smoking is the main cause (~80% of cases) of lung cancer (Huang et al., 2021). Other causes are exposure to radon, secondhand smoke, and air pollution. In 2020, lung cancer was the second most common human cancer globally, there were 2,206,771 new cases (11.4% of all cases). The number of new lung cancer deaths was 17,966,144, accounting for 18% of all cancer deaths (Wild et al., 2020). Lung cancer can be divided into non-small cell lung cancer (NSCLC) and small cell lung cancer (SCLC) (Hanna and Onaitis, 2013). Treatment for lung cancer differs according to subtype and stage (Hayashi et al., 2011). Chemotherapy and radiotherapy have side effects (Albano et al., 2021), and even targeted immunotherapeutic have a considerable symptom burden (Lim et al., 2020). Therefore, research on new drugs and combined therapies is needed.

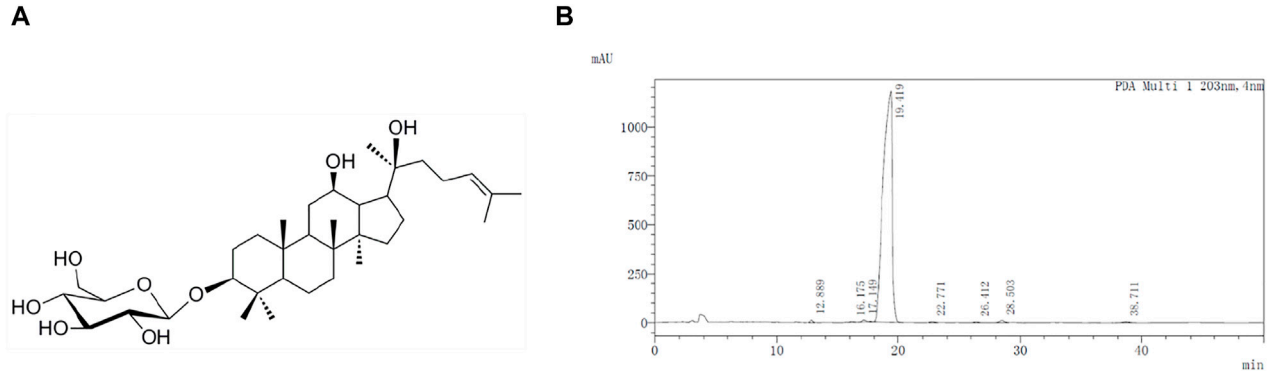

FIGURE 1 | Molecular structure **(A)** and HPLC profile **(B)** of G-Rh2.

Ginseng, a traditional Chinese herb, has been used as medicine for thousands of years. It is used in cancer treatment and prevention based on its multi-target activity and low toxicity. Ginsenosides are the main active constituents in ginseng. G-Rh2, a 20 (S)-protopanaxadiol saponin extracted from the root of *Panax ginseng* (Wong et al., 2015), has been reported to show cytotoxic activity and decreased cancer cells viability *via* JAK2/STAT3 pathway in human colorectal cancer cells (Han et al., 2016), stimulates ROS production in human HeLa cervical cancer cell lines (Liu et al., 2021). G-Rh2 was also reported with antitumor effects in liver, lung, prostate, and colorectal cancer (Ge et al., 2017; Shi et al., 2017; Wu et al., 2018; Zhang et al., 2021). G-Rh2 inhibits proliferation, metastasis, and apoptosis by activating the mitochondrial or membrane death receptor (Wang et al., 2017). However, the molecular targets and signaling pathways underlying the effect of G-Rh2 on lung cancer are unclear. Cancer is typically caused by multiple genes and risk factors, so identification of multiple targets is important for understanding the mechanisms underlying the effect of G-Rh2 on lung cancer.

Network pharmacology is a systematic approach that integrates pharmacologic, computational, and experimental methods to illuminate the molecular mechanisms of drugs (Zhao and He, 2018; Song et al., 2019; Zhou et al., 2020). It can describe the complex pharmacological mechanisms of traditional Chinese medicines from a network perspective by multitarget, multichannel, and multilink analysis (Li et al., 2015; Park et al., 2018). In this work, we used the network pharmacology approach to evaluate the molecular mechanisms underlying the effect of G-Rh2 in lung cancer.

MATERIALS AND METHODS

Materials and Reagents

G-Rh2 was purchased from Chengdu Phytoelite Bio-Technology Co., Ltd. (Chengdu, Sichuan, China) and the purity (>98%) was determined by high-performance liquid chromatography (**Figure 1**). 3-(4,5-Dimethylthiazol-2-yl)-2,5-diphenyltetrazolium bromide (MTT) and Annexin V-FITC apoptosis detection kit were purchased from Sigma-Alorich (St. Louis, MO, United States). The fetal bovine serum (FBS) was purchased from Corning (Medford, MA, United States). Antibiotics (100× penicillin/streptomycin) and 0.25% Trypsin-EDTA were purchased from Gibco (California, United States). Minimum essential medium (MEM) was purchased from Hyclone (Logan, UT, United States). RIPA Lysis Buffer and eECL Western Blot kit were purchased from CWBio (Taizhou, Jiangsu, China). The primary antibodies against p-AKT, AKT, p-PDK1, PDK1, p-p85, p85, p-IκBα, IκBα, and anti-rabbit IgG HRP (#7074) were from Cell Signaling Technology (Danvers, MA, United States).

Potential Targets Screening

The chemical structure of G-Rh2 was imported into PharmMapper server (http://www.lilab-ecust.cn/pharmmapper/, version 2017) (Xia et al., 2017), STITCH database http://stitch.embl.de/, version 5.0) (Szklarczyk et al., 2016), SwissTargetPrediction (http://www.swisstargetprediction.ch/) (David et al., 2014), and Similarity ensemble approach (http://sea.bkslab.org/) (Keiser et al., 2007) to obtained the related targets of G-Rh2.

Lung Cancer-Related Targets Screening

The potential targets of Lung cancer were identified by the Genetic Association Database (https://geneticassociationdb.nih.gov/), which is a database of genetic association data from complex diseases and disorders. Lung cancer was imported as a keyword and the disease targets associated with it were provided in the database.

Network Construction

In order to explore the relationship between G-Rh2 related targets and lung cancer disease related targets, protein-protein interaction (PPI) were analysed by the Database of Interacting Proteins (DIP^{TM}), Biological General Repository for Interaction Datasets (BioGRID), Human Protein Reference Database (HPRD), IntAct Molecular Interaction Database (IntAct), Molecular INTeraction database (MINT), and biomolecular interaction network database (BIND) using the plug-in Bisogenet (Martin et al., 2010) of Cytoscape 3.7.1 software. The PPI networks of G-Rh2 putative targets and lung cancer-related targets were established and visualized by the plug-in Bisogenet of Cytoscape 3.7.1 software.

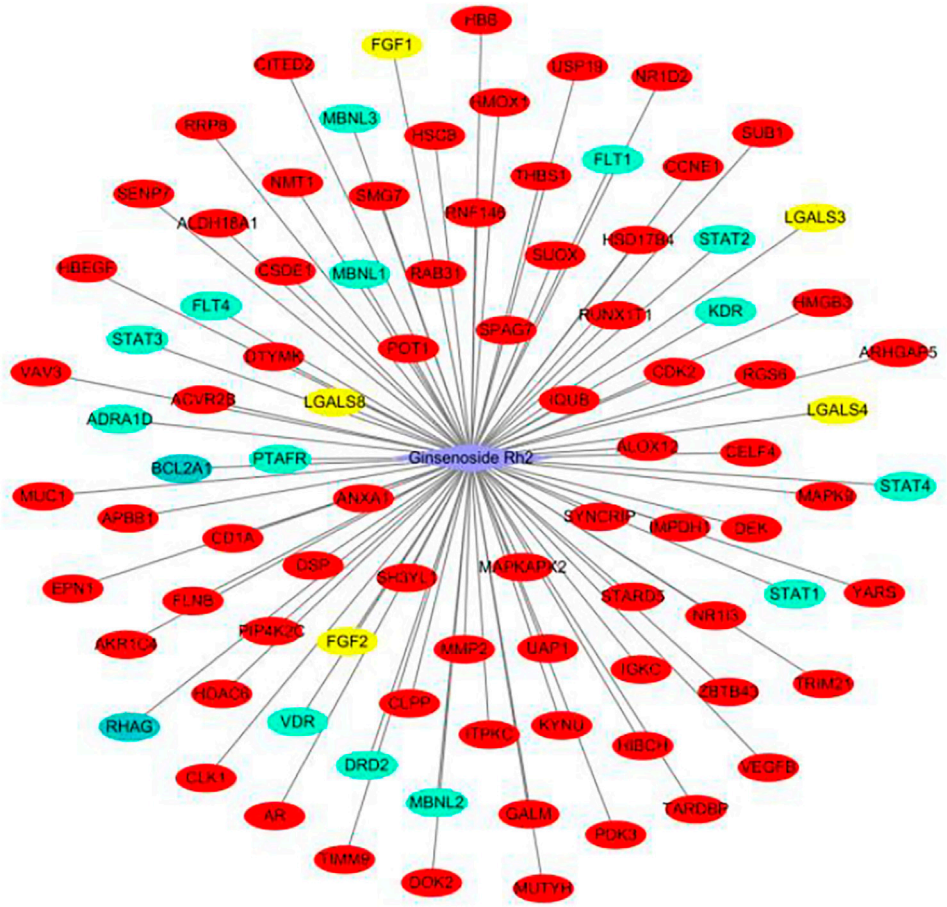

FIGURE 2 | Target network of G-Rh2. Red, yellow, green, and blue ovals, are targets obtained from PharmMapper Server, Similarity ensemble approach, SwissTargetPrediction, and the STITCH database.

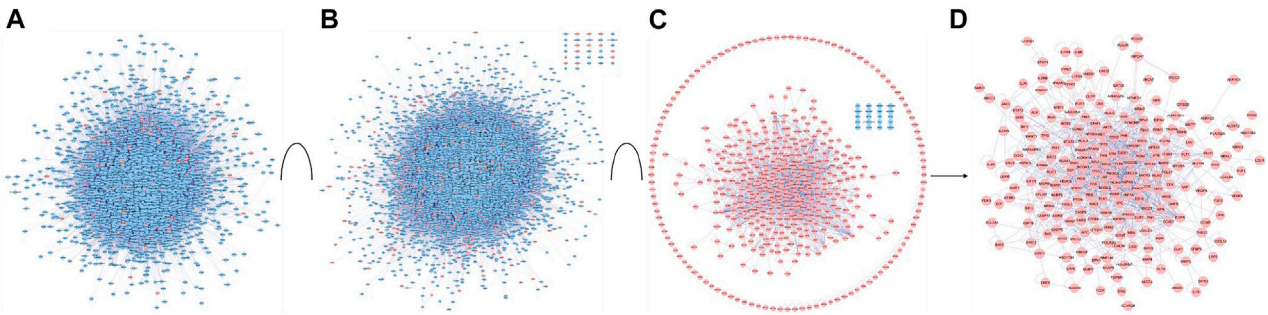

FIGURE 3 | PPI network construction and analysis for targets of G-Rh2 in lung cancer. **(A)** PPI network of G-Rh2 putative targets; **(B)** PPI network of lung cancer-related targets; **(C)** Interaction network of G-Rh2 targets and lung cancer-related targets; **(D)** Merged PPI network.

Bioinformatic Analysis

GO analysis with the biological process, cellular component, and molecular function was carried out using the Database for Annotation, Visualization and Integrated Discovery (DAVID, https://david.ncifcrf.gov/, v6.8) (Huang et al., 2009). Functional categories were enriched within genes (FDR <0.005) and the top 10 GO functional categories were selected. KOBAS 3.0 (http://kobas.cbi.pku.edu.cn/) that assigned Kyoto Encyclopedia of Genes and Genomes (KEGG) database was used for pathway analysis (Xie et al., 2011). The significantly changed pathways

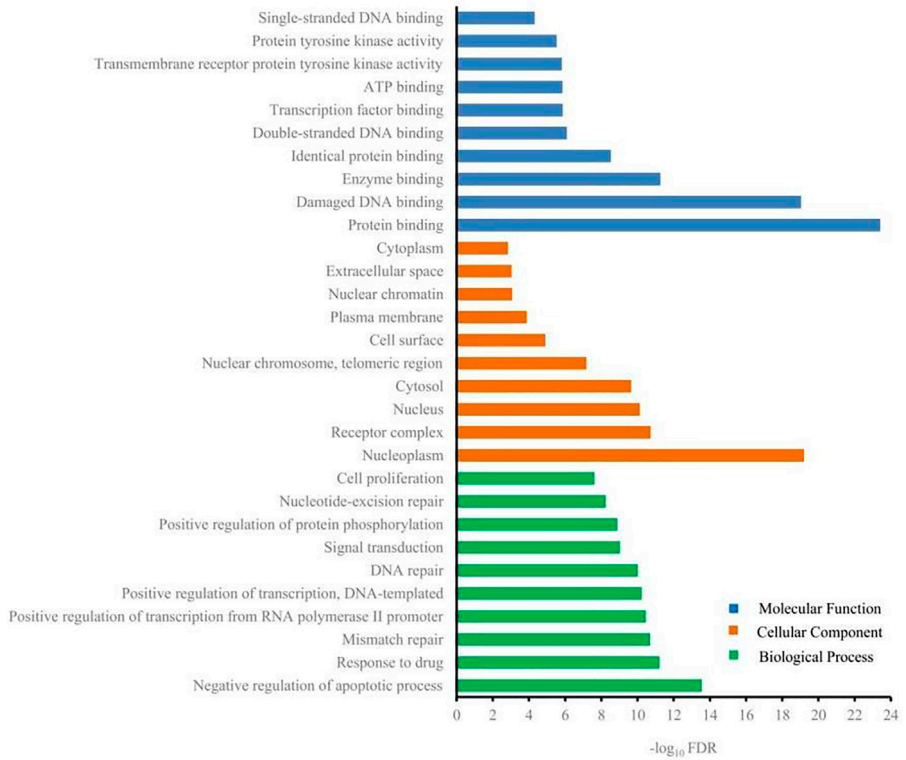

FIGURE 4 | Gene ontology terms of candidate targets for G-Rh2 in lung cancer.

which corrected p value <0.005 were selected and genes regulated these pathways were enriched by gene-pathway network analysis. The gene-pathway network was constructed to screen the key target genes for G-Rh2 against lung cancer.

Cell Line and Cell Culture

The A549 lung cancer cell line was purchased from the China Center for Type Culture Collection (Wuhan, Hubei, China) and cultured in MEM supplemented with 10% FBS, 100 U/mL penicillin and 100 μg/ml streptomycin at 37°C in a humidified atmosphere with 5% CO_2.

Cell Viability Assay

The viability of A549 cells was measured by MTT assay. Briefly, cells were seeded into 96-well plates at 2×10^4 cells/well. After adhered to the plates for overnight, cells were treated with different concentrations of G-Rh2 for 24 and 48 h. The medium was then removed and supplemented with 100 μL MTT solution for 4 h, following with 100 μL stopping buffer. The absorbance was determined at 550 nm using a microplate reader (Tecan Infinite M200 Pro, Männedorf, Switzerland).

Cell Apoptosis Assays

The apoptosis ratio of cells was analyzed by Annexin V-FITC Apoptosis Detection Kit according to the instruction of the manufacturer. In brief, the cells treated with different concentration of G-Rh2 for 24 h were harvested and centrifuged at 1,500 rpm for 3 min to remove the medium. The precipitation was then resuspended in 100 μL 1 × binding buffer. Subsequently, the cells were stained with Annexin-FITC and PI for 15 min in the dark. After added 400 μL 1 × binding buffer, the samples were evaluated by a Accuri C6 Plus flow cytometer (Becton, Dickinson and Company, CA, United States).

Western Blot Analysis

A total of 1×10^6 A549 cells were seeded into 40 mm Petri dish and grown for overnight. Then the cells were treated with G-Rh2 for different time points. After collection, the cells were lysed by RIPA lysis buffer and the protein content was determined by Bradford reagent, using bovine serum albumin (BSA) as a standard. Total protein were separated by 20% SDS-polyacrylamide gels for 1 h at 100 V, transferred to PVDF membranes, and blocked with 5% BSA in Tris-buffered saline containing Tween 20 (1 × TTBS) for 2 h. After washed with 1 × TTBS, the PVDF membranes were then incubated with primary antibodies (1:500–1:2000) in 5% BSA at 4°C for overnight, followed by washing and incubated for 1 h with HRP-conjugated secondary anti-IgG (1:500). The bands were then visualized by the eECL Kit and photographed using Tanon 5200 Multi imaging system (Tanon, China).

Statistical Analysis

The results have been represented as the mean ± SD. Variances among two groups were analyzed by Student's t-test. Data

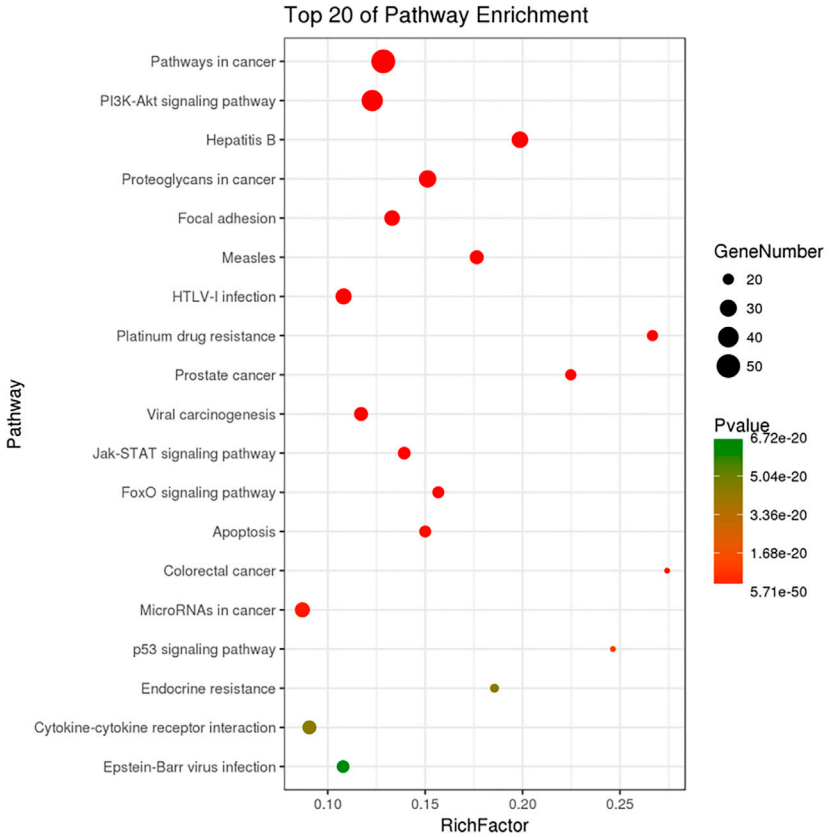

FIGURE 5 | KEGG pathway enrichment of candidate targets for G-Rh2 in lung cancer.

analysis was completed using SPSS 20.0 (SPSS Inc., Chicago, IL, United States). $p < 0.05$ indicated significant differences.

RESULTS AND DISCUSSION

Compound-Target Network Analysis

We evaluated the ability of G-Rh2 to inhibit the viability and induce apoptosis of A549 cells using a network pharmacology approach. The compound-target network was created by one approach. The network of G-Rh2 and its targets from PharmMapper server, SwissTargetPrediction, a similarity ensemble approach, and the STITCH database was constructed as shown in **Figure 2**. Ninety-one targets were obtained, among of which, 70 targets were obtained from PharmMapper server, 14 targets from SwissTargetPrediction, 5 from the similarity ensemble approach, and 2 from the STITCH database. After removing the duplicates, A total of 91 compound-targets was obtained.

Identification of Targets for G-Rh2

Biological networked systems include functional units or protein complexes in PPI networks and disease- or drug-target genes can be analyzed according to complex network theory (Peng et al., 2018). PPIs are important in the regulation of biological systems and are the targets of an increasing number of drugs (Scott et al., 2016). PPI networks of G-Rh2 putative targets and lung cancer-related targets were structured with PPI data. The PPI network of G-Rh2 putative targets contained 3444 nodes and 86990 edges, which represented 3444 interacting proteins and 86990 interactions (**Figure 3A**). The PPI network of lung cancer-related targets contained 7493 interacting proteins and 179815 interactions (**Figure 3B**).

The interaction network of G-Rh2 comprised 91 putative targets of G-Rh2 and 431 lung cancer-related targets. The interaction network encompassed 512 interacting proteins and 1,589 interactions (**Figure 3C**). The structured interaction network was merged with the PPI networks of G-Rh2 putative targets and lung cancer-related targets to identify targets for G-Rh2 in lung cancer. The new network had 217 nodes and 1,028 edges (**Figure 3D**); thus, 217 targets for G-Rh2 in lung cancer were identified.

GO and KEGG Pathway Enrichment Analysis

DAVID was used to carry out GO analysis to elucidate the function of 217 candidate targets in biological process, cellular component, and molecular function. One hundred and three GO terms with FDR <0.05 were significantly enriched: 73 in biological process, 11 in cellular component, and 19 in molecular function. The top 10 GO terms enriched in each sub-ontology are shown in **Figure 4**. Regulation of apoptotic

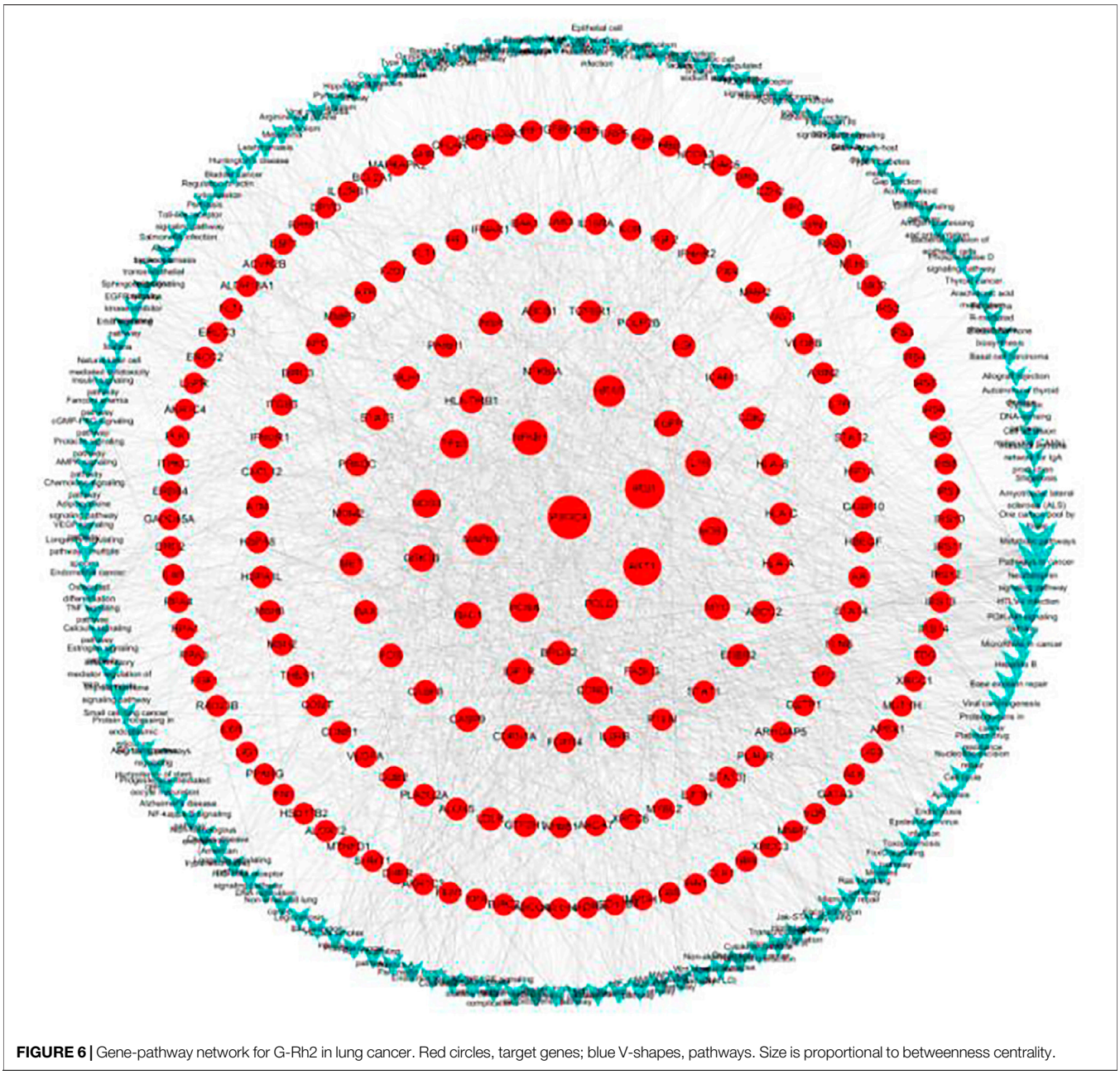

FIGURE 6 | Gene-pathway network for G-Rh2 in lung cancer. Red circles, target genes; blue V-shapes, pathways. Size is proportional to betweenness centrality.

process, regulation of transcription, nucleoplasm, nucleus, protein binding, and damaged DNA binding were the highly enriched GO terms. Anticancer agents activate several pathways simultaneously, positively or negatively regulating the death process (Solary et al., 2000). Regulation of apoptosis is the mechanism by which most chemotherapeutic drugs induce tumor cell death. Genetic alterations induce cancer and always result in dysregulated transcriptional programs. Almost every DNA, RNA, and protein component controlled by normal transcription is influenced by recurrent somatic mutations in tumor cells (Bradner et al., 2017). DNA binding of a new compound is an important aspect of its therapeutic potential for anticancer (Thangavel et al., 2018). Because of reversible binding or formation of covalent bonds with deoxyribonucleic acid, small DNA-interacting anticancer drugs abrogate the interaction between DNA and transcription factors in gene promoters (José, 2018). Therefore, G-Rh2 may reduce A549 cell viability by intervening in biological processes and affecting cellular components and molecular functions.

The KEGG pathway analysis was performed by KOBAS and 143 significantly enriched pathways (corrected $p < 0.005$) including pathways in cancer, the PI3K-Akt signaling pathway, proteoglycans in cancer, focal adhesion, the Jak-STAT signaling pathway, the FoxO signaling pathway, and apoptosis were obtained. **Figure 5** shows the top 20 enriched

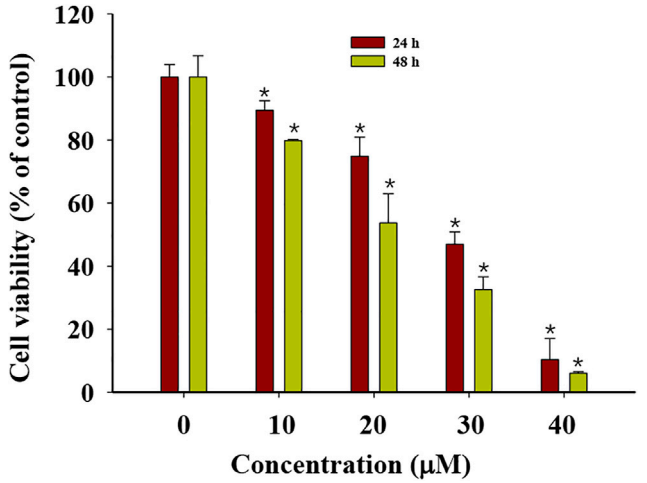

FIGURE 7 | Cytotoxicity of G-Rh2 to A549 cells. Cells were treated with G-Rh2 for 24 and 48 h and viability was evaluated by MTT assay. Values are means ± SD (n = 3).

pathways. The most significantly enriched pathways were related to pathways in cancer, followed by the PI3K-Akt signaling pathway. The PI3K-Akt signaling pathway is crucial in the development of many types of tumors (Lorusso, 2016; Zhang et al., 2017). Cell proliferation, growth, cell cycle, apoptosis, and protein synthesis are regulated by the PI3K-Akt signaling pathway (Zhu et al., 2018). Also, activation of the PI3K-Akt signaling pathway promotes cancer cell proliferation, survival, and angiogenesis. The PI3K-Akt signaling pathway is activated in cancer and is a potential therapeutic target (Chen et al., 2017). Xie et al. indicated that the PI3K-Akt signaling pathway is important in lung cancer and found that ginsenoside Rg3 promoted apoptosis by inhibiting the ratio of p-PI3K/PI3K and p-Akt/Akt in A549 cells (Xie et al., 2017). Our results suggest that G-Rh2 inhibits the viability of A549 cells by inducing apoptosis *via* the PI3K-Akt signaling pathway. In addition, the Wnt/β-catenin, mTOR, VEGF, EGFR, and metabolic signaling pathways are important in lung cancer (Cho, 2013).

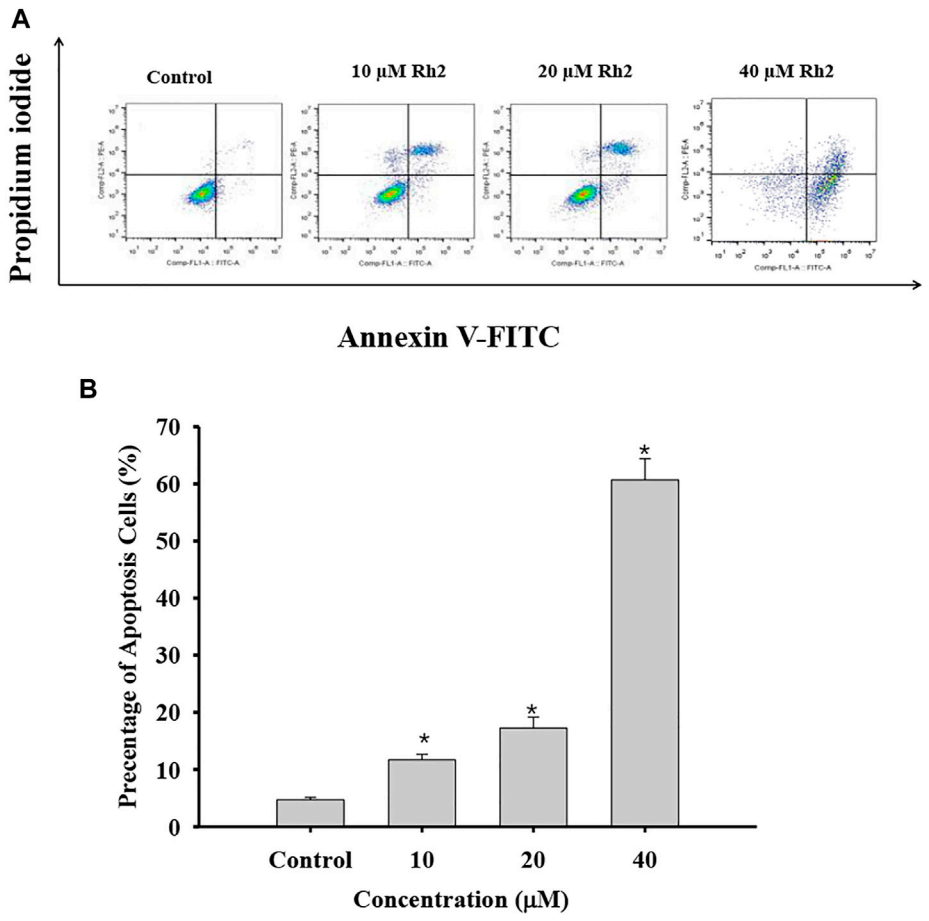

FIGURE 8 | Effect of G-Rh2 on apoptosis of A549 cells. **(A)** Cells were treated with G-Rh2, and the apoptotic rate was determined by Annexin V-FITC/PI staining. **(B)** Percentage of apoptotic cells, Values are means ± SD (n = 3).

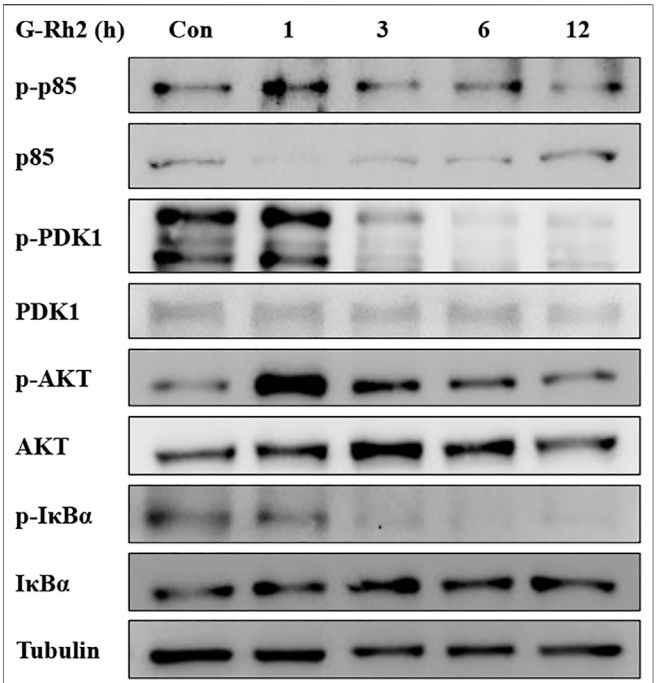

FIGURE 9 | Effects of G-Rh2 on apoptosis-related proteins and their phosphorylation levels in A549 cells. Cells were treated with G-Rh2 for 0, 1, 3, 6, and 12 h. The protein levels of p85/p-p85, PDK1/p-PDK1, Akt/p-Akt and IκBa/p-IκBa were measured by Western blotting.

Gene-Pathway Network Analysis

The significantly enriched pathways and genes were used to construct a gene-pathway network. As shown in **Figure 6**, 143 pathways and 191 genes were identified. Betweenness centrality (BC) was used to carry out the topological analysis. In the network, metabolic pathways had the highest BC, followed by pathways in cancer, the neurotrophin signaling pathway, HTLV-1 infection, and the PI3K-Akt signaling pathway. PIK3CA had the highest BC and several other genes including IRS1, AKT1, NFKB1, MAPK9, and POLD1 had larger BC. PIK3CA is one of the most commonly mutated oncogenes in human cancer and is used in the development of PI3 kinase inhibitors, which can be used as targeted therapies for cancers with these mutations (Jelovac et al., 2014). The PI3K signaling pathway is activated in cancers and is concerned with oncogenesis and cancer progression (Hennessy et al., 2005). PIK3CA mutations have been focused on as potential biomarkers of PI3K pathway activation (Ito et al., 2017). Activation of mutations and genomic amplification of the PIK3CA gene are closely related to increased PI3K activity in lung cancer (Yamamoto et al., 2008). Somatic mutations in the IA PI3K catalytic subunit p110α, encoded by PIK3CA, activate the PI3K signaling pathway (Sawa et al., 2017). IRS1 regulates many cancer-cell processes and PI3K within malignant cells (Houghton et al., 2010; Porter et al., 2013). A549 cell survival, proliferation, malignancy, and metastasis are suppressed by Akt1 knockdown (Jere et al., 2009). Also, constitutional activation of the PI3K-Akt signaling pathway can be caused by oncogenic mutations in the AKT1 gene, increasing the malignant potential of the affected cells. Our results indicate that G-Rh2 induces A549-cell apoptosis mainly by regulating the expression of PIK3CA, thus inhibiting activation of the PI3K-Akt signaling pathway. Also, regulation of IRS1, AKT1, NFKB1, MAPK9, and POLD1 may explain the G-Rh2-mediated inhibition of the viability of A549 cells.

G-Rh2 Inhibits A549 Cell Viability and Promotes Apoptosis

G-Rh2 suppresses cell proliferation, causes G1-phase arrest, enhances the activity of capase-3, and induces apoptosis in A549 cells (An et al., 2013). To validate the anti-proliferation effect of G-Rh2 on A549 cells, a MTT assay was carried out. A549 cells were treated with G-Rh2 at different concentrations for 24 h or 48 h. As shown in **Figure 7**, G-Rh2 significantly inhibited A549 cells proliferation in a dose-dependent manner. Based on the results of MTT assay, IC_{50} of G-Rh2 on A549 cells at 24 and 48 h were calculated respectively as 42.75 and 36.25 μM which was consist with previous report (Zhang et al., 2011).

Apoptosis, an orderly process of programmed cell death, is central to development of cancers. It involves of the activation, expression and regulation of a series of genes, and inhibits the growth of tumor cells. Apoptosis may not the main way for the death of many cancers response to common treatments (Brown and Attardi, 2005). G-Rh2 were reported to induces apoptosis of many cancer cells, such as human epidermoid carcinoma A431cells (Park et al., 2010), human malignant melanoma A375-S2 cells (Fei et al., 2002), and hepatocellular carcinoma HepG2 cells (Zhang et al., 2019). In order to determine whether G-Rh2 can regulates A549 cell death by inducing apoptosis in this study, A549 cells treated with 10, 20, and 40 μM G-Rh2 were stained by Annexin-PI based on a flow cytometry. As shown in **Figure 8**, the apoptosis rate increased significantly from 4.4% in the control group to 15.92, 23.72, and 78.7% at 10, 20, and 40 μM G-Rh2, respectively. It is indicate that G-Rh2 can significantly induce A549 cells apoptosis to regulate this lung cancer cell death, and is consistent with literatures (Cheng et al., 2005; Wang et al., 2018).

The PI3K/Akt signaling pathway operates by phosphorylation and dephosphorylation of the substrate-level (Sang and Li, 2007; Yu et al., 2021). PI3K, phosphoinositide 3-kinase, a lipid kinase family protein, which was constructed by two subunit including a regulatory subunit (P85) and a catalytic subunit (P110). When the growth factors binds to their receptor tyrosine kinase (RTK) or G protein-coupled receptors (GPCR), PI3K isoforms were stimulated and catalyzes the production of phosphatidylinositol-3,4,5-triphosphate (PIP3) at the cell membrane. PIP3, serves as a secondary messenger, is in turn to help the phosphorylation and activation of PDK1 and AKT. AKT is a serine/threonine kinase, once activated, it controls key cellular processes including the inhibition of apoptosis (Liu et al., 2009), and promotes cell survival by activating CREB and NF-κB activity (Park et al., 2010). Therefore, PI3K/Akt as a most commonly activated signaling pathway in human cancer, presents both an opportunity and a challenge for cancer therapy (Liu et al., 2009). In the present study, G-Rh2 was confirmed to down

regulate the phosphorylation of P85, PDK1, Akt and IκBα in A549 cells by western blot analyses (**Figure 9**). The inactivation of P85, PDK1 and Akt by G-Rh2 treatment indicating that G-Rh2 can induces cancer cells to apoptosis *via* inhibiting the PI3K/Akt signaling pathway. Similarly, the inactivation of IκBα means G-Rh2 suppress the cell survival *via* inhibiting the NF-κB signaling pathway and to induces cancer cells death. These results are consistent with that deduced from network pharmacology analyses.

CONCLUSION

The potential targets and signaling pathways of G-Rh2 on human lung cancer were predicted in this work by network pharmacology approach. According to the network pharmacology analyses results, 217 genes/proteins were predicted as potential targets for G-Rh2. Besides, bioinformatics analysis on the predicted targets revealed that over 140 pathways, of which PI3K-Akt signaling pathway is top signaling pathway involved in the underlying mechanisms of G-Rh2. Confirmatory experiments showed that G-Rh2 inhibits proliferation of human lung cancer A549 cells, and induces cells apoptosis *via* inhibiting the PI3K-Akt signaling pathway. It is consistent to the predicted results in the network pharmacology analyses.

DATA AVAILABILITY STATEMENT

The raw data supporting the conclusion of this article will be made available by the authors, without undue reservation.

AUTHOR CONTRIBUTIONS

LW and JZ contributed to design of the study. CS and JZ carried out the network pharmacology analyses. ZH, YH and YX performed the experiments. JZ, CS and JZ wrote and the manuscript. YY, NL, and CS contributed to manuscript revision. All authors read and approved the submitted version.

REFERENCES

Albano, D., Benenati, M., Bruno, A., Bruno, F., Calandri, M., Caruso, D., et al. (2021). Imaging Side Effects and Complications of Chemotherapy and Radiation Therapy: a Pictorial Review from Head to Toe. *Insights Imaging* 12, 1–28. doi:10.1186/s13244-021-01017-2

An, I. S., An, S., Kwon, K. J., Kim, Y. J., and Bae, S. (2013). Ginsenoside Rh2 Mediates Changes in the microRNA Expression Profile of Human Non-small Cell Lung Cancer A549 Cells. *Oncol. Rep.* 29 (2), 523–528. doi:10.3892/or.2012.2136

Bradner, J. E., Hnisz, D., and Young, R. A. (2017). Transcriptional Addiction in Cancer. *Cell.* 168 (4), 629–643. doi:10.1016/j.cell.2016.12.013

Brown, J. M., and Attardi, L. D. (2005). The Role of Apoptosis in Cancer Development and Treatment Response. *Nat. Rev. Cancer* 5, 231–237. doi:10.1038/nrc1560

Chen, Q., Duan, X., Fan, H., Xu, M., Tang, Q., Zhang, L., et al. (2017). Oxymatrine Protects against DSS-Induced Colitis via Inhibiting the PI3K/AKT Signaling Pathway. *Int. Immunopharmacol.* 53, 149–157. doi:10.1016/j.intimp.2017.10.025

Cheng, C. C., Yang, S. M., Huang, C. Y., Chen, J. C., Chang, W. M., and Hsu, S. L. (2005). Molecular Mechanisms of Ginsenoside Rh2-Mediated G1 Growth Arrest and Apoptosis in Human Lung Adenocarcinoma A549 Cells. *Cancer Chemother. Pharmacol.* 55, 531–540. doi:10.1007/s00280-004-0919-6

Cho, W. C. (2013). Targeting Signaling Pathways in Lung Cancer Therapy. *Expert Opin. Ther. Targets* 17 (2), 107–111. doi:10.1517/14728222.2013.729043

David, G., Aurélien, G., Matthias, W., Antoine, D., Olivier, M., and Vincent, Z. (2014). Swisstargetprediction: a Web Server for Target Prediction of Bioactive Small Molecules. *Nucleic Acids Res.* 42 (Web Server issue), W32–W38. doi:10.1093/nar/gku293

Fei, X. F., Wang, B. X., Tashiro, S., Li, T. J., Ma, J. S., and Ikejima, T. (2002). Apoptotic Effects of Ginsenoside Rh2 on Human Malignant Melanoma A375-S2 Cells. *Acta Pharmacol. Sin.* 23 (4), 315–322. doi:10.1016/S0300-483X(02)00008-2

Ge, G., Yan, Y., and Cai, H. (2017). Ginsenoside Rh2 Inhibited Proliferation by Inducing ROS Mediated ER Stress Dependent Apoptosis in Lung Cancer Cells. *Biol. Pharm. Bull.* 40, 2117–2124. doi:10.1248/bpb.b17-00463

Han, S., Jeong, A. J., Yang, H., Bin Kang, K., Lee, H., Yi, E. H., et al. (2016). Ginsenoside 20(S)-Rh2 Exerts Anti-cancer Activity through Targeting IL-6-induced JAK2/STAT3 Pathway in Human Colorectal Cancer Cells. *J. Ethnopharmacol.* 194, 83–90. doi:10.1016/j.jep.2016.08.039

Hanna, J. M., and Onaitis, M. W. (2013). Cell of Origin of Lung Cancer. *J. Carcinog.* 12, 6–12. doi:10.4103/1477-3163.109033

Hayashi, H., Kurata, T., and Nakagawa, K. (2011). Gemcitabine: Efficacy in the Treatment of Advanced Stage Nonsquamous Non-small Cell Lung Cancer. *Clin. Med. Insights Oncol.* 5, 177–184. doi:10.4137/CMO.S6252

Hennessy, B. T., Smith, D. L., RamDebra, P. T., LuPrahlad, Y., and Mills, G. B. (2005). Exploiting the PI3K/AKT Pathway for Cancer Drug Discovery. *Nat. Rev. Drug Discov.* 4 (12), 988–1004. doi:10.1038/nrd1902

Houghton, A. M., Rzymkiewicz, D. M., Ji, H., Gregory, A. D., Egea, E. E., Metz, H. E., et al. (2010). Neutrophil Elastase-Mediated Degradation of IRS-1 Accelerates Lung Tumor Growth. *Nat. Med.* 16 (2), 219–223. doi:10.1038/nm.2084

Huang, da. W., Sherman, B. T., and Lempicki, R. A. (2009). Systematic and Integrative Analysis of Large Gene Lists Using David Bioinformatics Resources. *Nat. Protoc.* 4 (1), 44–57. doi:10.1038/nprot.2008.211

Huang, Q. M., Liu, Y. H., and Suzuki, M. (2021). Role of POLD4 in Smoking-Induced Lung Cancer. *J. Mod. Oncol.* 29 (24), 4271–4275. doi:10.3969/j.issn.1672-4992.2021.24.002

Ito, C., Nishizuka, S. S., Ishida, K., Uesugi, N., Sugai, T., Tamura, G., et al. (2017). Analysis of PIK3CA Mutations and PI3K Pathway Proteins in Advanced Gastric Cancer. *J. Surg. Res.* 212, 195–204. doi:10.1016/j.jss.2017.01.018

Jelovac, D., Beaver, J. A., Balukrishna, S., Wong, H. Y., Toro, P. V., Cimino-Mathews, A., et al. (2014). A PIK3CA Mutation Detected in Plasma from a Patient with Synchronous Primary Breast and Lung Cancers. *Hum. Pathol.* 45 (4), 880–883. doi:10.1016/j.humpath.2013.10.016

Jere, D., Jiang, H. L., Kim, Y. K., Arote, R., Choi, Y. J., Yun, C. H., et al. (2009). Chitosan-graft-polyethylenimine for Akt1 siRNA Delivery to Lung Cancer Cells. *Int. J. Pharm.* 378 (1-2), 194–200. doi:10.1016/j.ijpharm.2009.05.046

José, P. (2018). Challenging Transcription by Dna-Binding Antitumor Drugs. *Biochem. Pharmacol.* 155, 336–345. doi:10.1016/j.bcp.2018.07.030

Keiser, M. J., Roth, B. L., Armbruster, B. N., Ernsberger, P., Irwin, J. J., and Shoichet, B. K. (2007). Relating Protein Pharmacology by Ligand Chemistry. *Nat. Biotechnol.* 25 (2), 197–206. doi:10.1038/nbt1284

Li, Y., Wang, J., Xiao, Y., Wang, Y., Chen, S., Yang, Y., et al. (2015). A Systems Pharmacology Approach to Investigate the Mechanisms of Action of Semen Strychni and Tripterygium Wilfordii Hook F for Treatment of Rheumatoid Arthritis. *J. Ethnopharmacol.* 175, 301–314. doi:10.1016/j.jep.2015.09.016

Lim, S. M., Hong, M. H., and Kim, H. R. (2020). Immunotherapy for Non-small Cell Lung Cancer: Current Landscape and Future Perspectives. *Immune Netw.* 20, e10–14. doi:10.4110/in.2020.20.e10

Liu, P., Cheng, H., Roberts, T. M., and Zhao, J. J. (2009). Targeting the Phosphoinositide 3-kinase Pathway in Cancer. *Nat. Rev. Drug Discov.* 8, 627–644. doi:10.1038/nrd2926

Liu, Y., Yu, S., Xing, X., Qiao, J., Yin, Y., Wang, J., et al. (2021). Ginsenoside Rh2 Stimulates the Production of Mitochondrial Reactive Oxygen Species and Induces Apoptosis of Cervical Cancer Cells by Inhibiting Mitochondrial Electron Transfer Chain Complex. *Mol. Med. Rep.* 24 (6), 873. doi:10.3892/mmr.2021.12513

Lorusso, P. M. (2016). Inhibition of the Pi3k/akt/mtor Pathway in Solid Tumors. *J. Clin. Oncol.* 34 (31), 3803–3815. doi:10.1200/JCO.2014.59.0018

Martin, A., Ochagavia, M. E., Rabasa, L. C., Miranda, J., Fernandez-de-Cossio, J., and Bringas, R. (2010). BisoGenet: A New Tool for Gene Network Building, Visualization and Analysis. *BMC Bioinformatics* 11, 91. doi:10.1186/1471-2105-11-91

Park, E. K., Lee, E. J., Lee, S. H., Koo, K. H., Sung, J. Y., Hwang, E. H., et al. (2010). Induction of Apoptosis by the Ginsenoside Rh2 by Internalization of Lipid Rafts and Caveolae and Inactivation of Akt. *Br. J. Pharmacol.* 160, 1212–1223. doi:10.1111/j.1476-5381.2010.00768.x

Park, S. Y., Park, J. H., Kim, H. S., Lee, C. Y., Lee, H. J., Kang, K. S., et al. (2018). Systems-level Mechanisms of Action of Panax Ginseng: a Network Pharmacological Approach. *J. Ginseng Res.* 42 (1), 98–106. doi:10.1016/j.jgr.2017.09.001

Peng, G. S., Yi, N. Q., Qi, G. M., and Chi, J. (2018). Identifying Influential Genes in Protein–Protein Interaction Networks. *Inf. Sci.* (454-455), 229–241. doi:10.1016/j.ins.2018.04.078

Porter, H. A., Perry, A., Kingsley, C., Tran, N. L., and Keegan, A. D. (2013). IRS1 Is Highly Expressed in Localized Breast Tumors and Regulates the Sensitivity of Breast Cancer Cells to Chemotherapy, while IRS2 Is Highly Expressed in Invasive Breast Tumors. *Cancer Lett.* 338 (2), 239–248. doi:10.1016/j.canlet.2013.03.030

Sang, C. L., and Li, Q. (2007). Research Progress of NF-Kb and its Relationship with Lung Cancer. *Chin. J. Pract. Intern. Med.* 27 (16), 1313–1315. doi:10.3969/j.issn.1005-2194.2007.16.029

Sawa, K., Koh, Y., Kawaguchi, T., Kambayashi, S., Asai, K., Mitsuoka, S., et al. (2017). PIK3CA Mutation as a Distinctive Genetic Feature of Non-small Cell Lung Cancer with Chronic Obstructive Pulmonary Disease: a Comprehensive Mutational Analysis from a Multi-Institutional Cohort. *Lung Cancer* 112, 96–101. doi:10.1016/j.lungcan.2017.07.039

Scott, D. E., Bayly, A. R., Abell, C., and Skidmore, J. (2016). Small Molecules, Big Targets: Drug Discovery Faces the Protein-Protein Interaction Challenge. *Nat. Rev. Drug Discov.* 15 (8), 533–550. doi:10.1038/nrd.2016.29

Shi, X., Jing, L. I., Ran, J., Xiong, W., Haixing, L. I., Guo, P., et al. (2017). Ginsenoside Rh2 Induced Human Colorectal Cancer Cell Apoptosis through PI3K/AKT/GSK-3βpathway. *Chin. Pharmacol. Bull.* 33 (1), 114–119. doi:10.3969/j.issn.1001-1978.2017.01.020

Solary, E., Droin, N., Bettaieb, A., Corcos, L., Dimanche-Boitrel, M. T., and Garrido, C. (2000). Positive and Negative Regulation of Apoptotic Pathways by Cytotoxic Agents in Hematological Malignancies. *Leukemia* 14 (10), 1833–1849. doi:10.1038/sj.leu.2401902

Song, X., Zhang, Y., Dai, E., Du, H., and Wang, L. (2019). Mechanism of Action of Celastrol against Rheumatoid Arthritis: A Network Pharmacology Analysis. *Int. Immunopharmacol.* 74, 105725. doi:10.1016/j.intimp.2019.105725

Szklarczyk, D., Santos, A., von Mering, C., Jensen, L. J., Bork, P., and Kuhn, M. (2016). STITCH 5: Augmenting Protein-Chemical Interaction Networks with Tissue and Affinity Data. *Nucleic Acids Res.* 44 (Database issue), D380–D384. doi:10.1093/nar/gkv1277

Thangavel, T., Sparkes, H. A., and Karuppannan, N. (2018). Quinoline Based Pd(II) Complexes: Synthesis, Characterization and Evaluation of Dna/protein Binding, Molecular Docking and *In Vitro* Anticancer Activity. *Inorg. Chim. Acta.* 482, 229–239. doi:10.1016/j.ica.2018.06.003

Tong-Lin Wu, T., Tong, Y. C., Chen, I. H., Niu, H. S., Li, Y., and Cheng, J. T. (2018). Induction of Apoptosis in Prostate Cancer by Ginsenoside Rh2. *Oncotarget* 9 (13), 11109–11118. doi:10.18632/oncotarget.24326

Wang, Y., Xu, H., Lu, Z., Yu, X., Lv, C., Tian, Y., et al. (2018). Pseudo-ginsenoside Rh2 Induces A549 Cells Apoptosis via the Ras/Raf/ERK/p53 Pathway. *Exp. Ther. Med.* 15, 4916–4924. doi:10.3892/etm.2018.6067

Wang, Y. S., Lin, Y., Li, H., Li, Y., Song, Z., and Jin, Y. H. (2017). The Identification of Molecular Target of (20S) Ginsenoside Rh2 for its Anti-cancer Activity. *Sci. Rep.* 7 (1), 12408–12412. doi:10.1038/s41598-017-12572-4

Wild, C., Weiderpass, E., and Stewart, B. W. (2020). *World Cancer Report: Cancer Research for Cancer Prevention*. Lyon, France: IARC Press.

Wong, A. S., Che, C. M., and Leung, K. W. (2015). Recent Advances in Ginseng as Cancer Therapeutics: a Functional and Mechanistic Overview. *Nat. Prod. Rep.* 32 (2), 256–272. doi:10.1039/c4np00080c

Xia, W., Yihang, S., Shiwei, W., Shiliang, L., Weilin, Z., and Xiaofeng, L. E. A. (2017). Pharmmapper 2017 Update: a Web Server for Potential Drug Target Identification with a Comprehensive Target Pharmacophore Database. *Nucleic Acids Res.* 45 (W1), W356–W360. doi:10.1093/nar/gkx374

Xie, C., Mao, X., Huang, J., Ding, Y., Wu, J., Dong, S., et al. (2011). KOBAS 2.0: a Web Server for Annotation and Identification of Enriched Pathways and Diseases. *Nucleic Acids Res.* 39 (Suppl. l_2), W316–W322. doi:10.1093/nar/gkr483

Xie, Q., Wen, H., Zhang, Q., Zhou, W., Lin, X., Xie, D., et al. (2017). Inhibiting PI3K-AKt Signaling Pathway Is Involved in Antitumor Effects of Ginsenoside Rg3 in Lung Cancer Cell. *Biomed. Pharmacother.* 85, 16–21. doi:10.1016/j.biopha.2016.11.096

Yamamoto, H., Shigematsu, H., Nomura, M., Lockwood, W. W., Sato, M., Okumura, N., et al. (2008). PIK3CA Mutations and Copy Number Gains in Human Lung Cancers. *Cancer Res.* 68 (17), 6913–6921. doi:10.1158/0008-5472.CAN-07-5084

Yu, T., Yu, W. J., and Wang, H. Y. (2021). Research Progress on the Role of PI3K/AKT Signaling Pathway in Non-small Cell Lung Cancer. *Chin. J. Clin. Res.* 34 (02), 248–250+254. doi:10.13429/j.cnki.cjcr.2021.02.026

Zhang, C., Yu, H., and Hou, J. (2011). [Effects of 20 (S) -ginsenoside Rh2 and 20 (R) -ginsenoside Rh2 on Proliferation and Apoptosis of Human Lung Adenocarcinoma A549 Cells]. *Zhongguo Zhong Yao Za Zhi* 36 (12), 1670–1674. doi:10.4268/cjcmm20111228

Zhang, H., Song, P., Huang, H., Kim, E., and Kim, M. (2021). Anticancer Effects and Potential Mechanisms of Ginsenoside Rh2 in Various Cancer Types (Review). *Oncol. Rep.* 45 (4), 1–10. doi:10.3892/or.2021.7984

Zhang, J., Li, W., Yuan, Q., Zhou, J., Zhang, J., Cao, Y., et al. (2019). Transcriptome Analyses of the Anti-proliferative Effects of 20(S)-Ginsenoside Rh2 on HepG2 Cells. *Front. Pharmacol.* 10, 1331. doi:10.3389/fphar.2019.01331

Zhang, Y., Kwok-Shing Ng, P., Kucherlapati, M., Chen, F., Liu, Y., Tsang, Y. H., et al. (2017). A Pan-Cancer Proteogenomic Atlas of PI3K/AKT/mTOR Pathway Alterations. *Cancer Cell.* 31 (6), 820–e3. doi:10.1016/j.ccell.2017.04.013

Zhao, R. L., and He, Y. M. (2018). Network Pharmacology Analysis of the Anti-cancer Pharmacological Mechanisms of Ganoderma Lucidum Extract with Experimental Support Using Hepa1-6-Bearing C57 BL/6 Mice. *J. Ethnopharmacol.* 210, 287–295. doi:10.1016/j.jep.2017.08.041

Zhou, Z., Chen, B., Chen, S., Lin, M., Chen, Y., Jin, S., et al. (2020). Applications of Network Pharmacology in Traditional Chinese Medicine Research. *Evid. Based Complement. Altern. Med.* 2020 (6), 1646905–1646907. doi:10.1155/2020/1646905

Zhu, X., Li, Z., Li, T., Long, F., Lv, Y., Liu, L., et al. (2018). Osthole Inhibits the PI3K/AKT Signaling Pathway via Activation of PTEN and Induces Cell Cycle Arrest and Apoptosis in Esophageal Squamous Cell Carcinoma. *Biomed. Pharmacother.* 102, 502–509. doi:10.1016/j.biopha.2018.03.106

Conflict of Interest: Author NL is employed by Beijing Increasepharm Safety and Efficacy Co., Ltd.

The remaining authors declare that the research was conducted in the absence of any commercial or financial relationships that could be construed as a potential conflict of interest.

Publisher's Note: All claims expressed in this article are solely those of the authors and do not necessarily represent those of their affiliated organizations, or those of the publisher, the editors and the reviewers. Any product that may be evaluated in this article, or claim that may be made by its manufacturer, is not guaranteed or endorsed by the publisher.

frontiers | Frontiers in Pharmacology

ORIGINAL RESEARCH
published: 07 July 2022
doi: 10.3389/fphar.2022.946900

Steamed *Panax notoginseng* and its Saponins Inhibit the Migration and Induce the Apoptosis of Neutrophils in a Zebrafish Tail-Fin Amputation Model

Yin Xiong[1,2,3]†, Mahmoud Halima[2,3]†, Xiaoyan Che[1]†, Yiming Zhang[1], Marcel J. M. Schaaf[2], Minghui Li[1], Min Gao[1], Liqun Guo[4], Yan Huang[4], Xiuming Cui[1] and Mei Wang[3,4,5]**

[1]Faculty of Life Science and Technology, Kunming University of Science and Technology, Kunming, China, [2]Institute of Biology Leiden, Leiden University, Leiden, Netherlands, [3]Leiden University–European Center for Chinese Medicine and Natural Compounds, Institute of Biology Leiden, Leiden University, Leiden, Netherlands, [4]Center for Drug Discovery & Technology Development of Yunnan Traditional Medicine, Kunming, China, [5]SU Biomedicine B.V., Leiden, Netherlands

OPEN ACCESS

Edited by:
Guangbo Fu,
Huaian No. 1 People's Hospital
Nanjing Medical University, China

Reviewed by:
Kunming Qin,
Jiangsu Ocean Universiity, China
Waqas Ahmad,
University of Science Malaysia, Malaysia
Furong Xu,
Yunnan University of Traditional Chinese Medicine, China

***Correspondence:**
Yin Xiong
yhsiung@163.com
Mei Wang
mei.wang@subiomedicine.com

†These authors have contributed equally to this work

Specialty section:
This article was submitted to Experimental Pharmacology and Drug Discovery, a section of the journal Frontiers in Pharmacology

Received: 18 May 2022
Accepted: 16 June 2022
Published: 07 July 2022

Citation:
Xiong Y, Halima M, Che X, Zhang Y, Schaaf MJM, Li M, Gao M, Guo L, Huang Y, Cui X and Wang M (2022) Steamed Panax notoginseng and its Saponins Inhibit the Migration and Induce the Apoptosis of Neutrophils in a Zebrafish Tail-Fin Amputation Model. Front. Pharmacol. 13:946900. doi: 10.3389/fphar.2022.946900

Panax notoginseng (PN) is a Chinese medicinal herb that is traditionally used to treat inflammation and immune-related diseases. Its major active constituents are saponins, the types and levels of which can be changed in the process of steaming. These differences in saponins are causally relevant to the differences in the therapeutic efficacies of raw and steamed PN. In this study, we have prepared the extracts of steamed PN (SPNE) with 70% ethanol and investigated their immunomodulatory effect using a zebrafish tail-fin amputation model. A fingerprint-effect relationship analysis was performed to uncover active constituents of SPNE samples related to the inhibitory effect on neutrophil number. The results showed that SPNE significantly inhibited the neutrophil number at the amputation site of zebrafish larvae. And SPNE extracts steamed at higher temperatures and for longer time periods showed a stronger inhibitory effect. Ginsenosides Rh_1, Rk_3, Rh_4, 20(*S*)-Rg_3, and 20(*R*)-Rg_3, of which the levels were increased along with the duration of steaming, were found to be the major active constituents contributing to the neutrophil-inhibiting effect of SPNE. By additionally investigating the number of neutrophils in the entire tail of zebrafish larvae and performing TUNEL assays, we found that the decreased number of neutrophils at the amputation site was due to both the inhibition of their migration and apoptosis-inducing effects of the ginsenosides in SPNE on neutrophils. Among them, Rh_1 and 20(*R*)-Rg_3 did not affect the number of neutrophils at the entire tail, suggesting that they only inhibit the migration of neutrophils. In contrast, ginsenosides Rk_3, Rh_4, 20(*S*)-Rg_3, and SPNE did not only inhibit the migration of neutrophils but also promoted neutrophilic cell death. In conclusion, this study sheds light on how SPNE, in particular the ginsenosides it contains, plays a role in immune modulation.

Keywords: steamed *Panax notoginseng*, saponin, neutrophil, migration, apoptosis, zebrafish, immune modulation

Abbreviations: Beclo, beclomethasone; dpf, days post-fertilization; Hpf, hours post-fertilization; PLSR, Partial least squares regression; PN, *Panax notoginseng*; RPN, raw *Panax notoginseng*; RPNE, raw *Panax notoginseng* extrac; SPN, steamed *Panax notoginseng*; SPNE, steamed *Panax notoginseng* extract; Veh, vehicle

1 INTRODUCTION

Panax notoginseng (PN) (Burk.) F. H. Chen, also named *sanqi*, is a renowned medicinal herb that has been used in Asia to treat inflammation and blood diseases for thousands of years. More than 300 species of Chinese herbal preparations contain PN root and/or rhizome, which are widely applied clinically for disorders such as cardiovascular diseases, atherosclerosis, diabetes, trauma and hemorrhage (Wang et al., 2016; Duan et al., 2017). Saponins are considered to be the major active components of PN, which can be obtained through ethanol extraction (Hu et al., 2018a; Xu et al., 2019). Previous research in our laboratory showed that a high temperature and long steaming time promoted the conversion of saponins in PN, which led to a differentiation in the bioactivities and clinical efficacies between raw and steamed forms of PN (Xiong et al., 2017; Xiong et al., 2019). For example, raw PN (RPN) is better in relieving swelling and easing pain, whereas steamed PN (SPN) shows more tonifying effects such as enhancing immunity and ameliorating anemia. Both of those effects could be related to the immune-modulating activity of these herbal medicines, but the corresponding active components and related mechanisms are still unknown, which hinders the application and further development of this herbal medicine (Kang and Min, 2012; He et al., 2018).

Zebrafish is a widely used animal model that has emerged in recent years as a model system for drug discovery and research of mechanisms underlying multiple disorders, which is utilized as a rapid and high-throughput drug screening system (Wang et al., 2013). The immune system of zebrafish is similar to that of humans, and zebrafish are therefore increasingly used to study diseases related to the immune system, such as inflammation and cancer (Trede et al., 2004). Within only 3 days, zebrafish embryos develop into the larval stage with an immune system consisting of neutrophils and macrophages which orchestrate the innate immune response. Using different transgenic lines in which these cells are fluorescently marked, the activation of the innate immune system can be visualized by imaging the migration of immune cells in a zebrafish tail-fin amputation model (Li et al., 2012). This approach is well suited to study the immunomodulatory activity of the active components of PN. In a previous study (He et al., 2020), we have investigated the immunomodulation by the ginsenoside Rg_1 using zebrafish larvae as an animal model. And we found that it acted as a selective glucocorticoid receptor agonist with anti-inflammatory action without affecting tissue regeneration.

In the present study, the powdered PN samples were extracted using 70% ethanol and purified to obtain the extracts of PN based on our previously reported methods (Hu et al., 2018a; Hu et al., 2018b). The immunomodulatory effects of these extracts were studied by determining the number of neutrophils migrating towards the wounded site of the zebrafish larval tail after amputation. And beclomethasone (Beclo), a classical glucocorticoid receptor agonist, was used as the positive control. Meanwhile, we developed the HPLC chromatographic fingerprints of PN samples, and investigated the correlation between the effects and fingerprints by using multivariate regression techniques. Major peaks predicted to be correlated with the immunomodulation by PN were then identified to be several ginsenosides, of which the activities were finally verified by pharmacological tests.

2 MATERIALS AND METHODS

2.1 Chemicals

The reference standards of ginsenosides Rh_1, Rk_3, Rh_4, 20(*R*)-Rg_3, and 20(*S*)-Rg_3 were purchased from Shanghai Yuanye Biotechnology Co., Ltd. (Shanghai, China), with the purity ≧ 98%. Methyl alcohol and acetonitrile (HPLC grade) were purchased from Sigma-Aldrich, Inc. (St. Louis, MO, United States). Ultrapure water was generated with an UPT-I-20T ultrapure water system (Chengdu Ultrapure Technology Inc., Chengdu, China). All other chemicals used were of analytical grade.

2.2 Sample Preparation

The preparation of samples was performed as described in previous studies from our laboratory (Hu et al., 2018a; Xiong et al., 2018). PN was obtained from a single batch of root in Yunnan, China (104°077′E, 23°188′N), which had been identified by Prof. Xiuming Cui in Kunming University of Science and Technology. The specimen (No. WSPN15101) has been deposited in Yunnan Key Laboratory of *P. notoginseng*, Kunming University of Science and Technology (Kunming, China), which can be fully validated using http://mpns.kew.org/mpns-portal/?_ga=1.111763972. 1427522246.1459077346. The quality of PN was consistent with the requirements of the Chinese Pharmacopoeia of 2020 edition (Chinese Pharmacopoeia Commission, 2020). SPN was prepared by steaming the crushed RPN in an autoclave (Shanghai, China) for 2, 4, 6, 8, and 10 h at 105°C, 110°C, and 120°C. The steamed powder was dried in a heating-air drying oven at about 45°C to constant weight, then powdered and sieved through a 40-mesh sieve. The powdered PN of 5.0 g was extracted using 50 ml of 70% ethanol at 85°C in a water bath for 1.5 h. After three times of extraction, the ethanol-reflux extracts were combined. Subsequently, the combined extract was centrifuged, filtered, concentrated, and dried to obtain the crude PN extracts. To purify the above crude PN extracts to obtain higher concentrations of saponins, an optimized purification process with macroporous resin was performed, with the concentration of saponin solution of 11.22 mg/ml, loading volume of 4.97 BV, washing volume of 2 BV, ethanol concentration of 70%, and ethanol elution volume of 3.31 BV.

2.3 HPLC Analyses

The sample solutions were prepared as described in a previous study (Xiong et al., 2017). Briefly, HPLC analyses were done on an Agilent 1260 series system (Agilent Technologies, Santa Clara, CA, United States) consisting of a G1311B Pump, a G4212B diode array detector, and a G1329B autosampler. A Vision HT C18 column (250 mm × 4.6 mm, 5 μm) was adopted for the analyses. The mobile phase consisted of A (ultra-pure water) and B (acetonitrile). The gradient mode was as follows: 0–20 min,

80% A; 20–45 min, 54% A; 45–55 min, 45% A; 55–60 min, 45% A; 60–65 min, 100% B; 65–70 min, 80% A; 70–90 min, 80% A. The flow rate was set at 1.0 ml/min. The detection wavelength was set at 203 nm, the column temperature at 30°C and the sample volume at 10 μl.

2.4 Zebrafish Lines and Maintenance

Zebrafish (*Danio rerio*) were maintained and handled according to the guidelines from the Zebrafish Model Organism Database (http://zfin.org) and in compliance with the directives of the local animal welfare committee of Leiden University. They were exposed to a 14 h light and 10 h dark cycle to maintain circadian rhythmicity. Fertilization was performed by natural spawning at the beginning of the light period. Eggs were collected and raised at 28°C in egg water (60 μg/ml Instant Ocean sea salts and 0.0025% methylene blue). The following transgenic zebrafish lines were used in this study: *Tg*(*mpx:GFP*^{i114}/*mpeg1:mCherry-F*^{umsF001}) and *Tg*(*mpx:GFP*)^{i114}.

2.5 Tail Fin Amputation and Drug Treatments

Three-day-old zebrafish larvae were utilized for the tail fin amputation experiments. In each experiment, 20 larvae were used in each treatment group. The administration included a vehicle (Veh) group treated with 0.01% DMSO as the negative control, a group treated with Beclo of 25 μM as the positive control, and groups subjected to the following treatments: RPN powder at 50 μg/ml; RPN extract (RPNE) at 50 μg/ml; SPN powder at 50 μg/ml; SPN extract (SPNE) at 30 μg/ml; and three concentrations (at 30, 60, and 90 μM) each for Rh_1, Rk_3, Rh_4, 20(*R*)-Rg_3, and 20(*S*)-Rg_3. In a pilot experiment, no toxicity on the survival of zebrafish larvae was observed for any group (data not shown). All groups were pretreated with Veh/Beclo/experimental treatment for 2 h before tail fin amputation, and received the same treatment for 4 h after the amputation. Next, larvae were anesthetized in egg water containing 0.02% buffered amino benzoic acid ethyl ester (Sigma-Aldrich Chemie N.V., Zwijndrecht, Netherlands). Larvae were placed on petri dishes coated with 2% agarose under a Leica M165C stereomicroscope, and the tail fins were partly amputated using a 1 mm sapphire blade. For quantification of leukocyte migration, larvae were fixed overnight in 4% paraformaldehyde at 4°C.

2.6 Visualization and Quantification of Neutrophils

Imaging of the *Tg*(*mpx:GFP*^{i114}/*mpeg1:mCherry-F*^{umsF001}) larvae was performed utilizing a LeicaMZ16FA fluorescence stereomicroscope supported by LAS 3.7 software. The neutrophils were detected based on the green fluorescence of their GFP lalabed. To quantify the number neutrophils recruited to the wounded area, the cells in a defined area of the tail as well as in the entire tail were counted manually.

2.7 Partial Least Squares Regression

PLSR is performed to find the inner relationship between the independent variables (X) and dependent variables (Y), which are simultaneously modeled by taking into account X variance, and the covariance between X and Y (Martens and Naes, 1991). In our study, the X matrix is composed of the enhanced fingerprints, and the Y vector is constructed with the relative inhibition rate (RI_i%) calculated by **Eq. 1**. Then, X and Y are decomposed in a product of another two matrices of scores and loadings, as described by **Eqs 2**, **3**:

$$RI_i\% = ((n_{\max} - n_i)/n_{\max}) \times 100\% \quad (1)$$

$$X = TP^T + E \quad (2)$$

$$Y = UQ^T + F \quad (3)$$

Where $n_{\max}$ is the maximal number of migrated neutrophils at the amputation site found in any of the treated groups, n_i is the number of migrated neutrophils treated by PN sample i, and RI_i% is the reference inhibition rate of neutrophils determined for PN sample i. TP^T approximates the chromatographic data and UQ^T to the true Y values; notice that the relationship between the T and U scores is a summary of the relationship between X and Y. The terms E and F from the equations are error matrices. Hence, the PLSR algorithm attempts to find latent variables that maximize the amount of variation explained in X that is relevant for predicting Y; i.e., capture variance and achieve correlation (Brereton, 2007).

2.8 Terminal Deoxynucleotidyl Transferase dUTP Nick-End Labeling Assay

Apoptotic cell death was detected by the Transferase dUTP Nick-End Labeling (TUNEL) assay with the *In Situ* Cell Death Detection Kit, Fluorescein (Roche Diagnostics GmbH, Mannheim, Germany). Briefly, *Tg*(*mpx:GFP*)^{i114} zebrafish larvae at 3 days post-fertilization (dpf) were euthanized, fixed, dehydrated, digested, and post-fixed following the manufacturer's protocol. The neutrophils and apoptotic neutrophils were labeled with green and red fluorescence, respectively. Then, the quantification of migrated neutrophils was performed as described above.

2.9 Statistical Analyses

All data are expressed as means ± standard deviation. IBM SPSS Statistics 20.0 software (IBM North America, New York, NY, United States) and GraphPad Prism 6 (GraphPad Software, San Diego, CA, United States) was applied to carry out the two-tailed unpaired t-test and one-way ANOVA. Umetrics SIMCA-P 11.5 software (Sartorius Stedim Biotech GmbH, Goettingen, Germany) was applied for PLSR analysis. A value of $p < 0.05$ was considered significant, and a value of $p < 0.01$ was considered highly significant.

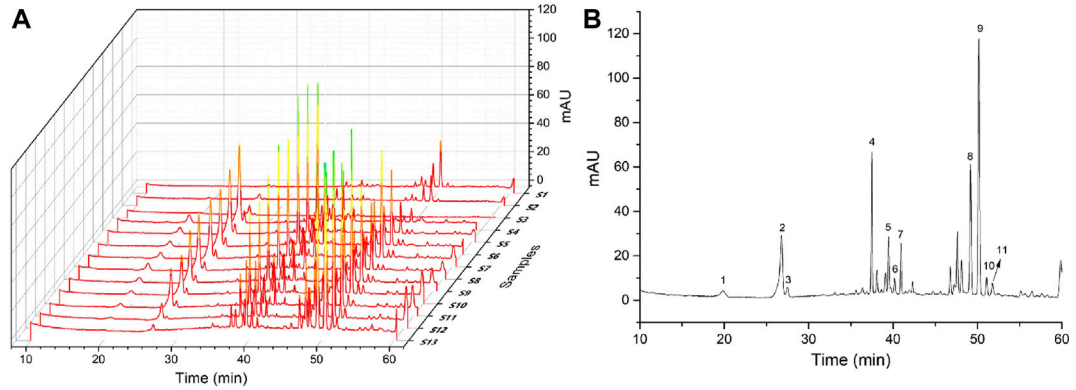

FIGURE 1 | (A) Chemical chromatograms of 13 batches of PN samples and **(B)** 11 selected peaks marked on the chromatogram of S10.

TABLE 1 | Peak areas of eleven common peaks in PN and PNE samples.

No.	Sample[a]	Peak number										
		1	2	3	4	5	6	7	8	9	10	11
S1	RPN	38.24	191.17	0.00	113.23	0.00	0.00	31.63	0.00	0.00	0.00	0.00
S2	SPN120°C-2 h	0.00	0.00	0.00	28.59	44.53	16.01	12.39	182.32	360.13	32.97	0.00
S3	SPN120°C-6 h	0.00	0.00	0.00	65.43	30.23	0.00	24.24	100.48	193.62	0.00	0.00
S4	RPNE	246.46	1533.16	249.52	866.13	90.59	15.00	285.18	50.82	100.80	55.62	0.00
S5	SPNE105°C-2 h	329.95	1432.35	261.00	885.48	81.51	21.68	279.02	120.20	246.94	66.24	0.00
S6	SPNE105°C-4 h	263.97	1380.61	174.94	1152.93	133.25	60.53	400.48	364.69	710.97	125.74	28.17
S7	SPNE105°C-6 h	281.04	1363.17	151.30	910.12	126.03	75.15	305.61	512.12	1019.41	139.13	39.10
S8	SPNE110°C-2 h	257.58	1342.24	0.00	867.53	98.59	39.23	269.37	298.42	602.43	88.43	23.05
S9	SPNE110°C-4 h	213.23	1180.66	187.59	827.83	110.62	49.81	273.76	459.39	910.72	110.56	29.82
S10	SPNE110°C-6 h	192.64	908.16	0.00	679.83	111.31	90.79	241.45	773.01	1560.13	172.65	57.94
S11	SPNE120°C-2 h	189.05	901.29	144.66	716.86	114.82	84.19	235.62	664.81	1322.47	139.68	42.01
S12	SPNE120°C-4 h	0.00	415.83	0.00	140.49	121.31	160.20	122.98	1334.54	2620.14	225.45	98.12
S13	SPNE120°C-6 h	0.00	0.00	0.00	142.15	128.92	191.16	64.80	1466.95	2913.80	254.35	105.24
	C.V.[b] (%)	78.71	71.71	113.27	68.16	43.85	92.07	62.77	92.72	92.46	70.23	106.95

[a]*RPN, raw* Panax notoginseng*; SPN, steamed* Panax notoginseng*; RPNE, raw* Panax notoginseng *extract; SPNE, steamed* Panax notoginseng *extract.*
[b]*C.V. (%) = δ/μ × 100; δ is the standard deviation, μ is the average value of peak area.*

3 RESULTS

3.1 HPLC Analyses

The information and HPLC fingerprints of 13 batches of PN samples, i.e., powder and extract of RPN and SPN prepared under different steaming time periods and temperatures, are shown in **Figure 1**. These fingerprints indicate a distinct difference in the chemical composition between raw and steamed samples, as well as a much higher level of major peaks in the extract compared to powder of the same steaming condition. Consecutive peaks with good segregation and large areas were determined as the common peaks of PN samples. As a result, 11 peaks were selected by comparing their ultraviolet spectra and HPLC retention time, which were then used for further analysis of the fingerprint-effect relationship. The areas of these 11 peaks in the 13 batches of PN samples are listed in **Table 1**. Along with the duration of steaming time and rise of temperature, the area and height of major peaks (peaks 1–4, and 7) were decreased gradually, while other peaks (peaks 5, 6, 8–11) were increased or formed. The peak area was defined as 0 when a peak was absent in a chromatogram. The coefficients of variance for all common peaks were higher than 43.85%, which is due to the diversity in the levels of components contained in samples under different processing conditions. Besides, the areas and height of PNE were much larger than the powder, suggesting a higher level of active constituents and possibly stronger bioeffects.

3.2 Inhibition of Zebrafish Neutrophils by *Panax notoginseng* Samples

The transgenic *Tg*(*mpx:GFP*^{i114}/*mpeg1:mCherry-F*^{umsF001}) zebrafish line in which neutrophils are labeled by GFP, enables the analysis of the behaviour of neutrophils *in vivo*. By visualizing the neutrophils that have migrated to the wounded area in the zebrafish tail fin amputation model, compounds that affect neutrophil behaviour and affect the immunomodulation response can be screened (Renshaw et al., 2006; Wang et al., 2013; Chatzopoulou et al., 2016). In this study, the neutrophil

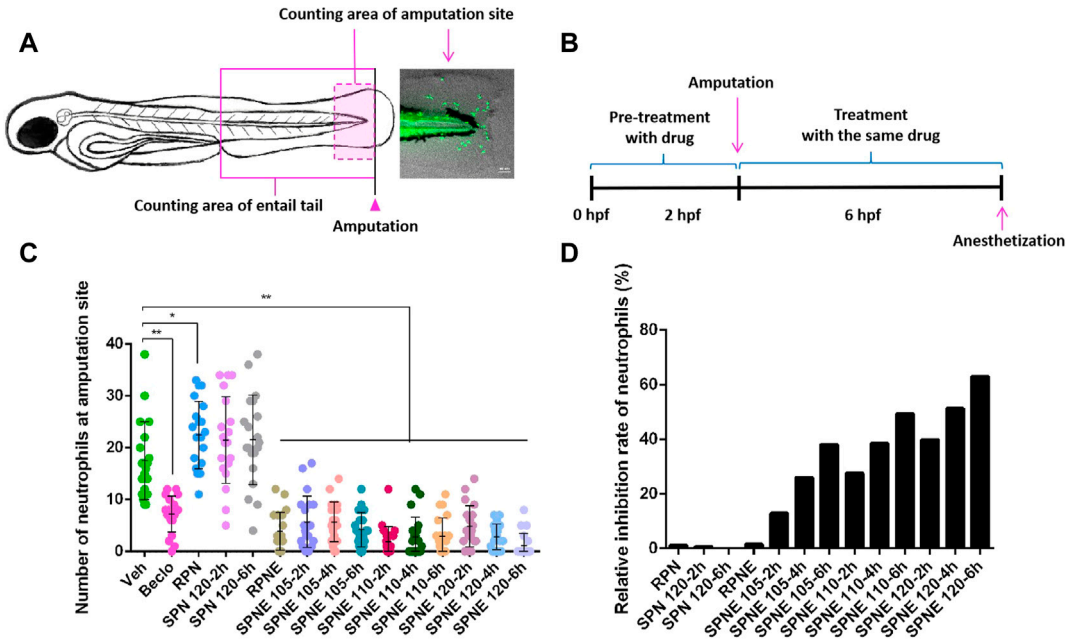

FIGURE 2 | The effect of different PN samples on neutrophil recruitment in the zebrafish tail fin amputation assay. **(A)** The counting areas for the quantification of neutrophils, and a representative fluorescence microscopy image of amputation-induced migration of neutrophils in zebrafish larvae at 3 dpf. **(B)** Schematic of the drug treatment in the zebrafish tail fin amputation experiments. **(C)** The number of neutrophils at the amputation site at 4 h after amputation upon treatment with different PN samples. **(D)** The relative inhibition rate of neutrophils after treating with different PN samples. Hpf, hours post-fertilization; Veh, vehicle; Beclo, beclomethasone; RPN, raw *Panax notoginseng*; RPNE, raw *Panax notoginseng* extract; SPN, steamed *Panax notoginseng*; SPNE, steamed *Panax notoginseng* extract. $^{*}p < 0.05$ and $^{**}p < 0.01$.

number at the injury region was determined in zebrafish larvae at 3 days post-fertilization (dpf) at 4 h after amputation (**Figure 2A**). After pre-treatment with different drugs for 2 h, the amputation was performed, following a 4-h treatment with the same drug (**Figure 2B**). The results showed that RPN and SPN powder did not significantly inhibit the number of neutrophils at the amputation site. In contrast, the number of neutrophils at the amputation site was decreased significantly upon treatment with Beclo or PNE. SPNE samples steamed at a higher temperature and for longer periods of time showed a stronger inhibiting effect (compared to the Veh group) on neutrophil number at the amputation site (**Figure 2C**) and higher relative inhibition rate (**Figure 2D**). To identify the constituents of SPNE responsible for the inhibition on neutrophils, a multivariate data analysis was subsequently performed to correlate the chemical data.

3.3 Uncovering Active Constituents by Multivariate Data Analysis

3.3.1 Prediction

Currently, methods for uncovering active constituents of herbal medicines that are used for treating diseases mainly rely on retrospective analysis. However, this method depends on a large consumption of manpower and material resources. To address this issue, the relative inhibition rates of neutrophils at the amputation site were determined for 13 batches of PN samples, and they were linked with the peak areas in the corresponding chemical fingerprints to construct a "fingerprint-effect relationship" by PLSR. By analyzing the relationship model and weight coefficients, active constituents could be preliminarily predicted despite changes in the peaks and their areas in the chromatogram. Since the total number of samples (13) was small and the prediction for new samples was not our first concern, no division was made into a calibration set to build a PLSR model and a test set to validate the predictive properties. PLSR models were built from the normalized data matrix X containing the 13 PN fingerprints and the response matrix Y of the reference inhibition rate of neutrophils at the amputation site. For the model, two principle components were determined, accounting for an explained variance of 94.9% for the X variable, 92.0% for the Y variable, and a predictive ability (Q^2) of 84.8%, indicating that the obtained model was excellent. As shown in the coefficient matrix in **Figure 3A**, the correlation coefficients between peaks 6, 8, 9, 10, and 11 and the reference inhibition rate were higher than 0.9, indicating that the area of these peaks had a very high level of correlation with the inhibiting effect of PN. Besides, the importance of the X-variables for the model could be summarized by variable importance for the projection (VIP) values (usually with a threshold > 1.0), which showed that these VIP values of peaks 6, 8, 9, 10, and 11 were all higher than 1.0 (**Figure 3B**). Thus, constituents corresponding to peaks 6, 8, 9, 10, and 11 were

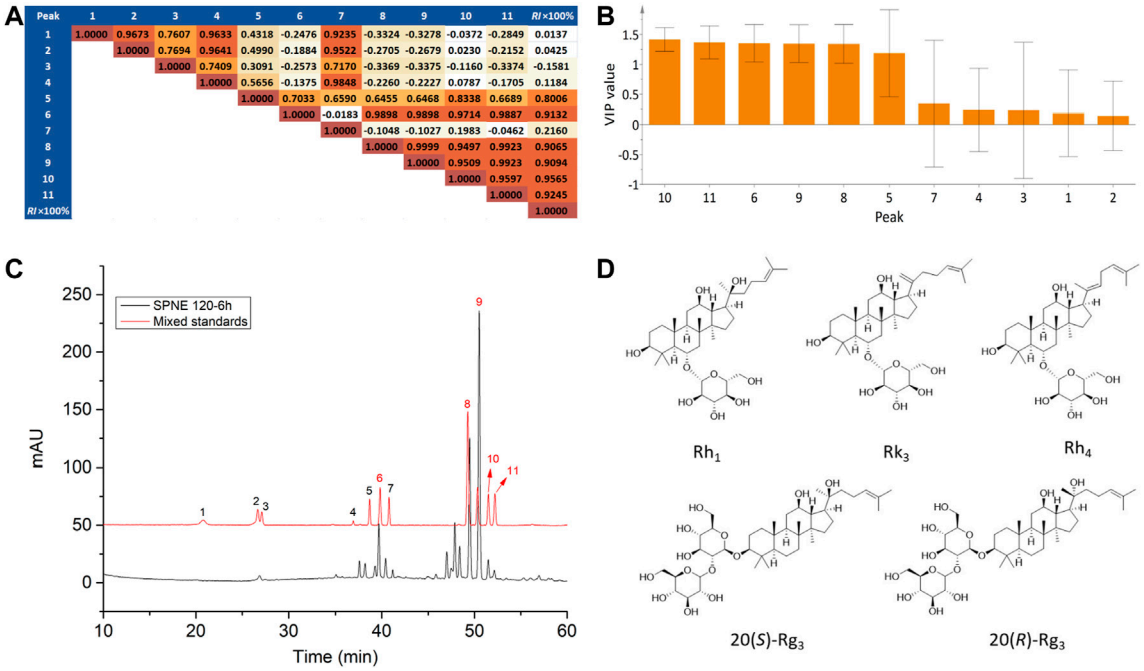

FIGURE 3 | Uncovering active constituents by multivariate data analysis. **(A)** Correlation matrix and **(B)** VIP values of peak areas correlating with the relative inhibition rates of PN samples. **(C)** The chromatograms of the mixed standards solution and SPNE sample steamed at 120°C for 6 h. Peaks 6, 8, 9,10 and 11 correspond to ginsenosides Rh_1, Rk_3, Rh_4, 20(*S*)-Rg_3, and 20(*R*)-Rg_3, respectively. **(D)** Structures of the ginsenosides Rh_1, Rk_3, Rh_4, 20(*S*)-Rg_3, and 20(*R*)-Rg_3.

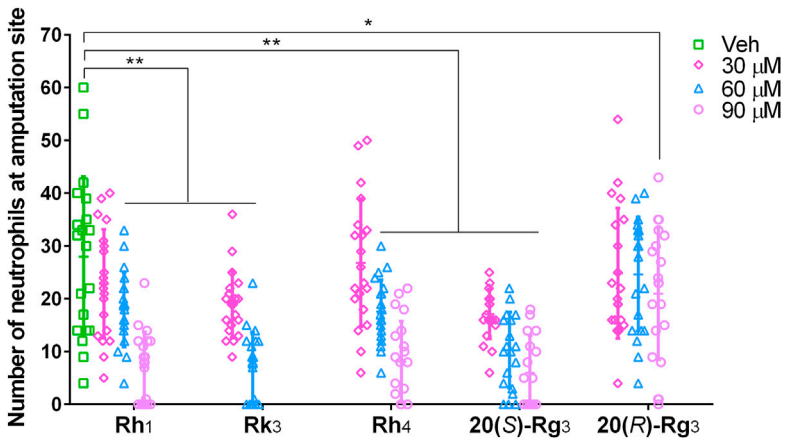

FIGURE 4 | Inhibiting effects of different doses of ginsenosides Rh_1, Rk_3, Rh_4, 20(*S*)-Rg_3, and 20(*R*)-Rg_3 on neutrophil recruitment at the amputation site of zebrafish larvae. Veh, vehicle. $^*p < 0.05$ and $^{**}p < 0.01$.

considered to be related to the inhibition of the neutrophil migration by different PN samples.

By comparing the chromatograms of PN samples to that of the mixture of reference substances (**Figure 3C**), peaks 6, 8, 9, 10, and 11 were identified as ginsenosides Rh_1, Rk_3, Rh_4, 20(*S*)-Rg_3, and 20(*R*)-Rg_3 respectively (**Figure 3D**). As shown in **Table 1** and **Figure 1**, the areas of peaks 6, 8, 9, 10, and 11 of SPNE samples were increased along with the steaming time and elevation of steaming temperature. Thus, the ginsenosides Rh_1, Rk_3, Rh_4, 20(*S*)-Rg_3, and 20(*R*)-Rg_3, might play a major role in the neutrophil-inhibiting effect of SPNE.

3.3.2 Verification

In order to verify the predicted result, the effects of ginsenosides Rh_1, Rk_3, Rh_4, 20(*S*)-Rg_3, and 20(*R*)-Rg_3 on neutrophil number were evaluated using the zebrafish tail fin amputation model.

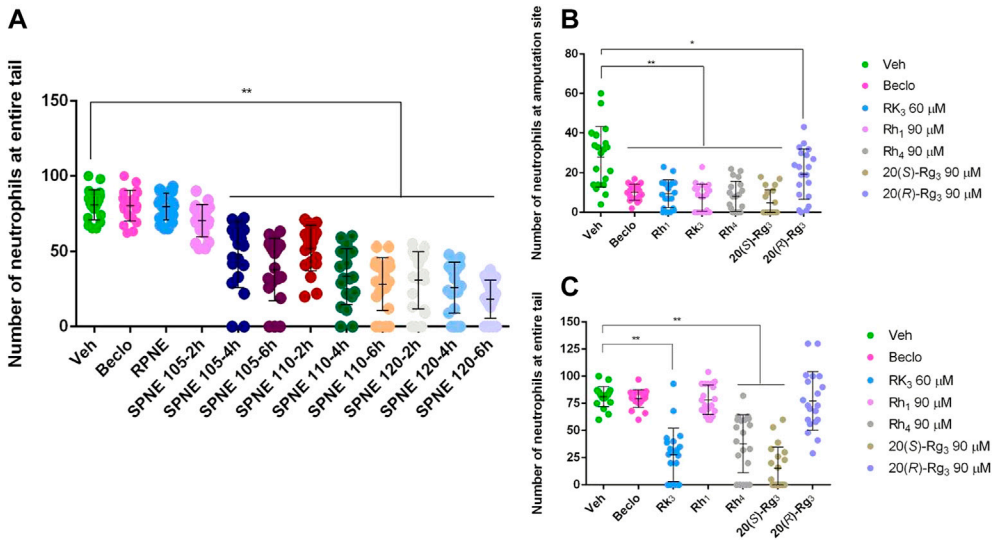

FIGURE 5 | The effect of SPNE and its major ginsenosides on neutrophil migration. **(A)** The number of neutrophils in the entire tail of amputated zebrafish larvae after treatment with different PNE samples. **(B,C)** The number of neutrophils at the amputation site **(B)** and in the entire tail **(C)** of amputated zebrafish larvae after treatment with ginsenosides Rh_1, Rk_3, Rh_4, 20(*S*)-Rg_3, and 20(*R*)-Rg_3. Beclo, beclomethasone; RPNE, raw *Panax notoginseng* extract; SPNE, steamed *Panax notoginseng* extract; Veh, vehicle. $^*p < 0.05$ and $^{**}p < 0.01$.

According to the results shown in **Figure 4**, the five ginsenosides all decreased the number of neutrophils at the amputation site in a dose-dependent way. Rh_1 and Rh_4 at 60 and 90 μM, Rk_3 at 30 and 60 μM, and 20(*S*)-Rg_3 at 30, 60 and 90 μM showed a highly significant inhibitory effect ($p < 0.01$). The ginsenoside 20(*R*)-Rg_3 at 90 μM also significantly decreased the neutrophil number ($p < 0.05$). Since Rk_3 at 90 μM appeared to be lethal to the zebrafish larvae, this concentration was excluded in the effective doses of Rk_3 in this case. Taking the results above together, we verified that ginsenosides Rh_1, Rk_3, Rh_4, 20(*S*)-Rg_3, and 20(*R*)-Rg_3 were the major active constituents of SPNE to inhibit neutrophil number in the zebrafish tail fin amputation model.

3.4 Steamed *Panax notoginseng* Extract and Its Major Ginsenosides Inhibit the Migration and Also Induce Apoptosis of Neutrophils

Neutrophils migrate rapidly to sites of inflammation. The resolution of this inflammatory response can be achieved by either reversing the migration of neutrophils or by the well-characterized process of neutrophil apoptosis (Renshaw et al., 2006; Loynes et al., 2010). To better understand the mechanism underlying the decreased number of neutrophils in the zebrafish tail fin amputation model upon treatment with SPNE and its major active ginsenosides, we investigated the number of neutrophils in the entire tail after amputation. Interestingly, no inhibition on the total number of neutrophils in the entire tail was observed after treatment with Beclo, RPNE, and SPNE steamed at the lowest temperature of 105°C and at the shortest time of 2 h (**Figure 5A**). This, combined with the result in **Figure 2C**, indicates that they mainly inhibit the migration of neutrophils to the injury site. In contrast, SPNE prepared at a higher temperature or for a longer period of time all induced a significant decrease in the total number of neutrophils in the entire tail (**Figure 5A**). This indicates that the decreased number of neutrophils at the amputation site observed after these treatments (**Figure 2D**) could be due to both the migration-inhibiting and elimination effects of SPNE on neutrophils.

To further explore if the previously identified five active constituents of SPNE showed similar effects on the total number of neutrophils in the tail, we compared the effects of ginsenosides Rh_1, Rk_3, Rh_4, 20(*S*)-Rg_3, and 20(*R*)-Rg_3 on the number of neutrophils at the amputation site and in the entire tail of zebrafish larvae. As shown in **Figures 5B,C**, all five ginsenosides at the tested dose significantly inhibited the number of neutrophils at the amputation site, confirming the results shown in **Figure 4**. However, Rh_1 and 20(*R*)-Rg_3 did not affect the number of neutrophils in the entire tail, suggesting they only inhibit the migration of neutrophils to the amputation site. In contrast, ginsenosides Rk_3, Rh_4, and 20(*S*)-Rg_3 induced a significant decrease in the number of neutrophils in the entire tail, indicating that these three compounds not only inhibit the migration of neutrophils but also promote the death of neutrophils.

Based on the above results, we hypothesized that the death of neutrophils could be due to apoptosis. This hypothesis was tested using TUNEL staining of the zebrafish larvae, which detects DNA fragmentation that is characteristic for (but not specific to) apoptotic cells. Images resulting from the application of this assay to larvae from the *Tg(mpx:GFP)*^{i114} show the neutrophils labeled in green and apoptotic neutrophils labeled in red (**Figure 6A**). These images showed that SPNE, ginsenosides Rk_3, Rh_4, and 20(*S*)-Rg_3 triggered the apoptosis of neutrophils

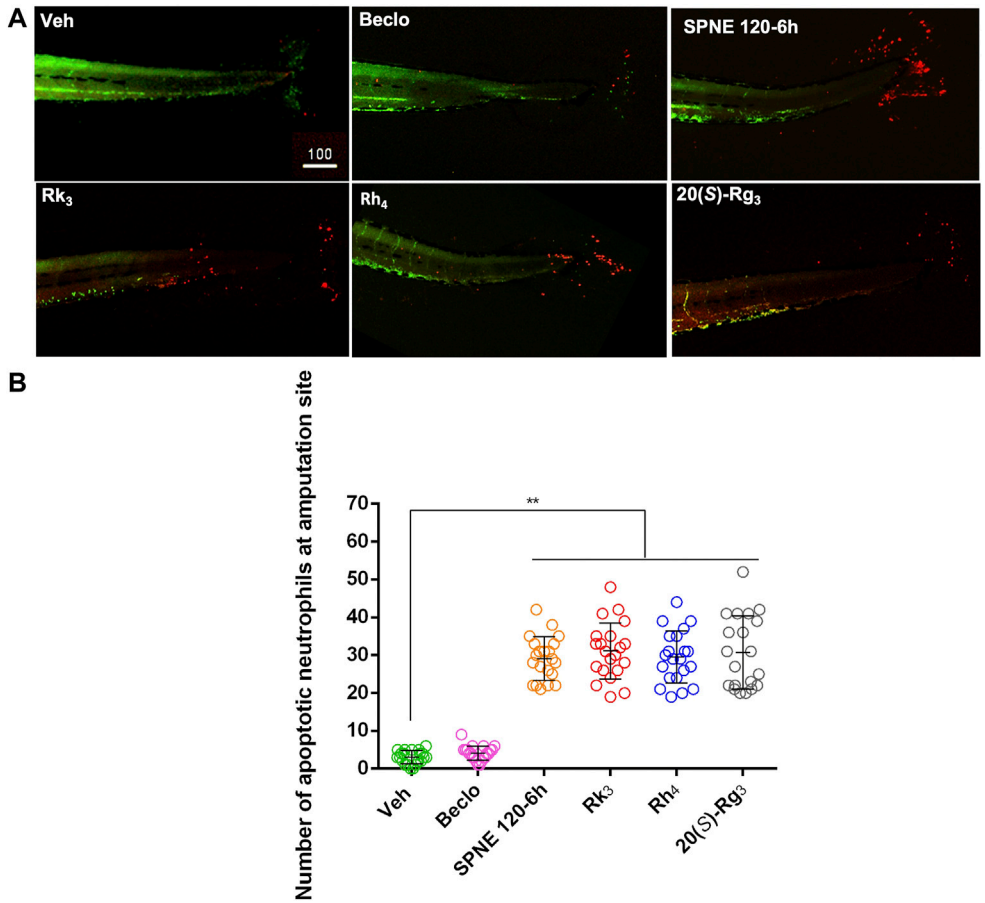

FIGURE 6 | The effect of SPNE and its major ginsenosides on apoptotic neutrophils. **(A)** Apoptotic neutrophils labeled by TUNEL staining in amputated tails of zebrafish larvae. **(B)** The number of apoptotic neutrophils at the amputation site after treating with ginsenosides Rh_1, Rk_3, Rh_4, 20(*S*)-Rg_3, and 20(*R*)-Rg_3. Beclo, beclomethasone; SPNE, steamed *Panax notoginseng* extract; Veh, vehicle. $^*p < 0.05$ and $^{**}p < 0.01$.

mainly at the amputation site of zebrafish larvae (**Figure 6A**). Compared to the Veh group, the numbers of apoptotic neutrophils were significantly increased by treatments with SPNE, and the ginsenosides Rk_3, Rh_4, and 20(*S*)-Rg_3 (**Figure 6B**).

4 DISCUSSION

Both raw and steamed forms of PN have been used in traditional Chinese medicine to regulate the immune system and treat diseases related to inflammation. Dammarane-type saponins are considered to be the major active constituents of PN, which could be enriched by the ethanol extraction process (Sun et al., 2016; Hu et al., 2018b). The chemical structures of saponins are often changed during the steaming process (Wang et al., 2013). As shown in **Figure 1**, the areas of major peaks in raw samples were decreased and some other new peaks were produced along with the rise of steaming time and temperature. Such variation in the chemical composition contributes to the difference in the pharmacological effects and clinical efficacies between raw and steamed forms (Xiong et al., 2019). This was illustrated in our study by the observation that SPNE could inhibit the migration of neutrophils and promote their apoptosis, whereas RPNE only impacted the migration (**Figures 2**, **5**).

Neutrophils constitute about 40%–60% of circulating white blood cells in the human body and are highly evolved for host defense through phagocytosis, degranulation, and the formation of reactive oxygen species and neutrophil extracellular traps (Wang et al., 2013). In the meantime, the uncontrolled neutrophilic activity and continued recruitment of neutrophils to inflammatory sites can result in persistent inflammation and exacerbate chronic human diseases related to the immune system (Gernez et al., 2010). Amputation of the tail fin of zebrafish larvae induces the migration of neutrophils towards the wounded site, which enables studying anti-inflammatory drug effects in an *in vivo* vertebrate animal model (Renshaw et al., 2006; Chatzopoulou et al., 2016).

To uncover the specific constituents responsible for the inhibitory effect on neutrophil migration, the multivariate data analysis of PLSR was performed to analyze the "fingerprint-

effect relationship" of PN samples. Compared with traditional extraction and separation approaches, this method has several advantages such as being less time- and solvent-consuming, low operating costs, and little pollution to the environment, and has therefore been widely applied to discover active compounds in complex mixtures of herbal medicines (Xu et al., 2014; Feng et al., 2020). Based on the results presented in **Figures 3**, **4**, ginsenosides Rh_1, Rk_3, Rh_4, 20(*S*)-Rg_3, and 20(*R*)-Rg_3 were predicted and verified to be the active ones involved in the effect on the number of neutrophils at the amputation site. These ginsenosides were also the major constituents of SPNE.

Combined with our previous results (Xiong et al., 2017; Xiong et al., 2019), notoginsenoside R_1, ginsenosides Re, Rb_1, Rg_1 and Rd were major constituents in raw PN samples. During the steaming process, the hydrolyzation of xylosyl at C-6 of notoginsenoside R_1 and rhamnosyl at C-6 of ginsenoside Re produced Rg_1. The further hydrolysis of the glucosyl at C-20 of Rg_1 yielded Rh_1 which then formed Rh_4 and Rk_3 through dehydration at C-20. Ginsenoside Rb_1 could be hydrolyzed at the glucosyl of C-20 to yield ginsenoside Rd. Similarly, the hydrolysation of the glucosyl at C-20 of Rd produced Rg_3 (Wang et al., 2012). This transformation indicated the change of major peaks in the chromatograms of PN samples during the steaming. The levels of ginsenosides Rh_1, Rk_3, Rh_4, 20(*S*)-Rg_3, and 20(*R*)-Rg_3 in SPNE were elevated along with the increase of steaming time and temperature, which explained why SPNE processed for longer time periods and at higher temperatures exhibited stronger inhibition on the migration of neutrophils as well as the pro-apoptosis effect on neutrophils.

SPN is traditionally used as a tonic to attenuate the syndrome of "blood deficiency" and help patients to recover from chronic disease in traditional Chinese medicine. Patients or animals with this syndrome often suffer from impaired hematopoietic function, peripheral blood pancytopenia, hypofunction of internal organs, malnutrition, or even hemolysis which promote inflammatory reactions (Zhang et al., 2014; Ji et al., 2017). Activated by inflammatory stimuli, circulating neutrophils are recruited to the injury or infectious sites as the first responders during an innate immune response, of which the retention, however, could lead to tissue damage and even develop to other complications. Therefore, the resolution of neutrophil-mediated inflammation by reversing the migration and inducing the apoptosis of neutrophils could be one of the mechanisms of drugs to alleviate anemia (Da Guarda et al., 2017; Mooney et al., 2018). In our previous studies, SPNE and its saponins were verified to show an anti-anemia effect by reversing the decrease of bloods cells in mice with blood deficiency syndrome (Zhang et al., 2019). The treatments of Rk_3 and 20(*S*)-Rg_3 of certain doses could reverse the decreased levels of heme and ferrochelatase, of which the abnormal synthesis can lead to anemia. In the presence of high level of heme, the neutrophil death could be accelerated by antioxidant reagents released by red blood cells (Luo and Loison, 2008). This might explain how SPNE and its ginsenosides played the role in the treatment of anemia by promoting the apoptosis of over retentive neutrophils. One thing should be noted that the effect of a ginsenoside on neutrophil was previously shown in our group to be mediated by the glucocorticoid receptor (He et al., 2020). But no effects of activation of this receptor has been found on apoptosis, which suggests that the effect of SPNE on apoptosis is most likely not mediated by this receptor but through activation of another pathway. Besides, the inappropriate delay of neutrophil death within tissues has been often implicated in a variety of inflammatory and immunological diseases. Neutrophil apoptosis in patients with both infective and non-infective insults-elicited systemic inflammatory response syndrome decreases significantly (Jimenez, 1997; Melley et al., 2005). With the anti-neutrophil treatment, the damage to the lung and liver could be both attenuated (Mercer-Jones et al., 1997). Therefore, SPNE and its ginsenosides showed the potential to be developed as drugs with neutrophil-inhibiting effect for the treatment of immune diseases.

5 CONCLUSION

By using the zebrafish larval tail fin amputation model, the effects on neutrophil recruitment of SPNE obtained using different steaming conditions were investigated in the present study. Combined with the chemical analysis and fingerprint-effect relationship of PN samples, ginsenosides Rh_1, Rk_3, Rh_4, 20(*S*)-Rg_3, and 20(*R*)-Rg_3 were found to be the active ones correlated to the effect of SPNE on neutrophils. Among them, Rh_1 and 20(*R*)-Rg_3 only inhibited the migration of neutrophils to the amputation site, whereas Rk_3, Rh_4, and 20(*S*)-Rg_3 could also promote the apoptosis of neutrophils. The results shed light on how SPNE and its ginsenosides impact immunity and treat related diseases.

DATA AVAILABILITY STATEMENT

The original contributions presented in the study are included in the article/Supplementary Material, further inquiries can be directed to the corresponding authors.

ETHICS STATEMENT

Ethical review and approval was not required for the animal study because according to the EU Directive 2010/63/EU on the protection of animals used for scientific purposes, early life-stages of zebrafish are not protected as animals until the stage of being capable of independent feeding (5 days post fertilization). Therefore, the animal ethical approval is not provided. Zebrafish were maintained and handled according to the guidelines from the Zebrafish Model Organism Database (http://zfin.org) and in compliance with the directives of the local animal welfare committee of Leiden University.

AUTHOR CONTRIBUTIONS

YX supervised the project, wrote this paper and carried out parts of data analyses; MH, XC, and YZ performed the

pharmacologic tests, chemical analyses and parts of data analyses; MS provided the technical support for the pharmacologic tests and revised the manuscript; ML, MG, LG, and YH did the literature studies; XC provided technical support for the methodology; MW supervised the project and revised the manuscript. All the authors read and approve the final manuscript.

FUNDING

This work was supported by the Fund of Yunnan Quality and Technology Supervision Bureau (KKPT202126008), Key R&D Project of Yunnan Provincial Science and Technology Department (202003AC100013), MW Expert Workstation of Yunnan Province (201905AF150001), and Major S&T Project of Yunnan Provincial Science and Technology Department (202102AA310045).

REFERENCES

Brereton, R. G. (2007). Applied Chemometrics for Scientists. *Calibration*. 1. 193–220. doi:10.1002/9780470057780

Chatzopoulou, A., Heijmans, J. P., Burgerhout, E., Oskam, N., Spaink, H. P., Meijer, A. H., et al. (2016). Glucocorticoid-induced Attenuation of the Inflammatory Response in Zebrafish. *Endocrinology* 157, 2772–2784. doi:10.1210/en.2015-2050

Chinese Pharmacopoeia Commission (2020). *Pharmacopoeia of the People's Republic of China*. Beijing, China: Chinese Medical Science and Technology Press.

Guarda, C. C. D., Santiago, R. P., Fiuza, L. M., Aleluia, M. M., Ferreira, J. R. D., Figueiredo, C. V. B., et al. (2017). Heme-mediated Cell Activation: the Inflammatory Puzzle of Sickle Cell Anemia. *Expert Rev. Hematol.* 10, 533–541. doi:10.1080/17474086.2017.1327809

Duan, L., Xiong, X., Hu, J., Liu, Y., Li, J., and Wang, J. (2017). *Panax Notoginseng* Saponins for Treating Coronary Artery Disease: a Functional and Mechanistic Overview. *Front. Pharmacol.* 8, 702. doi:10.3389/fphar.2017.00702

Feng, Y., Teng, L., Wang, Y., Gao, Y., Ma, Y., Zhou, H., et al. (2020). Using Spectrum-Effect Relationships Coupled with LC-TOF-MS to Screen Anti-arrhythmic Components of the Total Flavonoids in Hypericum Attenuatum Extracts. *J. Chromatogr. Sci.* 59, 246–261. doi:10.1093/chromsci/bmaa101

Gernez, Y., Tirouvanziam, R., and Chanez, P. (2010). Neutrophils in Chronic Inflammatory Airway Diseases: Can We Target Them and How? *Eur. Respir. j.* 35, 467–469. doi:10.1183/09031936.00186109

He, M., Huang, X., Liu, S., Guo, C., Xie, Y., Meijer, A. H., et al. (2018). The Difference between White and Red Ginseng: Variations in Ginsenosides and Immunomodulation. *Planta. Med.* 84, 845–854. doi:10.1055/a-0641-6240

He, M., Halima, M., Xie, Y., Schaaf, M. J. M., Meijer, A. H., and Wang, M. (2020). Ginsenoside Rg1 Acts as a Selective Glucocorticoid Receptor Agonist with Anti-inflammatory Action without Affecting Tissue Regeneration in Zebrafish Larvae. *Cells* 9, 1107. doi:10.3390/cells9051107

Hu, Y., Cui, X., Zhang, Z., Chen, L., Zhang, Y., Wang, C., et al. (2018a). Optimisation of Ethanol-Reflux Extraction of Saponins from Steamed *Panax Notoginseng* by Response Surface Methodology and Evaluation of Hematopoiesis Effect. *Molecules* 23, 1206. doi:10.3390/molecules23051206

Hu, Y. P., Cui, X. M., Zhang, Z. J., Chen, L. J., Yu, W., and Xiong, Y. (2018b). Optimization of Purification Process of Saponins in Steamed *Panax Notoginseng* by Failure Mode and Effects Analysis and Central Composite Design-Response Surface Methodology. *Chin. Herb. Med.* 49, 3009–3016. doi:10.7501/j.issn.0253-2670.2018.13.009

Ji, P., Wei, Y., Hua, Y., Zhang, X., Yao, W., Ma, Q., et al. (2017). A Novel Approach Using Metabolomics Coupled with Hematological and Biochemical Parameters to Explain the Enriching-Blood Effect and Mechanism of Unprocessed Angelica Sinensis and its 4 Kinds of Processed Products. *J. Ethnopharmacol.* 211, 101–116. doi:10.1016/j.jep.2017.09.028

Jimenez, M. F., Watson, R. W., Parodo, J., Evans, D., Foster, D., Steinberg, M., et al. (1997). Dysregulated Expression of Neutrophil Apoptosis in the Systemic Inflammatory Response Syndrome. *Arch. Surg.* 132, 1263–1270. doi:10.1001/archsurg.1997.01430360009002

Kang, S., and Min, H. (2012). Ginseng, the 'Immunity Boost': The Effects of Panax Ginseng on Immune System. *J. Ginseng Res.* 36, 354–368. doi:10.5142/jgr.2012.36.4.354

Li, L., Yan, B., Shi, Y. Q., Zhang, W. Q., and Wen, Z. L. (2012). Live Imaging Reveals Differing Roles of Macrophages and Neutrophils during Zebrafish Tail Fin Regeneration. *J. Biol. Chem.* 287, 25353–25360. doi:10.1074/jbc.M112.349126

Loynes, C. A., Martin, J. S., Robertson, A., Trushell, D. M., Ingham, P. W., Whyte, M. K., et al. (2010). Pivotal Advance: Pharmacological Manipulation of Inflammation Resolution during Spontaneously Resolving Tissue Neutrophilia in the Zebrafish. *J. Leukoc. Biol.* 87, 203–212. doi:10.1189/jlb.0409255

Luo, H. R., and Loison, F. (2008). Constitutive Neutrophil Apoptosis: Mechanisms and Regulation. *Am. J. Hematol.* 83, 288–295. doi:10.1002/ajh.21078

Martens, H. E., and Naes, T. (1991). Multivariate Calibration. *Biometrics* 47, 1203–1205.

Melley, D. D., Evans, T. W., and Quinlan, G. J. (2005). Redox Regulation of Neutrophil Apoptosis and the Systemic Inflammatory Response Syndrome. *Clin. Sci. (Lond)* 108, 413–424. doi:10.1042/CS20040228

Mercer-Jones, M. A., Heinzelmann, M., Peyton, J. C., Wickel, D., Cook, M., and Cheadle, W. G. (1997). Inhibition of Neutrophil Migration at the Site of Infection Increases Remote Organ Neutrophil Sequestration and Injury. *Shock* 8, 193–199. doi:10.1097/00024382-199709000-00007

Mooney, J. P., Galloway, L. J., and Riley, E. M. (2018). Malaria, Anemia, and Invasive Bacterial Disease: a Neutrophil Problem? *J. Leukoc. Biol.* 105, 645–655. doi:10.1002/JLB.3RI1018-400R

Renshaw, S. A., Loynes, C. A., Trushell, D. M., Elworthy, S., Ingham, P. W., and Whyte, M. K. (2006). A Transgenic Zebrafish Model of Neutrophilic Inflammation. *Blood* 108, 3976–3978. doi:10.1182/blood-2006-05-024075

Sun, S., Wang, C.-Z., Tong, R., Li, X.-L., Fishbein, A., Wang, Q., et al. (2010). Effects of Steaming the Root of *Panax Notoginseng* on Chemical Composition and Anticancer Activities. *Food Chem.* 118, 307–314. doi:10.1016/j.foodchem.2009.04.122

Trede, N. S., Langenau, D. M., Traver, D., Look, A. T., and Zon, L. I. (2004). The Use of Zebrafish to Understand Immunity. *Immunity* 20, 367–379. doi:10.1016/S1074-7613(04)00084-6

Wang, D., Liao, P.-Y., Zhu, H.-T., Chen, K.-K., Xu, M., Zhang, Y.-J., et al. (2012). The Processing of *Panax Notoginseng* and the Transformation of its Saponin Components. *Food Chem.* 132, 1808–1813. doi:10.1016/j.foodchem.2011.12.010

Wang, X., Robertson, A. L., Li, J., Chai, R. J., Haishan, W., Sadiku, P., et al. (2013). Inhibitors of Neutrophil Recruitment Identified Using Transgenic Zebrafish to Screen a Natural Product Library. *Dis. Model. Mech.* 7, 163–169. doi:10.1242/dmm.012047

Wang, T., Guo, R., Zhou, G., Zhou, X., Kou, Z., Sui, F., et al. (2016). Traditional Uses, Botany, Phytochemistry, Pharmacology and Toxicology of *Panax Notoginseng* (Burk.) F.H. Chen: a Review. *J. Ethnopharmacol.* 188, 234–258. doi:10.1016/j.jep.2016.05.005

Xiong, Y., Chen, L., Hu, Y., and Cui, X. (2017). Uncovering Active Constituents Responsible for Different Activities of Raw and Steamed *Panax Notoginseng* Roots. *Front. Pharmacol.* 8, 745. doi:10.3389/fphar.2017.00745

Xiong, Y., Hu, Y., Chen, L., Zhang, Z., Zhang, Y., Niu, M., et al. (2018). Unveiling Active Constituents and Potential Targets Related to the Hematinic Effect of Steamed *Panax Notoginseng* Using Network Pharmacology Coupled with Multivariate Data Analyses. *Front. Pharmacol.* 9, 1514. doi:10.3389/fphar.2018.01514

Xiong, Y., Chen, L., Man, J., Hu, Y., and Cui, X. (2019). Chemical and Bioactive Comparison of *Panax Notoginseng* Root and Rhizome in Raw and Steamed Forms. *J. Ginseng Res.* 43, 385–393. doi:10.1016/j.jgr.2017.11.004

Xu, G. L., Xie, M., Yang, X. Y., Song, Y., Yan, C., Yang, Y., et al. (2014). Spectrum-effect Relationships as a Systematic Approach to Traditional Chinese Medicine Research: Current Status and Future Perspectives. *Molecules* 19, 17897–17925. doi:10.3390/molecules191117897

Xu, C., Wang, W., Wang, B., Zhang, T., Cui, X., Pu, Y., et al. (2019). Analytical Methods and Biological Activities of *Panax Notoginseng* Saponins: Recent Trends. *J. Ethnopharmacol.* 236, 443–465. doi:10.1016/j.jep.2019.02.035

Zhang, H., Wang, H. F., Liu, Y., Huang, L. J., Wang, Z. F., and Li, Y. (2014). The Haematopoietic Effect of *Panax Japonicus* on Blood Deficiency Model Mice. *J. Ethnopharmacol.* 154, 818–824. doi:10.1016/j.jep.2014.05.008

Zhang, Z., Zhang, Y., Gao, M., Cui, X., Yang, Y., van Duijn, B., et al. (2019). Steamed *Panax Notoginseng* Attenuates Anemia in Mice with Blood Deficiency Syndrome via Regulating Hematopoietic Factors and JAK-STAT Pathway. *Front. Pharmacol.* 10, 1578. doi:10.3389/fphar.2019.01578

Conflict of Interest: Author MW was employed by SU Biomedicine B.V.

The remaining authors declare that the research was conducted in the absence of any commercial or financial relationships that could be construed as a potential conflict of interest.

Publisher's Note: All claims expressed in this article are solely those of the authors and do not necessarily represent those of their affiliated organizations, or those of the publisher, the editors and the reviewers. Any product that may be evaluated in this article, or claim that may be made by its manufacturer, is not guaranteed or endorsed by the publisher.

frontiers | Frontiers in Pharmacology

REVIEW
published: 07 July 2022
doi: 10.3389/fphar.2022.946752

A Review of Neuroprotective Effects and Mechanisms of Ginsenosides From Panax Ginseng in Treating Ischemic Stroke

Aimei Zhao[1†], Nan Liu[2†], Mingjiang Yao[3], Yehao Zhang[3], Zengyu Yao[1], Yujing Feng[4], Jianxun Liu[3] and Guoping Zhou[1*]*

[1]Department of Acupuncture and Moxibustion, Neuroscience Centre, Integrated Hospital of Traditional Chinese Medicine, Southern Medical University, Guangzhou, China, [2]Beijing Increasepharm Safety and Efficacy Co., Ltd., Beijing, China, [3]Beijing Key Laboratory of Pharmacology of Chinese Materia Region, Institute of Basic Medical Sciences, Xiyuan Hospital of China Academy of Chinese Medical Sciences, Beijing, China, [4]Department of Anesthesiology, Punan Hospital, Shanghai, China

OPEN ACCESS

Edited by:
Guangbo Fu,
Huaian No. 1 People's Hospital
Nanjing Medical University, China

Reviewed by:
Hongliang Li,
Yangzhou University, China
Jian Huang,
Princeton University, United States

***Correspondence:**
Jianxun Liu
liujx0324@sina.com
Guoping Zhou
doctorzgp@sina.com

[†]These authors have contributed equally to this work and share first authorship

Specialty section:
This article was submitted to Experimental Pharmacology and Drug Discovery, a section of the journal Frontiers in Pharmacology

Received: 18 May 2022
Accepted: 14 June 2022
Published: 07 July 2022

Citation:
Zhao A, Liu N, Yao M, Zhang Y, Yao Z, Feng Y, Liu J and Zhou G (2022) A Review of Neuroprotective Effects and Mechanisms of Ginsenosides From Panax Ginseng in Treating Ischemic Stroke. Front. Pharmacol. 13:946752. doi: 10.3389/fphar.2022.946752

Ischemic stroke has been considered one of the leading causes of mortality and disability worldwide, associated with a series of complex pathophysiological processes. However, effective therapeutic methods for ischemic stroke are still limited. Panax ginseng, a valuable traditional Chinese medicine, has been long used in eastern countries for various diseases. Ginsenosides, the main active ingredient of Panax ginseng, has demonstrated neuroprotective effects on ischemic stroke injury during the last decade. In this article, we summarized the pathophysiology of ischemic stroke and reviewed the literature on ginsenosides studies in preclinical and clinical ischemic stroke. Available findings showed that both major ginsenosides and minor ginsenosides (such as Rg3, Rg5, and Rh2) has a potential neuroprotective effect, mainly through attenuating the excitotoxicity, Ca^{2+} overload, mitochondria dysfunction, blood-brain barrier (BBB) permeability, anti-inflammation, anti-oxidative, anti-apoptosis, anti-pyroptosis, anti-autophagy, improving angiogenesis, and neurogenesis. Therefore, this review brings a current understanding of the mechanisms of ginsenosides in the treatment of ischemic stroke. Further studies, especially in clinical trials, will be important to confirm the clinical value of ginseng and ginsenosides.

Keywords: panax ginseng, ginsenosides, traditional Chinese medicine, cerebral ischemic stroke, neuroprotection mechanisms

INTRODUCTION

Stroke is one of the leading causes of disability and mortality worldwide, which creates a significant economic burden on the healthcare system (Johnson et al., 2019). Ischemic stroke (IS) is the primary stroke subtype, accounting for approximately 87% of stroke cases (Virani et al., 2020). The middle cerebral artery (MCA) is the most commonly affected vascular territory in cerebral ischemic stroke (Navarro-Orozco and Sánchez-Manso, 2022), and an intravascular blood clot or thrombus usually causes vascular occlusion. Clinically, thrombolytic therapy and thrombectomy are the only approved methods for treating acute ischemic stroke (Campbell and Khatri, 2020), restoring blood flow to the ischemic brain and rescuing damaged neurons in the ischemic penumbra. However, these treatments have limited time windows, intravenous alteplase (rtPA) restricted within 4.5 h, endovascular

thrombectomy within 24 h (Lees et al., 2010; Powers et al., 2019), to reduce the risk of hemorrhagic transformation, and only a minority of patients benefit from the treatments timely. Therefore, exploring new drugs or therapies is necessary to prolong the therapeutic window and improve patient outcomes.

In ischemic stroke, the obstruction of brain blood vessels deprives the essential nutrients and oxygen to brain cells, causing a sudden onset of neurological deficit. The ischemic insult may lead to irreversible damage or death to neurons in the ischemic core, while the neurons in the penumbral area surrounding the ischemic core may be salvageable with effective brain-protective treatments. Ischemic stroke involves a variety of mechanisms, such as excitotoxicity, mitochondrial dysfunction, oxidative stress, inflammation, autophagy, and blood-brain barrier (BBB) damage (George and Steinberg, 2015; Chamorro et al., 2016; Wang P. et al., 2018). Mitochondrial dysfunction occurs within minutes of ischemic stroke, resulting in depletion of adenosine triphosphate (ATP) and membrane depolarization, followed by sustained glutamate release and intracellular Ca^{2+} overload. The increased intracellular calcium leads to the overproduction of reactive oxygen species (ROS) and activates inflammatory responses, triggering the death of damaged neurons and the leakage of BBB (Zhou et al., 2018). These pathophysiological mechanisms overlap and correlate with the development of ischemic stroke and are potential pharmacological targets for treating ischemic stroke.

As a traditional herbal medicine, Panax ginseng has been widely used in treating and preventing diseases for thousands of years in East Asian countries, especially in China, Korea, and Japan. The botanical name "Panax" implies "all-healing" in Greek, which stemmed from the traditional belief that ginseng has healing properties in all aspects of the body (Kim, 2018). Among the eleven ginseng species, Panax ginseng (Asian or Korean ginseng), Panax quinquefolius (North American ginseng), and Panax notoginseng are three particularly important for medicinal use (Wang et al., 2020). Panax ginseng contains various pharmacological components, such as ginsenosides, polysaccharides, and polyphenols (Zheng et al., 2017). Ginsenosides are considered the main active ingredients of Panax ginseng, Panax quinquefolius, and Panax notoginseng for the pharmaceutical functions, which are mainly accumulated in roots, stems, leaves, flowers buds, and berries (Kim et al., 2018). About 200 ginsenosides have been identified from ginseng, including major ginsenosides (Rd, Rb1, Rb2, Rc, Re, Rg1, etc.) and minor ginsenosides (Rh1, Rh2, Rg3, Rg5, etc.) (Hyun et al., 2022). According to the chemical structures, ginsenosides can be divided into protopanaxadiol (PPD), protopanaxatriol (PPT), and oleanolic acid. PPD mainly includes ginsenosides Rd, Rb1, Rb2, Rb3, Rg3, Rg5, Rh2, F2, and compound K. PPT includes the ginsenosides Rg1, Rg2, Re, Rf, Rh1, and F1, while the typical representative ginsenoside of the oleanolic acid is ginsenoside Ro (Lu et al., 2022). As a natural product, ginseng has a wide range of pharmacological effects, such as anti-oxidative and anti-cancer, enhancing immunity, energy, and sexuality, and combating neurological diseases, diabetes mellitus, and cardiovascular diseases (Ratan et al., 2021). Currently, growing evidence shows that ginsenosides have neuroprotective effects *in vivo* and *in vitro* and have excellent potential as novel candidate agents for ischemic stroke. It can be used to treat ischemic stroke *via* reducing neurotoxicity (Zhang C. et al., 2020), anti-oxidant (Chu et al., 2019), anti-inflammation (Zhu et al., 2012), anti-apoptosis (Li et al., 2010), anti-autophagy (Huang et al., 2020), regulating blood-brain barrier permeability (Zhang X. et al., 2020), promoting angiogenesis (Chen J. et al., 2019) and neurogenesis (Gao et al., 2010) to alleviate nerve damage and promote nerve repair.

This article reviews the literature on treating ischemic stroke with ginsenosides, including preclinical and clinical experimental studies. Studies of ginsenosides in treating cerebral ischemia published until March 2022 were identified from the PubMed database. We summarized the pathophysiologies of cerebral ischemia stroke and the potential mechanisms of ginsenosides in treating ischemic stroke. Our work brings a current understanding of the mechanisms of ginsenosides in the treatment of ischemic stroke.

PATHOPHYSIOLOGIES OF ISCHEMIC STROKE

Excitotoxicity

Excitotoxicity is one of the significant events in cerebral ischemia, playing a key role in neuronal death (Rothman and Olney, 1986). After cerebral ischemia, rapid and massive release and uptake inhibition of the excitatory amino acid glutamate leads to energy failure (Chamorro et al., 2016). The function of ion pumps is required with ATP to transform the sodium (Na^+), potassium (K^+), and Ca^{2+} between intracellular and extracellular. With ATP depletion, the Ca^{2+} cannot be pumped out of neuron cells and causes glutamate release (Luoma et al., 2011). Postsynaptic receptors of glutamate include ionotropic receptors or metabotropic receptors (mGluRs), the ionotropic type receptor, NMDA (N-methyl-D-aspartate) receptor, which primarily regulates the excitotoxic response (Kaplan-Arabaci et al., 2022). Overactivation of glutamate receptors leads to the opening of receptor-gated calcium channels and Ca^{2+} influx, and the increase of intracellular Ca^{2+} causes a series of pathological reactions in the cytoplasm and nucleus (Lai et al., 2014). Moreover, Ca^{2+} overload in mitochondrial activates the downstream apoptotic pathway, inducing mitochondrial destruction and cell apoptosis (Szydlowska and Tymianski, 2010). Astrocyte glutamate transporter excitatory amino-acid transporter 2 (EAAT2 or GLT-1) is the primary glutamate transporter in the brain, playing a pivotal role in sustaining glutamate homeostasis (Tzingounis and Wadiche, 2007). Therefore, regulating the excitatory neurotransmitter glutamate and Ca^{2+} influx significantly reduces the excitotoxicity after cerebral ischemia.

Inflammation

Inflammatory response plays a crucial role in ischemic stroke pathogenesis, which contributes to all the stages of ischemic stroke (Drieu et al., 2018). Inflammatory response at the

blood-endothelial interface, including adhesion molecules, cytokines, chemokines, and leukocytes, is an essential cerebral infarction tissue injury mechanism (Zhu et al., 2022). Astrocytes and microglia are the primary cells in the brain that mediate inflammatory responses in response to ischemic brain injury (Mo et al., 2020). Astrocyte hypertrophy and proliferation are extensive responses to neuronal injury. Stroke-induced brain injury activates microglia polarization into pro-inflammatory, classical (M1) or anti-inflammatory, alternative (M2) phenotypes (Song et al., 2019). M1 microglia produce large amounts of pro-inflammatory mediators, such as tumor necrosis factor α (TNFα), interleukin (IL)-1β, IL-6, interferon-γ (IFN-γ), inducible nitric oxide synthase (iNOS), and proteolytic enzymes (Yenari et al., 2010). While M2 microglia is characterized by the effects of pro-angiogenic and anti-inflammatory, producing IL-4, IL-10, transforming growth factor β (TGF-β), and vascular endothelial growth factor (VEGF) (Qin et al., 2019). Inflammation after cerebral ischemia with contrasting effects, as it can promote nerve repair as well as aggravate secondary brain damage. Toll-like receptors (TLRs), nuclear factor-kappa B (NF-κB), and mitogen-activated protein kinases (MAPK) signaling pathways are related to the activation of inflammation in ischemic stroke (Mo et al., 2020). TLRs are transmembrane proteins expressed in microglia, astrocytes, neurons, and cerebral endothelium (Marsh et al., 2009), which can induce inflammatory responses by regulating cytokine and chemokine production. NF-κB participates in transcriptional induction of pro-inflammatory genes, such as cell adhesion molecules, cytokines, matrix metalloproteinases (MMP), and growth factors. p38 MAPK plays a vital role in inflammation-mediated ischemic injury (Sun and Nan, 2016). In addition, the NOD-like receptor (NLR) family, pyrin domain containing 3(NLRP3) inflammasome can detect tissue damage and pathogen invasion through innate immune cell sensor components commonly known as pattern recognition receptors (PRRs). PRRs promote activation NF-κB and MAPK pathways, thus increasing the transcription of protein-coding genes associated with NLRP3 (Xu et al., 2021).

Oxidative Stress

Oxidative and nitrosative stress present a challenge to ischemic stroke, which is caused by the excessive production of reactive oxygen species (ROS) and reactive nitrogen species (RNS) (Allen and Bayraktutan, 2009). Excessive ROS can result in lipid peroxidation and damage proteins and DNA, initiating a cascade of deleterious cellular processes that promote cell death. It often results from ROS/RNS production and antioxidant systems imbalance. Under physiological conditions, ROS and RNS can be scavenged by endogenous antioxidant enzymes or non-enzyme, including superoxide dismutase (SOD), catalase (CAT), glutathione peroxidase (GPX), glutathione-S-transferase (GST), and glutathione (GSH) (Tang D. et al., 2019). After cerebral ischemia, ROS and RNS have been shown in phagocytes, vascular cells, and glial cells in the penumbra. ROS is composed of superoxide anions (O_2^-), hydrogen peroxide, hydroxyl radical, and hydroperoxyl radicals, a by-product of oxygen metabolism in mitochondria. RNS mainly includes nitric oxide (NO) and peroxynitrite anion ($ONOO^-$), while $ONOO^-$ is formed by the rapid reaction of NO and O_2^- (He et al., 2021). Nuclear factor erythroid 2-related factor (Nrf2) is a transcription factor that regulates the expression of endogenous antioxidant enzymes, and Nrf2/ARE is an important endogenous anti-oxidative stress signaling pathway (Wu et al., 2020). Actively protecting mitochondrial function, antioxidation, free radical scavenging, and slowing down oxidative stress have become effective strategies in saving neurons from the pathological processes of cerebral ischemia-reperfusion. Anti-oxidative stress, scavenging free radicals, and protecting mitochondrial function have become effective strategies to save neurons from the pathological process of ischemic injury.

Apoptosis/Pyroptosis/Ferroptosis

Multiple cell death pathways are implicated in the pathogenesis of ischemic stroke (Tuo et al., 2022). Apoptosis is a typical form of programmed or regulated cell death. Recent studies have revealed novel programmed or regulated cell death types, including pyroptosis and ferroptosis (Galluzzi et al., 2018).

Apoptosis can be triggered through either the intrinsic or the extrinsic pathway. The initial morphological changes in apoptosis have been observed in post-ischemic stroke neurons, which involve cell shrinkage and cytoplasmatic condensation, nuclear membrane breakdown, and formation of apoptotic bodies (Linnik et al., 1993). The intrinsic signaling cascade of apoptosis can be mediated by calpain, ROS, and DNA damage. Excessive accumulation of Ca^{2+} and ROS in intracellular triggers activation of calpains and one of the substrates-B-cell leukemia/lymphoma 2 (Bcl-2). Bcl-2 is an anti-apoptotic protein that could interact with Bax on the mitochondrial membrane, causing a release of various proapoptotic factors, including cytochrome C (Cytc) and apoptosis-inducing factor (AIF) (Chao and Korsmeyer, 1998). Cystic complexes form an apoptosome with apoptotic protein-activating factor-1 and procaspase-9, activating caspase-3 and initiating cell death (Wang et al., 2019). ROS can damage the plasma membrane and DNA; DNA damage activates the nuclear pathway of cell death through the phosphorylation of p53 or translocation of nucleophosmin (Culmsee and Krieglstein, 2007). The extrinsic apoptosis pathway is triggered by the extracellular death ligands (TRAIL, FasL, TNF-α) that bind to death receptors (TRAILR, Fas, TNFR1) and Fas-associated death domain (FADD), creating a death-inducing signaling complex with procaspase-8. Activated caspase-8 activates downstream effector caspases (such as caspase-3) by direct proteolytic cleavage (Muhammad et al., 2018; Tuo et al., 2022).

Pyroptosis is an inflammatory form of programmed cell death that inflammasome activation can cause. The inflammasome is a protein complex that can be activated by infection, metabolic imbalances, and tissue injury (Broz and Dixit, 2016). Several inflammasome sensor proteins have been identified, including the NLRP1, NLRP3, NLRP4, and absent in melanoma 2 (AIM2), which trigger the downstream inflammatory response (Fann et al., 2013a). Inflammasomes, including canonical and noncanonical types, canonical inflammasomes like the NLRP3

activate caspase-1, whereas noncanonical inflammasomes activate mouse caspase-11 or human caspase-4 and caspase-5 (Hu J. J. et al., 2020). Gasdermin D (GSDMD) is the key effector of pyroptosis, downstream of inflammasome pathways, and a substrate for inflammatory caspases-1,4, 5, and 11 (Liu Z. et al., 2019). Caspase-1 or caspase-11 can cleave GSDMD into an N-terminal fragment (GSDMD-N) and C-terminal product (GSDMD-C) (Shi et al., 2015). Once caspase-1 is activated, pro-IL-1β and pro-IL18 can be divided into biologically active, mature, pro-inflammatory cytokines released into the extracellular environment, causing neuronal cell toxicity (Tuo et al., 2022). Inhibition or knockout of caspase-1 is neuroprotective in focal stroke models (Fann et al., 2013b).

Ferroptosis is an iron-dependent form of regulated cell death (Dixon et al., 2012), with iron accumulation and lipid peroxidation. Excessive intracellular iron accumulation elevates ROS by Fenton reaction, leading to ferroptosis cell death by irresistible lipid peroxidation. Studies have shown that iron deposition, lipid peroxidation, and neuronal death in the brain were significantly increased in an adult rat model of ischemic stroke (Kondo et al., 1997; Park U. J. et al., 2011). Glutathione peroxidase 4 (GPX4) plays an important role in suppressing ferroptosis, which functions to reduce lipid peroxides in cellular membranes. GPX4 uses GSH to eliminate the production of phospholipid hydroperoxides (PLOOH), the primary mediator of chain reactions in lipoxygenases (Tang D. L. et al., 2019). GSH is the most abundant antioxidant in the cell, synthesized from glutamate, cysteine, and glycine, among which cysteine is the rate-limiting precursor (Lee et al., 2020). The intracellular cysteine level mainly depends on extracellular cystine uptake by system Xc^- (Koppula et al., 2018), which consists of a regulatory subunit solute carrier family 3 member 2 (SLC3A2) and a catalytic subunit solute carrier family 7 member 11 (SLC7A11). Correspondingly, the inactivation of GPX4 or SLC7A11 induces ferroptosis. The levels of GPx4 and SLC7A11 were found to be decreased in MCAO rats compared with those in the sham group (Lan et al., 2020).

Autophagy

Autophagy-dependent death, known as type 2 programmed cell death (Shen et al., 2013), plays a vital role in maintaining cellular homeostasis after cerebral ischemia. Ischemia and hypoxia cause cell dysfunction of energy metabolism, leading to the destruction of the cytoskeleton and loss of homeostasis (Mo et al., 2020). Autophagy is initiated by nucleating a double membrane, which elongates into an autophagosomal vesicle that encapsulates damaged macromolecules and organelles (Klionsky et al., 2016). A cascade of autophagy-related proteins (ATGs) plays critical roles in autophagic membrane dynamics and processes (Liu and Levine, 2015). LC3-II is a biological marker of autophagosome formation localized to the autophagosome membrane. Mammalian target of rapamycin (mTOR) is one of the critical targets for autophagy regulation, a serine/threonine-protein kinase that belongs to the phosphatidylinositol 3-kinase (PI3K) related kinase family (Glick et al., 2010). Typical autophagy is triggered through a core pre-activation complex composed of ULK1/2, ATG13, and FIP200 proteins. AMPK is a central regulator of metabolism and autophagy and can phosphorylate ULK1 to activate autophagy (Jia et al., 2020), a potential therapeutic target for ischemic stroke (Jiang et al., 2018). In moderate hypoxia, hypoxia-inducible factor-1α (HIF-1α) regulates autophagy through upregulating expression of Bcl-2 and 19-kDa interacting protein 3 (BNIP3), while BNIP3 mediates autophagy by disrupting the interaction of Beclin-1 with Bcl-2 (Matsui et al., 2008). A report showed that knockdown of Beclin-1 can prevent secondary neurodegenerative damage after focal cerebral infarction by inhibiting autophagy activation (Xing et al., 2012).

Others

Cerebral ischemia initiates a complex cascade of pathophysiological events. In addition to the pathophysiologic reviewed above, BBB permeability, angiogenesis, and neurogenesis are crucial mechanisms for cerebral ischemia and reperfusion. The BBB is a cellular barrier composed of tight junctions between vascular endothelial cells interfaced with pericytes and astrocytes (Singh et al., 2016), which protects the central nervous system (CNS) by regulating the transport of substances between the blood and brain. Inflammatory cytokines, such as TNF-α and IL-1β, can increase the permeability of BBB to entrance into the CNS (Smith et al., 2016). The increased biphasic permeability of BBB leads to cerebral angiogenic edema, hemorrhage, and mortality during ischemic stroke-reperfusion (Knowland et al., 2014). Angiogenesis involves sprouting new vessels from existing vessels, predominantly induced by vascular endothelial growth factor (VEGF) (Ferrara and Adamis, 2016). It is critical to repair tissue regeneration under wound healing, hypoxia, and chronic ischemia (Fan et al., 2018). Under hypoxic conditions, HIF-1α plays a crucial role in pathophysiological angiogenesis by directly regulating VEGF, and HIF-1α/VEGF may be an important pathway for the regulation of angiogenesis (Hu Q. et al., 2020). Neurogenesis is a complex process that generates new functional neurons and glial cells from neural stem cells (NSCs), mainly in the subventricular zone (SVZ) and the subgranular zone of the dentate gyrus (DG) of the hippocampus, involving proliferation, differentiation, migration, and maturation (Nada et al., 2014). Accumulative evidence supports that newborn neurons have critical physiological functions in neuroplasticity, learning and memory, and emotion regulation (Berg et al., 2019). After cerebral ischemia, the increased expression of brain-derived neurotrophic factor (BDNF), platelet-derived growth factor-B (PDGF-B), transforming growth factor-beta (TGF-β), fibroblast growth factor 2 (FGF2), and VEGF, may promote both angiogenesis and axonal outgrowth (Hatakeyama et al., 2020). Therefore, activation of endogenous neurogenesis plays a vital role in promoting neurological function recovery.

NEUROPROTECTIVE EFFECTS OF GINSENG AND GINSENOSIDES IN ISCHEMIC STROKE

Ginseng, the root of Panax ginseng, has been widely used to treat cerebrovascular diseases in Asian countries. Ginsenosides are the major bioactive components of ginseng, responsible for its

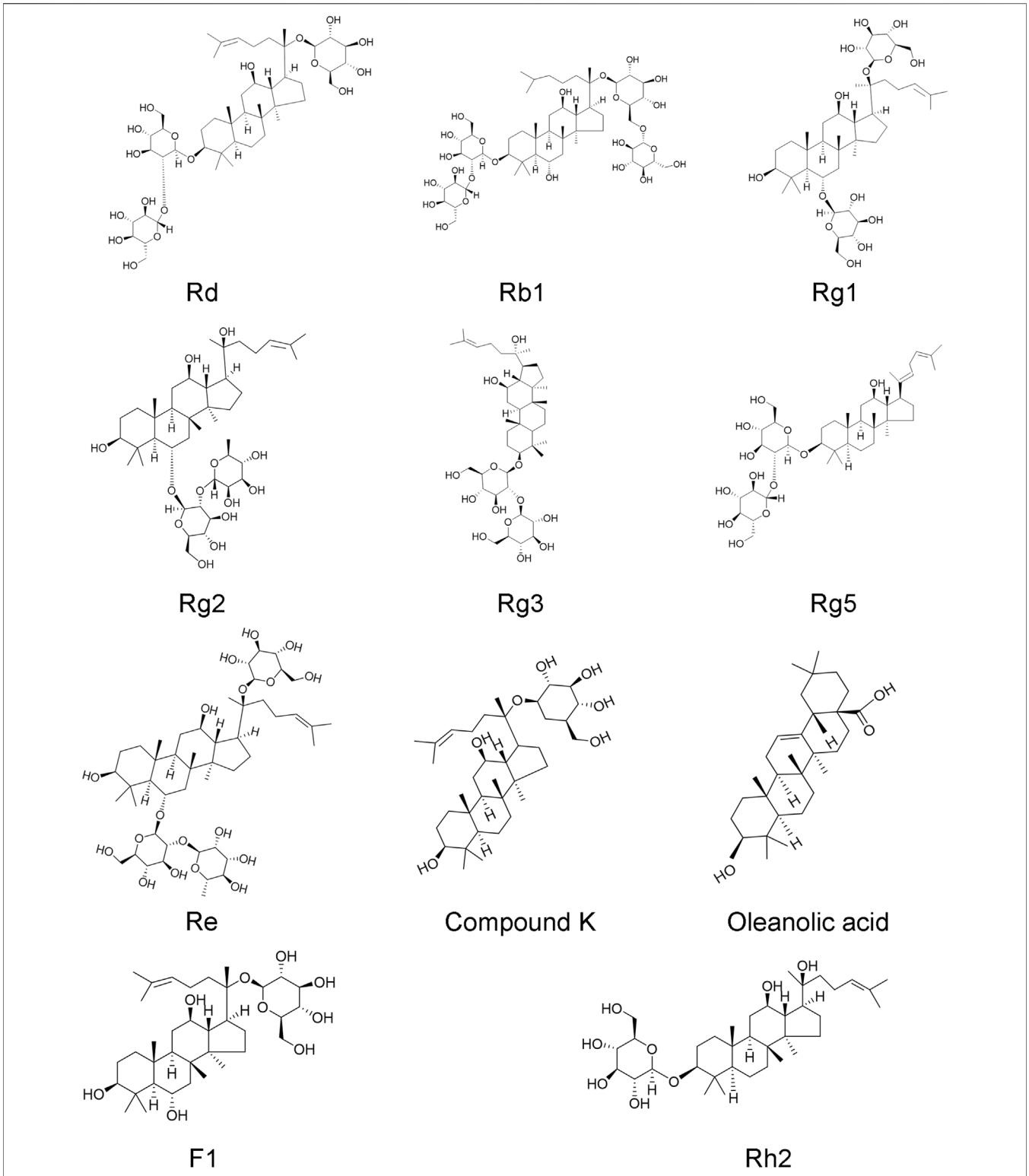

FIGURE 1 | Chemical structures of ginsenoside Rd, Rb1, Rg1, Rg2, Rg3, Rg5, Re, Rh2, F1, compound K, and oleanolic acid.

pharmacological activities (Kim et al., 2020). Now, accumulated studies show that ginseng and ginsenosides have many positive effects on treating and preventing cerebral ischemic stroke. Ginsenosides with neuroprotective effects mainly include ginsenoside Rb1 (Liu A. et al., 2018), ginsenoside Rd (Zhang X. et al., 2020), ginsenoside Re (Chen et al., 2008), ginsenoside

TABLE 1 | Summary of effects and mechanisms of ginseng and ginsenosides *in vitro* and *in vivo* models.

Gensing and gensinosides	Content of ginsenosides in panax ginseng	Animals/Cells and Dosage	Model	Mechanisms	Effects	References
KRG		C57BL/6 mice, 100 mg/kg	HI	Nrf2↑ AQP4↓	Antioxidant	Liu et al. (2020)
KRG		C57BL/6 mice, 100 mg/kg	HI	NQO1, HO1, SOD2, Gpx1, IL-10↑ IL-1β, iNOS↓	Antioxidant, anti-inflammation	Liu et al. (2019b)
KRG		C57BL/6 mice, 100 mg/kg	pdMCAO	Nrf2↑ AQP4↓	Oxidative stress, inflammation, improve long-term recovery	Liu et al. (2019a)
KRG		C57BL/6 mice, 100 mg/kg	pdMCAO	NQO1, HO1, SOD2, Gpx1↑ Nrf2 pathway	Antioxidant, attenuate acute sensorimotor deficits, improve long-term functional recovery	Liu et al. (2018b)
RGE		C57BL/6 mice, 360 mg/kg	MCAO	ASK1, ROS, TUNEL↓	Oxidative stress, apoptosis	Cheon et al. (2013)
KRG		SD rats, 100 mg/kg	MCAO/R	MDA↑ GPx, SOD, CAT↓	Antioxidant	Ban et al. (2012)
BG		SD rats, 100 or 400 mg/kg	MCAO	Cholinergic immunoreactivity, NADPH-d↑	Improve learning and memory	Park et al. (2011a)
KRG		SD rats, 100 mg/kg	tMCAO	TNF-α, IL-1β, IL-6↓	Inflammation	Lee et al. (2011)
PGE		Wistar rats, 200 mg/kg	TGCI	SOD, GPx↑ MDA↓	Antioxidant	Kim et al. (2009)
KGT		Swiss albino rat, 350 mg/kg	MCAO	GSH, GR, CAT, GST, GPx, SOD↑ LPO↓	Antioxidant	Shah et al. (2005)
GTS		Wistar rats, 25 mg/kg	MCAO	BrdU+/NeuN+↑	Neurogenesis	Zheng et al. (2011)
Rd	0.07 ± 0.03%Park et al. (2013) 0.07–0.19%Chen et al. (2019b)	C57BL/6 mice, 10, 20, 40 mg/kg Cortical neuron, 5, 10, 20 μM	MCAO/R OGD/R	miR-139-5p, Nrf2↑ NLRP3, ASC, Caspase 1 p20, and GSDMD-N, FoxO1, Keap1, ROS, TXNIP↓ miR-139-5p/FoxO1/Keap1/Nrf2 axis	Pyroptosis	Yao et al. (2022)
Rd		SD rats, 30 mg/kg	MCAO	NF-κB, MMP-9↓ NF-κB/MMP-9 pathway	BBB inflammation	Zhang et al. (2020b)
Rd		SD rats, 10 mg/kg Cortical neurons, 0 μM, 3 μM, 10 μM, 100 μM	MCAO OGD	P-NR2b at Ser-1303, calcineurin↓	Excitotoxicity	Zhang et al. (2020a)
Rd		C57BL/6 J mice, 10 or 30 mg/kg Neuronal Cell, 0.1, 1.0, and 10 μM	CCH OGD/R	BDNF↑ caspase-3, Ac-H3, HDAC2↓	Epigenetic modulation apoptosis	Wan et al. (2017)
Rd		SD rats, 50 mg/kg Cortical neurons, 10 μM	MCAO OGD	NR2B, P- Ser-1303, P-Tyr-1472, P- Ser-1480↓	Neuroprotection	Xie et al. (2016)
Rd		SD rats, 10 mg/kg BV2 cells, 10 μM	MCAO OGD	IL-1α, IL-1β, IL-6, IL-10, IL-18, TNF-α, IFN-γ, IκBα, p65, NF-κB↓	Inflammation	Zhang et al. (2016)
Rd		SD rats, 30 mg/kg	MCAO	NEIL1, NEIL3 ↑ mtDNA and nDNA damages, caspase-3, TUNEL↓	Attenuate DNA damage, apoptosis	Yang et al. (2016)
Rd		PC12 cells, 0.1, 1, 10, 50 or 100 μm		GAP-43, ERK1/2, AKT↑ MAPK/ERK and PI3K/AKT pathways	Neurite outgrowth, neuronal repair	Wu et al. (2016a)
Rd		SD rats, 1, 2.5, and 5 mg/kg PC12 cells, 25, 50, and 100 μmol/L	MCAO OGD	BrdU/DCX, Nestin/GFAP, VEGF, BDNF, pAkt, pERK↑ PI3K/Akt and ERK1/2 pathways	Neurogenesis	Liu et al. (2015)
Rd		SD rats, 30 and 10 mg/kg Neuron cells, 10 μM	MCAO OGD	PKB/AKT↑ ptau, GSK-3β↓ PI3K/AKT/GSK-3β pathway	Attenuates tau protein, reduce sequential cognition impairment	Zhang et al. (2014)
Rd		SD rats, 30 mg/kg Astrocytes, 10 and 50 μM	MCAO OGD	GLT-1, p-PKB/Akt, p-ERK1/2↑ glutamate↓	Glutamate clearance	Zhang et al. (2013)
Rd		SD rats, 10 mg/kg	MCAO	NF-κB p65, PARP-1 ↓	Inflammation, apoptosis	Hu et al. (2013)
Rd		Hippocampal neurons, 0.1, 1, 10 μM	Glutamate-induced	Ca^{2+} Influx, TUNEL and caspase-3↓	Ca^{2+} Influx	Zhang et al. (2012a)
Rd		SD rats, 10 mg/kg	MCAO	ASIC2a↑ TRPM7, ASIC1a↓	Ca^{2+} Influx	Zhang et al. (2012b)
Rd		SD rats, 50 mg/kg	MCAO	ROS, CytoC, AIF↓	Mitochondrial protection, energy restoration, inhibition of apoptosis	Ye et al. (2011d)
Rd		SD rats, 0.1–200 mg/kg	MCAO	iNOS and COX-2↓	Oxidative, inflammatory	Ye et al. (2011c)
Rd		SD rats, 10–50 mg/kg	MCAO	BBB permeability↑	Wider therapeutic window	Ye et al. (2011a)
Rd		C57BL/6 mice, 10–50 mg/kg	MCAO	CAT, SOD2, GPX, GST, GSH/GSSG, complexes I-IV↑ ROS↓	Redox imbalance, oxidative damage, mitochondrial function	Ye et al. (2011b)
Rd		Cortical neurons, 1, 3, 10, 30 and 60 μM	Glutamate-induced	caspase 3, Ca^{2+} influx↓	Apoptosis	Li et al. (2010)
Rd		Hippocampal neurons, 0.1–10 μM	OGD	GPX, SOD, CAT↑ MDA, GSH, GSSG, ROS↓	Oxidative stress	Ye et al. (2009)

(Continued on following page)

TABLE 1 | (*Continued*) Summary of effects and mechanisms of ginseng and ginsenosides *in vitro* and *in vivo* models.

Gensing and gensinosides	Content of ginsenosides in panax ginseng	Animals/Cells and Dosage	Model	Mechanisms	Effects	References
Rb1	0.11 ± 0.02%Park et al. (2013) 0.29–2.0%Chen et al. (2019b)	C57BL/6 mic, 50 mg/kg	dMCAO	GAP43, BDA, cAMP, PKA, pCREB↑ cAMP/PKA/CREB Pathway	Axonal regeneration, motor functional recovery	Gao et al. (2020b)
Rb1, Rg1		Astrocyte cultures Rb1, 2, 5, 10 μM Rg1, 2, 5, 10 μM	OGD/R	CAT, complexes I-V, ATP↑ ROS↓	Mitochondrial oxidative	Xu et al. (2019)
Rb1, Rh2, Rg1, Rg3, Rg5, Re		PC12 cells Rb1, 50 μg/ml Rh2, 0.5 μg/ml Rg1, 5 μg/ml Rg3, 20 μg/ml Rg5, 100 μg/ml Re, 5 μg/ml	$CoCl_2$-induced	ROS, TLR4, MyD88, SIRT1, P65, IL-1β, TNF-α, IL-6↓	Apoptosis, mitochondrial membrane potential, inflammation	Cheng et al. (2019)
Rb1		SD rats, 50 or 100 mg/kg SH-SY5Y cells, 10 μmol/L	Microperfusion of Glu and $CaCl_2$ OGD/R	P-Akt, P-mTOR↑ P-PTEN↓P-AKT/ P-mTOR pathway	Neuroprotection, microenvironment	Guo et al. (2018)
Rb1		Wistar rats, 50, 10, 200 mg/kg	MCAO	caspase-3, caspase-9, HMGB1, NF-κB, TNF-α, IL-6, NO↓	Apoptosis, inflammation	Liu et al. (2018a)
Rb1		C57BL/6 J mice, 0.5, 1, 5 or 10 mg/kg	MCAO	GSH↑ MDA, NO, ROS, NOX-1, NOX-4, NADPH, pERK1/2↓	Antioxidant	Dong et al. (2017)
Rb1		ICR mice, 5, 20 or 40 mg/kg	MCAO	MMP-9, NOX-4 ↓	BBB	Chen et al. (2015)
Rb1		Microglial cell, 100 μg/ml	H_2O_2-induced	TNF-α, NO, O2-↓	Apoptosis	Ke et al. (2014)
Rb1		SH-SY5Y cells, 1.0, 10 and 100 μM	OGD	p-Akt↑ LC3II, Beclin1 ↓ PI3K/Akt Pathway	Aautophagy	Luo et al. (2014)
Rb1		SD rats, 100 mg/kg	MCAO	BDNF, GAP-43, NF↑ IL-1, TNF-α↓	Neuroprotection	Jiang et al. (2013)
Rb1		SD rats, 12.5 mg/kg	MCAO	NF-κB/p65, IKK-α, IκB-α, TNF-α, IL-6↓	Inflammation	Zhu et al. (2012)
Rb1		SD rats, 12.5 mg/kg	MCAO	LC3, Beclin 1↓	Autophagy	Lu et al. (2011)
Rb1		Wistar rats, 40 mg/kg	MCAO	BDNF↑ caspase-3↓	Neurogenesis	Gao et al. (2010)
Rb1		Cynomolgus monkeys, 300 μg/kg	TSM	NeuN↑ TUNEL, GFAP↓	Neuroprotection	Yoshikawa et al. (2008)
Rb1		SHR-SP rats, 20 μg/kg	MCAO	VEGF, Bcl-xL↑	Neuroprotection	Sakanaka et al. (2007)
Rb1		Wistar rats, 40 mg/kg	MCAO	GDNF, Bcl-2↑ bax↓	Apoptotic	Yuan et al. (2007)
Rb1		SHR-SP rats, 20 μg/kg	MCAO	Bcl-xL↑	Apoptotic	Zhang et al. (2006)
Rb1		SHR-SP rats, 20 μg/kg	MCAO	Infarcted area↓ scavenging free radicals	neuroprotection	Zhang et al. (1998)
Rb1		Mongolian gerbils, 80 μg/kg	TFI	Hippocampal blood flow↑ scavenging free radicals	neuroprotection	Lim et al. (1997)
Rg1	0.27 ± 0.04%Park et al. (2013) 0.32–1.55%Chen et al. (2019b)	SD rats, 40 mg/kg	MCAO	Bcl2 ↑ Bax, TUNEL, p-PERK, p-eIF2, ATF4↓ PERK-eIF2-α-ATF4 signaling pathway	ER, apoptosis	Gu et al. (2020)
Rg1		SD rats, 50 mg/kg	MCAO	Glycolysis or gluconeogenesis, amino acid metabolism, lipid metabolism↓	Energy metabolism, amino acids metabolism, lipids metabolism	Gao et al. (2020a)
Rg1		SD rats, 20 mg/kg PC12 cells, 0.01–1 μmol/L	tMCAO OGD/R	Nrf2, ARE, HO-1, NQO-1, GCLC, GCLM↑ miR-144 ↓ miR-144/Nrf2/ARE pathway	Oxidative stress	Chu et al. (2019)
Rg1		SD rats, 10, 20, or 40 mg/kg	MCAO	p-IκBα, P65, IL-6, IL-1β, TNF-α, IFN-γ↓	Inflammation	Zheng et al. (2019)
Rg1		C57BL/6 mice,10, 20 or 40 mg/kg hCMEC/D3 cells,0.1–1,000 μM	dMCAO OGD	BrdU+/CD31+, BrdU+/GFAP+, VEGF, HIF-1α, p-Akt, p-mTOR↑ PI3K/Akt/mTOR signaling pathway	Angiogenesis	Chen et al. (2019a)
Rg1		C57BL/6 mice, 20, 40 mg/kg	MCAO	BDNF↑ IL-1β, TNF-α, IL-6, Glu, Asp↓	Neuroprotection	Wang et al. (2018b)
Rg1		SD rats, 6 mg/kg BV2, 8 μg/ml	MCAO OGD	miR-155-5p↓	Neuroprotection	Wang et al. (2018a)
Rg1		SD rats, 30 or 60 mg/kg Cortical neurons, 30 or 60 μM	MCAO OGD	SOD, CAT, PPARγ↑ MPO, TNF-α, IL-6↓	Antioxidative, anti-Inflammatory	Li et al. (2017a)
Rg1		NSCs, 0.01–50 μM	OGD	Bcl-2↑ Caspase3, Bax, p-p38, p-JNK2↓	Apoptosis	Li et al. (2017b)
Rg1		SD rats, 40 mg/kg	MCAO	PAR-1↓	BBB permeability	Xie et al. (2015)
Rg1		SD rats, 20, 40 or 60 mg/kg	MCAO	PPARγ, HO-1, bcl-2↑ caspase-3, caspase-9, IL-1β, TNF-α, HMGB1, RAGE↓	Inflammation, apoptosis	Yang et al. (2015)

(Continued on following page)

TABLE 1 | (*Continued*) Summary of effects and mechanisms of ginseng and ginsenosides *in vitro* and *in vivo* models.

Gensing and gensinosides	Content of ginsenosides in panax ginseng	Animals/Cells and Dosage	Model	Mechanisms	Effects	References
				PPARγ/Heme oxygenase-1 (HO-1) signaling		
Rg1		SD rats, 30, 60 mg/kg	MCAO	Regulate systemic metabolic	Neuroprotection	Lin et al. (2015)
Rg1		Hippocampal neurons, 5, 20, 60 mM	OGD	Calcium influx↓ nNOS↑	Neuroprotection	He et al. (2014)
Rg1		BALB/c mice, 20 or 40 mg/kg Astrocytes, 10 μM	MCAO H_2O_2-induced	mitochondrial membrane potential↑ Ca^{2+}, ROS↓	Apoptosis Ca^{2+} overload	Sun et al. (2014)
Rg1		SD rats, 20 mg/kg	MCAO	AQP4↓	BBB	Zhou et al. (2014)
Rg1		PC12 cells, 0.1–10 uM	H_2O_2- induced	Akt, ERK1/2 ↑ p-IkBα, p-IKKβ, p65↓ NF-kB pathway	Oxidative stress	Liu et al. (2011)
Rg1		SD rats, 20 mg/kg Hippocampal neurons, 110,100 uM	MCAO OGD	Ca^{2+}↓ NMDA receptors and L-type voltage-dependent Ca^{2+} channels	Neuroprotection	Zhang et al. (2008b)
Rg1		Mongolian gerbils, 5 and 10 mg/kg	MCAO	Brdu↑	Neurogenesis cell proliferation	Shen and Zhang, (2003)
Rg2	0.06 ± 0.04%Park et al. (2013) 0.01–0.09%Chen et al. (2019b)	SD rats, 2.5, 5 and 10 mg/kg	MCAO	BCL-2, P53↑ BAX, HSP70↓	Apoptosis	Zhang et al. (2008a)
Rg3	0.05 ± 0.04%Park et al. (2013) 0.001–0.003% Chen et al. (2019b)	SD rats, 20 mg/kg	MCAO/R	22 differentially expressed miRNAs 415 differentially expressed mRNAs cGMP-PKG, cAMP and MAPK signaling pathways	Neuroprotection	Zhang et al. (2022)
Rg3		SD rats, 20 mg/kg	MCAO/R	239 differentially expressed lncRNAs 538 differentially expressed mRNAs TNF, NF-κB, cytokine, and other receptor signaling pathways	Neuroprotection	Yang et al. (2022)
Rg3		SH-SY5Y cells, 1, 5, 25, 125 μmol/L	OGD/R	Bcl-2↑ Bax, cleaved caspase-3↓	Apoptosis	He et al. (2017)
Rg3		SD rats, 10 and 20 mg/kg	MCAO	calpain I, caspase-3, TUNEL↓	Neuroprotection, apoptosis	He et al. (2012)
Rg3		Mitochondria, 2–16 μM	Ca^{2+}, H2O2 induced	ATP, respiratory control ratio ↑ MPTP↓	Neuroprotection	Tian et al. (2009)
Rg3		Wistar rats, 10 and 5 mg/kg	MCAO	MDA, ATP ↑ SOD, GSH-Px ↓	Lipid peroxides, oxidative stress, energy metabolism	Tian et al. (2005)
Re	0.22 ± 0.03%Park et al. (2013) 0.44–1.2%Chen et al. (2019b)	SD rats, 5, 10 or 20 mg/kg	MCAO	MDA, H^+ -ATPase↓ decrease mitochondrial swelling	Oxidative stress	Chen et al. (2008)
Re		Wistar rats, 5, 10, 20 mg/kg	MCAO	SOD, GSH-Px↑ MDA↓	Oxidative stress	Zhou et al. (2006)
CK		PC12 cells, 2, 4, 8 μM	OGD/R	p-mTOR↑p-AMPK, p62, Atg7, Atg5, LC3II/I↓ AMPK-mTOR pathway	Autophagy, apoptosis	Huang et al. (2020)
CK		C57BL/6 mice, 30 mg/kg BV2, 25, 50, 75 μM	MCAO LPS	HO-1↑ IL-6, MCP-1, MMP-3, and MMP-9↓ ROS, MAPKs, NF-κB/AP-1, and HO-1/ARE signaling pathways	Anti-inflammation	Park et al. (2012)
OA		SD rats, 10, 20 mg/kg SH-SY5Y cells, 10, 20, and 40 μM	MCAO OGD/R	Nissl+, NeuN+↑ GSK-3β, HO-1, ROS, TUNEL ↓ GSK-3β/HO-1 pathway	Antioxidative	Lin et al. (2021)
F1		SD rats, 50 mg/kg	MCAO	MVD, IGF-1/IGF1R↑ IGF-1/IGF1R pathway	Angiogenesis, improve focal cerebral blood perfusion	Zhang et al. (2019)
Rh2	0.001–0.006% Chen et al. (2019b)	BV2, 5, 25 μM	LPS and IFN-γ-induced	IL-10↑ NO, COX-2, TNF-α, IL-1↓ AP-1 and PKA pathway	Inflammation	Bae et al. (2006)

KRG, Korean red ginseng; BG, Black ginseng; KGT, Korean ginseng tea; RGE, Red Ginseng Extract; PGE, Panax ginseng extract; GTS, Ginseng total saponins; GTS, Ginseng total saponins; CK, Compound K; OA, Oleanolic acid; HI, Hypoxia-Ischemia; pdMCAO, permanent distal middle cerebral artery occlusion; tMCAO, transient middle cerebral artery occlusion; MCAO/R, middle cerebral artery occlusion/reperfusion; TGCI, transient global cerebral ischemia; TSM,T hromboembolic stroke model; TFI, transient forebrain ischemia; OGD/R, oxygen-glucose deprivation/reoxygenation; CCH, chronic cerebral hypoperfusion; NSCs, Neural stem cells; ASK1, apoptosis signal-regulating kinase 1; NADPH-d, nicotinamide adenine dinucleotide phosphate-diaphorase; TNF-α, tumor necrosis factor-α; IL-1β, interleukin-1 beta; MDA, malondialdehyde; SOD, superoxide dismutase; GPx, glutathione peroxidase; LPO, lipid peroxidation; GSH, glutathione; GR, glutathione reductase; CAT, catalase; GST, glutathione-S-transferase; Ac-H3, acetylated histone H3; HDAC2, histone deacetylase 2; mtDNA, mitochondrial DNA; ROS, reactive oxygen species; ATP, adenosine triphosphate; HMGB1, High-mobility group box 1; MMP-9, matrix metalloproteinase-9; NOX, nicotinamide adenine dinucleotide phosphate oxidase; HSP70, heat shock protein 70; BBB, blood–brain barrier; ER, endoplasmic reticulum stress; MPTP, mitochondrial permeability transition pore; MVD, microvessel density.

Rg1 (Zheng et al., 2019), ginsenoside Rg2 (Zhang G. et al., 2008), ginsenoside Rg3 (He et al., 2017), ginsenoside Rg5 (Cheng et al., 2019), ginsenoside Rh2 (Bae et al., 2006), ginsenoside F1 (Zhang et al., 2019), Compound K (Huang et al., 2020), Oleanolic acid (Lin et al., 2021) (**Figure 1**). Overall, the neuroprotective effects of ginseng and ginsenosides against cerebral ischemia are mediated by the regulation of excitotoxicity, Ca^{2+} overload, inflammation, mitochondria dysfunction, oxidative stress, apoptosis, pyroptosis, autophagy, BBB permeability, angiogenesis, and neurogenesis, as shown in **Table 1** and **Table 2**. The content of ginsenosides in Panax ginseng is also shown in **Table 1**.

Panax Ginseng and its Neuroprotective Effects

According to the manufacturing processing technique of ginseng, Panax ginseng can be divided into three types: white ginseng, red ginseng, and black ginseng (Hyun et al., 2022). White ginseng is produced by dehydration in the sun without cooking, and red ginseng is steamed at 90–100°C for 2–3 h. Until now, red ginseng is mainly processed in Korea, which is also named Korea red ginseng (KRG). While black ginseng is generated by steaming red ginseng nine times (Jo et al., 2009; Wan et al., 2021). The therapeutic effects of KRG on permanent and transient hypoxic-ischemic brain damage were studied in rats and mice at 100–360 mg/kg per day. In hypoxic-ischemic (HI) mice, 7 days before HI pretreated with KRG, reduced infarct volume, cerebral edema, and degeneration of hippocampal neurons were observed at 6 h, 24 h, 7 days, and 28 days after HI (Liu et al., 2019a; Liu et al., 2020). What's more, red ginseng pretreatment could also suppress apoptosis in ischemic lesions (Cheon et al., 2013). Recent studies have shown that KRG pretreatment has elicited robust and prolonged anti-oxidative and anti-inflammatory effects after hypoxia-ischemia *via* an Nrf2-dependent manner. While Nrf2-dependent endogenous neuroprotection effects attenuate sensorimotor deficits and gliosis reactive in microglia and astrocytes, they regulate dynamic glutamine synthetase (GS) and aquaporin 4 (AQP4) expressions, thus improving long-term functional recovery (Liu L. et al., 2018; Liu et al., 2019b; Liu et al., 2020). Red ginseng could play the effect of anti-oxidant by reducing the level of lipid peroxidation (Ban et al., 2012), and increasing the expression of GSH, CAT, GST, glutathione peroxidase GPx and SOD (Kim et al., 2009) (Shah et al., 2005). Meanwhile, the neuroprotection of anti-inflammation may raise IL-10 expression and reduce the levels of TNF-α, IL-1β, and IL-6 in serum (Lee et al., 2011). In addition, black ginseng is helpful for the treatment of vascular dementia *via* reduced loss of cholinergic immunoreactivity and nicotinamide adenine dinucleotide phosphate-diaphorase (NADPH-d)-positive neurons in the hippocampus (Park H. J. et al., 2011). Ginseng total saponins could increase the number of BrdU+/NeuN+ cells to induce endogenous neural stem cell activation (Zheng et al., 2011), further supporting the beneficial role of ginseng in ischemic stroke.

Ginsenoside Rd and its Neuroprotective Effect

Ginsenoside Rd is one of the major ginsenosides responsible for pharmaceutical activities and has been demonstrated to exert significant neuroprotective in preclinical and clinical studies. *In vitro* and *in vivo* studies show that ginsenoside Rd could improve neuron survival and decrease neuron apoptosis. Ginsenoside Rd modulates the balance between acetylated histone H3 (Ac-H3) and histone deacetylase [histone deacetylase 2 (HDAC2)], thus upregulating BDNF in chronic cerebral hypoperfusion (CCH) mice and OGD/R neurons (Wan et al., 2017). Ginsenoside Rd significantly inhibits glutamate-induced Ca^{2+} entry in cortical neurons and prevents cell apoptosis (Li et al., 2010). A recent study shows that ginsenoside Rd regulates cerebral ischemia/reperfusion injury by exerting an anti-pyroptotic effect through the miR-139-5p/FoxO1/Keap1/Nrf2 axis (Yao et al., 2022). What's more, ginsenoside Rd administration could enhance ischemic stroke-induced cognitive impairment and downregulate tau protein phosphorylation *via* the PI3K/AKT/GSK-3β pathway (Zhang et al., 2014). Glutamate is essential for excitatory synapse transmission; however, overstimulation of ionic glutamate receptors can trigger excessive calcium influx, leading to excitotoxicity of neurons. Ginsenoside Rd protects neurons against glutamate-induced excitotoxicity by inhibiting Ca^{2+} influx (Zhang C. et al., 2012), attenuating the expression of transient receptor potential melastatin 7 (TRPM7) and acid-sensing ion channels 1a (ASIC1a) (Zhang Y. et al., 2012), and mitigating DAPK1-mediated NR2b phosphorylation and attenuating calcineurin activity (Xie et al., 2016; Zhang C. et al., 2020). Ginsenoside Rd administration promotes glutamate clearance by upregulating the expression of glial glutamate transporter-1 (GLT-1) through PI3K/AKT and ERK1/2 pathways (Zhang et al., 2013).

Pretreatment of ginsenoside Rd plays antiapoptotic and anti-inflammatory effects in MCAO rats through inhibiting poly (ADP-ribose) polymerase-1, preventing the mitochondrial release of apoptosis-inducing factor (AIF), and reducing the accumulation of NF-κB p65 subunit nuclear (Hu et al., 2013). Another study showed that ginsenoside Rd could eliminate inflammatory injury by inhibiting the expression of iNOS and cyclooxygenase-2 (COX-2) (Ye et al., 2011c). Oxidative stress caused by ischemic stroke leads to DNA damage and triggers cell death. Ginsenoside Rd could upregulate the endogenous antioxidant system, preserve the mitochondrial respiratory chain complex and aconitase activities, downregulate mitochondrial hydrogen peroxide production, and stabilize mitochondrial membrane potential (Ye et al., 2009; Ye et al., 2011b; Yang et al., 2016). Another similar report showed that ginsenoside Rd minimizes mitochondria-mediated apoptosis following focal ischemia by reducing the mitochondrial release of cytochrome c (CytoC) and AIF. *In vitro* studies further exhibited that ginsenoside Rd could attenuate mitochondrial swelling, preserve MMP, and decrease ROS production (Ye et al., 2011d). Following ischemic stroke, impaired cell volume regulation can lead to cytotoxic cell swelling, disruption of BBB integrity, and brain edema. Ginsenoside Rd could pass through

TABLE 2 | Summary of clinical trials of ginsenosides interventions in cerebarl ischemic stroke patients.

Gensinosides	Model	Sample sizes	Inclusion criteria	Evaluaive critera	Results	References
Rd	Acute ischaemic stroke	Ginsenoside Rd group (n = 290) placebo group (n = 96)	1) 18–75 years of age; 2) had received a clinical diagnosis of primary acute ischaemic stroke and were able to receive the study drug within 72 h after the onset of symptoms; 3) had a score of 5–22 on the NIHSS	NIHSS BI	Ginsenoside Rd improved the NIHSS and mRs scores, and had an acceptable adverse event profile.	Liu et al. (2012)
Rd	Acute ischaemic stroke	Ginsenoside-Rd 10 mg (n = 65) ginsenoside-Rd 20 mg (n = 67) placebo group (n = 67)	1) between 18 and 75 years of age; 2) had a clinical diagnosis of primary acute ischaemic stroke with an onset of the first episode within the previous 72 h; 3) had a score of 5–22 on the NIHSS	NIHSS BI mRs	Ginsenoside Rd improved NIHSS scores at 15 days, no significance of BI and mRs scores at 15 and 90 days.	Liu et al. (2009)

NIHSS, national institutes of health stroke scale; mRs, modified Rankin scalel; BI, barthel index.

the intact BBB and exert neuroprotection effects in transient and permanent MCAO rat models (Ye et al., 2011a). In addition, ginsenoside Rd attenuates BBB by inhibiting proteasome activity and sequentially suppressing the NF-κB/MMP-9 pathway (Zhang X. et al., 2020). At the same time, ginsenoside Rd could promote neurogenesis *via* upregulating the expression of VEGF, BDNF, and growth-associated protein of 43 kDa (GAP-43) and activating the PI3K/Akt and ERK1/2 dependent pathways (Liu et al., 2015; Wu S. D. et al., 2016).

Two randomized, double-blind, placebo-controlled, phase II multicenter clinical trials involving 199 patients (Liu et al., 2009) and 390 patients (Liu et al., 2012) with acute ischemic stroke showed that Rd could improve patients' neurologic deficits scores at 15 or 90 days and ameliorate disability by modified Rankin Scale (mRS) score at 90 days after stroke. The therapeutic effect of ginsenoside Rd may be related to its capability to suppress microglial proteasome and secondary inflammation (Zhang et al., 2016). The studies suggested that ginsenoside Rd is a promising neuroprotectant in acute ischemic patients.

Ginsenoside Rb1 and its Neuroprotective Effects

Ginsenoside Rb1 is one of the main bioactive saponins in ginseng, which could alleviate cerebral ischemia injury *via* modulating apoptosis, autophagy, oxidative, inflammation, BBB permeability, and promoting neurogenesis (Jiang et al., 2013; Luo et al., 2014; Chen et al., 2015; Cheng et al., 2019). Apoptotic caspases further classified as initiator caspases (Caspase-8, -9, -10), and effector caspases (Caspase-3, -6, -7) based on their functions (Wu Y. et al., 2016). Ginsenoside Rb1 could inhibit apoptosis and attenuate damaged neurons by downregulation of the expression of caspase-3, caspase-9 (Liu A. et al., 2018), nitric oxide, and superoxide (Ke et al., 2014), and up-regulating the expression of the mitochondrion associated antiapoptotic factor Bcl-xL (Zhang et al., 2006). Ginsenoside Rb1 could inhibit the expression of Beclin-1 and LC3-II *via* activation of PI3K/Akt pathway (Lu et al., 2011; Luo et al., 2014). The neuroprotective effect of ginsenoside Rb1 is also related to the activation of Akt/mTOR signaling pathway and inhibition of P-PTEN protein (Guo et al., 2018).

Free radicals can be excessively produced following cerebral ischemia. Ginsenoside Rbl protects the cerebral cortex and hippocampal CA1 neurons against ischemic damage by scavenging free radicals (Lim et al., 1997; Zhang et al., 1998). Administration of Rb1 or Rg1 could improve the mitochondrial and reduce ROS production in OGD/R cultured astrocytes, with increased activity of CAT, complexes I, II, III, and V, elevated level of mtDNA and ATP, and attenuated the MMP depolarization (Xu et al., 2019). Furthermore, ginsenoside Rb1 also showed an antioxidative effect in aged mice (Dong et al., 2017). Inflammation plays an important role in the pathophysiological process after ischemic stroke, which could induce secondary brain damage (Rajkovic et al., 2018). Ginsenoside Rbl could exert anti-inflammatory effects by downregulating the expression of IL-6, and TNF-α (Zhu et al., 2012), which is associated with TLR4/MyD88 and SIRT1 signaling pathways (Cheng et al., 2019). High mobility group box1 (HMGB1) is a highly abundant non-histone DNA-binding nuclear protein and is a crucial pro-inflammatory factor in ischemic stroke. Administration of Ginsenoside Rb1 could also attenuate cerebral ischemic reperfusion-induced apoptosis and inflammation *via* inhibiting HMGB1inflammatory signals (Liu A. et al., 2018). In addition, ginsenoside Rb1 protects BBB integrity following cerebral ischemia and reduces brain edema by suppressing neuroinflammation induction of MMP-9 and NOX4-derived free radicals (Chen et al., 2015). Ginsenoside Rb1 has a positive effect on neurogenesis, probably *via* improving the expression of NeuN, BDNF, glial-derived neurotrophic factor (GDNF), and growth-associated protein 43 (GAP43), while decreasing the expression of TUNEL, caspase-3, and GFAP (Yuan et al., 2007; Yoshikawa et al., 2008) (Jiang et al., 2013) (Gao et al., 2010). Intravenous infusion of ginsenoside Rb1 prevents ischemic brain damage through upregulation of VEGF and Bcl-xL (Sakanaka et al., 2007). In addition, ginsenoside Rb1could promote functional motor recovery in post-stroke

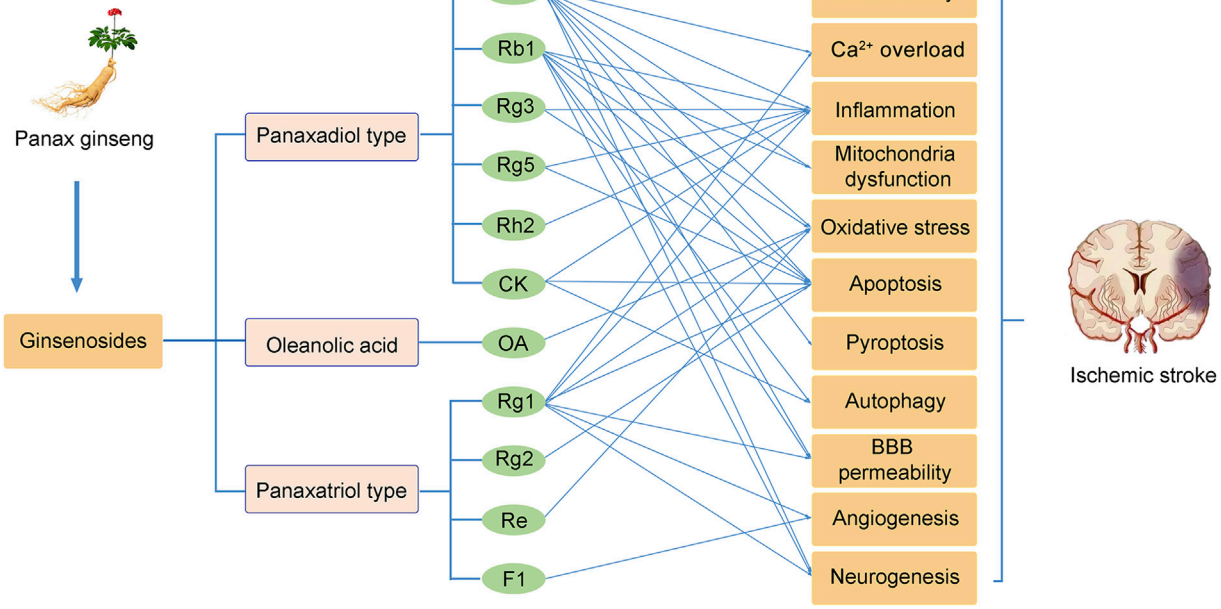

FIGURE 2 | The neuroprotective effects of ginsenosides on cerebral ischemic stroke.

mice by stimulating axonal regeneration and brain repair by regulating the cAMP/PKA/CREB pathway (Gao X. et al., 2020).

Ginsenosides Rg1, Rg2, Rg3, Rg5 and Their Neuroprotective Effects

Ginsenoside Rg, including Rg1, Rg2, Rg3, and Rg5, has been widely used in cerebral ischemic stroke with therapeutic effects of anti-apoptosis (Zhang G. et al., 2008), antioxidant (Li et al., 2017a), anti-inflammation (Zheng et al., 2019), regulating energy metabolism (Gao J. et al., 2020), and promoting angiogenesis (Chen J. et al., 2019) and neurogenesis (Shen and Zhang, 2003).

Ginsenoside Rg1 could reduce the neurological deficit scores, brain edema, and infarct volume in MCAO mice and inhibit intracellular Ca^{2+} overload and ROS production in astrocytes (Sun et al., 2014). Neuron apoptosis, inflammation, and oxidative stress are the main pathological characteristics of cerebral ischemia stroke. Ginsenoside Rg1 protects NSCs from OGD-induced cell apoptosis and oxidative stress *via* inhibiting the phosphorylation of p38/JNK2 (Li et al., 2017b), while Rg1 combined with mannitol protects neurons against apoptosis through the PERK-eIF2-α-ATF4 signaling pathway (Gu et al., 2020). PPARγ/Heme oxygenase-1 (HO-1) signaling was critical in mediating apoptosis and inflammation, while ginsenoside Rg1 could activate PPARγ/HO-1 and provide neuroprotective effects *via* modulating the expression of levels of PPARγ, Bcl-2, cleaved caspase-3, cleaved caspase-9, IL-1β, TNF-α, HMGB1 (Yang et al., 2015). Similarly, ginsenoside Rg2 and Rg3 exert a neuroprotective effect against apoptosis by decreasing the levels of Bax, and increasing the levels of Bcl-2 (He et al., 2012; He et al., 2017) [86]. Ginsenoside Rg1, Rg3, Rg5, Rb1, Rh2, and Re could reduce cerebral ischemic damage by inhibiting NF-κB transcriptional activity and the expression of pro-inflammatory cytokines (Cheng et al., 2019; Zheng et al., 2019). Administration of ginsenoside Rg1 in combination with geniposide protected against focal cerebral ischemia injury *via* microglial microRNA-155-5p inhibition (Wang J. et al., 2018). Moreover, the neuroprotection of ginsenoside Rg3 against ischemic injury is associated with multiple lncRNAs, miRNAs sand mRNAs, which mainly related to the tumor necrosis factor (TNF), NF-κB, cytokine, and cGMP-PKG, cAMP and MAPK signaling pathways (Yang et al., 2022; Zhang et al., 2022).

A previous study confirmed that ginsenoside Rg1 exerts the neuroprotective effect of antioxidant *via* downregulation of the NF-kB signaling pathway, and activation of Akt and ERK1/2 in H_2O_2-induced cell injury (Liu et al., 2011). *In vitro* and *in vivo* studies showed that Ginsenoside Rg1 significantly increased PPARγ expression and regulated the oxidative stress and inflammation after ischemic injury (Li et al., 2017a). Additionally, ginsenoside Rg1 could alleviate oxidative stress *via* inhibiting miR-144 and promoting the Nrf2/ARE pathway after ischemic/reperfusion injury (Chu et al., 2019). What's more, ginsenoside Rg1 exerts neuroprotective effects by blocking the intracellular calcium overload and decreasing the concentration of free calcium and iNOS activity after OGD exposure (He et al., 2014), the inhibition of calcium influx *via* NMDA receptors and L-type voltage-dependent Ca^{2+} channels (Zhang Y. F. et al., 2008). Metabolic changes play an important role in cerebral ischemic damage. The potential therapeutic effect of

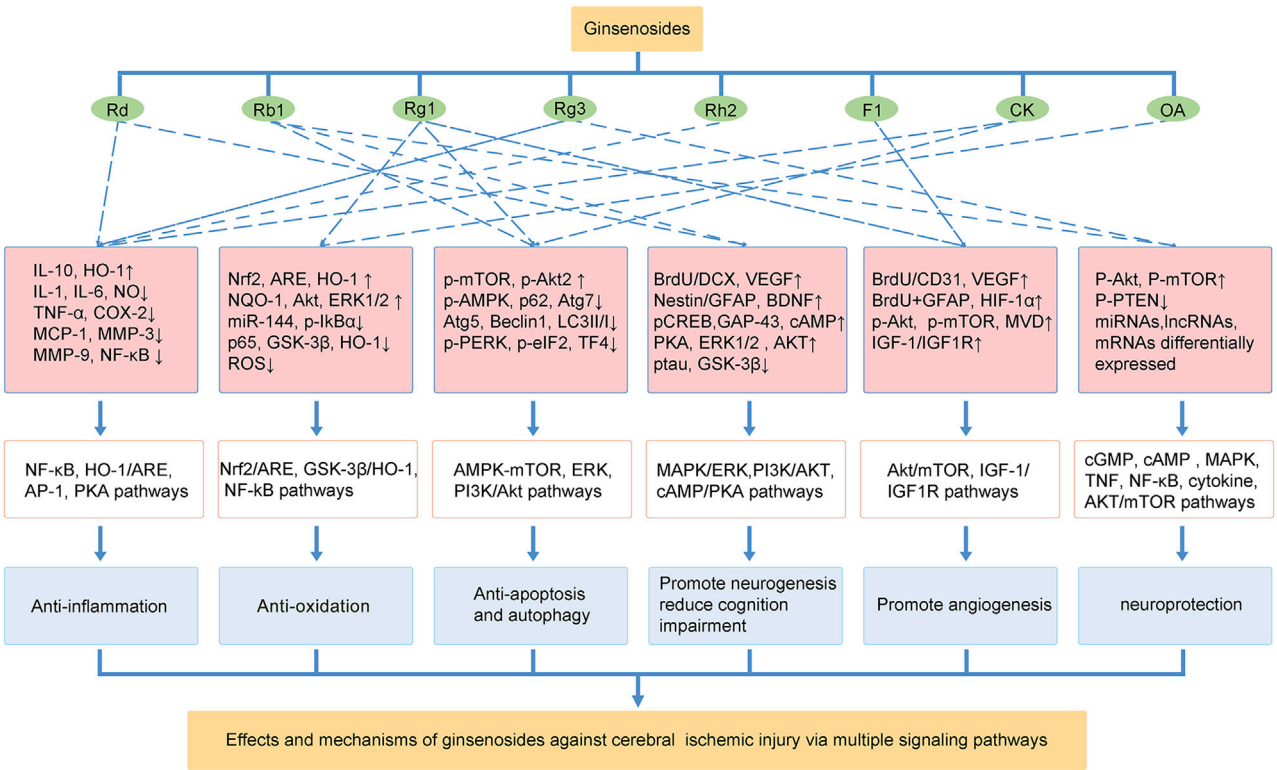

FIGURE 3 | The effects and mechanisms of ginsenosides against cerebral ischemic injury *via* multiple signaling pathways.

ginsenoside Rg1 is possible *via* suppressing the systemic metabolic changes in cerebral injury rats (Lin et al., 2015). NSCs transplantation combined with ginsenoside Rg1 could significantly improve the cerebral infarct and neurological deficits *via* intervening energy metabolism, amino acids metabolism, and lipids metabolism (Gao J. et al., 2020). Besides, ginsenoside Rg3 could decrease the activities of SOD and GSH-Px, and enhance MDA and ATP levels after cerebral ischemia, which provide neuroprotection *via* reducing lipid peroxides, scavenging free radicals, and improving mitochondrial energy metabolism (Tian et al., 2005; Tian et al., 2009).

Angiogenesis plays a crucial role in reconstructing brain tissue and recovering neurological function after an ischemic stroke. Ginsenoside Rg1 could promote cerebral angiogenesis through the PI3K/Akt/mTOR signaling pathway, *via* upregulating the expressions of VEGF, HIF-1α, PI3K, p-Akt, and p-mTOR, and significantly increase the proliferation, migration and tube formation of endothelial cells (Chen J. et al., 2019). Besides, ginsenoside Rg1 exerts neuroprotection in cerebral ischemic injury *via* increasing the expression of BDNF in the hippocampal CA1 region and decreasing the expression of IL-1β, IL-6, and TNF-α in serum (Wang L. et al., 2018), as well as promoting the neurogenesis in the dentate gyrus of gerbils after global ischemia (Shen and Zhang, 2003). Ginsenoside Rg1 could also ameliorate neurological injury by attenuating BBB permeability, which is related to the downregulation of PAR-1 and aquaporin 4 expressions (Xie et al., 2015) (Zhou et al., 2014).

Other Ginsenosides and Their Neuroprotective Effects

In addition to ginsenosides summarized above, ginsenoside Re, Rh2, F1, and Compound K, Oleanolic acid may also play a neuroprotective role in treating cerebral ischemic stroke. Ginsenoside Re significantly improved mitochondrial membrane fluidity and decreased mitochondrial swelling, which ameliorated lipid peroxidation and protected neurons *via* improving the activities of SOD and GSH-Px, and reducing the content of MDA in the rat brain (Zhou et al., 2006; Chen et al., 2008). Oleanolic acid (OA) exerts neuroprotective effects *via* reducing ROS production and suppressing the activation of GSK-3β, and upregulating the expression of HO-1throgh GSK-3β/HO-1 signaling pathway in OGD/R induced SH-SY5Y cells and MCAO rats (Lin et al., 2021). Compound K (CK), a ginseng saponin metabolite, showed the neuroprotective effect of anti-inflammatory *via* suppressing microglial activation through inhibiting ROS, MAPK, and NF-κB/activator protein-1 (AP-1) and enhancement of HO-1 signaling (Park et al., 2012). Pretreatment of CK protects against neuron damage by increasing cell viability and decreasing ROS generation, mitochondrial damage, and Ca^{2+}

overload. What's more, OGD/R-induced autophagy and apoptosis in neurons could be regulated by modulating the AMP-activated protein kinase (AMPK) and mTOR pathway (Huang et al., 2020). Ginsenoside Rh2 inhibited the expression of COX-2, TNF-α, and IL-1β, and promoted the anti-inflammatory cytokine IL-10, depending on the AP-1 and protein kinase A (PKA) pathway, which is more potent than the anti-inflammatory effect of ginsenoside Rg3 (Bae et al., 2006). Ginsenoside F1 could promote angiogenesis through the insulin-like growth factor 1 (IGF-1)/insulin-like growth factor 1 receptor (IGF1R) pathway and might also enhance focal cerebral blood perfusion and increase cerebral microvessel density in MCAO rats (Zhang et al., 2019).

CONCLUSION AND PERSPECTIVES

Currently, effective therapies for preventing and treating patients with ischemic stroke remain a challenge. Panax ginseng has been widely used in eastern countries for various diseases. The neuroprotective effects of ginseng or ginsenosides on preclinical and clinical ischemic stroke injury have been demonstrated during the last decade. This review concludes our recent findings related to the effects of ginseng and ginsenosides against ischemic stroke. As shown in **Figure 2**, ginsenoside Rd, Rb1 and Rg1 are the most commonly used in treating ischemic stroke. Mechanisms underlying the neuroprotective effects of ginseng or ginsenosides include regulation of excitotoxicity, Ca^{2+} overload, inflammation, mitochondria dysfunction, oxidative stress, apoptosis, pyroptosis, autophagy, BBB permeability, improving angiogenesis and neurogenesis. These effects can potentially improve abnormal neurobehaviors, such as sensorimotor or cognitive deficits. Ginseng and ginsenosides exert neuroprotective effects *via* modulating multiple signaling pathways, such as MAPK/ERK, PI3K/AKT, cAMP/PKA, AMPK/mTOR, NF-κB, Nrf2, GSK-3β/HO-1, IGF-1/IGF1R pathways, to block the pathological damage of neurons and promote the neural remodeling of stroke (**Figure 3**).

Although numerous preclinical studies have been conducted on the neuroprotective effects of ginseng and ginsenosides in the treatment of ischemic stroke, there are few clinical trials of ginsenosides in treating ischemic stroke. Thus, further high-quality studies are needed to establish the clinical efficacy of ginsenosides. In addition, most experimental stroke models were induced by MCAO in young rats or mice, and only a few aged animals or models with diabetes were used, while the clinical patients are more likely to be associated with hypertension, hyperlipidemia, hyperglycemia, or other diseases. Therefore, it is necessary to study the neuroprotective effects of Panax ginseng or ginsenosides against ischemic stroke with pseudo-clinical models, which will provide a reliable basis for the clinical application of ginseng. Overall, this review describes the recent progress of pharmacological research on ginseng and ginsenosides in ischemic stroke and points out the issues that future research should focus on, which is of great importance for understanding the use of ginseng in the prevention and treatment of ischemic stroke.

AUTHOR CONTRIBUTIONS

JL and GZ designed and supervised the review, AZ and NL collected, analyzed, and drafted the main manuscript; YZ, ZY, and YF checked references, figures and tables; MY revised the manuscript. All authors have read and approved the final version.

FUNDING

This study was supported by the National Natural Science Foundation of China (NSFC 82030124, NSFC 81873041).

REFERENCES

Allen, C. L., and Bayraktutan, U. (2009). Oxidative Stress and its Role in the Pathogenesis of Ischaemic Stroke. *Int. J. Stroke* 4, 461–470. doi:10.1111/j.1747-4949.2009.00387.x

Bae, E. A., Kim, E. J., Park, J. S., Kim, H. S., Ryu, J. H., and Kim, D. H. (2006). Ginsenosides Rg3 and Rh2 Inhibit the Activation of AP-1 and Protein Kinase A Pathway in Lipopolysaccharide/interferon-Gamma-Stimulated BV-2 Microglial Cells. *Planta Med.* 72, 627–633. doi:10.1055/s-2006-931563

Ban, J. Y., Kang, S. W., Lee, J. S., Chung, J. H., Ko, Y. G., and Choi, H. S. (2012). Korean Red Ginseng Protects against Neuronal Damage Induced by Transient Focal Ischemia in Rats. *Exp. Ther. Med.* 3, 693–698. doi:10.3892/etm.2012.449

Berg, D. A., Su, Y., Jimenez-Cyrus, D., Patel, A., Huang, N., Morizet, D., et al. (2019). A Common Embryonic Origin of Stem Cells Drives Developmental and Adult Neurogenesis. *Cell.* 177, 654–e15. doi:10.1016/j.cell.2019.02.010

Broz, P., and Dixit, V. M. (2016). Inflammasomes: Mechanism of Assembly, Regulation and Signalling. *Nat. Rev. Immunol.* 16, 407–420. doi:10.1038/nri.2016.58

Campbell, B. C. V., and Khatri, P. (2020). Stroke. *Lancet* 396, 129–142. doi:10.1016/s0140-6736(20)31179-x

Chamorro, Á., Dirnagl, U., Urra, X., and Planas, A. M. (2016). Neuroprotection in Acute Stroke: Targeting Excitotoxicity, Oxidative and Nitrosative Stress, and Inflammation. *Lancet Neurol.* 15, 869–881. doi:10.1016/S1474-4422(16)00114-9

Chao, D. T., and Korsmeyer, S. J. (1998). BCL-2 Family: Regulators of Cell Death. *Annu. Rev. Immunol.* 16, 395–419. doi:10.1146/annurev.immunol.16.1.395

Chen, J., Zhang, X., Liu, X., Zhang, C., Shang, W., Xue, J., et al. (2019a). Ginsenoside Rg1 Promotes Cerebral Angiogenesis via the PI3K/Akt/mTOR Signaling Pathway in Ischemic Mice. *Eur. J. Pharmacol.* 856, 172418. doi:10.1016/j.ejphar.2019.172418

Chen, L. M., Zhou, X. M., Cao, Y. L., and Hu, W. X. (2008). Neuroprotection of Ginsenoside Re in Cerebral Ischemia-Reperfusion Injury in Rats. *J. Asian Nat. Prod. Res.* 10, 439–445. doi:10.1080/10286020801892292

Chen, W., Balan, P., and Popovich, D. G. (2019b). Analysis of Ginsenoside Content (Panax Ginseng) from Different Regions. *Molecules* 24. doi:10.3390/molecules24193491

Chen, W., Guo, Y., Yang, W., Zheng, P., Zeng, J., and Tong, W. (2015). Protective Effect of Ginsenoside Rb1 on Integrity of Blood-Brain Barrier Following Cerebral Ischemia. *Exp. Brain Res.* 233, 2823–2831. doi:10.1007/s00221-015-4352-3

Cheng, Z., Zhang, M., Ling, C., Zhu, Y., Ren, H., Hong, C., et al. (2019). Neuroprotective Effects of Ginsenosides against Cerebral Ischemia. *Molecules* 24. doi:10.3390/molecules24061102

Cheon, S. Y., Cho, K. J., Lee, J. E., Kim, H. W., Lee, S. K., Kim, H. J., et al. (2013). Cerebroprotective Effects of Red Ginseng Extract Pretreatment against

Ischemia-Induced Oxidative Stress and Apoptosis. *Int. J. Neurosci.* 123, 269–277. doi:10.3109/00207454.2012.758120

Chu, S. F., Zhang, Z., Zhou, X., He, W. B., Chen, C., Luo, P., et al. (2019). Ginsenoside Rg1 Protects against Ischemic/reperfusion-Induced Neuronal Injury through miR-144/Nrf2/ARE Pathway. *Acta Pharmacol. Sin.* 40, 13–25. doi:10.1038/s41401-018-0154-z

Culmsee, C., and Krieglstein, J. (2007). Ischaemic Brain Damage after Stroke: New Insights into Efficient Therapeutic Strategies. International Symposium on Neurodegeneration and Neuroprotection. *EMBO Rep.* 8, 129–133. doi:10.1038/sj.embor.7400892

Dixon, S. J., Lemberg, K. M., Lamprecht, M. R., Skouta, R., Zaitsev, E. M., Gleason, C. E., et al. (2012). Ferroptosis: an Iron-dependent Form of Nonapoptotic Cell Death. *Cell.* 149, 1060–1072. doi:10.1016/j.cell.2012.03.042

Dong, X., Zheng, L., Lu, S., and Yang, Y. (2017). Neuroprotective Effects of Pretreatment of Ginsenoside Rb1 on Severe Cerebral Ischemia-Induced Injuries in Aged Mice: Involvement of Anti-oxidant Signaling. *Geriatr. Gerontol. Int.* 17, 338–345. doi:10.1111/ggi.12699

Drieu, A., Levard, D., Vivien, D., and Rubio, M. (2018). Anti-inflammatory Treatments for Stroke: from Bench to Bedside. *Ther. Adv. Neurol. Disord.* 11, 1756286418789854. doi:10.1177/1756286418789854

Fan, Y., Lu, H., Liang, W., Garcia-Barrio, M. T., Guo, Y., Zhang, J., et al. (2018). Endothelial TFEB (Transcription Factor EB) Positively Regulates Postischemic Angiogenesis. *Circ. Res.* 122, 945–957. doi:10.1161/CIRCRESAHA.118.312672

Fann, D. Y., Lee, S. Y., Manzanero, S., Chunduri, P., Sobey, C. G., and Arumugam, T. V. (2013a). Pathogenesis of Acute Stroke and the Role of Inflammasomes. *Ageing Res. Rev.* 12, 941–966. doi:10.1016/j.arr.2013.09.004

Fann, D. Y., Lee, S. Y., Manzanero, S., Tang, S. C., Gelderblom, M., Chunduri, P., et al. (2013b). Intravenous Immunoglobulin Suppresses NLRP1 and NLRP3 Inflammasome-Mediated Neuronal Death in Ischemic Stroke. *Cell. Death Dis.* 4, e790. doi:10.1038/cddis.2013.326

Ferrara, N., and Adamis, A. P. (2016). Ten Years of Anti-vascular Endothelial Growth Factor Therapy. *Nat. Rev. Drug Discov.* 15, 385–403. doi:10.1038/nrd.2015.17

Galluzzi, L., Vitale, I., Aaronson, S. A., Abrams, J. M., Adam, D., Agostinis, P., et al. (2018). Molecular Mechanisms of Cell Death: Recommendations of the Nomenclature Committee on Cell Death 2018. *Cell. Death Differ.* 25, 486–541. doi:10.1038/s41418-017-0012-4

Gao, J., Bai, P., Li, Y., Li, J., Jia, C., Wang, T., et al. (2020a). Metabolomic Profiling of the Synergistic Effects of Ginsenoside Rg1 in Combination with Neural Stem Cell Transplantation in Ischemic Stroke Rats. *J. Proteome Res.* 19, 2676–2688. doi:10.1021/acs.jproteome.9b00639

Gao, X. Q., Yang, C. X., Chen, G. J., Wang, G. Y., Chen, B., Tan, S. K., et al. (2010). Ginsenoside Rb1 Regulates the Expressions of Brain-Derived Neurotrophic Factor and Caspase-3 and Induces Neurogenesis in Rats with Experimental Cerebral Ischemia. *J. Ethnopharmacol.* 132, 393–399. doi:10.1016/j.jep.2010.07.033

Gao, X., Zhang, X., Cui, L., Chen, R., Zhang, C., Xue, J., et al. (2020b). Ginsenoside Rb1 Promotes Motor Functional Recovery and Axonal Regeneration in Post-stroke Mice through cAMP/PKA/CREB Signaling Pathway. *Brain Res. Bull.* 154, 51–60. doi:10.1016/j.brainresbull.2019.10.006

George, P. M., and Steinberg, G. K. (2015). Novel Stroke Therapeutics: Unraveling Stroke Pathophysiology and its Impact on Clinical Treatments. *Neuron* 87, 297–309. doi:10.1016/j.neuron.2015.05.041

Glick, D., Barth, S., and Macleod, K. F. (2010). Autophagy: Cellular and Molecular Mechanisms. *J. Pathol.* 221, 3–12. doi:10.1002/path.2697

Gu, Y., Ren, K., Wang, L., Jiang, C., and Yao, Q. (2020). Rg1 in Combination with Mannitol Protects Neurons against Glutamate-Induced ER Stress via the PERK-eIF2 α-ATF4 Signaling Pathway. *Life Sci.* 263, 118559. doi:10.1016/j.lfs.2020.118559

Guo, Y., Wang, L. P., Li, C., Xiong, Y. X., Yan, Y. T., Zhao, L. Q., et al. (2018). Effects of Ginsenoside Rb1 on Expressions of Phosphorylation Akt/Phosphorylation mTOR/Phosphorylation PTEN in Artificial Abnormal Hippocampal Microenvironment in Rats. *Neurochem. Res.* 43, 1927–1937. doi:10.1007/s11064-018-2612-x

Hatakeyama, M., Ninomiya, I., and Kanazawa, M. (2020). Angiogenesis and Neuronal Remodeling after Ischemic Stroke. *Neural Regen. Res.* 15, 16–19. doi:10.4103/1673-5374.264442

He, B., Chen, P., Xie, Y., Li, S., Zhang, X., Yang, R., et al. (2017). 20(R)-Ginsenoside Rg3 Protects SH-Sy5y Cells against Apoptosis Induced by Oxygen and Glucose Deprivation/reperfusion. *Bioorg Med. Chem. Lett.* 27, 3867–3871. doi:10.1016/j.bmcl.2017.06.045

He, B., Chen, P., Yang, J., Yun, Y., Zhang, X., Yang, R., et al. (2012). Neuroprotective Effect of 20(R)-ginsenoside Rg(3) against Transient Focal Cerebral Ischemia in Rats. *Neurosci. Lett.* 526, 106–111. doi:10.1016/j.neulet.2012.08.022

He, J., Liu, J., Huang, Y., Tang, X., Xiao, H., and Hu, Z. (2021). Oxidative Stress, Inflammation, and Autophagy: Potential Targets of Mesenchymal Stem Cells-Based Therapies in Ischemic Stroke. *Front. Neurosci.* 15. doi:10.3389/fnins.2021.641157

He, Q., Sun, J., Wang, Q., Wang, W., and He, B. (2014). Neuroprotective Effects of Ginsenoside Rg1 against Oxygen-Glucose Deprivation in Cultured Hippocampal Neurons. *J. Chin. Med. Assoc.* 77, 142–149. doi:10.1016/j.jcma.2014.01.001

Hu, G., Wu, Z., Yang, F., Zhao, H., Liu, X., Deng, Y., et al. (2013). Ginsenoside Rd Blocks AIF Mitochondrio-Nuclear Translocation and NF-Kb Nuclear Accumulation by Inhibiting poly(ADP-Ribose) Polymerase-1 after Focal Cerebral Ischemia in Rats. *Neurol. Sci.* 34, 2101–2106. doi:10.1007/s10072-013-1344-6

Hu, J. J., Liu, X., Xia, S., Zhang, Z., Zhang, Y., Zhao, J., et al. (2020a). FDA-Approved Disulfiram Inhibits Pyroptosis by Blocking Gasdermin D Pore Formation. *Nat. Immunol.* 21, 736–745. doi:10.1038/s41590-020-0669-6

Hu, Q., Liu, L., Zhou, L., Lu, H., Wang, J., Chen, X., et al. (2020b). Effect of Fluoxetine on HIF-1α- Netrin/VEGF Cascade, Angiogenesis and Neuroprotection in a Rat Model of Transient Middle Cerebral Artery Occlusion. *Exp. Neurol.* 329, 113312. doi:10.1016/j.expneurol.2020.113312

Huang, Q., Lou, T., Wang, M., Xue, L., Lu, J., Zhang, H., et al. (2020). Compound K Inhibits Autophagy-Mediated Apoptosis Induced by Oxygen and Glucose Deprivation/reperfusion via Regulating AMPK-mTOR Pathway in Neurons. *Life Sci.* 254, 117793. doi:10.1016/j.lfs.2020.117793

Hyun, S. H., Bhilare, K. D., In, G., Park, C.-K., and Kim, J.-H. (2022). Effects of Panax Ginseng and Ginsenosides on Oxidative Stress and Cardiovascular Diseases: Pharmacological and Therapeutic Roles. *J. Ginseng Res.* 46, 33–38. doi:10.1016/j.jgr.2021.07.007

Jia, J., Bissa, B., Brecht, L., Allers, L., Choi, S. W., Gu, Y., et al. (2020). AMPK, a Regulator of Metabolism and Autophagy, Is Activated by Lysosomal Damage via a Novel Galectin-Directed Ubiquitin Signal Transduction System. *Mol. Cell.* 77, 951–969. doi:10.1016/j.molcel.2019.12.028

Jiang, S., Li, T., Ji, T., Yi, W., Yang, Z., Wang, S., et al. (2018). AMPK: Potential Therapeutic Target for Ischemic Stroke. *Theranostics* 8, 4535–4551. doi:10.7150/thno.25674

Jiang, Z., Wang, Y., Zhang, X., Peng, T., Lu, Y., Leng, J., et al. (2013). Preventive and Therapeutic Effects of Ginsenoside Rb1 for Neural Injury during Cerebral Infarction in Rats. *Am. J. Chin. Med.* 41, 341–352. doi:10.1142/S0192415X13500250

Jo, E.-J., Kang, S. J., and Kim, A.-J. (2009). Effects of Steam- and Dry-Processing Temperatures on the Benzo(a)pyrene Content of Black and Red Ginseng. *Korean J. Food Nutr.* 22, 199–204.

Johnson, C. O., Minh, N., Roth, G. A., Nichols, E., Alam, T., Abate, D., et al. (2019). Global, Regional, and National Burden of Stroke, 1990-2016: a Systematic Analysis for the Global Burden of Disease Study 2016. *Lancet Neurol.* 18, 439–458. doi:10.1016/S1474-4422(19)30034-1

Kaplan-Arabaci, O., Acari, A., Ciftci, P., and Gozuacik, D. (2022). Glutamate Scavenging as a Neuroreparative Strategy in Ischemic Stroke. *Front. Pharmacol.* 13, 866738. doi:10.3389/fphar.2022.866738

Ke, L., Guo, W., Xu, J., Zhang, G., Wang, W., and Huang, W. (2014). Ginsenoside Rb1 Attenuates Activated Microglia-Induced Neuronal Damage. *Neural Regen. Res.* 9, 252–259. doi:10.4103/1673-5374.128217

Kim, D., Park, M., Haleem, I., Lee, Y., Koo, J., Na, Y. C., et al. (2020). Natural Product Ginsenoside 20(S)-25-Methoxyl-Dammarane-3β, 12β, 20-Triol in Cancer Treatment: A Review of the Pharmacological Mechanisms and Pharmacokinetics. *Front. Pharmacol.* 11, 521. doi:10.3389/fphar.2020.00521

Kim, J. H. (2018). Pharmacological and Medical Applications of Panax Ginseng and Ginsenosides: a Review for Use in Cardiovascular Diseases. *J. Ginseng Res.* 42, 264–269. doi:10.1016/j.jgr.2017.10.004

Kim, N. H., Jayakodi, M., Lee, S. C., Choi, B. S., Jang, W., Lee, J., et al. (2018). Genome and Evolution of the Shade-Requiring Medicinal Herb Panax Ginseng. *Plant Biotechnol. J.* 16, 1904–1917. doi:10.1111/pbi.12926

Kim, Y. O., Kim, H. J., Kim, G. S., Park, H. G., Lim, S. J., Seong, N. S., et al. (2009). Panax Ginseng Protects against Global Ischemia Injury in Rat hippocampus. *J. Med. Food* 12, 71–76. doi:10.1089/jmf.2007.0614

Klionsky, D. J., Abdelmohsen, K., Abe, A., Abedin, M. J., Abeliovich, H., Acevedo Arozena, A., et al. (2016). Guidelines for the Use and Interpretation of Assays for Monitoring Autophagy. *Autophagy* 12, 1–222. doi:10.1080/15548627.2015.1100356. 3rd edition

Knowland, D., Arac, A., Sekiguchi, K. J., Hsu, M., Lutz, S. E., Perrino, J., et al. (2014). Stepwise Recruitment of Transcellular and Paracellular Pathways Underlies Blood-Brain Barrier Breakdown in Stroke. *Neuron* 82, 603–617. doi:10.1016/j.neuron.2014.03.003

Kondo, Y., Asanuma, M., Nishibayashi, S., Iwata, E., and Ogawa, N. (1997). Late-onset Lipid Peroxidation and Neuronal Cell Death Following Transient Forebrain Ischemia in Rat Brain. *Brain Res.* 772, 37–44. doi:10.1016/s0006-8993(97)00836-6

Koppula, P., Zhang, Y., Zhuang, L., and Gan, B. (2018). Amino Acid Transporter SLC7A11/xCT at the Crossroads of Regulating Redox Homeostasis and Nutrient Dependency of Cancer. *Cancer Commun.* 38. doi:10.1186/s40880-018-0288-x

Lai, T. W., Zhang, S., and Wang, Y. T. (2014). Excitotoxicity and Stroke: Identifying Novel Targets for Neuroprotection. *Prog. Neurobiol.* 115, 157–188. doi:10.1016/j.pneurobio.2013.11.006

Lan, B., Ge, J. W., Cheng, S. W., Zheng, X. L., Liao, J., He, C., et al. (2020). Extract of Naotaifang, a Compound Chinese Herbal Medicine, Protects Neuron Ferroptosis Induced by Acute Cerebral Ischemia in Rats. *J. Integr. Medicine-Jim* 18, 344–350. doi:10.1016/j.joim.2020.01.008

Lee, H., Zandkarimi, F., Zhang, Y., Meena, J. K., Kim, J., Zhuang, L., et al. (2020). Energy-stress-mediated AMPK Activation Inhibits Ferroptosis. *Nat. Cell. Biol.* 22, 225–234. doi:10.1038/s41556-020-0461-8

Lee, J. S., Choi, H. S., Kang, S. W., Chung, J. H., Park, H. K., Ban, J. Y., et al. (2011). Therapeutic Effect of Korean Red Ginseng on Inflammatory Cytokines in Rats with Focal Cerebral Ischemia/reperfusion Injury. *Am. J. Chin. Med.* 39, 83–94. doi:10.1142/S0192415X1100866X

Lees, K. R., Bluhmki, E., Von Kummer, R., Brott, T. G., Toni, D., Grotta, J. C., et al. (2010). Time to Treatment with Intravenous Alteplase and Outcome in Stroke: an Updated Pooled Analysis of ECASS, ATLANTIS, NINDS, and EPITHET Trials. *Lancet* 375, 1695–1703. doi:10.1016/S0140-6736(10)60491-6

Li, X. Y., Liang, J., Tang, Y. B., Zhou, J. G., and Guan, Y. Y. (2010). Ginsenoside Rd Prevents Glutamate-Induced Apoptosis in Rat Cortical Neurons. *Clin. Exp. Pharmacol. Physiol.* 37, 199–204. doi:10.1111/j.1440-1681.2009.05286.x

Li, Y., Guan, Y., Wang, Y., Yu, C. L., Zhai, F. G., and Guan, L. X. (2017a). Neuroprotective Effect of the Ginsenoside Rg1 on Cerebral Ischemic Injury *In Vivo* and *In Vitro* Is Mediated by PPARγ-Regulated Antioxidative and Anti-inflammatory Pathways. *Evid. Based Complement. Altern. Med.* 2017, 7842082. doi:10.1155/2017/7842082

Li, Y., Suo, L., Liu, Y., Li, H., and Xue, W. (2017b). Protective Effects of Ginsenoside Rg1 against Oxygen-Glucose-Deprivation-Induced Apoptosis in Neural Stem Cells. *J. Neurol. Sci.* 373, 107–112. doi:10.1016/j.jns.2016.12.036

Lim, J. H., Wen, T. C., Matsuda, S., Tanaka, J., Maeda, N., Peng, H., et al. (1997). Protection of Ischemic Hippocampal Neurons by Ginsenoside Rb1, a Main Ingredient of Ginseng Root. *Neurosci. Res.* 28, 191–200. doi:10.1016/s0168-0102(97)00041-2

Lin, K., Zhang, Z., Zhang, Z., Zhu, P., Jiang, X., Wang, Y., et al. (2021). Oleanolic Acid Alleviates Cerebral Ischemia/Reperfusion Injury via Regulation of the GSK-3β/HO-1 Signaling Pathway. *Pharm. (Basel)* 15. doi:10.3390/ph15010001

Lin, M., Sun, W., Gong, W., Ding, Y., Zhuang, Y., and Hou, Q. (2015). Ginsenoside Rg1 Protects against Transient Focal Cerebral Ischemic Injury and Suppresses its Systemic Metabolic Changes in Cerabral Injury Rats. *Acta Pharm. Sin. B* 5, 277–284. doi:10.1016/j.apsb.2015.02.001

Linnik, M. D., Zobrist, R. H., and Hatfield, M. D. (1993). Evidence Supporting a Role for Programmed Cell Death in Focal Cerebral Ischemia in Rats. *Stroke* 24, 2002–2008. discussion 2008-2009. doi:10.1161/01.str.24.12.2002

Liu, A., Zhu, W., Sun, L., Han, G., Liu, H., Chen, Z., et al. (2018a). Ginsenoside Rb1 Administration Attenuates Focal Cerebral Ischemic Reperfusion Injury through Inhibition of HMGB1 and Inflammation Signals. *Exp. Ther. Med.* 16, 3020–3026. doi:10.3892/etm.2018.6523

Liu, L., Kelly, M. G., Wierzbicki, E. L., Escober-Nario, I. C., Vollmer, M. K., and Doré, S. (2019a). Nrf2 Plays an Essential Role in Long-Term Brain Damage and Neuroprotection of Korean Red Ginseng in a Permanent Cerebral Ischemia Model. *Antioxidants (Basel)* 8, 273. doi:10.3390/antiox8080273

Liu, L., Vollmer, M. K., Ahmad, A. S., Fernandez, V. M., Kim, H., and Doré, S. (2019b). Pretreatment with Korean Red Ginseng or Dimethyl Fumarate Attenuates Reactive Gliosis and Confers Sustained Neuroprotection against Cerebral Hypoxic-Ischemic Damage by an Nrf2-dependent Mechanism. *Free Radic. Biol. Med.* 131, 98–114. doi:10.1016/j.freeradbiomed.2018.11.017

Liu, L., Vollmer, M. K., Fernandez, V. M., Dweik, Y., Kim, H., and Doré, S. (2018b). Korean Red Ginseng Pretreatment Protects against Long-Term Sensorimotor Deficits after Ischemic Stroke Likely through Nrf2. *Front. Cell. Neurosci.* 12, 74. doi:10.3389/fncel.2018.00074

Liu, L., Vollmer, M. K., Kelly, M. G., Fernandez, V. M., Fernandez, T. G., Kim, H., et al. (2020). Reactive Gliosis Contributes to Nrf2-dependent Neuroprotection by Pretreatment with Dimethyl Fumarate or Korean Red Ginseng against Hypoxic-Ischemia: Focus on Hippocampal Injury. *Mol. Neurobiol.* 57, 105–117. doi:10.1007/s12035-019-01760-0

Liu, Q., Kou, J. P., and Yu, B. Y. (2011). Ginsenoside Rg1 Protects against Hydrogen Peroxide-Induced Cell Death in PC12 Cells via Inhibiting NF-Kb Activation. *Neurochem. Int.* 58, 119–125. doi:10.1016/j.neuint.2010.11.004

Liu, X., Wang, L., Wen, A., Yang, J., Yan, Y., Song, Y., et al. (2012). Ginsenoside-Rd Improves Outcome of Acute Ischaemic Stroke - a Randomized, Double-Blind, Placebo-Controlled, Multicenter Trial. *Eur. J. Neurol.* 19, 855–863. doi:10.1111/j.1468-1331.2011.03634.x

Liu, X., Xia, J., Wang, L., Song, Y., Yang, J., Yan, Y., et al. (2009). Efficacy and Safety of Ginsenoside-Rd for Acute Ischaemic Stroke: a Randomized, Double-Blind, Placebo-Controlled, Phase II Multicenter Trial. *Eur. J. Neurol.* 16, 569–575. doi:10.1111/j.1468-1331.2009.02534.x

Liu, X. Y., Zhou, X. Y., Hou, J. C., Zhu, H., Wang, Z., Liu, J. X., et al. (2015). Ginsenoside Rd Promotes Neurogenesis in Rat Brain after Transient Focal Cerebral Ischemia via Activation of PI3K/Akt Pathway. *Acta Pharmacol. Sin.* 36, 421–428. doi:10.1038/aps.2014.156

Liu, Y., and Levine, B. (2015). Autosis and Autophagic Cell Death: the Dark Side of Autophagy. *Cell. Death Differ.* 22, 367–376. doi:10.1038/cdd.2014.143

Liu, Z., Wang, C., Yang, J., Zhou, B., Yang, R., Ramachandran, R., et al. (2019c). Crystal Structures of the Full-Length Murine and Human Gasdermin D Reveal Mechanisms of Autoinhibition, Lipid Binding, and Oligomerization. *Immunity* 51, 43–49. doi:10.1016/j.immuni.2019.04.017

Lu, J., Wang, X., Wu, A., Cao, Y., Dai, X., Liang, Y., et al. (2022). Ginsenosides in Central Nervous System Diseases: Pharmacological Actions, Mechanisms, and Therapeutics. *Phytother. Res.* doi:10.1002/ptr.7395

Lu, T., Jiang, Y., Zhou, Z., Yue, X., Wei, N., Chen, Z., et al. (2011). Intranasal Ginsenoside Rb1 Targets the Brain and Ameliorates Cerebral Ischemia/reperfusion Injury in Rats. *Biol. Pharm. Bull.* 34, 1319–1324. doi:10.1248/bpb.34.1319

Luo, T., Liu, G., Ma, H., Lu, B., Xu, H., Wang, Y., et al. (2014). Inhibition of Autophagy via Activation of PI3K/Akt Pathway Contributes to the Protection of Ginsenoside Rb1 against Neuronal Death Caused by Ischemic Insults. *Int. J. Mol. Sci.* 15, 15426–15442. doi:10.3390/ijms150915426

Luoma, J. I., Kelley, B. G., and Mermelstein, P. G. (2011). Progesterone Inhibition of Voltage-Gated Calcium Channels Is a Potential Neuroprotective Mechanism against Excitotoxicity. *Steroids* 76, 845–855. doi:10.1016/j.steroids.2011.02.013

Marsh, B., Stevens, S. L., Packard, A. E. B., Gopalan, B., Hunter, B., Leung, P. Y., et al. (2009). Systemic Lipopolysaccharide Protects the Brain from Ischemic Injury by Reprogramming the Response of the Brain to Stroke: A Critical Role for IRF3. *J. Neurosci.* 29, 9839–9849. doi:10.1523/JNEUROSCI.2496-09.2009

Matsui, Y., Kyoi, S., Takagi, H., Hsu, C. P., Hariharan, N., Ago, T., et al. (2008). Molecular Mechanisms and Physiological Significance of Autophagy during Myocardial Ischemia and Reperfusion. *Autophagy* 4, 409–415. doi:10.4161/auto.5638

Mo, Y., Sun, Y.-Y., and Liu, K.-Y. (2020). Autophagy and Inflammation in Ischemic Stroke. *Neural Regen. Res.* 15, 1388–1396. doi:10.4103/1673-5374.274331

Muhammad, I. F., Borné, Y., Melander, O., Orho-Melander, M., Nilsson, J., Söderholm, M., et al. (2018). FADD (Fas-Associated Protein with Death

Domain), Caspase-3, and Caspase-8 and Incidence of Ischemic Stroke. *Stroke* 49, 2224–2226. doi:10.1161/STROKEAHA.118.022063

Nada, S. E., Tulsulkar, J., and Shah, Z. A. (2014). Heme Oxygenase 1-mediated Neurogenesis Is Enhanced by Ginkgo Biloba (EGb 761®) after Permanent Ischemic Stroke in Mice. *Mol. Neurobiol.* 49, 945–956. doi:10.1007/s12035-013-8572-x

Navarro-Orozco, D., and Sánchez-Manso, J. C. (2022). "Neuroanatomy, Middle Cerebral Artery," in StatPearls. *(Treasure Island (FL)* (Florida: StatPearls Publishing LLC.). StatPearls Publishing Copyright © 2022.

Park, H. J., Shim, H. S., Kim, K. S., and Shim, I. (2011a). The Protective Effect of Black Ginseng against Transient Focal Ischemia-Induced Neuronal Damage in Rats. *Korean J. Physiol. Pharmacol.* 15, 333–338. doi:10.4196/kjpp.2011.15.6.333

Park, H. W., In, G., Han, S. T., Lee, M. W., Kim, S. Y., Kim, K. T., et al. (2013). Simultaneous Determination of 30 Ginsenosides in Panax Ginseng Preparations Using Ultra Performance Liquid Chromatography. *J. Ginseng Res.* 37, 457–467. doi:10.5142/jgr.2013.37.457

Park, J. S., Shin, J. A., Jung, J. S., Hyun, J. W., Van Le, T. K., Kim, D. H., et al. (2012). Anti-inflammatory Mechanism of Compound K in Activated Microglia and its Neuroprotective Effect on Experimental Stroke in Mice. *J. Pharmacol. Exp. Ther.* 341, 59–67. doi:10.1124/jpet.111.189035

Park, U. J., Lee, Y. A., Won, S. M., Lee, J. H., Kang, S. H., Springer, J. E., et al. (2011b). Blood-derived Iron Mediates Free Radical Production and Neuronal Death in the Hippocampal CA1 Area Following Transient Forebrain Ischemia in Rat. *Acta Neuropathol.* 121, 459–473. doi:10.1007/s00401-010-0785-8

Powers, W. J., Rabinstein, A. A., Ackerson, T., Adeoye, O. M., Bambakidis, N. C., Becker, K., et al. (2019). Amer Heart Assoc StrokeGuidelines for the Early Management of Patients with Acute Ischemic Stroke: 2019 Update to the 2018 Guidelines for the Early Management of Acute Ischemic Stroke: A Guideline for Healthcare Professionals from the American Heart Association/American Stroke Association. *Stroke* 50, E344–E418. doi:10.1161/str.0000000000000211

Qin, C., Zhou, L. Q., Ma, X. T., Hu, Z. W., Yang, S., Chen, M., et al. (2019). Dual Functions of Microglia in Ischemic Stroke. *Neurosci. Bull.* 35, 921–933. doi:10.1007/s12264-019-00388-3

Rajkovic, O., Potjewyd, G., and Pinteaux, E. (2018). Regenerative Medicine Therapies for Targeting Neuroinflammation after Stroke. *Front. Neurol.* 9, 734. doi:10.3389/fneur.2018.00734

Ratan, Z. A., Haidere, M. F., Hong, Y. H., Park, S. H., Lee, J.-O., Lee, J., et al. (2021). Pharmacological Potential of Ginseng and its Major Component Ginsenosides. *J. Ginseng Res.* 45, 199–210. doi:10.1016/j.jgr.2020.02.004

Rothman, S. M., and Olney, J. W. (1986). Glutamate and the Pathophysiology of Hypoxic-Iischemic Brain Damage. *Ann. Neurol.* 19, 105–111. doi:10.1002/ana.410190202

Sakanaka, M., Zhu, P., Zhang, B., Wen, T. C., Cao, F., Ma, Y. J., et al. (2007). Intravenous Infusion of Dihydroginsenoside Rb1 Prevents Compressive Spinal Cord Injury and Ischemic Brain Damage through Upregulation of VEGF and Bcl-XL. *J. Neurotrauma* 24, 1037–1054. doi:10.1089/neu.2006.0182

Shah, Z. A., Gilani, R. A., Sharma, P., and Vohora, S. B. (2005). Cerebroprotective Effect of Korean Ginseng Tea against Global and Focal Models of Ischemia in Rats. *J. Ethnopharmacol.* 101, 299–307. doi:10.1016/j.jep.2005.05.002

Shen, J., Zheng, H., Ruan, J., Fang, W., Li, A., Tian, G., et al. (2013). Autophagy Inhibition Induces Enhanced Proapoptotic Effects of ZD6474 in Glioblastoma. *Br. J. Cancer* 109, 164–171. doi:10.1038/bjc.2013.306

Shen, L., and Zhang, J. (2003). Ginsenoside Rg1 Increases Ischemia-Induced Cell Proliferation and Survival in the Dentate Gyrus of Adult Gerbils. *Neurosci. Lett.* 344, 1–4. doi:10.1016/s0304-3940(03)00318-5

Shi, J., Zhao, Y., Wang, K., Shi, X., Wang, Y., Huang, H., et al. (2015). Cleavage of GSDMD by Inflammatory Caspases Determines Pyroptotic Cell Death. *Nature* 526, 660–665. doi:10.1038/nature15514

Singh, A., Kim, W., Kim, Y., Jeong, K., Kang, C. S., Kim, Y., et al. (2016). Multifunctional Photonics Nanoparticles for Crossing the Blood-Brain Barrier and Effecting Optically Trackable Brain Theranostics. *Adv. Funct. Mater* 26, 7057–7066. doi:10.1002/adfm.201602808

Smith, J. R., Galie, P. A., Slochower, D. R., Weisshaar, C. L., Janmey, P. A., and Winkelstein, B. A. (2016). Salmon-Derived Thrombin Inhibits Development of Chronic Pain through an Endothelial Barrier Protective Mechanism Dependent on APC. *Biomaterials* 80, 96–105. doi:10.1016/j.biomaterials.2015.11.062

Song, Y., Li, Z., He, T., Qu, M., Jiang, L., Li, W., et al. (2019). M2 Microglia-Derived Exosomes Protect the Mouse Brain from Ischemia-Reperfusion Injury via Exosomal miR-124. *Theranostics* 9, 2910–2923. doi:10.7150/thno.30879

Sun, C., Lai, X., Huang, X., and Zeng, Y. (2014). Protective Effects of Ginsenoside Rg1 on Astrocytes and Cerebral Ischemic-Reperfusion Mice. *Biol. Pharm. Bull.* 37, 1891–1898. doi:10.1248/bpb.b14-00394

Sun, J., and Nan, G. (2016). The Mitogen-Activated Protein Kinase (MAPK) Signaling Pathway as a Discovery Target in Stroke. *J. Mol. Neurosci.* 59, 90–98. doi:10.1007/s12031-016-0717-8

Szydlowska, K., and Tymianski, M. (2010). Calcium, Ischemia and Excitotoxicity. *Cell. Calcium* 47, 122–129. doi:10.1016/j.ceca.2010.01.003

Tang, D., Kang, R., Berghe, T. V., Vandenabeele, P., and Kroemer, G. (2019a). The Molecular Machinery of Regulated Cell Death. *Cell. Res.* 29, 347–364. doi:10.1038/s41422-019-0164-5

Tang, D. L., Kang, R., Vanden Berghe, T., Vandenabeele, P., and Kroemer, G. (2019b). The Molecular Machinery of Regulated Cell Death. *Cell. Res.* 29, 347–364. doi:10.1038/s41422-019-0164-5

Tian, J., Fu, F., Geng, M., Jiang, Y., Yang, J., Jiang, W., et al. (2005). Neuroprotective Effect of 20(S)-ginsenoside Rg3 on Cerebral Ischemia in Rats. *Neurosci. Lett.* 374, 92–97. doi:10.1016/j.neulet.2004.10.030

Tian, J., Zhang, S., Li, G., Liu, Z., and Xu, B. (2009). 20(S)-ginsenoside Rg3, a Neuroprotective Agent, Inhibits Mitochondrial Permeability Transition Pores in Rat Brain. *Phytother. Res.* 23, 486–491. doi:10.1002/ptr.2653

Tuo, Q. Z., Zhang, S. T., and Lei, P. (2022). Mechanisms of Neuronal Cell Death in Ischemic Stroke and Their Therapeutic Implications. *Med. Res. Rev.* 42, 259–305. doi:10.1002/med.21817

Tzingounis, A. V., and Wadiche, J. I. (2007). Glutamate Transporters: Confining Runaway Excitation by Shaping Synaptic Transmission. *Nat. Rev. Neurosci.* 8, 935–947. doi:10.1038/nrn2274

Virani, S. S., Alonso, A., Benjamin, E. J., Bittencourt, M. S., Callaway, C. W., Carson, A. P., et al. (2020). Heart Disease and Stroke Statistics-2020 Update: A Report from the American Heart Association. *Circulation* 141, e139–e596. doi:10.1161/CIR.0000000000000757

Wan, Q., Ma, X., Zhang, Z. J., Sun, T., Xia, F., Zhao, G., et al. (2017). Ginsenoside Reduces Cognitive Impairment during Chronic Cerebral Hypoperfusion through Brain-Derived Neurotrophic Factor Regulated by Epigenetic Modulation. *Mol. Neurobiol.* 54, 2889–2900. doi:10.1007/s12035-016-9868-4

Wan, Y., Wang, J., Xu, J.-F., Tang, F., Chen, L., Tan, Y.-Z., et al. (2021). Panax Ginseng and its Ginsenosides: Potential Candidates for the Prevention and Treatment of Chemotherapy-Induced Side Effects. *J. Ginseng Res.* 45, 617–630. doi:10.1016/j.jgr.2021.03.001

Wang, J., Li, D., Hou, J., and Lei, H. (2018a). Protective Effects of Geniposide and Ginsenoside Rg1 Combination Treatment on Rats Following Cerebral Ischemia Are Mediated via Microglial microRNA-155-5p Inhibition. *Mol. Med. Rep.* 17, 3186–3193. doi:10.3892/mmr.2017.8221

Wang, L. J., Huang, Y., Yin, G., Wang, J., Wang, P., Chen, Z. Y., et al. (2020). Antimicrobial Activities of Asian Ginseng, American Ginseng, and Notoginseng. *Phytotherapy Res.* 34, 1226–1236. doi:10.1002/ptr.6605

Wang, L., Zhao, H., Zhai, Z. Z., and Qu, L. X. (2018b). Protective Effect and Mechanism of Ginsenoside Rg1 in Cerebral Ischaemia-Reperfusion Injury in Mice. *Biomed. Pharmacother.* 99, 876–882. doi:10.1016/j.biopha.2018.01.136

Wang, P., Shao, B. Z., Deng, Z., Chen, S., Yue, Z., and Miao, C. Y. (2018c). Autophagy in Ischemic Stroke. *Prog. Neurobiol.* 163-164, 98–117. doi:10.1016/j.pneurobio.2018.01.001

Wang, R., Dong, Y., Lu, Y., Zhang, W., Brann, D. W., and Zhang, Q. (2019). Photobiomodulation for Global Cerebral Ischemia: Targeting Mitochondrial Dynamics and Functions. *Mol. Neurobiol.* 56, 1852–1869. doi:10.1007/s12035-018-1191-9

Wu, L., Xiong, X., Wu, X., Ye, Y., Jian, Z., Zhi, Z., et al. (2020). Targeting Oxidative Stress and Inflammation to Prevent Ischemia-Reperfusion Injury. *Front. Mol. Neurosci.* 13, 28. doi:10.3389/fnmol.2020.00028

Wu, S. D., Xia, F., Lin, X. M., Duan, K. L., Wang, F., Lu, Q. L., et al. (2016a). Ginsenoside-Rd Promotes Neurite Outgrowth of PC12 Cells through MAPK/ERK- and PI3K/AKT-dependent Pathways. *Int. J. Mol. Sci.* 17. doi:10.3390/ijms17020177

Wu, Y., Lindblad, J. L., Garnett, J., Kamber Kaya, H. E., Xu, D., Zhao, Y., et al. (2016b). Genetic Characterization of Two Gain-Of-Function Alleles of the

Effector Caspase DrICE in Drosophila. *Cell. Death Differ.* 23, 723–732. doi:10.1038/cdd.2015.144

Xie, C. L., Li, J. H., Wang, W. W., Zheng, G. Q., and Wang, L. X. (2015). Neuroprotective Effect of Ginsenoside-Rg1 on Cerebral Ischemia/reperfusion Injury in Rats by Downregulating Protease-Activated Receptor-1 Expression. *Life Sci.* 121, 145–151. doi:10.1016/j.lfs.2014.12.002

Xie, Z., Shi, M., Zhang, C., Zhao, H., Hui, H., and Zhao, G. (2016). Ginsenoside Rd Protects against Cerebral Ischemia-Reperfusion Injury via Decreasing the Expression of the NMDA Receptor 2B Subunit and its Phosphorylated Product. *Neurochem. Res.* 41, 2149–2159. doi:10.1007/s11064-016-1930-0

Xing, S., Zhang, Y., Li, J., Zhang, J., Li, Y., Dang, C., et al. (2012). Beclin 1 Knockdown Inhibits Autophagic Activation and Prevents the Secondary Neurodegenerative Damage in the Ipsilateral Thalamus Following Focal Cerebral Infarction. *Autophagy* 8, 63–76. doi:10.4161/auto.8.1.18217

Xu, M., Ma, Q., Fan, C., Chen, X., Zhang, H., and Tang, M. (2019). Ginsenosides Rb1 and Rg1 Protect Primary Cultured Astrocytes against Oxygen-Glucose Deprivation/Reoxygenation-Induced Injury via Improving Mitochondrial Function. *Int. J. Mol. Sci.* 20. doi:10.3390/ijms20236086

Xu, Q. X., Zhao, B., Ye, Y. Z., Li, Y. N., Zhang, Y. G., Xiong, X. X., et al. (2021). Relevant Mediators Involved in and Therapies Targeting the Inflammatory Response Induced by Activation of the NLRP3 Inflammasome in Ischemic Stroke. *J. Neuroinflammation* 18. doi:10.1186/s12974-021-02137-8

Yang, L. X., Zhang, X., and Zhao, G. (2016). Ginsenoside Rd Attenuates DNA Damage by Increasing Expression of DNA Glycosylase Endonuclease VIII-like Proteins after Focal Cerebral Ischemia. *Chin. Med. J. Engl.* 129, 1955–1962. doi:10.4103/0366-6999.187851

Yang, Y., He, B., Yang, R., Chen, D., Zhang, X., Li, F., et al. (2022). Comprehensive Analysis of lncRNA Expression Profiles in Rats with Cerebral Ischemia-Reperfusion Injury after Treatment with 20(R)-ginsenoside Rg3. *J. Integr. Neurosci.* 21, 16. doi:10.31083/j.jin2101016

Yang, Y., Li, X., Zhang, L., Liu, L., Jing, G., and Cai, H. (2015). Ginsenoside Rg1 Suppressed Inflammation and Neuron Apoptosis by Activating PPARγ/HO-1 in hippocampus in Rat Model of Cerebral Ischemia-Reperfusion Injury. *Int. J. Clin. Exp. Pathol.* 8, 2484–2494.

Yao, Y., Hu, S., Zhang, C., Zhou, Q., Wang, H., Yang, Y., et al. (2022). Ginsenoside Rd Attenuates Cerebral Ischemia/reperfusion Injury by Exerting an Anti-pyroptotic Effect via the miR-139-5p/FoxO1/Keap1/Nrf2 axis. *Int. Immunopharmacol.* 105, 108582. doi:10.1016/j.intimp.2022.108582

Ye, R., Kong, X., Yang, Q., Zhang, Y., Han, J., Li, P., et al. (2011a). Ginsenoside Rd in Experimental Stroke: Superior Neuroprotective Efficacy with a Wide Therapeutic Window. *Neurotherapeutics* 8, 515–525. doi:10.1007/s13311-011-0051-3

Ye, R., Kong, X., Yang, Q., Zhang, Y., Han, J., and Zhao, G. (2011b). Ginsenoside Rd Attenuates Redox Imbalance and Improves Stroke Outcome after Focal Cerebral Ischemia in Aged Mice. *Neuropharmacology* 61, 815–824. doi:10.1016/j.neuropharm.2011.05.029

Ye, R., Li, N., Han, J., Kong, X., Cao, R., Rao, Z., et al. (2009). Neuroprotective Effects of Ginsenoside Rd against Oxygen-Glucose Deprivation in Cultured Hippocampal Neurons. *Neurosci. Res.* 64, 306–310. doi:10.1016/j.neures.2009.03.016

Ye, R., Yang, Q., Kong, X., Han, J., Zhang, X., Zhang, Y., et al. (2011c). Ginsenoside Rd Attenuates Early Oxidative Damage and Sequential Inflammatory Response after Transient Focal Ischemia in Rats. *Neurochem. Int.* 58, 391–398. doi:10.1016/j.neuint.2010.12.015

Ye, R., Zhang, X., Kong, X., Han, J., Yang, Q., Zhang, Y., et al. (2011d). Ginsenoside Rd Attenuates Mitochondrial Dysfunction and Sequential Apoptosis after Transient Focal Ischemia. *Neuroscience* 178, 169–180. doi:10.1016/j.neuroscience.2011.01.007

Yenari, M. A., Kauppinen, T. M., and Swanson, R. A. (2010). Microglial Activation in Stroke: Therapeutic Targets. *Neurotherapeutics* 7, 378–391. doi:10.1016/j.nurt.2010.07.005

Yoshikawa, T., Akiyoshi, Y., Susumu, T., Tokado, H., Fukuzaki, K., Nagata, R., et al. (2008). Ginsenoside Rb1 Reduces Neurodegeneration in the Peri-Infarct Area of a Thromboembolic Stroke Model in Non-human Primates. *J. Pharmacol. Sci.* 107, 32–40. doi:10.1254/jphs.fp0071297

Yuan, Q. L., Yang, C. X., Xu, P., Gao, X. Q., Deng, L., Chen, P., et al. (2007). Neuroprotective Effects of Ginsenoside Rb1 on Transient Cerebral Ischemia in Rats. *Brain Res.* 1167, 1–12. doi:10.1016/j.brainres.2007.06.024

Zhang, B., Hata, R., Zhu, P., Sato, K., Wen, T. C., Yang, L., et al. (2006). Prevention of Ischemic Neuronal Death by Intravenous Infusion of a Ginseng Saponin, Ginsenoside Rb(1), that Upregulates Bcl-X(L) Expression. *J. Cereb. Blood Flow. Metab.* 26, 708–721. doi:10.1038/sj.jcbfm.9600225

Zhang, B., Matsuda, S., Tanaka, J., Tateishi, N., Maeda, N., Wen, T. C., et al. (1998). Ginsenoside Rb(1) Prevents Image Navigation Disability, Cortical Infarction, and Thalamic Degeneration in Rats with Focal Cerebral Ischemia. *J. Stroke Cerebrovasc. Dis.* 7, 1–9. doi:10.1016/s1052-3057(98)80015-3

Zhang, C., Du, F., Shi, M., Ye, R., Cheng, H., Han, J., et al. (2012a). Ginsenoside Rd Protects Neurons against Glutamate-Induced Excitotoxicity by Inhibiting Ca(2+) Influx. *Cell. Mol. Neurobiol.* 32, 121–128. doi:10.1007/s10571-011-9742-x

Zhang, C., Liu, X., Xu, H., Hu, G., Zhang, X., Xie, Z., et al. (2020a). Protopanaxadiol Ginsenoside Rd Protects against NMDA Receptor-Mediated Excitotoxicity by Attenuating Calcineurin-Regulated DAPK1 Activity. *Sci. Rep.* 10, 8078. doi:10.1038/s41598-020-64738-2

Zhang, G., Liu, A., Zhou, Y., San, X., Jin, T., and Jin, Y. (2008a). Panax Ginseng Ginsenoside-Rg2 Protects Memory Impairment via Anti-apoptosis in a Rat Model with Vascular Dementia. *J. Ethnopharmacol.* 115, 441–448. doi:10.1016/j.jep.2007.10.026

Zhang, G., Xia, F., Zhang, Y., Zhang, X., Cao, Y., Wang, L., et al. (2016). Ginsenoside Rd Is Efficacious against Acute Ischemic Stroke by Suppressing Microglial Proteasome-Mediated Inflammation. *Mol. Neurobiol.* 53, 2529–2540. doi:10.1007/s12035-015-9261-8

Zhang, J., Liu, M., Huang, M., Chen, M., Zhang, D., Luo, L., et al. (2019). Ginsenoside F1 Promotes Angiogenesis by Activating the IGF-1/IGF1R Pathway. *Pharmacol. Res.* 144, 292–305. doi:10.1016/j.phrs.2019.04.021

Zhang, R., Chen, D. Y., Luo, X. W., Yang, Y., Zhang, X. C., Yang, R. H., et al. (2022). Comprehensive Analysis of the Effect of 20(R)-Ginsenoside Rg3 on Stroke Recovery in Rats via the Integrative miRNA-mRNA Regulatory Network. *Molecules* 27. doi:10.3390/molecules27051573

Zhang, X., Liu, X., Hu, G., Zhang, G., Zhao, G., and Shi, M. (2020b). Ginsenoside Rd Attenuates Blood-Brain Barrier Damage by Suppressing Proteasome-Mediated Signaling after Transient Forebrain Ischemia. *Neuroreport* 31, 466–472. doi:10.1097/WNR.0000000000001426

Zhang, X., Shi, M., Bjørås, M., Wang, W., Zhang, G., Han, J., et al. (2013). Ginsenoside Rd Promotes Glutamate Clearance by Up-Regulating Glial Glutamate Transporter GLT-1 via PI3K/AKT and ERK1/2 Pathways. *Front. Pharmacol.* 4, 152. doi:10.3389/fphar.2013.00152

Zhang, X., Shi, M., Ye, R., Wang, W., Liu, X., Zhang, G., et al. (2014). Ginsenoside Rd Attenuates Tau Protein Phosphorylation via the PI3K/AKT/GSK-3β Pathway after Transient Forebrain Ischemia. *Neurochem. Res.* 39, 1363–1373. doi:10.1007/s11064-014-1321-3

Zhang, Y. F., Fan, X. J., Li, X., Peng, L. L., Wang, G. H., Ke, K. F., et al. (2008b). Ginsenoside Rg1 Protects Neurons from Hypoxic-Ischemic Injury Possibly by Inhibiting Ca2+ Influx through NMDA Receptors and L-type Voltage-dependent Ca2+ Channels. *Eur. J. Pharmacol.* 586, 90–99. doi:10.1016/j.ejphar.2007.12.037

Zhang, Y., Zhou, L., Zhang, X., Bai, J., Shi, M., and Zhao, G. (2012b). Ginsenoside-Rd Attenuates TRPM7 and ASIC1a but Promotes ASIC2a Expression in Rats after Focal Cerebral Ischemia. *Neurol. Sci.* 33, 1125–1131. doi:10.1007/s10072-011-0916-6

Zheng, G. Q., Cheng, W., Wang, Y., Wang, X. M., Zhao, S. Z., Zhou, Y., et al. (2011). Ginseng Total Saponins Enhance Neurogenesis after Focal Cerebral Ischemia. *J. Ethnopharmacol.* 133, 724–728. doi:10.1016/j.jep.2010.01.064

Zheng, Q., Bao, X. Y., Zhu, P. C., Tong, Q., Zheng, G. Q., and Wang, Y. (2017). Ginsenoside Rb1 for Myocardial Ischemia/Reperfusion Injury: Preclinical Evidence and Possible Mechanisms. *Oxid. Med. Cell. Longev.* 2017, 6313625. doi:10.1155/2017/6313625

Zheng, T., Jiang, H., Jin, R., Zhao, Y., Bai, Y., Xu, H., et al. (2019). Ginsenoside Rg1 Attenuates Protein Aggregation and Inflammatory Response Following Cerebral Ischemia and Reperfusion Injury. *Eur. J. Pharmacol.* 853, 65–73. doi:10.1016/j.ejphar.2019.02.018

Zhou, X. M., Cao, Y. L., and Dou, D. Q. (2006). Protective Effect of Ginsenoside-Re against Cerebral Ischemia/reperfusion Damage in Rats. *Biol. Pharm. Bull.* 29, 2502–2505. doi:10.1248/bpb.29.2502

Zhou, Y., Li, H. Q., Lu, L., Fu, D. L., Liu, A. J., Li, J. H., et al. (2014). Ginsenoside Rg1 Provides Neuroprotection against Blood Brain Barrier Disruption and Neurological Injury in a Rat Model of Cerebral Ischemia/reperfusion through Downregulation of Aquaporin 4 Expression. *Phytomedicine* 21, 998–1003. doi:10.1016/j.phymed.2013.12.005

Zhou, Z., Lu, J., Liu, W. W., Manaenko, A., Hou, X., Mei, Q., et al. (2018). Advances in Stroke Pharmacology. *Pharmacol. Ther.* 191, 23–42. doi:10.1016/j.pharmthera.2018.05.012

Zhu, H., Hu, S. P., Li, Y. T., Sun, Y., Xiong, X. X., Hu, X. Y., et al. (2022). Interleukins and Ischemic Stroke. *Front. Immunol.* 13. doi:10.3389/fimmu.2022.828447

Zhu, J., Jiang, Y., Wu, L., Lu, T., Xu, G., and Liu, X. (2012). Suppression of Local Inflammation Contributes to the Neuroprotective Effect of Ginsenoside Rb1 in Rats with Cerebral Ischemia. *Neuroscience* 202, 342–351. doi:10.1016/j.neuroscience.2011.11.070

Conflict of Interest: NL was employed by the company Beijing Increasepharm Safety and Efficacy Co., Ltd.

The remaining authors declare that the research was conducted in the absence of any commercial or financial relationships that could be construed as a potential conflict of interest.

Publisher's Note: All claims expressed in this article are solely those of the authors and do not necessarily represent those of their affiliated organizations, or those of the publisher, the editors and the reviewers. Any product that may be evaluated in this article, or claim that may be made by its manufacturer, is not guaranteed or endorsed by the publisher.

frontiers | Frontiers in Pharmacology

TYPE Review
PUBLISHED 01 August 2022
DOI 10.3389/fphar.2022.972813

OPEN ACCESS

EDITED BY
Weicheng Hu,
Huaiyin Normal University, China

REVIEWED BY
Lun Wang,
Chengdu Institute of Biology (CAS), China
Haifeng Wu,
Chinese Academy of Medical Sciences and Peking Union Medical College, China
Kunming Qin,
Jiangsu Ocean Universiity, China

*CORRESPONDENCE
Mingxin Liu,
liumx@gdou.edu.cn
Shuai Wei,
weishuaiws@126.com

SPECIALTY SECTION
This article was submitted to Experimental Pharmacology and Drug Discovery, a section of the journal Frontiers in Pharmacology

RECEIVED 19 June 2022
ACCEPTED 04 July 2022
PUBLISHED 01 August 2022

CITATION
Yang Z, Deng J, Liu M, He C, Feng X, Liu S and Wei S (2022), A review for discovering bioactive minor saponins and biotransformative metabolites in Panax quinquefolius L.. *Front. Pharmacol.* 13:972813. doi: 10.3389/fphar.2022.972813

A review for discovering bioactive minor saponins and biotransformative metabolites in *Panax quinquefolius* L.

Zhiyou Yang[1,2], Jiahang Deng[1], Mingxin Liu[3]*, Chuantong He[1], Xinyue Feng[1], Shucheng Liu[1,2] and Shuai Wei[1,2]*

[1]Guangdong Provincial Key Laboratory of Aquatic Product Processing and Safety, Guangdong Province Engineering Laboratory for Marine Biological Products, Key Laboratory of Advanced Processing of Aquatic Product of Guangdong Higher Education Institution, Guangdong Provincial Engineering Technology Research Center of Seafood, College of Food Science and Technology, Guangdong Ocean University, Zhanjiang, China, [2]Collaborative Innovation Centre of Seafood Deep Processing, Dalian Polytechnic University, Dalian, China, [3]College of Electrical and Information Engineering, Guangdong Ocean University, Zhanjiang, China

Panax quinquefolius L. has attracted extensive attention worldwide because of its prominent pharmacological properties on type 2 diabetes, cancers, central nervous system, and cardiovascular diseases. Ginsenosides are active phytochemicals of *P. quinquefolius*, which can be classified as propanaxdiol (PPD)-type, propanaxtriol (PPT)-type, oleanane-type, and ocotillol-type oligoglycosides depending on the skeleton of aglycone. Recently, advanced analytical and isolated methods including ultra-performance liquid chromatography tandem with mass detector, preparative high-performance liquid chromatography, and high speed counter-current chromatography have been used to isolate and identify minor components in *P. quinquefolius*, which accelerates the clarification of the material basis. However, the poor bioavailability and undetermined bio-metabolism of most saponins have greatly hindered both the development of medicines and the identification of their real active constituents. Thus, it is essential to consider the bio-metabolism of constituents before and after absorption. In this review, we described the structures of minor ginsenosides in *P. quinquefolius*, including naturally occurring protype compounds and their *in vivo* metabolites. The preclinical and clinical pharmacological studies of the ginsenosides in the past few years were also summarized. The review will promote the reacquaint of minor saponins on the growing appreciation of their biological role in *P. quinquefolius*.

KEYWORDS

***Panax quinquefolius*, minor ginsenosides, metabolites, structural diversity, pharmacological effects**

Introduction

Ginseng root has historically been used as medicine food homology plant for thousand years in oriental countries. It occupies a prominent position in the list of best-selling natural medicines worldwide (Qi et al., 2011). *Panax ginseng* C.A. Meyer (known as Asian or Korean ginseng), *P. quinquefolius* (known as American ginseng), and *P. notoginseng* (Burkill) F.H. Chen (known as Sanchi ginseng) are three reputable folk medicine around the world. *P. quinquefolius* is one of the top 10 selling natural health products in the United States. Despite its high chemical similarity with Asian ginseng, *P. quinquefolius* instead exhibits heat-clearing and refreshing functions as a tonic medicinal plant (Yang et al., 2014). Modern pharmacological studies indicated *P. quinquefolius* exert a wide range of biological activities, such as hypoglycemic, cardiovascular protective, anti-diabetic, anti-tumor, anti-inflammatory, anti-obesity, anti-aging, and antimicrobial effects (Assinewe et al., 2003; Szczuka et al., 2019).

It is well documented that the triterpenoid saponins, called ginseng saponins or ginsenosides, are the major active compounds in *P. quinquefolius* (Yuan et al., 2010). The ginsenoside profile varies in this herb due to the cultivation in different areas in terms of total ginsenosides, the ratio of protopanaxadiol (PPD) to protopanaxatriol (PPT), and other marker ginsenosides. The type and contents of ginsenosides are also different in the root, stem/leaves, flower bud, and fruits. Thus, a wide spectrum of advanced analytical methods including ultra-performance liquid chromatography tandem with mass detector, preparative high-performance liquid chromatography, and high-speed counter-current chromatography have been used to isolate and identify minor components in *P. quinquefolius*, which accelerates the clarification of its material basis.

Rb1, Rb2, Rc, Re, and Rg1 are considered as major ginsenosides with high contents in *P. quinquefolius*. The multitude of sugar moieties in major ginsenosides affects their bioavailability after oral intake, as well as the biological activities. The bioactive ginsenosides *in vitro* do not always represent the real active form *in vivo*, due to the bio-metabolism of constituents by trillions of gut microbiota in the gastrointestinal tract and enzymes in blood and tissues after absorption. To link the health benefits of major ginsenosides to their effects, it is warranted to determine the profiles of *P. quinquefolius* and its minor metabolites.

In this review, the structural diversities of ginsenosides in different parts of *P. quinquefolius* are described, especially naturally occurring minor ginsenosides and those resulting from biotransformation. Preclinical and clinical studies of *P. quinquefolius* and ginsenosides are also delineated. Finally, special attention is paid to future research trends for *P. quinquefolius*, and targets identification of bioactive ginsenosides and their underlying mechanism exploration are discussed and prospected.

FIGURE 1
Geographical distribution of *P. quinquefolius* based on GMPGIS. The map was plotted using online ArcGIS (ESRI, Redland, CA, United States. URL: http://www.learngis2.maps.arcgis.com/). Flags showing cultivated or wild resources of *P. quinquefolius*.

TABLE 1 The natural occurring ginsenosides in different parts of *P. quinquefolius*.

No	Name	Type	Medicinal parts				Identification methods	References
			Root	Stem/ leaves	Flower buds	Fruits		
1	Rb1	PPD	√	√			NMR	Chen et al. (1981)
2	Rb2	PPD	√	√			NMR	Chen et al. (1981)
3	Rb3	PPD	√	√			NMR	Chen et al. (1981)
4	Rc	PPD	√	√			HPLC	Li et al. (1996)
5	Rd	PPD	√	√			NMR	Chen et al. (1981)
6	Q-I	PPD	√				NMR	Yoshikawa et al. (1998)
7	Q-II	PPD	√				NMR	Yoshikawa et al. (1998)
8	Q-III	PPD	√				NMR	Yoshikawa et al. (1998)
9	Q-V	PPD	√				NMR	Yoshikawa et al. (1998)
10	Malonyl-G-Rb1	PPD	√		√		NMR	Yoshikawa et al. (1998)
11	Pseudo-G-Rc1	PPD	√				NMR	Yoshikawa et al. (1998)
12	G-F2	PPD	√				NMR	Yoshikawa et al. (1998)
13	Gypenoside XVII	PPD	√				NMR	Yoshikawa et al. (1998)
14	Malonyl-G-Rb2	PPD	√		√		LC/MS/MS, NMR	Wang et al. (1999)
15	Malonyl-G-Rc	PPD	√		√		LC/MS/MS, NMR	Wang et al. (1999)
16	20(S)-G-Rh2	PPD		√			LC-MS/MS	Popovich and Kitts, (2004)
17	Rs1	PPD			√		NMR	Nakamura et al. (2007)
18	Pseudo-G-F8	PPD			√		NMR	Nakamura et al. (2007)
19	Q-L10	PPD		√			NMR	Chen et al. (2009)
20	Q-L14	PPD		√			NMR	Chen et al. (2009)
21	Q-L16	PPD		√			NMR	Chen et al. (2009)
22	20(S)-G-Rg3	PPD	√				NMR	Qi et al. (2011)
23	G-F8	PPD	√				NMR	Qi et al. (2011)
24	Malonyl-G-Rd	PPD			√		NMR	Wang et al. (2015b)
25	20(R)-G-Rg3	PPD	√				NMR	Qi et al. (2011)
26	20(R)-G-Rh2	PPD	√				NMR	Qi et al. (2011)
27	20(S)-PPD	PPD	√				NMR	Qi et al. (2011)
28	20(R)-PPD	PPD	√				NMR	Qi et al. (2011)
29	Q-IV	Modified PPD	√				NMR	Yoshikawa et al. (1998)
30	Notoginsenoside G	Modified PPD	√				NMR	Yoshikawa et al. (1998)
31	Notoginsenoside C	Modified PPD	√				NMR	Yoshikawa et al. (1998)
32	floralquinquenoside D	Modified PPD			√		NMR	Nakamura et al. (2007)
33	ginsenoside I	Modified PPD			√		NMR	Nakamura et al. (2007)
34	Notoginsenoside E	Modified PPD			√		NMR	Nakamura et al. (2007)
35	Notoginsenoside K	Modified PPD	√				NMR	Yoshikawa et al. (1998)
36	quinquenoside L3	Modified PPD		√			NMR	Wang et al. (1998)
37	Notoginsenoside A	Modified PPD	√				NMR	Yoshikawa et al. (1998)
38	quinquenoside L2	Modified PPD		√			NMR	Wang et al. (2001)
39	quinquenoside L1	Modified PPD		√			NMR	Wang et al. (2001)
40	Rg1	PPT	√	√			NMR	Chen et al. (1981)
41	Re	PPT	√	√			NMR	Chen et al. (1981)
42	Rf	PPT	√				NMR	Yoshikawa et al. (1998)
43	Rg2	PPT	√				NMR	Yoshikawa et al. (1998)
44	Rh1	PPT	√				NMR	Dou et al. (2006)
45	F1	PPT	√				NMR	Dou et al. (2006)

(Continued on following page)

TABLE 1 (*Continued*) The natural occurring ginsenosides in different parts of *P. quinquefolius*.

No	Name	Type	Medicinal parts				Identification methods	References
			Root	Stem/ leaves	Flower buds	Fruits		
46	F3	PPT			√		NMR	Nakamura et al. (2007)
47	Q-L17	PPT		√			NMR	Li et al. (2009)
48	Q-F6	PPT				√	NMR	Lu et al. (2012)
49	6'-O-Ac-G-Rg1	PPT	√				NMR	Qi et al. (2011)
50	20(S)-Ac-G-Rg2	PPT	√				NMR	Qi et al. (2011)
51	20(R)-Ac-G-Rg2	PPT	√				NMR	Qi et al. (2011)
52	F-E	PPT	√				NMR	Qi et al. (2011)
53	Malonyl-G-Re	PPT			√		NMR	Wang et al. (2015c)
54	Rg8	Modified PPT	√				NMR	Dou et al. (2006)
55	F4	Modified PPT	√				NMR	Dou et al. (2006)
56	floralquinquenoside E	PPT			√		NMR	Nakamura et al. (2007)
57	floralquinquenoside A	Modified PPT			√		NMR	Nakamura et al. (2007)
58	floralquinquenoside B	Modified PPT			√		NMR	Nakamura et al. (2007)
59	floralquinquenoside C	Modified PPT			√		NMR	Nakamura et al. (2007)
60	quinquenoside L9	Modified PPT			√		NMR	Nakamura et al. (2007)
61	24(R)-pseudo-G-F11	Ocotillol		√			NMR	Chen et al. (1981)
62	24(S)-pseudo-G-F11	Ocotillol			√		NMR	Nakamura et al. (2007)
63	pseudo-RT5	Ocotillol			√		NMR	Nakamura et al. (2007)
64	24(R)-vina-G-R1	Ocotillol			√		NMR	Nakamura et al. (2007)
65	12-one-pseudo-G-F11	Ocotillol		√			NMR	Qi et al. (2020)
66	Ocotillol	Ocotillol		√			NMR	Han et al. (2014)
67	3α-ocotillol	Ocotillol		√			NMR	Han et al. (2014)
68	pseudo-ginsenoside RT6	Modified Ocotillol		√			NMR	Liu et al. (2013)
69	pseudoginsengenin R1	Modified Ocotillol		√			NMR	Liu et al. (2013)
70	Chikusetsusaponin IVa	Oleanane	√				NMR	Yoshikawa et al. (1998)
71	G-Ro	Oleanane	√				NMR	Qi et al. (2011)
72	ginsenoside 1a	Modified type			√		NMR	Nakamura et al. (2007)
73	quinquefoloside-Ld	Modified type		√			NMR	Xiang et al. (2013)
74	quinquefoloside-Le	Modified type		√			NMR	Xiang et al. (2013)
75	dammar-20(S), 25(S)-epoxy-3β, 12β, 26-triol	Modified type	√				NMR	Han et al. (2016)

P. quinquefolius: Geographical distribution and application

P. quinquefolius was first found in 1716 by father Joseph-François Lafitau, a Jesuit priest in Canada. He stumbled across *P. quinquefolius* growing in the woods near Montreal. It is distributed native to the temperate forest regions of North America, from 67° to 95°W longitude and 30° to 48°N latitude, including North of Quebec and Ontario and South of Mississippi, Arkansas, and Georgia. Wild ginseng is still harvested from areas in Wisconsin, Pennsylvania, and New York State. *P. quinquefolius* was first introduced to China in 1975, and the major producing areas are Heilongjiang, Jilin, Liaoning, Hebei, Shandong, and Shanxi Provinces (Figure 1) (Shen et al., 2019).

P. quinquefolius can be cultivated in large number of countries except for the abovementioned places. Based on the environmental variables over 30 years from 1970 to 2000, and 226 global distribution areas of *P. quinquefolius*, the maximum entropy model (MaxEnt) was used to predict the global ecological suitable areas for *P. quinquefolius*. The potential ecological suitable places of *P. quinquefolius* were primarily in Changbai Mountain in China and Appalachian Mountain in America, in the range of 35°N–50°N, 110°E–145° and E35°N–50°N,

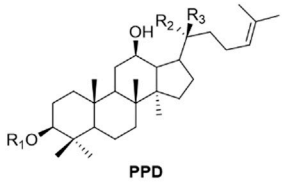

PPD

No	Name	R1	R2	R3
1	Rb1	glc^{2}→glc	CH_3	*O*-glc^{6}→glc
2	Rb2	glc^{2}→glc	CH_3	*O*-glc^{6}→arap
3	Rb3	glc^{2}→glc	CH_3	*O*-glc^{6}→xyl
4	Rc	glc^{2}→glc	CH_3	*O*-glc^{6}→araf
5	Rd	glc^{2}→glc	CH_3	*O*-glc
6	Q-I	glc^{2}→glc^{6}→Butenoyl	CH_3	*O*-glc
7	Q-II	glc^{2}→glc^{6}→Octenoyl	CH_3	*O*-glc^{6}→glc
8	Q-III	Ac←^{6}glc^{2}→glc	CH_3	*O*-glc
9	Q-V	glc^{2}→glc	CH_3	*O*-glc^{6}→glc^{4}→glc
10	Malonyl-G-Rb1	glc^{2}→^{1}glc^{6}→mal	CH_3	*O*-glc^{6}→glc
11	Pseudo-G-Rc1	glc^{2}→^{1}glc^{6}→Ac	CH_3	*O*-glc
12	G-F2	glc	CH_3	*O*-glc
13	Gypenoside XVII	glc	CH_3	*O*-glc^{6}→glc
14	Malonyl-G-Rb2	glc^{2}→^{1}glc^{6}→mal	CH_3	*O*-glc^{6}→arap
15	Malonyl-G-Rc	glc^{2}→^{1}glc^{6}→mal	CH_3	*O*-glc^{6}→araf
16	20*S*-G-Rh2	glc	CH_3	OH
17	Rs1	glc^{2}→^{1}glc^{6}→Ac	CH_3	*O*-glc^{6}→arap
18	Pseudo-G-F8	Ac←^{6}glc^{2}→glc	CH_3	*O*-glc^{6}→arap
19	Q-L10	glc	CH_3	*O*-glc^{6}→arap
20	Q-L14	glc^{2}→glc	CH_3	*O*-arap
21	Q-L16	glc^{2}→glc	CH_3	*O*-glc^{6}→glc
22	20*S*-G-Rg3	glc^{2}→glc	CH_3	OH
23	G-F8	Ac←^{6}glc^{2}→glc	CH_3	*O*-glc^{6}→arap
24	Malonyl-G-Rd	glc^{2}→glc^{6}→mal	CH_3	*O*-glc
25	20*R*-G-Rg3	glc^{2}→glc	OH	CH_3
26	20*R*-G-Rh2	glc	OH	CH_3
27	20*S*-PPD	H	CH_3	OH
28	20*R*-PPD	H	OH	CH_3

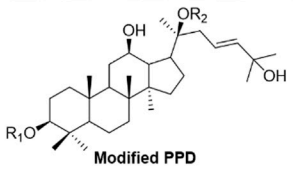

Modified PPD

No	Name	R1	R2
36	quinquenoside L3	glc	glc^{6}→xyl
37	Notoginsenoside A	glc^{2}→glc	glc^{6}→glc

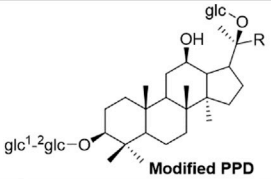

Modified PPD

No	Name	R
38	quinquenoside L2	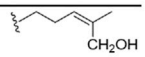
39	quinquenoside L1	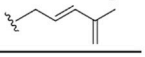

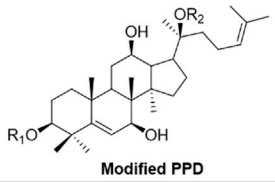

Modified PPD

No	Name	R1	R2
29	Q-IV	glc^{2}→glc	glc^{6}→glc
30	Notoginsenoside G	glc^{2}→glc	glc

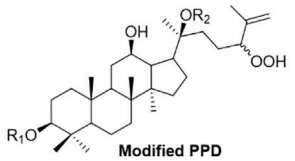

Modified PPD

No	Name	R1	R2
31	Notoginsenoside C	glc^{2}→glc	glc^{6}→glc
32	floralquinquenoside D	glc	glc
33	ginsenoside I	glc^{2}→glc	glc

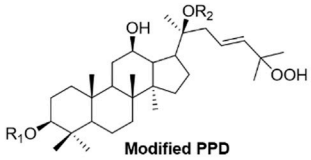

Modified PPD

No	Name	R1	R2
34	Notoginsenoside E	glc^{2}→glc	glc
35	Notoginsenoside K	glc^{2}→glc	glc^{6}→glc

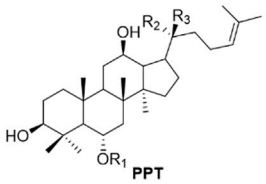

PPT

No	Name	R1	R2	R3
40	Rg1	glc	CH_3	*O*-glc
41	Re	glc^{2}→rha	CH_3	*O*-glc
42	Rf	glc^{2}→glc	CH_3	OH
43	Rg2	glc^{2}→rha	CH_3	OH
44	Rh1	glc	CH_3	OH
45	F1	H	CH_3	*O*-glc
46	F3	H	CH_3	*O*-glc^{6}→arap
47	Q-L17	glc	CH_3	*O*-glc^{6}→xyl
48	Q-F6	glc	CH_3	*O*-glc^{6}→araf
49	6'-*O*-Ac-G-Rg1	glc^{6}→Ac	CH_3	*O*-glc
50	20*S*-Ac-G-Rg2	glc^{2}→Ac	CH_3	OH
51	20*R*-Ac-G-Rg2	glc^{2}→Ac	OH	CH_3
52	F-E	glc^{2}→rha	CH_3	*O*-glc^{6}→xyl
53	Malonyl-G-Re	glc^{2}→rha	CH_3	*O*-glc^{6}→mal

FIGURE 2
Ginsenosides characterized from *P. quinquefolius*. PPD, Protopanaxadiol; PPT, protopanaxatriol; G, ginsenoside; Q, quinquenoside.

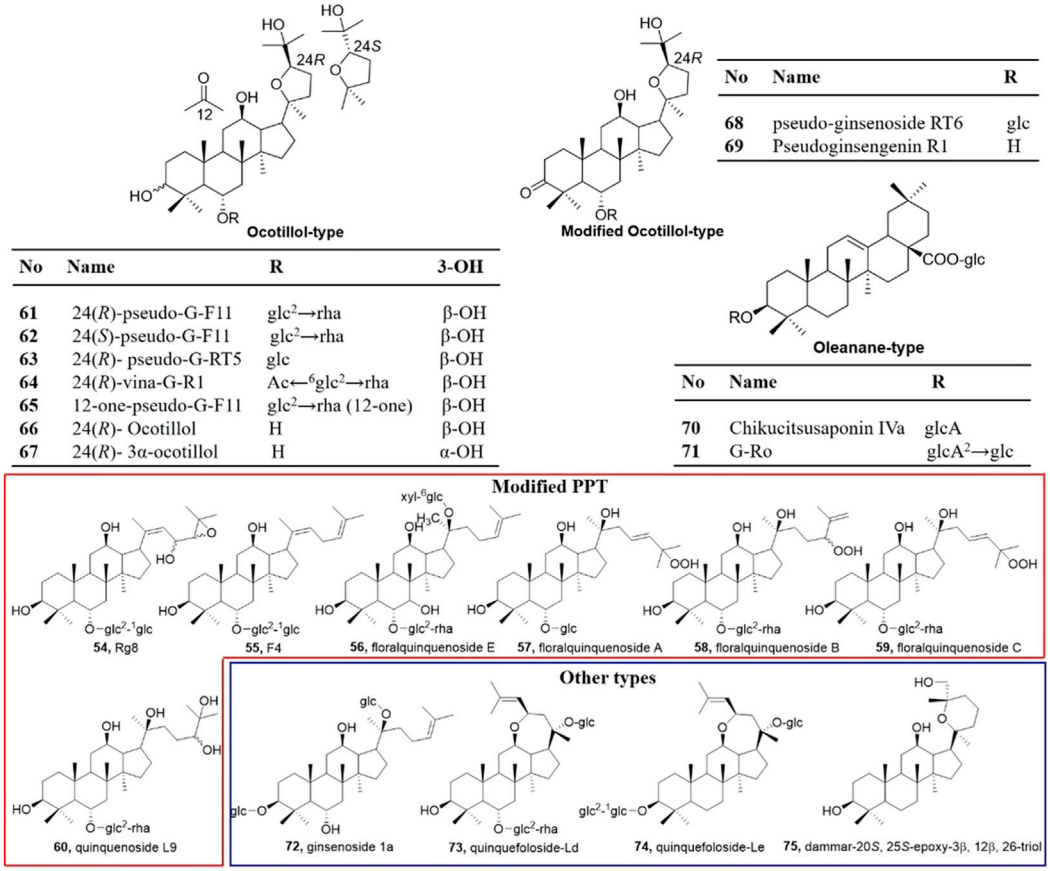

No	Name	R	3-OH
61	24(*R*)-pseudo-G-F11	glc^2→rha	β-OH
62	24(*S*)-pseudo-G-F11	glc^2→rha	β-OH
63	24(*R*)- pseudo-G-RT5	glc	β-OH
64	24(*R*)-vina-G-R1	Ac←^{6}glc^2→rha	β-OH
65	12-one-pseudo-G-F11	glc^2→rha (12-one)	β-OH
66	24(*R*)- Ocotillol	H	β-OH
67	24(*R*)- 3α-ocotillol	H	α-OH

No	Name	R
68	pseudo-ginsenoside RT6	glc
69	Pseudoginsengenin R1	H

No	Name	R
70	Chikucitsusaponin IVa	glcA
71	G-Ro	glcA^2→glc

glcA: β-D-glucopyranosiduronic acid; **glc**: β-D-glucopyranosyl; **mal:** malonyl; **rha:** α-L-rhamnopyranosyl; **araf:** α-L-arabinofuranosyl; **arap:** α-L-arabinopyranosyl; **Ac:** acetyl; **xyl:** β-D-xylpyranosyl

FIGURE 2
Continued.

60°W–120°W, respectively, including Canada, the United States, China, North and South Korea, Russia and Japan. Japan and South Korea were the potential producing regions (Zhang et al., 2018).

P. quinquefolius has been used by native Americans for a long history. It was used in Cherokee medicine for coughing, shortness of breath, headaches, digestive upset, fatigue, convulsions, female reproductive problems, and general weakness. An assortment of products containing *P. quinquefolius* are currently available on the market, including capsule, tablet, powder, and tea. The roots are implemented in drugs, cosmetic and skin care, food and feed additives. In United States, *P. quinquefolius* extracts are used in candies and drinks, while in China, they are used in alcoholic beverages (Szczuka et al., 2019).

Structural diversity of ginsenosides in *P. quinquefolius*

Ginsenosides, which share a unique dammarane type triterpenoid saponin structure (Fuzzati, 2004), are the major characteristic constituents of *P. quinquefolius*. More than 100 ginsenosides have been identified in *P. quinquefolius*, including naturally occurring compounds and those resulting from steaming and biotransformation (Yuan et al., 2010). The contents and types of ginsenosides vary from the roots, leaves, stems, flower buds and fruits of *P. quinquefolius* (Table 1). A comprehensive study was conducted to compare the components among different parts of *P. quinquefolius* and found that the root contains much more abundant Rb1, Ro, and mRb1 isomer, compared with the other parts. The stem leaf and flower bud show similar saponin composition, with richer m-Rb2, Rb3, and p-F11, than the root (Wang et al., 2019). Differences were found in sugar moieties, numbers, and sugar attachment at positions C-3, C-6, or C-20 and they provided diversity in ginsenoside structures (Qi et al., 2011). The carbonylation at C-3, dehydrogenation at C-5, 6 and changeable C-20 side-chain, and stereoisomerism further enrich the structural diversity of ginsenosides.

As summarized in Figure 2, ginsenosides in *P. quinquefolius* are generally classified into four groups, consisting of

TABLE 2 Biotransformation of major ginsenosides into rare ginsenosides.

Transformation pathways	Enzymes	Biotransformation conditions	Yield	Ref.
	Enzymatic transformation			
Rb1→Rd→20(S)-Rg3	*M. esteraromaticum* (β-glucosidase bgp1)	pH 7.0, 37°C, 6 h	74.3%	Quan et al. (2012d)
Rb1→Rd→Compound K	*M. esteraromaticum* (β-glucosidase bgp3)	pH 7.0, 40°C, 1 h	77%	Quan et al. (2012b)
Rb1→Compound K	*L. mesenteroides* DC102 (Crude glycosidase)	pH 6–8, 30°C, 72 h	99%	Quan et al. (2011)
Rb1→Rd	*A. niger* (β-glucosidase immobilized with amino-based silica)	pH 5.5, 45°C, 1 h	3.30-fold	Wu et al. (2021)
Rb1, Rb2, Rc, Rd→Ginsenoside F2	*Sphingomonas* sp. 2F2 (β-glucosidase bglSp)	pH 5.0, 37°C	—	Wang et al. (2011)
Rb2→Compound Y→Compound K	*M. esteraromaticum* (β-glycosidase)	pH 7.0, 40°C	—	Quan et al. (2012a)
Rb2→Rd→Compound K, Rb2→C-O→Compound K	*A. mellea* mycelium (β-glucosidase)	pH 4–4.5, 45–60°C, 72–96 h	—	Kim et al. (2018)
Rb2→Rd	α-L-Arabinopyranosidase	pH 7.0, 40°C, 1 h	—	Kim et al. (2020)
Rc→Rd	*T. thermarum* DSM5069 (a-L-arabinofuranosidase)	pH 5.0, 95°C	99.4%	Xie et al. (2016)
Re→Rg2, Rg1→Rh1	β-glucosidase (Bgp1)	pH 7.0, 37°C	100%, 78%	Quan et al. (2012c)
Rf→Rh1	*A. niger* (β-glucosidase (Bgl1))	pH 7.5, 37°C	—	Ruan et al. (2009)
Rf→Protopanaxatriol	*A. niger* (β-glucosidase)	pH 5.0, 55°C	90.4%	Liu et al. (2010a)
Rg1→Ginsenoside F1	*S. keddieii* (glycosidase bglSk)	pH 8.0, 25°C	100%	Kim et al. (2012)
	Microbial Transformation			
Rb1→Rd	*B. pyrrocinia* GP16, *Bacillus megaterium* GP27, *Sphingomonas echinoides* GP50	30°C, 48 h	99.5%–99.8%	Kim et al. (2005)
Rb1→Gypenoside LXXV	Fungus *E. vermicola* CNU 120806	pH 5.0, 50°C	95.4%	Hou et al. (2012)
Rb1→Ginsenoside XVII→Ginsenoside F2	*Intrasporangium* sp. GS603	27°C, 160 rpm, 72 h	—	Cheng et al. (2007)
Rb1→Ginsenoside F2	Rat Intestinal *Enterococcus gallinarum*	pH 7.0, 40°C	45%	Yan et al. (2021)
Rb1→Compound K	*L. mesenteroides* KFRI 690	37°C, 96 h	97.8%	Park et al. (2012)
Rb1→Compound K	Fungi *Arthrinium* sp. GE 17–18	30°C, 24 h	100%	Fu et al. (2016)
Rb1→3-keto and dehydrogenated C-K	*P. bainier* sp. 229	28°C, 5 days	—	Zhou et al. (2018)
Rb1→Rd→Rg3	*Microbacterium* sp. GS514	30°C, 48 h	41.4%	Cheng et al. (2008)
Rb1→Rd→Rg3	Bacterium *Burkholderia* sp. GE 17–7	pH 7.0, 30°C, 15 h	98%	Fu et al. (2017)
Rb1→Rd→Rg3	Bacterium *Flavobacterium* sp. GE 32	30°C, 72 h	—	Fu, (2019)
Rb1→Rd, Re→Rg2, Rg1→Rh1, Ginsenoside F1	*Cellulosimicrobium* sp. TH-20	pH 7.0, 30°C, 5 days	38%–96%	Yu et al. (2017)
Rb1→Compound K, Rg1→F1	*Cladosporium cladosporioides*	pH 7.0, 30°C	74.2%, 89.3%	Wu et al. (2012)
Rc→Rg3	*Leuconostoc* sp. BG78	37°C, 96 h	70%–75%	Ten et al. (2014a)
Rc→C-MC1	*Sphingopyxis* sp. BG97	37°C, 72 h	75%	Ten et al. (2014b)

(Continued on following page)

TABLE 2 (*Continued*) Biotransformation of major ginsenosides into rare ginsenosides.

Transformation pathways	Enzymes	Biotransformation conditions	Yield	Ref.
Rd→Compound K	*Lactobacillus pentosus* DC101	pH 7.0, 30°C, 3 days	97%	Quan et al. (2010)
Rg1→25-OH-20(*S*/*R*)-Rh1	*Cordyceps Sinensis*	28°C, 150 rpm, 6 days	82.5%	Sui et al. (2020)
Saponins→mainly Rg3, F2, Compound K	Human fecal microflora	37°C, 24 h	—	Wan et al. (2013)
Rb1, Rb2, Rb3, Rc→Compound K	Human intestinal bacteria	37°C, 48 h	83.5%–88.7%	Zheng et al. (2021)
	***In vivo* Transformation**			
Rb1→Rg3, Rh2→ Protopanaxadiol	Rat intestinal microbiota	Rat feces	—	Qian and Cai, (2010)
Rb1→Rb1+O	Rat plasma and urine	Plasma and urine	—	Wang et al. (2015a)
Rb1→Rd→Protopanaxadiol	Rat intestinal microbiota	Plasma, urine, and feces	—	Kang et al. (2016)
Rg1→Rg1+O	Rat plasma and urine	Plasma and urine	—	Wang et al. (2016)
Rg1, Re, Rf→Rh1→Protopanaxatriol	Rat intestinal microbiota	Plasma, urine, and feces	—	Dong et al. (2018)
Rg1, Re→Rh1, Rg2→F1, Rh1, Rg1	Human stomach and intestine	Plasma and urine	—	Tawab et al. (2003)
Rb1, Rc, Rd→Rg3, F2→Rh2, Compound K→Protopanaxadiol	Human intestinal microbiota	Plasma	—	Wan et al. (2016)

protopanaxadiol-type (PPD), protopanaxatriol-type (PPT), ocotillol-type, and oleanolic acid-type. PPD and PPT are the major groups of ginsenosides and are usually found in neutral forms. In the PPD-type, sugar residues are attached to β-OH at C-3 and/or C-20. Natural occurring PPD compounds include compounds 1–28. Compounds 29–30 with modified PPD structure were characterized by a double bond between C-5 and C-6 and a hydroxyl group in C-7 was isolated from the roots of *P. quinquefolius* (Yoshikawa et al., 1998). Compounds 31–39 were clarified as modified PPD structures with variable C-20 side-chains. In the PPT group, sugar moieties are attached to the α-OH at C-6 and/or β-OH at C-20. PPT constituents include compounds 40–60. PPD and PPT type ginsenosides constitute the main saponins in *P. quinquefolius*, and reports have shown that Rb1, Rb2, Rc, Rg1, Re, and Rd account for 90% of the total saponins (Wang et al., 2015b). Minor ginsenosides isolated from *P. quinquefolius* include ocotillol-type (compounds 61–69), oleanane-type (compounds 70–71), and dammarane saponins with a modified aglycone skeleton (compounds 29–39 and 54–60). A variety of minor ginsenosides have been isolated and the structures were elucidated via MS/MS, and NMR analysis. For example, in 1998, Yoshikawa et al. identified 5 dammarane-type triterpene oligoglycosides named quinquenosides I–V from the root of *P. quinquefolius*, along with notoginsenoside A, C, G, K, malonyl G-Rb1, pseudo-G-Rc1, gypenoside XVII, and chikusetsusaponin Iva (Yoshikawa et al., 1998). Three new dammarane-type saponins named quinquenosides L1–3 were isolated from the leaves and stems of *P. quinquefolius* collected in Canada (Wang et al., 1998; Wang et al., 2001). By using LC/MS/MS, the ginsenosides malonyl G-Rb2 and malonyl G-Rc were characterized in the root of *P. quinquefolius* (Wang et al., 1999). In 2004, a new dammarane-type triterpenoid saponin, ginsenoside Rg8, was isolated from the roots of *P. quinquefolius*, along with (20E)-ginsenoside F4, Rh1, and F1 (Dou et al., 2006). In 2007, from the flower buds of *P. quinquefolius*, 5 new dammarane-type triterpene glycosides, floralquinquenosides A, B, C, D, and E, along with 18 known ginsenosides were isolated and identified by NMR analysis (Nakamura et al., 2007). Four new triterpenoid saponin quinquenoside L10, 14, 16, and 17 were isolated from the leaves and stems of *P. quinquefolius* in 2009 (Chen et al., 2009; Li et al., 2009). Quinquenoside F6 was isolated from the fruits of *P. quinquefolius* (Lu et al., 2012). Two new dammarane-type saponins quinquefoloside-Ld and Le with a novel heptatomic ring between C-12 and C-17 from leaves of *P. quinquefolius* were elucidated (Xiang et al., 2013). Two new ocotillol-type compounds were isolated from the leaves and stems of *P. quinquefolium* L. and identified as pseudo-ginsenoside RT6 and pseudoginsengenin R1 (Liu et al., 2013). A new ocotillol-type ginsenoside, namely 12-one-pseudoginsenoside F_{11} (12-one-Pseudo-G-F_{11}), was isolated from stems and leaves of *P. quinquefolium* (Qi et al., 2020).

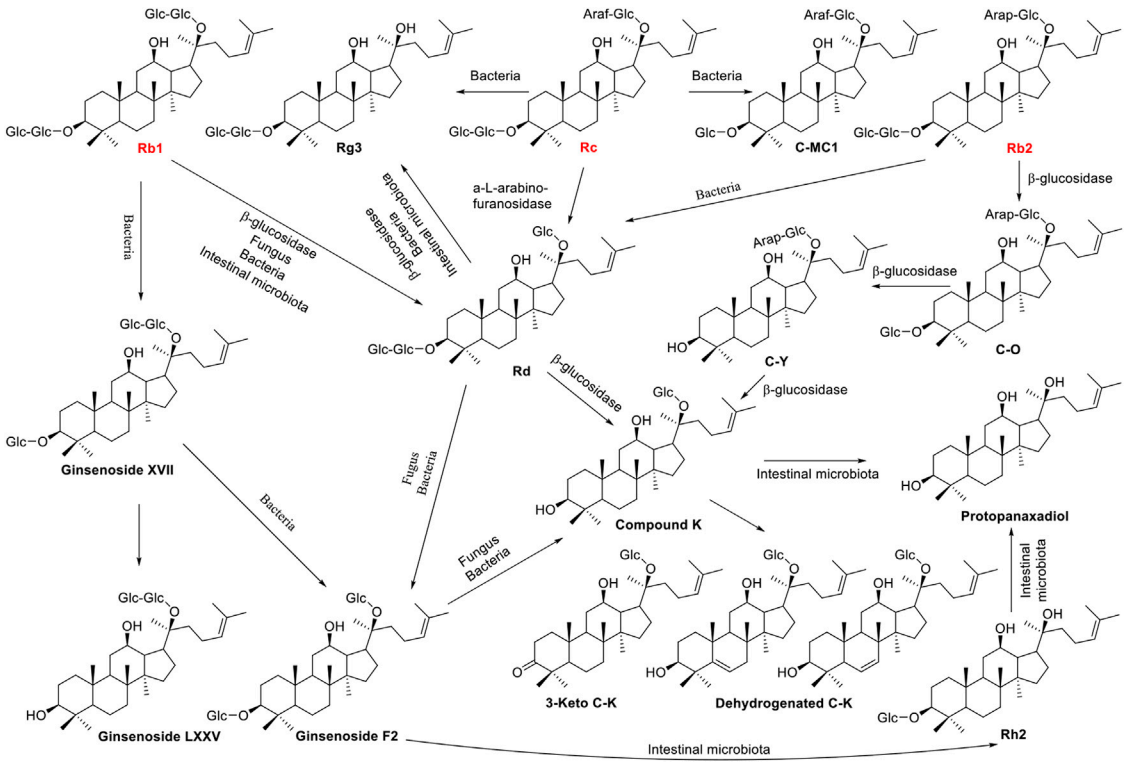

FIGURE 3
Schematic illustration of biotransformation of major PPD-type ginsenosides Rb1, Rb2, and Rc into minor ginsenosides.

The biotransformation of major ginsenosides into minor ginsenosides

The ginsenosides Rb1, Rb2, Rc, Re, and Rg1 are usually characterized as major ginsenosides, and account for more than 80% of total ginsenosides (Yu et al., 2017). The bioactive ginsenosides have been widely utilized in medical and chemical fields, which created a demand for their availability. However, the large size and poor cell membrane permeability of major ginsenosides restricted their absorption and bioavailability in human body after oral administration (Liu et al., 2010a). Therefore, the production of rare or minor smaller ginsenosides by transformation is urgently requisite. On the one hand, *in vitro* or *in vivo* biotransformation of major ginsenosides can generate an assortment of novel structural ginsenosides, resulted from the reduction of sugar moieties, substituent groups alteration and aglycone backbone changes. The small molecular ginsenosides are easily absorbed in the gastrointestinal tract after oral administration due to the deglucosylation (Ryu et al., 2017). In addition, a multitude of evidence showed that biotransformation of major ginsenosides to minor ginsenosides result in improved pharmacological activities (Quan et al., 2015; Ryu et al., 2017).

The deglycosylation of sugar moieties is mainly occurred in the transformation of major ginsenosides. Thermal and mild acid hydrolysis treatments show inefficient and low selective decomposition, while biotransformation including microbial enzymatic transformation, microbial transformation, and *in vivo* transformation, exerts high selectivity, lower by-products, and high targets yields. Thus, research on the biotransformation of major ginsenosides for increasing the bioavailability and pharmacological activities by structural modification of ginsenosides attracts more attention. The types, pathways, conditions, and yields of biotransformation were shown in Table 2.

Enzymatic transformation

Ginsenosides Rb1, Rb2, and Rc belong to protopanaxadiol (PPD) triterpenoid saponins, which are further modified by the glycosidation at the positions of C-3 and C-20 with different sugar moieties. The variable origin of microbial β-glucosidase determines the position and efficiency of deglycosylation. *Microbacterium esteraromaticum* derived β-glucosidase bgp1 catalyses ginsenoside Rb1 into 20(S)-Rg3 *via* intermediate product Rd, while β-glucosidase bgp3 transforms Rb1 into Compound K (C-K) *via* Rd (Quan et al., 2012b; Quan

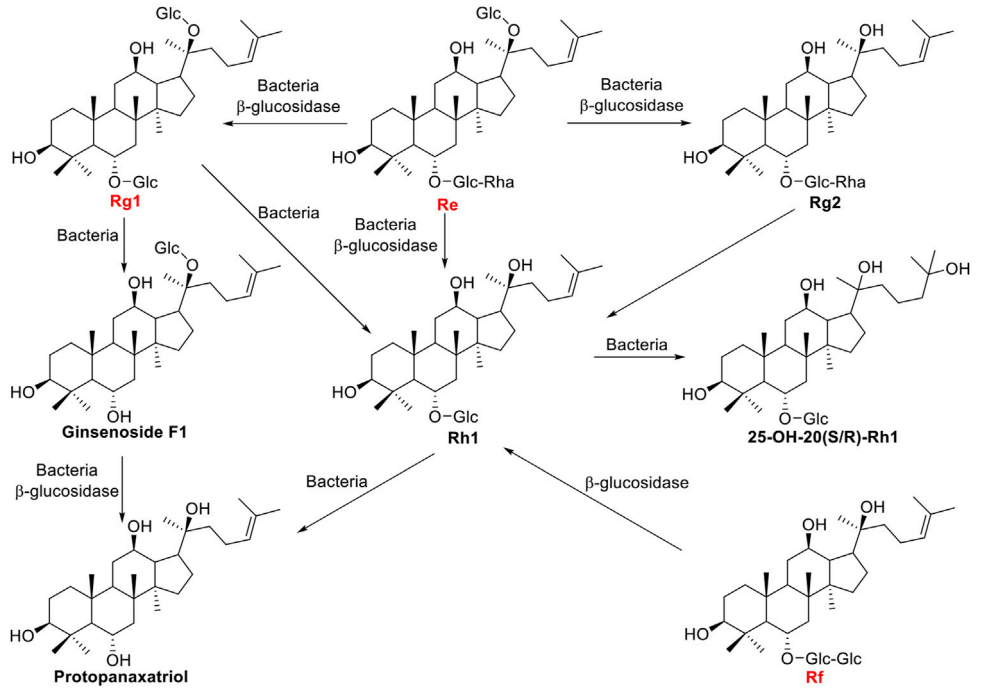

FIGURE 4
Schematic illustration of biotransformation of major PPT-type ginsenosides Re, Rf, and Rg1 into minor ginsenosides.

et al., 2012d). Intriguingly, crude glycosidase obtained from *Leuconostoc mesenteroides* DC102 transforms Rb1 into compound K with a yield of 99% after 3 days cultivation (Quan et al., 2011). In addition, an enzyme immobilization method was developed for the effective biotransformation of Rb1to Rd, and the catalytic efficiency of the immobilized β-glucosidase from *Aspergillus niger* was 3.30-fold higher than that of the free enzyme (Wu et al., 2021). Ginsenoside Rb2 can be transformed to Rd in the treatment of α-L-Arabinopyranosidase (Kim et al., 2020). While, after coculture Rb2 with β-glucosidase from *M. esteraromaticum* or *Armillaria mellea* mycelium, the product compound K was obtained via intermediate compounds Y, Rd, and C-O (Quan et al., 2012a; Kim et al., 2018). The a-L-arabinofuranosidase purified from *thermarum* DSM5069 catalyses ginsenoside Rc to Rd with a high yield of 99.4% (Xie et al., 2016). The biotransformation pathways were shown in Figure 3.

Ginsenosides Re, Rf, and Rg1 are another type of major ginsenosides belong to protopanaxatriol (PPT) triterpenoid saponins, and the positions of C-6 and C-20 are glycosidased with different sugar moieties. The β-glucosidase bgp1 gene consists of 2,496 bp encoding 831 amino acids which have homology to the glycosyl hydrolase families 3 protein domain. Recombinant β-glucosidase bgp1 transformed ginsenosides Re and Rg1 to ginsenosides Rg2 and Rh1, respectively (Quan et al., 2012c). A β-glucosidase gene isolated from *A. niger*, *bgl1*, was able to transform ginsenoside Rf into Rh1 (Ruan et al., 2009). The β-glucosidase finally transform Rh1 into PPT with a yield of 90.4% (Liu et al., 2010). Another β-glucosidase gene *bglSk*, isolated from *Sanguibacter keddieii*, consists of 1,857 bp and revealed significant homology to that of glycoside hydrolase family 3, which could convert major ginsenosides Rb1, Rb2, Rc, Rd, Re, and Rg1 into rare ginsenosides such as Compound Y, C-Mc, Compound K, Rg2(S), and F1. Kim et al. (2012) found *bglSk* could completely convert the Rg1 into F1. The biotransformation pathways were shown in Figure 4.

Collectively, the different β-glucosidase showed specialized catalysed position, and β-glucosidase bgp1 prefers to hydrolyse the glucosides at C-20 position, while β-glucosidase bglSk recognizes C-3 and C-6 position. However, β-glucosidase bgp3 and β-glucosidase isolated from *A. niger* do not show selectivity at C-6 and C-20.

Microbial transformation

Microbial transformation is effective in modifying ginsenosides to obtain new chemical derivatives and is also a major production method of minor ginsenosides. The enzymatic transformation showed advantages of a short reaction time, superior environmental protection, and high product yield and purity. However, the separation and purification processes of enzymes are high-cost and complicated, and the reaction

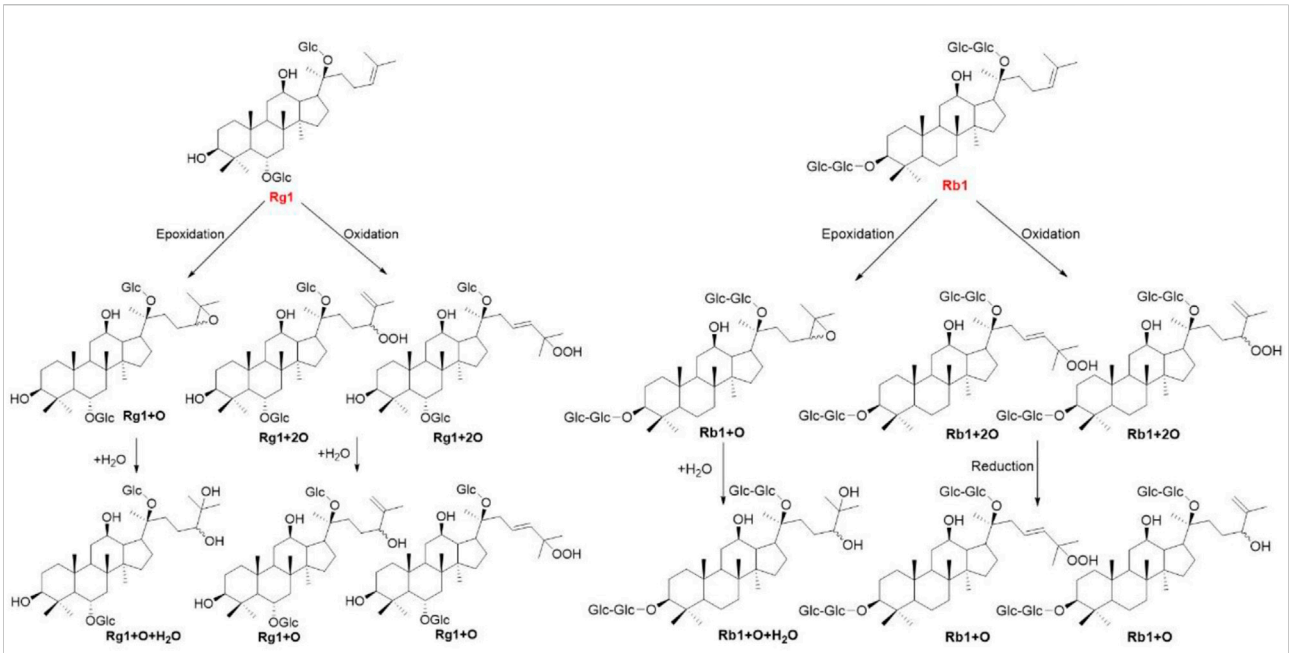

FIGURE 5
The oxygenated metabolites involved in *in vivo* biotransformation pathways of ginsenosides Rb1 and Rg1.

conditions are strictly controlled due to the susceptible enzyme activity. In contrast, microbial transformation is characterized by wide applications and low costs, but a dearth of high selectivity and a long conversion time. Thus, the combination of enzymatic and microbial transformation of ginsenosides could warrant the actual production process.

Burkholderia pyrrocinia GP16, *Bacillus megaterium* GP27, and *Sphingomonas echinoides* GP50 were screened from 70 strains of aerobic bacteria with β-glucosidase activity, and they almost completely transformed Rb1 to Rd (Kim et al., 2005). With the aid of bacteria *L. mesenteroides* KFRI 690 or Fungi *Arthrinium* sp. GE 17–18, ginsenoside Rb1 can be converted to Compound K efficiently with yields of 97.8% and 100%, respectively (Park et al., 2012; Fu et al., 2016). In addition, gypenoside LXXV and F2 were finally obtained *via* intermediate product Ginsenoside XVII without further conversion by Fungus *Esteya vermicola* CNU 120806 and bacteria *Intrasporangium* sp. GS603 transformation, respectively (Cheng et al., 2007; Hou et al., 2012). The scale-up fermentation was carried out using *Paecilomyces bainier* sp. 229, and ginsenoside Rb1 was converted to a known 3-keto C-K and two new dehydrogenated C-K metabolites (Figure 3), which were isolated through repeated silica gel column chromatography and high-pressure liquid chromatography (Zhou et al., 2018). Furthermore, several kinds of bacteria, such as *Microbacterium* sp. GS514, *Burkholderia* sp. GE 17–7, and *Flavobacterium* sp. GE 32, can transform Rb1 to Rg3 *via* the intermediate product Rd (Cheng et al., 2008; Fu et al., 2017; Fu, 2019). Rc was converted into minor ginsenosides Rg3 and C-MC1 with bacteria *Leuconostoc* sp. BG78 and *Sphingopyxis* sp. BG97, respectively (Ten et al., 2014a and Ten et al., 2014b). Sui et al. (2020) demonstrated that ginsenoside Rg1 could be thoroughly converted into 20(*S*/*R*)-Rh1 and 25-OH-20(*S*/*R*)-Rh1 by *Cordyceps Sinensis*, with a biocatalytic pathway established as Rg1→20(*S*/*R*)-Rh1→25-OH-20(*S*/*R*)-Rh1, and the molar bioconversion rate for total 25-OH-20(*S*/*R*)-Rh1 was 82.5%. Aside from bacteria and fungi, human fecal, and intestinal microflora could also transform ginsenosides. While human fecal microflora was prepared from a healthy Chinese man and subsequently incubated with *P. quinquefolius* saponins at 37°C for 24 h, three most abundant metabolites are identified with liquid chromatography/quadrupole time-of-flight mass spectrometry (LC–Q-TOF-MS) as 20(*S*)-ginsenoside Rg3, ginsenoside F2, and Compound K (Wan et al., 2013). Additionally, human intestinal bacteria were incubated with ginsenosides Rb_1, Rb_2, Rb_3 and Rc at 37°C under anaerobic conditions, and ginsenoside Compound K was identified as the transformed product after 48 h with transformation rates of 83.5%, 88.7%, 85.6%, and 84.2%, respectively (Zheng et al., 2021).

In vivo transformation

Gut microbiota mainly transform prototype ginsenosides into rare bioactive metabolites. Unlike *in vitro* enzyme and

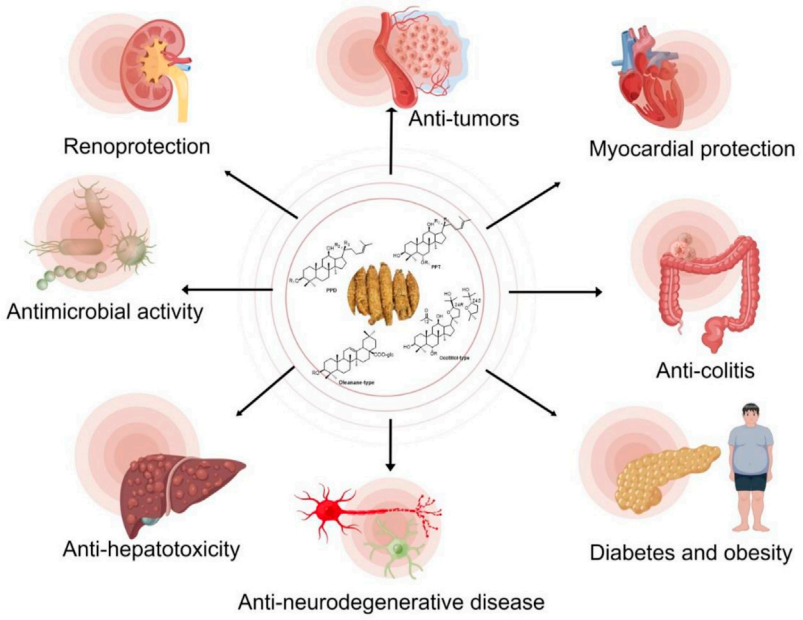

FIGURE 6
Biological and pharmacological activities of *P. quinquefolius* and its derived ginsenosides.

microbial transformation, the ginsenosides underlying anaerobically with pooled gut bacteria resulted in some novel metabolites in the plasma, bile, urine, and feces. After Rb1, Rg3, and Rh2 were administered to male Sprague Dawley rats at a dose of 100 mg/kg body weight, Rb1 and Rg3 could be metabolized to Rh2, while Rb1 could be metabolized to Rg3. The final products of Rb1, Rg3, and Rh2 were protopanaxadiol and monooxygenated protopanaxadiol (Qian and Cai, 2010). To further clarify the role of microbiota on metabolism of Rb1, ginsenoside Rb1 was administered to normal and antimicrobials treated rats, and the metabolites of Rb1, such as Rd, F2, and Compound K were detected in normal rat plasma but not in antimicrobials treated rats (Kang et al., 2016). Oxygenated metabolites have been considered as the major circulating metabolites of ginsenosides. After ginsenosides Rb1 and Rg1 were oral administered to rats for 24 h, totally 10 and 9 oxygenated metabolites were characterized by UHPLC-QTOF MS analysis, respectively (Figure 5) (Wang et al., 2015a; Wang et al., 2016). The degradation of ginsenosides has been thoroughly investigated in animals and *in vitro* using enzymes and microbiota, thus the elucidation of metabolites reaching the systemic circulation in human is of great importance. Six healthy male volunteers ingested 1 g of *P. quinquefolius* twice a day for 7 days. Totally, 5, 10, and 20 metabolites were detected in plasma, urine, and feces, respectively. And Compound K is found to be the major metabolite in all three samples (Wan et al., 2016).

Pharmacological activities of ginsenosides from *P. quinquefolius*

Anti-obesity and diabetes

PPD and PPT types of ginsenosides were purified from the leaves of *P. quinquefolius*, and the porcine pancreatic lipase activity was determined *in vitro*. PDG inhibited the pancreatic lipase activity in a dose-dependent manner at the concentrations of 0.25–1 mg/ml, while PPT showed no inhibitory activity. Moreover, PPD was effective in preventing and healing obesity, fatty liver and hypertriglyceridemia in mice fed with a high-fat diet (Liu et al., 2010b). Another clinical study indicated that the oral intake of *P. quinquefolius* extract with 1 g/meal (3 g/day) significantly reduced HbA1c and fasting blood glucose, and systolic blood pressure was also lowered (Vuksan et al., 2019). A dammarane from acid hydrolysates of *P. quinquefolius* total saponins, named 20(*R*)-dammarane-3β,12β,20,25-tetrahydroxy-3β-O-β-D-glucopyranoside, exhibited significantly inhibitory activity against α-glucosidase, and the IC_{50} value [(0.22 ± 0.21) μmol/L] was about 43-fold lower than the positive control acarbose, indicating the potential effects of saponins on diabetes (Han et al., 2020). After a 5-weeks treatment of malonyl ginsenosides from *P. quinquefolius*, the fasting blood glucose (FBG), triglyceride (TG), total cholesterol (TC), low-density lipoprotein cholesterol (LDL-C), nonesterified fatty acid (NEFA), alanine transaminase (ALT), and aspartate transaminase (AST) levels were significantly reduced and

glucose tolerance and insulin resistance were improved (Liu et al., 2021). IRS1/PI3K/Akt and IRS1/PI3K/Akt pathways are involved in the anti-T2DM effects of malonyl ginsenosides.

Anti-tumors

20(S)-PPD is a metabolite of ginseng saponin of *P. quinquefolius*, which significantly inhibited the growth and induced cell cycle arrest in HCT116 cells. An *in vivo* study showed that when i.p. administered (30 mg/kg) PPD once every 2 days for 3 weeks, xenograft tumor growth in athymic nude mice bearing HCT116 cells were inhibited (Gao et al., 2013). A structure-function relationship study indicated that sugar numbers within a ginsenoside exerted an inverse impact on tumor cells, and the sugar moiety at C-6 possess higher anti-cancer activity than that with linkages at C-3 or C-20, due to the increased steric hindrance to target proteins after C-6 was sugar substituted (Qi et al., 2010).

The number and position of hydroxyl groups in ginsenosides also affect their pharmacological activities. The substitution of hydroxyl or methoxyl groups at C-25 increases the anti-tumor effects of ginsenosides. Compared with 20(S)-Rh2, 20(S)-PPD and 20(S)-Rg3, 20(S)-25-OH-PPD showed the most apoptotic, antiproliferative, cell cycle arrest, and tumor growth inhibition effects *in vivo* (Wang et al., 2008b). In addition, usually 20(S) stereoisomers of ginsenosides show stronger chemopreventive effects than 20(R) stereoisomers (Qi et al., 2010).

Anti-neurodegenerative diseases

When fifty-two healthy volunteers (40–60 years old, mean age 51.63) received 200 mg of *P. quinquefolius* or a matching placebo for 1, 3, and 6 h according to a double-blind, placebo-controlled, balanced, crossover design, the result showed that cognitive performance on "Working Memory" was significantly improved after treatment for 3 h (Ossoukhova et al., 2015). In addition, Cereboost™, an extract of *P. quinquefolius* extract, restored Aβ1-42 which insulted downregulation of brain microtubule-associated protein 2 and synaptophysin as well as acetylcholine concentration, thus recovered the cognitive function (Shin et al., 2016). When APP/PS1 AD mice was administered by pseudoginsenoside-F11 at 8 mg/kg for 4 weeks, the expressions of β-amyloid precursor protein (APP) and Aβ1-40 in the cortex and hippocampus were significantly inhibited, and the activities of superoxide dismutase (SOD) and glutathione peroxidase (GSH-Px) were restored (Wang et al., 2013a). Additionally, pseudoginsenoside-F11 exerts anti-Parkinson effects through inhibiting free radical formation and stimulating endogenous antioxidant release in a 6-hydroxydopamine-lesioned rat model (Wang et al., 2013b).

Experimental autoimmune encephalomyelitis (EAE) is a commonly used experimental model for the demyelinating disease, multiple sclerosis (MS). An aqueous extract of ginseng (150 mg/kg body mass) was oral administered to MOG (35–55) peptide induced EAE mice, and the clinical signs of EAE, TNF-α expression, and iNOS and demyelination scores were significantly improved compared with model mice (Bowie et al., 2012). Pseudoginsenoside-F11 (4 and 8 mg/kg bw twice at a 4 h interval) significantly mitigated anxiety-like behavior in methamphetamine-induced rats, shortened the time of immobility in forced swimming test, and significantly decreased the number of errors in the T-maze test (Wu et al., 2003).

Others

The saponins from the leaves of *P. quinquefolius* showed a renoprotective effect in a mouse model of cisplatin-induced acute kidney injury. The further mechanism study clarified that saponins administration significantly suppressed the protein expression levels of Nox4, cleaved-Caspase-3, cleaved-Caspase-9, Bax, NF-κB, COX-2, and iNOS (Ma et al., 2017).

A MI/R model was constructed to investigate whether *P. quinquefolius* saponins decrease no-reflow phenomenon via suppression of inflammation, and the results showed that the inhibition of NLRP3 inflammasome *via* TLR4/MyD88/NF-κB signaling pathway is involved in *P. quinquefolius* saponins effects on cardiac functional improvement and pathological morphology changes of myocardium (Yu et al., 2021). Mice pretreated with saponins from the leaves of *P. quinquefolius* (150 or 300 mg/kg) by oral gavage for 7 days significantly reversed acetaminophen induced liver injury. Further study indicated that anti-oxidant, anti-apoptotic and anti-inflammatory activities were involved in its mechanism (Xu et al., 2017).

The heated *P. quinquefolius* could protect cell viability against H_2O_2-induced oxidative damage, and enhance the activities of superoxide dismutase and catalase dose dependently in V79-4 cells (Kim et al., 2007). Heat-processing reduced the content of ginsenosides Rb1, Re, Rc, and Rd, and increased the content of Rg2 and Rg3 in *P. quinquefolius*. After 2 h steaming, the percent content of ginsenoside Rg3 increased from 0.06% to 5.9%, and Rg3 showed the best antiproliferative effects in human breast cancer cell line MCF-7 *via* arresting cancer cells in G1-phase (Wang et al., 2008a).

Ginsenoside C-Y can be used as a potential botanical agent to protect premature skin from UVB-induced photodamage and prevent skin hyperpigmentation (Liu et al., 2019). Taken together, *P. quinquefolius* and its derived ginsenosides possess a variety of pharmacological activities (Figure 6), which is a promising medicinal plant for human health.

Conclusion and perspectives

Collectively, recent advances on the cultivation, chemical diversity, biotransformation, pharmacological, and clinical studies of *P. quinquefolius* were summarized in this review. A

total of 75 naturally occurring ginsenosides have been identified from the roots, leaves and stems, flower buds, and fruits of wild or cultivated *P. quinquefolius*. With the aid of advanced chemical and analytical techniques and the characterization of novel compounds, the diversity of ginsenosides is constantly revealed.

Major ginsenosides, the main components in *P. quinquefolius*, are usually difficult to be absorbed and exhibit low bioavailability. However, minor ginsenosides with relatively high bioavailability and pharmacological activities can be obtained by biotransformation. Some of *P. quinquefolius* associated bacteria, fungus or their enzymes were purified, with highly selectivity to the substituted sugar moieties in C-3, C-6 and C-20. The *in vitro* and *in vivo* metabolic pathways of major ginsenosides are also discussed. Moreover, the pharmacological activities of *P. quinquefolius* or its derived ginsenosides, including anti-tumor, anti-diabetes and obesity, anti-colitis, anti-hepatotoxicity, anti-neurodegenerative disease, myocardial, and renoprotection were exhibited and summarized.

In conclusion, *P. quinquefolius* is a very promising medicinal plant for the treatment of diverse diseases, while the greater attention of the following issues should be focused in the future: 1) Due to the low yields of naturally occurring minor ginsenosides, most of the novel compounds are not screened for their biological activities, and total or semi-synthesis and directional biotransformation may be efficient ways. 2) Although the pharmacological effects of some ginsenosides were investigated, the direct targets and mechanism are rarely discovered, which need to be further elucidated.

Author contributions

ZY generated the main idea, prepared the figures and tables, and wrote the manuscript. JD and CH performed literature search on pharmacological effects and biotransformation of ginsenosides. XF and SL performed literature search on ginsenoside structures. ZY performed the experiments and analysed the data. ML and SW performed a critical review of data and literature, edited the paper content and its final content.

Funding

This research was funded by the Natural Science Foundation of Guangdong Province of China (Nos. 2020A1515010779 and 2022A1515011419), National Natural Science Foundation of China (No. 62171143), and Special Program for Key Field of Guangdong Colleges (No. 2021ZDZX1060).

Conflict of interest

The authors declare that the research was conducted in the absence of any commercial or financial relationships that could be construed as a potential conflict of interest.

Publisher's note

References

Assinewe, V. A., Baum, B. R., Gagnon, D., and Arnason, J. T. (2003). Phytochemistry of wild populations of *Panax quinquefolius* L. (North American ginseng). *J. Agric. Food Chem.* 51, 4549–4553. doi:10.1021/jf030042h

Bowie, L. E., Roscoe, W. A., Lui, E. M., Smith, R., and Karlik, S. J. (2012). Effects of an aqueous extract of North American ginseng on MOG(35-55)-induced EAE in mice. *Can. J. Physiol. Pharmacol.* 90, 933–939. doi:10.1139/y2012-092

Chen, S. E., Staba, E. J., Taniyasu, S., Kasai, R., and Tanaka, O. (1981). Further study on dammarane-saponins of leaves and stems of American Ginseng, *Panax quinquefolium*. *Planta Med.* 42, 406–409. doi:10.1055/s-2007-971664

Chen, J., Zhao, R., Zeng, Y. M., Meng, H., Zuo, W. J., Li, X., et al. (2009). Three new triterpenoid saponins from the leaves and stems of *Panax quinquefolium*. *J. Asian Nat. Prod. Res.* 11, 195–201. doi:10.1080/10286020802682734

Cheng, L. Q., Na, J. R., Kim, M. K., Bang, M. H., and Yang, D. C. (2007). Microbial conversion of ginsenoside Rb1 to minor ginsenoside F2 and gypenoside XVII by *Intrasporangium* sp. GS603 isolated from soil. *J. Microbiol. Biotechnol.* 17, 1937–1943.

Cheng, L. Q., Na, J. R., Bang, M. H., Kim, M. K., and Yang, D. C. (2008). Conversion of major ginsenoside Rb1 to 20(*S*)-ginsenoside Rg3 by *Microbacterium* sp. GS514. *Phytochemistry* 69, 218–224. doi:10.1016/j.phytochem.2007.06.035

Dong, W. W., Han, X. Z., Zhao, J., Zhong, F. L., Ma, R., Wu, S., et al. (2018). Metabolite profiling of ginsenosides in rat plasma, urine and feces by LC-MS/MS and its application to a pharmacokinetic study after oral administration of *Panax ginseng* extract. *Biomed. Chromatogr.* 32, e4105. doi:10.1002/bmc.4105

Dou, D., Li, W., Guo, N., Fu, R., Pei, Y., Koike, K., et al. (2006). Ginsenoside Rg8, a new dammarane-type triterpenoid saponin from roots of *Panax quinquefolium*. *Chem. Pharm. Bull.* 54, 751–753. doi:10.1248/cpb.54.751

Fu, Y., Yin, Z. H., Wu, L. P., and Yin, C. R. (2016). Biotransformation of ginsenoside Rb1 to ginsenoside C-K by endophytic fungus *Arthrinium* sp. GE 17-18 isolated from *Panax ginseng*. *Lett. Appl. Microbiol.* 63, 196–201. doi:10.1111/lam.12606

Fu, Y., Yin, Z. H., and Yin, C. Y. (2017). Biotransformation of ginsenoside Rb1 to ginsenoside Rg3 by endophytic bacterium *Burkholderia* sp. GE 17-7 isolated from *Panax ginseng*. *J. Appl. Microbiol.* 122, 1579–1585. doi:10.1111/jam.13435

Fu, Y. (2019). Biotransformation of ginsenoside Rb1 to Gyp-XVII and minor ginsenoside Rg3 by endophytic bacterium *Flavobacterium* sp. GE 32 isolated from *Panax ginseng*. *Lett. Appl. Microbiol.* 68, 134–141. doi:10.1111/lam.13090

Fuzzati, N. (2004). Analysis methods of ginsenosides. *J. Chromatogr. B Anal. Technol. Biomed. Life Sci.* 812, 119–133. doi:10.1016/j.jchromb.2004.07.039

Gao, J. L., Lv, G. Y., He, B. C., Zhang, B. Q., Zhang, H., Wang, N., et al. (2013). Ginseng saponin metabolite 20(*S*)-protopanaxadiol inhibits tumor growth by targeting multiple cancer signaling pathways. *Oncol. Rep.* 30, 292–298. doi:10.3892/or.2013.2438

Han, L., Lin, M. Y., Zheng, Q., Liu, H. Y., Liu, H. Y., Dong, G., et al. (2014). A new epimer of ocotillol from stems and leaves of American ginseng. *Nat. Prod. Res.* 28, 935–939. doi:10.1080/14786419.2014.896008

Han, L., Li, Z., Zheng, Q., Liu, J. P., and Li, P. Y. (2016). A new triterpenoid compound from stems and leaves of American ginseng. *Nat. Prod. Res.* 30, 13–19. doi:10.1080/14786419.2015.1030403

Han, S., Shi, S., Zou, Y., Wang, Z., Wang, Y., Shi, L., et al. (2020). Chemical constituents from acid hydrolyzates of *Panax quinquefolius* total saponins and their inhibition activity to α-glycosidase and protein tyrosine phosphatase 1B. *Chin. Herb. Med.* 12, 195–199. doi:10.1016/j.chmed.2020.03.003

Hou, J. G., Xue, J. J., Sun, M. Q., Wang, C. Y., Liu, L., Zhang, D. L., et al. (2012). Highly selective microbial transformation of major ginsenoside Rb1 to gypenoside LXXV by *Esteya vermicola* CNU120806. *J. Appl. Microbiol.* 113, 807–814. doi:10.1111/j.1365-2672.2012.05400.x

Kang, A., Zhang, S., Zhu, D., Dong, Y., Shan, J., Xie, T., et al. (2016). Gut microbiota in the pharmacokinetics and colonic deglycosylation metabolism of ginsenoside Rb1 in rats: Contrary effects of antimicrobials treatment and restraint stress. *Chem. Biol. Interact.* 258, 187–196. doi:10.1016/j.cbi.2016.09.005

Kim, K. K., Lee, J. W., Lee, K. Y., and Yang, D. C. (2005). Microbial conversion of major ginsenoside rb(1) to pharmaceutically active minor ginsenoside rd. *J. Microbiol.* 43, 456–462. doi:10.1016/j.jgr.2015.11.004

Kim, K. T., Yoo, K. M., Lee, J. W., Eom, S. H., Hwang, I. K., Lee, C. Y., et al. (2007). Protective effect of steamed American ginseng (*Panax quinquefolius* L.) on V79-4 cells induced by oxidative stress. *J. Ethnopharmacol.* 111, 443–450. doi:10.1016/j.jep.2007.01.004

Kim, J. K., Cui, C. H., Yoon, M. H., Kim, S. C., and Im, W. T. (2012). Bioconversion of major ginsenosides Rg1 to minor ginsenoside F1 using novel recombinant ginsenoside hydrolyzing glycosidase cloned from *Sanguibacter keddieii* and enzyme characterization. *J. Biotechnol.* 161, 294–301. doi:10.1016/j.jbiotec.2012.06.021

Kim, M. J., Upadhyaya, J., Yoon, M. S., Ryu, N. S., Song, Y. E., Park, H. W., et al. (2018). Highly regioselective biotransformation of ginsenoside Rb2 into compound Y and compound K by β-glycosidase purified from *Armillaria mellea* mycelia. *J. Ginseng Res.* 42, 504–511. doi:10.1016/j.jgr.2017.07.001

Kim, J. H., Oh, J. M., Chun, S., Park, H. Y., and Im, W. T. (2020). Enzymatic biotransformation of ginsenoside Rb_2 into rd by recombinant α-L-arabinopyranosidase from *Blastococcus saxobsidens*. *J. Microbiol. Biotechnol.* 30, 391–397. doi:10.4014/jmb.1910.10065

Li, T. S. C., Mazza, G., Cottrell, A. C., and Gao, L. (1996). Ginsenosides in roots and leaves of American ginseng. *J. Agric. Food Chem.* 44, 717–720. doi:10.1021/jf950309f

Li, G. Y., Zeng, Y. M., Meng, H., Li, X., and Wang, J. H. (2009). A new triterpenoid saponin from the leaves and stems of *Panax quinquefolium* L. *Chin. Chem. Lett.* 20, 1207–1210. doi:10.1016/j.cclet.2009.05.017

Liu, J. P., Tian, X., Liu, H. Y., Zhang, Q. H., Lu, D., Li, P. Y., et al. (2013). Two novel dammarane-type compounds from the leaves and stems of *Panax quinquefolium* L. *J. Asian Nat. Prod. Res.* 15, 974–978. doi:10.1080/10286020.2013.794416

Liu, X. Y., Xiao, Y. K., Hwang, E., Haeng, J. J., and Yi, T. H. (2019). Antiphotoaging and antimelanogenesis properties of ginsenoside C-Y, a ginsenoside Rb2 metabolite from American ginseng PDD-ginsenoside. *Photochem. Photobiol.* 95, 1412–1423. doi:10.1111/php.13116

Liu, Z., Qu, C. Y., Li, J. X., Wang, Y. F., Li, W., Wang, C. Z., et al. (2021). Hypoglycemic and hypolipidemic effects of malonyl ginsenosides from American ginseng (*Panax quinquefolius* L.) on type 2 diabetic mice. *ACS Omega* 6, 33652–33664. doi:10.1021/acsomega.1c04656

Liu, L., Gu, L. J., Zhang, D. L., Wang, Z., Wang, C. Y., Li, Z., et al. (2010a). Microbial conversion of rare ginsenoside Rf to 20(*S*)-protopanaxatriol by *Aspergillus niger*. *Biosci. Biotechnol. Biochem.* 74, 96–100. doi:10.1271/bbb.90596

Liu, R., Zhang, J., Liu, W., Kimura, Y., and Zheng, Y. (2010b). Anti-Obesity effects of protopanaxdiol types of Ginsenosides isolated from the leaves of American ginseng (*Panax quinquefolius* L.) in mice fed with a high-fat diet. *Fitoterapia* 81, 1079–1087. doi:10.1016/j.fitote.2010.07.002

Lu, D., Li, P., and Liu, J. (2012). Quinquenoside F_6, a new triterpenoid saponin from the fruits of *Panax quinquefolium* L. *Nat. Prod. Res.* 26, 1395–1401. doi:10.1080/14786419.2011.592833

Ma, Z. N., Li, Y. Z., Li, W., Yan, X. T., Yang, G., Zhang, J., et al. (2017). Nephroprotective effects of saponins from leaves of *Panax quinquefolius* against cisplatin-induced acute kidney injury. *Int. J. Mol. Sci.* 18, 1407. doi:10.3390/ijms18071407

Nakamura, S., Sugimoto, S., Matsuda, H., and Yoshikawa, M. (2007). Medicinal flowers. XVII. New dammarane-type triterpene glycosides from flower buds of American ginseng, Panax quinquefolium L. *Chem. Pharm. Bull.* 55, 1342–1348. doi:10.1248/cpb.55.1342

Ossoukhova, A., Owen, L., Savage, K., Meyer, M., Ibarra, A., Roller, M., et al. (2015). Improved working memory performance following administration of a single dose of American ginseng (*Panax quinquefolius* L.) to healthy middle-age adults. *Hum. Psychopharmacol.* 30, 108–122. doi:10.1002/hup.2463

Park, S. J., Youn, S. Y., Ji, G. E., and Park, M. S. (2012). Whole cell biotransformation of major ginsenosides using *leuconostocs* and *lactobacilli*. *Food Sci. Biotechnol.* 21, 839–844. doi:10.1007/s10068-012-0108-z

Popovich, D. G., and Kitts, D. D. (2004). Mechanistic studies on protopanaxadiol, Rh2, and ginseng (*Panax quinquefolius*) extract induced cytotoxicity in intestinal Caco-2 cells. *J. Biochem. Mol. Toxicol.* 18, 143–149. doi:10.1002/jbt.20019

Qi, L. W., Wang, C. Z., and Yuan, C. S. (2010). American ginseng: potential structure-function relationship in cancer chemoprevention. *Biochem. Pharmacol.* 80, 947–954. doi:10.1016/j.bcp.2010.06.023

Qi, L. W., Wang, C. Z., and Yuan, C. S. (2011). Ginsenosides from American ginseng: chemical and pharmacological diversity. *Phytochemistry* 72, 689–699. doi:10.1016/j.phytochem.2011.02.012

Qi, Z., Wang, Z., Zhou, B., Fu, S., Hong, T., Li, P., et al. (2020). A new ocotillol-type ginsenoside from stems and leaves of *Panax quinquefolium* L. and its anti-oxidative effect on hydrogen peroxide exposed A549 cells. *Nat. Prod. Res.* 34, 2474–2481. doi:10.1080/14786419.2018.1543677

Qian, T., and Cai, Z. (2010). Biotransformation of ginsenosides Rb1, Rg3 and Rh2 in rat gastrointestinal tracts. *Chin. Med.* 5, 19. doi:10.1186/1749-8546-5-19

Quan, L. H., Cheng, L. Q., Kim, H. B., Kim, J. H., Son, N. R., Kim, S. Y., et al. (2010). Bioconversion of ginsenoside rd into compound k by *lactobacillus pentosus* dc101 isolated from kimchi. *J. Ginseng Res.* 34, 288–295. doi:10.5142/jgr.2010.34.4.288

Quan, L. H., Piao, J. Y., Min, J. W., Kim, H. B., Kim, S. R., Yang, D. U., et al. (2011). Biotransformation of ginsenoside Rb1 to prosapogenins, gypenoside XVII, ginsenoside rd, ginsenoside F2, and compound K by *Leuconostoc mesenteroides* DC102. *J. Ginseng Res.* 35, 344–351. doi:10.5142/jgr.2011.35.3.344

Quan, L. H., Jin, Y., Wang, C., Min, J. W., Kim, Y. J., Yang, D. C., et al. (2012a). Enzymatic transformation of the major ginsenoside Rb2 to minor compound Y and compound K by a ginsenoside-hydrolyzing β-glycosidase from *Microbacterium esteraromaticum*. *J. Ind. Microbiol. Biotechnol.* 39, 1557–1562. doi:10.1007/s10295-012-1158-1

Quan, L. H., Min, J. W., Jin, Y., Wang, C., Kim, Y. J., Yang, D. C., et al. (2012b). Enzymatic biotransformation of ginsenoside Rb1 to compound K by recombinant β-glucosidase from *Microbacterium esteraromaticum*. *J. Agric. Food Chem.* 60, 3776–3781. doi:10.1021/jf300186a

Quan, L. H., Min, J. W., Sathiyamoorthy, S., Yang, D. U., Kim, Y. J., and Yang, D. C. (2012c). Biotransformation of ginsenosides Re and Rg1 into ginsenosides Rg2 and Rh1 by recombinant β-glucosidase. *Biotechnol. Lett.* 34, 913–917. doi:10.1007/s10529-012-0849-z

Quan, L. H., Min, J. W., Yang, D. U., Kim, Y. J., and Yang, D. C. (2012d). Enzymatic biotransformation of ginsenoside Rb1 to 20(*S*)-Rg3 by recombinant β-glucosidase from *Microbacterium esteraromaticum*. *Appl. Microbiol. Biotechnol.* 94, 377–384. doi:10.1007/s00253-011-3861-7

Quan, K., Liu, Q., Wan, J. Y., Zhao, Y. J., Guo, R. Z., Alolga, R. N., et al. (2015). Rapid preparation of rare ginsenosides by acid transformation and their structure-activity relationships against cancer cells. *Sci. Rep.* 5, 8598. doi:10.1038/srep08598

Ruan, C. C., Zhang, H., Zhang, L. X., Liu, Z., Sun, G. Z., Lei, J., et al. (2009). Biotransformation of ginsenoside Rf to Rh1 by recombinant beta-glucosidase. *Molecules* 14, 2043–2048. doi:10.3390/molecules14062043

Ryu, J., Lee, H. W., Yoon, J., Seo, B., Kwon, D. E., Shin, U. M., et al. (2017). Effect of hydrothermal processing on ginseng extract. *J. Ginseng Res.* 41, 572–577. doi:10.1016/j.jgr.2016.12.002

Shen, L., Li, X. W., Meng, X. X., Wu, J., Tang, H., Huang, L. F., et al. (2019). Prediction of the globally ecological suitability of *Panax quinquefolius* by the geographic information system for global medicinal plants (GMPGIS). *Chin. J. Nat. Med.* 17, 481–489. doi:10.1016/S1875-5364(19)30069-X

Shin, K., Guo, H., Cha, Y., Ban, Y. H., Seo, da. W., Choi, Y., et al. (2016). Cereboost™, an American ginseng extract, improves cognitive function via up-regulation of choline acetyltransferase expression and neuroprotection. *Regul. Toxicol. Pharmacol.* 78, 53–58. doi:10.1016/j.yrtph.2016.04.006

Sui, X., Liu, J., Xin, Y., Qu, M., Qiu, Y., He, T., et al. (2020). Highly regioselective biotransformation of ginsenoside Rg1 to 25-OH derivatives of 20(S/R)-Rh1 by *Cordyceps Sinensis*. *Bioorg. Med. Chem. Lett.* 30, 127504. doi:10.1016/j.bmcl.2020.127504

Szczuka, D., Nowak, A., Zakłos-Szyda, M., Kochan, E., Szymańska, G., Motyl, I., et al. (2019). American ginseng (*Panax quinquefolium* L.) as a source of bioactive phytochemicals with pro-health properties. *Nutrients* 11, 1041. doi:10.3390/nu11051041

Tawab, M. A., Bahr, U., Karas, M., Wurglics, M., and Schubert-Zsilavecz, M. (2003). Degradation of ginsenosides in humans after oral administration. *Drug Metab. Dispos.* 31, 1065–1071. doi:10.1124/dmd.31.8.1065

Ten, L. N., Chae, S. M., and Yoo, S. A. (2014a). Transformation of ginsenoside rc into (20S)-Rg3 by the *bacterium Leuconostoc* sp. BG78. *Chem. Nat. Compd.* 50, 562–564. doi:10.1007/s10600-014-1018-5

Ten, L. N., Chae, S. M., and Yoo, S. A. (2014b). Biotransformation of ginsenoside rc into c-mc1 by the *bacterium sphingopyxis* sp. bg97. *Chem. Nat. Compd.* 50, 565–567. doi:10.1007/s10600-014-1019-4

Vuksan, V., Xu, Z. Z., Jovanovski, E., Jenkins, A. L., Beljan-Zdravkovic, U., Sievenpiper, J. L., et al. (2019). Efficacy and safety of American ginseng (*Panax quinquefolius* L.) extract on glycemic control and cardiovascular risk factors in individuals with type 2 diabetes: a double-blind, randomized, cross-over clinical trial. *Eur. J. Nutr.* 58, 1237–1245. doi:10.1007/s00394-018-1642-0

Wan, J. Y., Liu, P., Wang, H. Y., Qi, L. W., Wang, C. Z., Li, P., et al. (2013). Biotransformation and metabolic profile of American ginseng saponins with human intestinal microflora by liquid chromatography quadrupole time-of-flight mass spectrometry. *J. Chromatogr. A* 1286, 83–92. doi:10.1016/j.chroma.2013.02.053

Wan, J. Y., Wang, C. Z., Liu, Z., Zhang, Q. H., Musch, M. W., Bissonnette, M., et al. (2016). Determination of American ginseng saponins and their metabolites in human plasma, urine and feces samples by liquid chromatography coupled with quadrupole time-of-flight mass spectrometry. *J. Chromatogr. B Anal. Technol. Biomed. Life Sci.* 1015-1016, 62–73. doi:10.1016/j.jchromb.2016.02.008

Wang, J., Li, W., and Li, X. (1998). A new saponin from the leaves and stems of *Panax quinquefolium* L. collected in Canada. *J. Asian Nat. Prod. Res.* 1, 93–97. doi:10.1080/10286029808039849

Wang, X., Sakuma, T., Asafu-Adjaye, E., and Shiu, G. K. (1999). Determination of ginsenosides in plant extracts from *Panax ginseng* and *Panax quinquefolius* L. by LC/MS/MS. *Anal. Chem.* 71, 1579–1584. doi:10.1021/ac980890p

Wang, J. H., Li, W., Sha, Y., Tezuka, Y., Kadota, S., Li, X., et al. (2001). Triterpenoid saponins from leaves and stems of *Panax quinquefolium* L. *J. Asian Nat. Prod. Res.* 3, 123–130. doi:10.1080/10286020108041379

Wang, C. Z., Aung, H. H., Zhang, B., Sun, S., Li, X. L., He, H., et al. (2008a). Chemopreventive effects of heat-processed *Panax quinquefolius* root on human breast cancer cells. *Anticancer Res.* 28, 2545–2551.

Wang, W., Wang, H., Rayburn, E. R., Zhao, Y., Hill, D. L., Zhang, R., et al. (2008b). 20(*S*)-25-methoxyl-dammarane-3beta, 12beta, 20-triol, a novel natural product for prostate cancer therapy: activity *in vitro* and *in vivo* and mechanisms of action. *Br. J. Cancer* 98, 792–802. doi:10.1038/sj.bjc.6604227

Wang, L., Liu, Q. M., Sung, B. H., An, D. S., Lee, H. G., Kim, S. G., et al. (2011). Bioconversion of ginsenosides Rb(1), Rb(2), rc and rd by novel β-glucosidase hydrolyzing outer 3-O glycoside from *Sphingomonas sp*. 2F2: cloning, expression, and enzyme characterization. *J. Biotechnol.* 156, 125–133. doi:10.1016/j.jbiotec.2011.07.024

Wang, C. M., Liu, M. Y., Wang, F., Wei, M. J., Wang, S., Wu, C. F., et al. (2013a). Anti-amnesic effect of pseudoginsenoside-F11 in two mouse models of Alzheimer's disease. *Pharmacol. Biochem. Behav.* 106, 57–67. doi:10.1016/j.pbb.2013.03.010

Wang, J. Y., Yang, J. Y., Wang, F., Fu, S. Y., Hou, Y., Jiang, B., et al. (2013b). Neuroprotective effect of pseudoginsenoside-f11 on a rat model of Parkinson's disease induced by 6-hydroxydopamine. *Evid. Based. Complement. Altern. Med.* 2013, 152798. doi:10.1155/2013/152798

Wang, J. R., Yau, L. F., Tong, T. T., Feng, Q. T., Bai, L. P., Ma, J., et al. (2015a). Characterization of oxygenated metabolites of ginsenoside Rb1 in plasma and urine of rat. *J. Agric. Food Chem.* 63, 2689–2700. doi:10.1021/acs.jafc.5b00710

Wang, Y., Choi, H. K., Brinckmann, J. A., Jiang, X., and Huang, L. (2015b). Chemical analysis of *Panax quinquefolius* (North American ginseng): A review. *J. Chromatogr. A* 1426, 1–15. doi:10.1016/j.chroma.2015.11.012

Wang, Y. S., Jin, Y. P., Gao, W., Xiao, S. Y., Zhang, Y. W., Zheng, P. H., et al. (2015c). Complete (1)H-NMR and (13)C-NMR spectral assignment of five malonyl ginsenosides from the fresh flower buds of *Panax ginseng*. *J. Ginseng Res.* 40, 245–250. doi:10.1016/j.jgr.2015.08.003

Wang, J. R., Tong, T. T., Yau, L. F., Chen, C. Y., Bai, L. P., Ma, J., et al. (2016). Characterization of oxygenated metabolites of ginsenoside Rg1 in plasma and urine of rat. *J. Chromatogr. B Anal. Technol. Biomed. Life Sci.* 1026, 75–86. doi:10.1016/j.jchromb.2015.12.028

Wang, H., Zhang, C., Zuo, T., Li, W., Jia, L., Wang, X., et al. (2019). In-depth profiling, characterization, and comparison of the ginsenosides among three different parts (the root, stem leaf, and flower bud) of *Panax quinquefolius* L. by ultra-high performance liquid chromatography/quadrupole-Orbitrap mass spectrometry. *Anal. Bioanal. Chem.* 411, 7817–7829. doi:10.1007/s00216-019-02180-8

Wu, C. F., Liu, Y. L., Song, M., Liu, W., Wang, J. H., Li, X., et al. (2003). Protective effects of pseudoginsenoside-F11 on methamphetamine-induced neurotoxicity in mice. *Pharmacol. Biochem. Behav.* 76, 103–109. doi:10.1016/s0091-3057(03)00215-6

Wu, L., Jin, Y., Yin, C., and Bai, L. (2012). Co-transformation of Panax major ginsenosides Rb_1 and Rg_1 to minor ginsenosides C-K and F_1 by *Cladosporium cladosporioides*. *J. Ind. Microbiol. Biotechnol.* 39, 521–527. doi:10.1007/s10295-011-1058-9

Wu, X., Qu, B., Liu, Y., Ren, X., Wang, S., Quan, Y., et al. (2021). Highly enhanced activity and stability via affinity induced immobilization β-glucosidase from *Aspergillus niger* onto amino-based silica for the biotransformation of ginsenoside Rb1. *J. Chromatogr. A* 1653, 462388. doi:10.1016/j.chroma.2021.462388

Xiang, Z., Lv, J., Zhou, Z., Li, Y., Dou, D., Zhao, J., et al. (2013). Two new dammarane-type saponins from leaves of *Panax quinquefolium*. *Nat. Prod. Res.* 27, 1271–1276. doi:10.1080/14786419.2012.730045

Xie, J., Zhao, D., Zhao, L., Pei, J., Xiao, W., Ding, G., et al. (2016). Characterization of a novel arabinose-tolerant α-L-arabinofuranosidase with high ginsenoside Rc to ginsenoside Rd bioconversion productivity. *J. Appl. Microbiol.* 120, 647–660. doi:10.1111/jam.13040

Xu, X. Y., Hu, J. N., Liu, Z., Zhang, R., He, Y. F., Hou, W., et al. (2017). Saponins (ginsenosides) from the leaves of *Panax quinquefolius* ameliorated acetaminophen-induced hepatotoxicity in mice. *J. Agric. Food Chem.* 65, 3684–3692. doi:10.1021/acs.jafc.7b00610

Yan, C., Hao, C., Jin, W., Dong, W., and Quan, L. (2021). Biotransformation of ginsenoside Rb1 to ginsenoside F2 by recombinant β-glucosidase from rat intestinal *Enterococcus gallinarum*. *Biotechnol. Bioproc. E.* 26, 968–975. doi:10.1007/s12257-021-0008-2

Yang, W. Z., Hu, Y., Wu, W. Y., Ye, M., and Guo, D. A. (2014). Saponins in the genus *panax* L. (Araliaceae): a systematic review of their chemical diversity. *Phytochemistry* 106, 7–24. doi:10.1016/j.phytochem.2014.07.012

Yoshikawa, M., Murakami, T., Yashiro, K., Yamahara, J., Matsuda, H., Saijoh, R., et al. (1998). Bioactive saponins and glycosides. XI. Structures of new dammarane-type triterpene oligoglycosides, quinquenosides I, II, III, IV, and V, from American ginseng, the roots of *Panax quinquefolium* L. *Chem. Pharm. Bull.* 46, 647–654. doi:10.1248/cpb.46.647

Yu, S., Zhou, X., Li, F., Xu, C., Zheng, F., Li, J., et al. (2017). Microbial transformation of ginsenoside Rb1, Re and Rg1 and its contribution to the improved anti-inflammatory activity of ginseng. *Sci. Rep.* 7, 138. doi:10.1038/s41598-017-00262-0

Yu, P., Li, Y., Fu, W., Li, X., Liu, Y., Wang, Y., et al. (2021). *Panax quinquefolius L.* Saponins protect myocardial ischemia reperfusion No-reflow through inhibiting the activation of NLRP3 inflammasome via TLR4/MyD88/NF-κB signaling pathway. *Front. Pharmacol.* 11, 607813. doi:10.3389/fphar.2020.607813

Yuan, C. S., Wang, C. Z., Wicks, S. M., and Qi, L. W. (2010). Chemical and pharmacological studies of saponins with a focus on American ginseng. *J. Ginseng Res.* 34, 160–167. doi:10.5142/jgr.2010.34.3.160

Zhang, Q., Wen, J., Chang, Z. Q., Xie, C. X., and Song, J. Y. (2018). Evaluation and prediction of ecological suitability of medicinal plant American ginseng (*panax quinquefolius*). *Chin. Herb. Med.* 1, 80–85. doi:10.1016/j.chmed.2018.01.003

Zheng, F., Zhang, M. Y., Wu, Y. X., Wang, Y. Z., Li, F. T., Han, M. X., et al. (2021). Biotransformation of ginsenosides (Rb_1, Rb_2, Rb_3, rc) in human intestinal bacteria and its effect on intestinal flora. *Chem. Biodivers.* 18, e2100296. doi:10.1002/cbdv.202100296

Zhou, W., Huang, H., Zhu, H., Zhou, P., and Shi, X. (2018). New metabolites from the biotransformation of ginsenoside Rb1 by *Paecilomyces bainier* sp.229 and activities in inducing osteogenic differentiation by Wnt/β-catenin signaling activation. *J. Ginseng Res.* 42, 199–207. doi:10.1016/j.jgr.2017.03.004

frontiers | Frontiers in Pharmacology

TYPE Review
PUBLISHED 08 August 2022
DOI 10.3389/fphar.2022.974274

OPEN ACCESS

EDITED BY
Weicheng Hu,
Huaiyin Normal University, China

REVIEWED BY
Enhui Zhang,
Lanzhou Institute of Chemical Physics (CAS), China
Yu Huang,
City University of Hong Kong, Hong Kong SAR, China
Lin Dai,
Tianjin University of Science and Technology, China

*CORRESPONDENCE
Taoyun Wang,
wangtaoyun@mail.usts.edu.cn
Linmao Wang,
wanglinmao12345@sina.com

SPECIALTY SECTION
This article was submitted to Experimental Pharmacology and Drug Discovery, a section of the journal Frontiers in Pharmacology

RECEIVED 21 June 2022
ACCEPTED 11 July 2022
PUBLISHED 08 August 2022

CITATION
Ke Y, Huang L, Song Y, Liu Z, Liang L, Wang L and Wang T (2022), Preparation and pharmacological effects of minor ginsenoside nanoparticles: a review. *Front. Pharmacol.* 13:974274. doi: 10.3389/fphar.2022.974274

Preparation and pharmacological effects of minor ginsenoside nanoparticles: a review

Yue Ke[1], Lei Huang[1], Yu Song[1], Zhenxin Liu[1], Linshuang Liang[1], Linmao Wang[2]* and Taoyun Wang[1]*

[1]School of Chemistry and Life Sciences, Suzhou University of Science and Technology, Suzhou, China, [2]Department of Thoracic Surgery, The First People's Hospital of Yancheng, Affiliated Hospital 4 of Nantong University, Yancheng, China

Ginseng (*Panax ginseng*) is a perennial herbaceous plant belonging to *Panax* genus of Araliaceae. Ginsenosides are a kind of important compounds in ginseng and minor ginsenosides are secondary metabolic derivatives of ginsenosides. Studies have shown that minor ginsenosides have many pharmacological effects, such as antioxidant, anti-tumor, anti-platelet aggregation, and neuroprotective effects. However, the therapeutic effects of minor ginsenosides are limited due to poor solubility in water, short half-life, and poor targeting accuracy. In recent years, to improve the application efficiency, the research on the nanocrystallization of minor ginsenosides have attracted extensive attention from researchers. This review focuses on the classification, preparation methods, pharmacological effects, and action mechanisms of minor ginsenoside nanoparticles, as well as existing problems and future direction of relevant research, which provides a reference for the in-depth research of minor ginsenoside nanoparticles.

KEYWORDS

minor ginsenosides, nanoparticles, preparation, pharmacological effects, action mechanism

1 Introduction

Belonging to *Panax genus* of Araliaceae, ginseng is a perennial herbaceous plant with fleshy roots. It is also a traditional precious herb, a tonic that can enhance physical vitality (Park et al., 2005), known as the "king of herbs" (He et al., 2019). Ginseng can be used for the treatment of several diseases effectively, such as liver and stomach diseases, diabetes, cardiovascular diseases, etc., so it is widely used in the world. Ginsenoside is a tetracyclic triterpenoid saponin extracted from ginseng (Li et al., 2009), and it is the main active ingredient of ginseng. In recent years, the pharmacological effects of ginsenosides have been continuously discovered. According to the literature, ginsenosides have clinical applications such as anti-allergy (Yoo et al., 2016) and reducing hypertension (Zhou et al., 2017). Minor ginsenosides are secondary metabolic derivatives of ginsenosides, and they are the most important active ingredient in ginsenosides. At present, more than 60 minor ginsenosides have been found (Liu et al., 2019), mainly including Rg3, Rg5, Rh1, Rh2, Compound K (CK), etc. It has been confirmed that minor ginsenosides are easier to be

absorbed by the human body and have more prominent effects on promoting cell differentiation and regeneration, repairing nerves, and resisting tumors (Li et al., 2021a). However, minor ginsenosides show low solubility in water, low bioavailability and short half-life (Ye et al., 2014), which restricts the pharmacological effects of minor ginsenosides to a certain extent.

Nanotechnology is a modern technology which controls the material structure in 0.1–100 nm and makes the material show special properties (Kaehler, 1994). Professor Xu Bihui (Yang et al., 2000) took the lead in introducing nanotechnology into the field of traditional Chinese medicine and put forward the concept of "nano traditional Chinese medicine". Based on the different forms of nanoparticles, nano-drugs can be divided into two types: one is nano-drug crystal, that is, the material itself is nanosized or crushed to nano size; the other one is nano-drug carrier, which carries drugs with the help of nanoscale carrier materials (Zheng and Shi, 2012). Nano-drugs improve the utilization rate of drugs, enhance the original curative effects and improve the targeting effect (Liu et al., 2014). Therefore, in recent years, to improve the pharmacological effects of minor ginsenosides, the research of minor ginsenoside nanoparticles has attracted extensive attention from researchers in related fields.

Focusing on the current research hotspot of minor ginsenoside nanoparticles, this review summarizes the classification, preparation methods, pharmacological effects, and action mechanisms of minor ginsenoside nanoparticles, and provides a reference for the in-depth research of minor ginsenoside nanoparticles.

2 Preparation of minor ginsenoside nanoparticles

2.1 Preparation of minor ginsenoside nanocrystals

Nanocrystalline drugs do not have any matrix materials and can form a stable nano state only through the action of a small number of surfactants or polymers (Zheng and Song, 2012). Nanocrystalline drugs have the advantages of high solubility and dissolution, strong adhesion to biofilm, and low interference by food. There are mainly three types of nanocrystalline drug preparation technologies (Wang et al., 2014).

2.1.1 "Top-bottom" technology

"Top-bottom" technology is to crush large particles into nano-sized small particles (Dai et al., 2019), mainly including the medium grinding method, high-pressure homogenization method, and extrusion method. This technology has the advantages of low cost, large output, and simple operation (Shen et al., 2014). The disadvantage of "Top-bottom" technology is that reducing the particle size below 100 nm requires much processing time and is not easy to expand production (Sinha et al., 2013). Xie et al. (2016) prepared minor ginsenoside Rg3 nanocrystals by high-pressure homogenization and precipitation. The minor ginsenoside Rg3 was dissolved in methanol as the organic phase, and poloxamer 188 was dissolved in purified water as the aqueous phase. The organic phase was added to the aqueous phase to prepare the crude suspension. The nanosuspension was obtained by circulating 4 times under the pressure of 28 MPa and 10 times under the pressure of 48 MPa through a high-pressure homogenizer. The suspension mixed with mannitol were pre-frozen in an ultra-low temperature refrigerator, and then transferred into a freeze dryer for freeze-drying to obtain ginsenoside Rg3 nano freeze-dried powder. The prepared nanocrystals had a small particle size of (284 ± 14) nm, an ideal polydispersity coefficient of 0.156 ± 0.007 and good overall stability. It was measured that Rg3 contained in each gram of nano freeze-dried powder was 36.70 mg.

2.1.2 "Top-bottom" and "bottom-top" combined technology

The combined technology of "Top-bottom" and "Bottom-top" which to dissolve the drug in solvent and add the medicine solution to nonsolvent to precipitate it (Gao et al., 2012) takes one method as the pretreatment step, and then another method is used to prepare nano-drug crystals (Wang et al., 2014). This technology can make up for the shortcomings and make full use of the advantages of the two technologies. Wang et al. (2018) combined high-pressure homogenization technology with spray drying technology to prepare expandable particles to load with minor ginsenoside Rg3. Rg3 coarse powder was dispersed in aqueous solution. The dispersion was first treated by a high speed homogenizer at 15000 rpm for 2 min, and then it was processed through a high-pressure homogenizer that the cycle operation was carried out under different pressures. The prepared nanosuspension had a particle size of 400–500 nm, with the polydispersity coefficient less than 0.3.

2.1.3 Other preparation technology of minor ginsenoside nanocrystals

Aerosol solvent extraction system (ASES) means that supercritical fluid CO_2 and solution are pumped into a previously installed precipitation reactor through a nozzle, in which the solute is oversaturated and precipitated into nanoparticles through the extraction and absorption of CO_2 to the solvent and the diffusion of solvent molecules to CO_2 (Yu et al., 2006). Tao et al. (2018) synthesized minor ginsenoside Rh2 and re-drug nanocomposites using ASES technology. The author chose vapor-over-liquid, subcritical liquid and supercritical liquid to prepare. In contrast, as the operating pressure and temperature increased to subcritical conditions, the particle size decreased: the average particle size was 164 nm. And the aggregation behavior was significantly improved. The

zeta potential was −4.79 mV, and it had an excellent dissolution rate of 96.2%.

2.2 Preparation of minor ginsenoside nano-drug carrier

Nano-drug carrier has the advantages of improving the bioavailability, the pharmacokinetics of traditional chemotherapy drugs, and the accuracy of drugs reaching tumor cells. Nano-drug carrier also reduces the toxicity of drugs and prolongs the action time of drugs *in vivo*. At present, nano-drug carrier technology has been applied to the administration of minor ginsenosides. The commonly used preparation methods of minor ginsenoside nano-drug carrier include film hydration, emulsion solvent evaporation, desolvation and self-assembly.

2.2.1 Film hydration method

Film hydration usually refers to dissolving the carrier material and drug in an appropriate organic solvent, removing the solvent by rotary evaporation, forming a film between the drug and the film-forming material, and then hydrating the film to prepare nanoparticles. Yang et al. (2016) dissolved CK, phospholipids and D-α-tocopheryl polyethylene glycol 1000 succinate in ethanol by ultrasound. Subsequently, the evaporation solution was evaporated by rotary vacuum evaporation until the film was formed on the vessel wall. The film removed residual ethanol, rehydrated to form liposomes loaded with CK followed by lyophilization (GCKT-liposomes). The particle size was 119.3 ± 1.4 nm, the zeta potential was 1.9 ± 0.4 mV, and drug encapsulation efficiency was 98.4 ± 2.3%.

2.2.2 Emulsion solvent evaporation method

Emulsion solvent evaporation method refers to taking water-insoluble organic solvents (usually dichloromethane and chloroform) as the "oil phase", in which the carrier material is dissolved, and take acetone or methanol as the "aqueous phase" to dissolve the drug into the influent phase, then make the two phases mix evenly (Qiu et al., 2004). After sufficient emulsification, the organic solvent is removed by rotary evaporation to obtain nanoparticles. Youwen Zhang et al. (2017) added Rg3 dissolved in ethanol to polylactic-co-glycolic acid (PLGA) dissolved in dichloromethane as the oil phase, and added it to the water phase formed by mixing polyvinyl alcohol and ethanol. The mixture was emulsified by a probe sonicator, and then subjected to magnetic stirring, washing, ultracentrifugation and freeze-drying to obtain nano freeze-dried powder. The average size of nanoparticles was 97.5 nm. Drug encapsulation efficiency was 97.5%, and the drug loading rate was 70.2%. The zeta potential was -28 mV.

2.2.3 Desolvation method

Desolvation is commonly used in the preparation of albumin nanoparticles. This method dissolves albumin in water as the aqueous phase, and drugs are generally dissolved in absolute ethanol as the organic phase (Li et al., 2021b). The two phases are mixed evenly by magnetic stirring, and the mixed solution is treated by dialysis or centrifugal purification and other methods to remove organic solvents, then the solution is freeze-dried to obtain nanoparticles. Singh et al. (2017a) embedded minor ginsenoside CK in bovine serum albumin (BSA) by desolvation method to form BSA-CK nanoparticles. That is, BSA was dissolved in water and sonicated, then magnetic stirring. Then CK dissolved in ethanol was added to the BSA-water solution and stirring was continued. The mixture was then dialyzed against excess methanol/distilled water using a dialysis membrane for 1 day and against distilled water for 2 days. Finally, BSA-CK nanoparticles was obtained by lyophilization. The average particle size of BSA-CK nanoparticles is about 157.2 nm, and the zeta potential was −70.80 mV. Compared with non-nano CK, the solubility of BSA-CK were significantly enhanced.

2.2.4 Preparation method based on self-assembly

The chemical components of minor ginsenosides are complex and diverse. After decoction and dissolution, it is easy to use the electrostatic interaction between opposite charges, hydrogen bonding, and acid-base complexation to aggregate into self-assembled nanoparticles (Ma et al., 2021; Shen et al., 2021). Usually, the relevant drug ingredients are placed directly in water or buffer solution and stirred by heating to form self-assembled nanoparticles. Zhao et al. (2016) made that etoposide and ginsenoside Rh2 were covalently linked to both ends of polyethylene glycol (PEG) at the same time to form an amphiphilic polymer with hydrophobic ends and hydrophilic middle. The final yield of the target product was 62.9%. The particle size of nanoparticles was (112.64 ± 4.28) nm, the polydispersity index was (0.224 ± 0.002), and the surface potential was (-13.82 ± 2.74) mV.

3 Pharmacological effects and mechanism of nano minor ginsenoside

3.1 Pharmacological effects and mechanism of minor ginsenoside nanocrystals

3.1.1 Anticancer effect and related mechanism

Tao et al. (2018) prepared Rh2 nanoparticles using ASES technology. The cytotoxicity of Rh2 nanoparticles to cancer cell

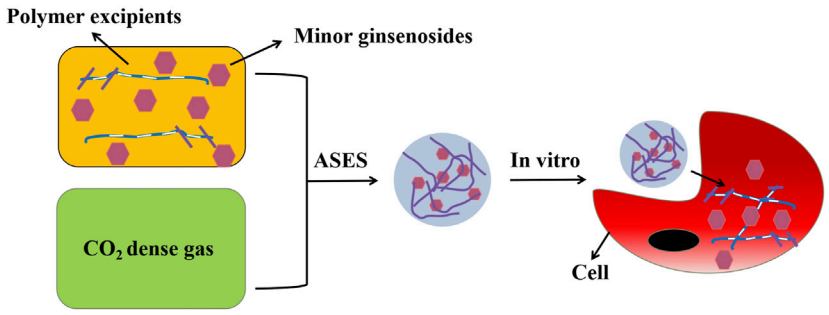

FIGURE 1
Preparation process and cell uptake diagram.

SCC-15 was measured by the MTT assay. The results showed that Rh2 nanoparticles had good anticancer activity, and the anticancer ability was more effective with the decrease in particle size. This may be through endocytosis, which promotes the uptake of nano drugs by cancer cells and further leads to apoptosis. At the same time, X-ray diffraction showed that there were very few crystalline substances and no valuable diffraction peaks, indicating that Rh2 nanoparticles showed an amorphous shape after being treated by the ASES process. This situation may be due to the rapid precipitation in the process of ASES, which makes the drug form a metastable region, and then reduces the crystallinity of the drug. This transformation from crystalline state to amorphous state may reduce the water insolubility of drugs, improve the dissolution efficiency, and then improve the bioavailability. This may also be the reason for improved anticancer activity. (Figure 1).

3.1.2 Antitumor activity of minor ginsenoside nanocrystals

Xie et al. (2016) prepared ginsenoside Rg3 nanocrystals and evaluated the antitumor effect of Rg3 nanocrystal suspension *in vitro* by the MTT method. Compared with commercial *Shenyi* capsule, the results showed that the two drugs had strong inhibitory effects on HepG2 cells and A549 cells. And when the drug concentration was greater than 50 μg/ml, nano-drugs showed better inhibition of tumor cell proliferation than *Shenyi* capsules. This result shows that Rg3 nanocrystals have good antitumor activity.

3.2 Pharmacological effects and mechanism of minor ginsenoside nanocarrier drug delivery system

According to different carrier materials, nano-drug carriers can be classified into organic nanocarriers, inorganic nanocarriers and composite nanocarriers (Zhou, 2020). The pharmacological effects of minor ginsenosides were significantly enhanced by the introduction of nano-drug carriers (Table 1). The typical feature of this kind of drug carriers is that it can carry out targeted delivery, and the action mechanism of its pharmacological effects can be classified into passive targeting and active targeting (Figure 2). Drugs of passive targeting type enter pathological sites through the intercellular space of the inner wall of blood vessels, and use the high enhanced permeability and retention (EPR) effect to make drugs accumulate in tumor, inflammation and other pathological sites (Iyer et al., 2006), so that the required drug level in the blood can be maintained for a long time (Torchilin, 2010). The active targeting type mainly refers to the target site has some special receptors. The antibody specifically bound to it or some modification is carried out on the carrier, and the targeted ligand is linked to the surface of the carrier. Through the mutual recognition of the ligand and the receptor, a specific binding with the target is realized, and then the drug is released at a specific location (Dong et al., 2017). Nano drugs are engulfed by tumor or other pathological cell membrane invagination to form endocytosomes (Sahay et al., 2010), and then the drugs are released to achieve the therapeutic effect. The pharmacological activities and specific mechanisms are introduced according to different carrier types as follows.

3.2.1 Organic nanocarrier drug delivery system

3.2.1.1 Pharmacological effects and mechanism of minor ginsenoside liposome drug delivery system

Liposomes are vesicle structures composed of lipid bilayers with high biocompatibility (Pei et al., 2021). It can improve the solubility of drugs, enhance the hold time of drugs *in vivo* and reduce toxicity (Liu and Feng, 2015). Cholesterol is an important component of liposomes, but it can lead to allergic reactions and cardiopulmonary side effects (Moein Moghimi et al., 2006), so it needs to be replaced. Ginsenoside has a steroid structure similar to cholesterol (Nag et al., 2012), which can make the arrangement of phospholipids in the liposome bilayer more compact (Hui

TABLE 1 Enhanced effect of minor ginsenoside nano drug delivery system on minor ginsenoside.

Minor ginsenoside types	Type of drug carriers	Enhanced effects of nano-drug delivery system	References
CK	Liposomes	Improving encapsulation efficiency; enhanced uptake efficiency and cytotoxicity of A549 cells	Yang et al. (2016)
	Liposomes	Increase drug solubility; increased tumor targeting; enhancement of anti-tumor effect	Jin et al. (2018)
	Micelles	Enhanced the cytotoxicity of HepG2 and Huh-7 cells *in vitro*; enhanced uptake efficiency; sustained drug release	Zhang et al. (2020)
	Micelles	Cytotoxicity to A549 cells; increased tumor targeting	Shaozhi Zhang et al. (2017)
	Micelles	Improved CK water solubility; promoted tumor cell apoptosis, inhibited tumor cell invasion, metastasis and efflux; increased tumor targeting	Lei Yang et al. (2017)
	Chitosan-based nanoparticles	Improved CK water solubility; anti-proliferation effect on HepG2 cells; greater cytotoxicity and higher apoptosis rate	Zhang et al. (2018)
	Chitosan-based nanoparticles	Enhanced uptake efficiency and cytotoxicity of PC3 cells	Zhang et al. (2021)
	Chitosan-based nanoparticles	Improved CK water solubility; higher cytotoxicity to HT29 and HepG2 cells	Mathiyalagan et al. (2014)
	Albumin-based nanoparticles	Improved CK water solubility; higher toxicity to cancer cells; enhanced anti-inflammatory effect	Singh et al. (2017a)
	Gold nanoparticles	Slightly high cytotoxicity to A549 and HT29 cells; increased apoptosis of cancer cells	Kim et al. (2019)
	Mesoporous silicas	Good biocompatibility to normal cell line (HaCaT skin cells); higher cytotoxicity to A549, HepG2 and HT29 cell lines; better anti-inflammatory effect on RAW264.7 cells	Singh et al. (2017b)
Rg3	Liposomes	Increased uptake, antiproliferative and targeting of glioma spheres	Zhu et al. (2021)
	Liposomes	More pronounced sustained release	Cui et al. (2020)
	Liposomes	Improved the bioavailability; enhanced cytotoxicity ; inhibited angiogenesis and growth of lung cancer	Yu et al. (2013)
	Liposomes	Enhanced inhibition of tumor cell proliferation	Li et al. (2014a)
	Liposomes	Enhanced inhibition of tumor cell proliferation; Increased tumor targeting	Wei et al. (2014)
	Liposomes	Enhance the inhibitory efficiency on HepG2 cells and HUVEC cells; increased cellular uptake	Li et al. (2014b)
	Liposomes	Inhibition of A375 melanoma cells	Ye et al. (2014)
	Microemulsions	Microemulsion with optimum physical and chemical stability	Hou et al. (2019)
	Microemulsions	Controlled drug release	Liu et al. (2008)
	Micelles	Inhibition of tumor angiogenesis	Yu et al. (2015)
	Micelles	Improved water solubility and bioavailability of Rg3; reduced adriamycin - induced cardiotoxicity and enhanced its anticancer effect	Lan Li et al. (2017)
	Polymer-based nanoparticles	Improved cardiac function and reduced infarct size	Li et al. (2020)
	Polymer-based nanoparticles	Targeted cancer cells ; significantly inhibited tumor proliferation; circulated in blood longer	Qiu et al. (2019)
	Polymer-based nanoparticles	Sustained drug release; inhibited the proliferation of A431 cancer cells and induced apoptosis	Wei Zhang et al. (2017)
	Polymer-based nanoparticles	More easily through the blood brain barrier; inhibition of proliferation of C6 glioma cells	Su et al. (2020)
	Polymer-based nanoparticles	Sustained drug release and delivery	Cao et al. (2022)
	Polymer-based nanoparticles	Sustained drug release	Pan et al. (2015)
	Polymer-based nanoparticles	Drug release regulated with temperature; inhibitory effect on HepG2 hepatoma cells	Zhang W N et al. (2017)
	Polymer-based nanoparticles	Inhibited tumor angiogenesis ; sustained drug release	Geng et al. (2014a)
	Polymer-based nanoparticles	Improved antitumor activity	Geng et al. (2016)
		Sustained drug release; Improved anti-angiogenic activity	Geng et al. (2014b)

(Continued on following page)

TABLE 1 (*Continued*) Enhanced effect of minor ginsenoside nano drug delivery system on minor ginsenoside.

Minor ginsenoside types	Type of drug carriers	Enhanced effects of nano-drug delivery system	References
	Polymer-based nanoparticles		
	Chitosan-based nanoparticles	Sustained drug release; higher fatigue resistance	Youwen Zhang et al. (2017)
	Albumin-based nanoparticles	Higher antitumor activity in HepG2 and A549 cells	Zhang et al. (2019)
	Albumin-based nanoparticles	Sustained drug release; inhibitory effect on proliferation of A549 cells	Cheng and Zheng, (2014)
	Albumin-based nanoparticles	Sustained drug release; inhibitory effect on Hela cells of cervical cancer	Chen et al. (2013)
	Gold nanoparticles	Improved Rg3 water solubility	Park et al. (2011)
	Gold nanoparticles	Enhanced anti-inflammatory effect	Kang et al. (2016)
	Mesoporous silicas	Inhibited the proliferation of A549 cells; improved drug dissolution rate	Jiang et al. (2016)
	Magnetic nanoparticles	Nontoxic safety; automatic targeting of mouse liver	Zhao et al. (2018)
	Magnetic nanoparticles	Sustained drug release; inhibition of HeLa cell proliferation	Yang et al. (2014)
	Composite nano carriers	Sustained drug release; improved cell uptake efficiency	Lee et al. (2014)
	Nanofibers	Higher inhibitory effect on hypertrophic scar formation	Sun et al. (2014)
Rg5	Liposomes	Tumor targeting; inhibited tumor growth	Hong et al. (2019)
	Liposomes	Tumor targeting; inhibited tumor growth	Xue Wang et al. (2021)
	Albumin-based nanoparticles	Inhibited tumor growth	Dong et al. (2019)
Rh1	Liposomes	Improved encapsulation efficiency and solubility	Choi et al. (2015)
	Self - microemulsions	Enhanced intestinal cellular uptake and oral utilization	Lei Yang et al. (2017)
	Polymer-based nanoparticles	Increased cytotoxicity to lung cancer	Mathiyalagan et al. (2019)
Rh2	Liposomes	Sustained drug release; enhanced uptake and cytotoxicity of PC3 cells	Zare-Zardini et al. (2020)
	Liposomes	Extended blood circulation; inhibited tumor growth	Hong et al. (2020)
	Liposomes	Higher inhibitory activity against HepG2 xenografts	Weiguo Xu et al. (2015)
	Microemulsions	Inhibited the growth of A549 tumor xenografts	Qu et al. (2017a)
	Microemulsions	Accumulation in tumors; improved antitumor effect	Qu et al. (2017b)
	Self - microemulsions	Enhanced intestinal cellular uptake and oral utilization	Feifei Yang et al. (2017)
	Micelles	Improved Rh2 water solubility; enhanced drug uptake; extended drug retention; improved antitumor effect	Xia et al. (2020)
	Micelles	Increased cell uptake; inhibited the proliferation of A549 cells; longer blood retention period	Peng Li et al. (2017)
	Micelles	Increased solubility; inhibited tumor growth	Chen et al. (2014)
	Polymer-based nanoparticles	Increased cytotoxicity to lung cancer	Mathiyalagan et al. (2019)
	Polymer-based nanoparticles	Sustained drug release; increased the residence time of drugs in inflammatory tissues	Xu et al. (2022)
	Polymer-based nanoparticles	Increased solubility; longer circulation time; improved antitumor effect	Xu et al. (2020)
	Polymer-based nanoparticles	Increased solubility; sustained drug release; increased inhibition of glioma cell proliferation; improved antitumor effect	Zou et al. (2016)
	Chitosan-based nanoparticles	Higher cytotoxicity to A549 cells	Gu et al. (2021)
	Albumin-based nanoparticles	Improved water solubility; enhanced the anticancer effect on A549 lung cancer cells and HT29 colon cancer cells; higher anti-inflammatory ability	Singh et al. (2017a)
	Mesoporous silicas	Good biocompatibility to normal cell line (HaCaT skin cells); higher cytotoxicity to A549, HepG2 and HT29 cell lines; better anti-inflammatory effect on RAW264.7 cells	Singh et al. (2017b)
		Higher antitumor activity; reduced toxicity to the coagulation system and heart tissue	

(Continued on following page)

TABLE 1 (*Continued*) Enhanced effect of minor ginsenoside nano drug delivery system on minor ginsenoside.

Minor ginsenoside types	Type of drug carriers	Enhanced effects of nano-drug delivery system	References
	Graphene-based nanoparticles		Zare-Zardini et al. (2018a)
	Graphene-based nanoparticles	Higher anticancer activity; reduced side effects on normal cells (red blood cells, heart tissue, etc.)	Zare-Zardini et al. (2018b)

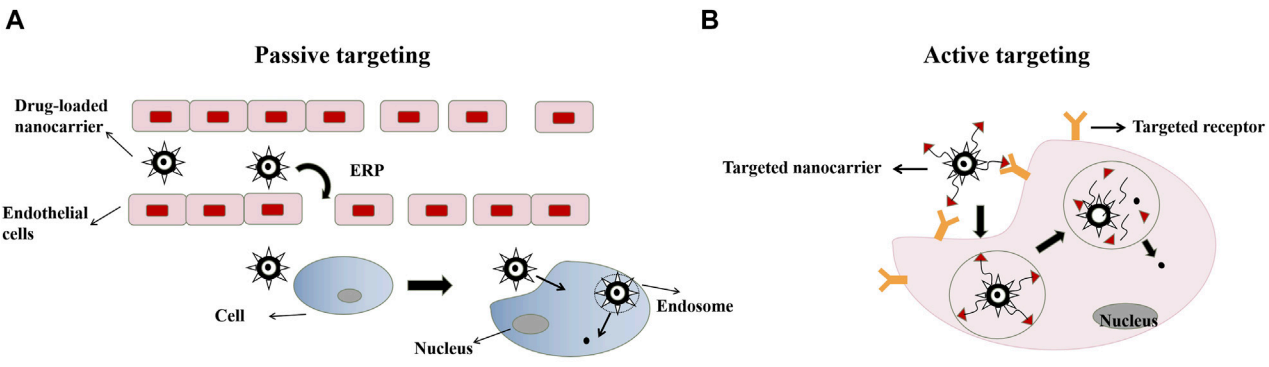

FIGURE 2
Main action mechanism: Passive targeting **(A)**; Active targeting **(B)**.

et al., 2014), and reduce the particle size of liposomes. The membrane stability of liposomes was improved by changing the thermodynamic parameters of bilayer phospholipids (Fukuda et al., 1985; Hong et al., 2020). Zhu et al. (2021) studied a minor ginsenoside Rg3-based liposomal system (Rg3-LPs). Rg3 was used to replace cholesterol in liposomes. Compared with cholesterol liposomes (C-LPs), Rg3-LPs improved the uptake and targeting of glioma spheres *in vitro*, and the anti-proliferation effect of paclitaxel-loaded Rg3-LPs on glioma cells was significantly stronger than that of paclitaxel loaded C-LPs. Hong et al. (2020) developed a new nanocarrier, the ginsenoside Rh2 liposome (Rh2-lipo), in which cholesterol was replaced by Rh2 and paclitaxel (PTX). The results showed that compared with ordinary liposomes, Rh2-lipo loaded with PTX could significantly inhibit tumor growth and reverse the immunosuppressive microenvironment in the tumor microenvironment (TME).

TME is still the main challenge of drug therapy. Data show that some immune cells have immunosuppressive properties, which lead to the production of cancer stem cells and promote the proliferation of cancer cells, thus reducing the efficacy of drugs (Arneth, 2019). Minor ginsenosides themselves have excellent antitumor and anticancer activities, and some also show good immunomodulatory effects in reshaping the TME. Therefore, the combination of TME remodeling ability and smaller particle size improves its tumor penetration effect and uptake rate (Zhu et al., 2021). At the same time, the interaction between glucose transporters of tumor cells and minor ginsenosides significantly increases the accumulation of liposomes in tumors. After endocytosis, nanoparticles can be separated from lysosomes, so that drugs can be released and take effect in the cytoplasm (Figure 3).

3.2.1.2 Pharmacological effects and mechanism of minor ginsenoside microemulsion and self microemulsion drug delivery systems

The microemulsion is a thermodynamic stable system composed of water, oil and amphiphilic substances (Pei et al., 2021). It can improve the utilization and absorption rate, enhance the solubility and make the drugs play a better effect. Qu et al. (2017a) studied a multicomponent microemulsion (ECG-MEs) composed of etoposide, coix seed oil and minor ginsenoside Rh2. ECG-MEs may effectively enter various types of tumor cells and have good synergistic antitumor effect. The reason may be that microemulsions have very low surface tension and small droplet size, resulting in high absorption and penetration (Talegaonkar et al., 2008). The addition of an appropriate amount of Rh2 not only maintains the stable nanostructure of the multicomponent microemulsion, but also stimulates the

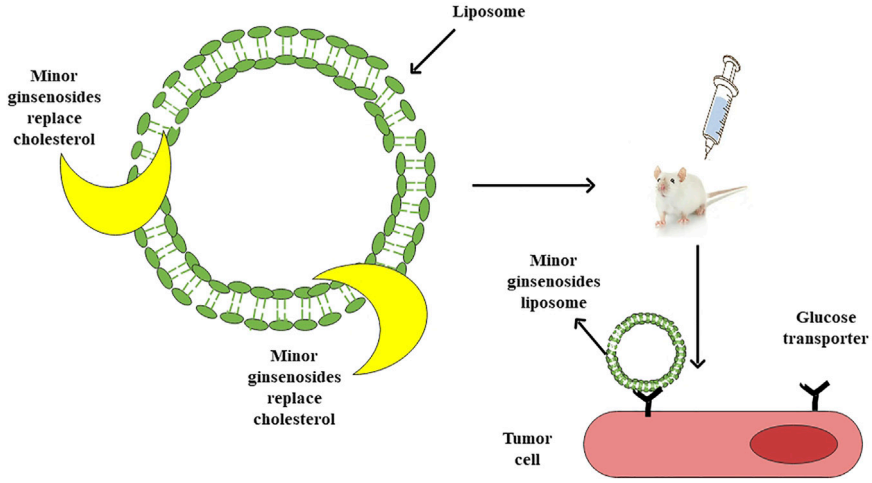

FIGURE 3
Minor ginsenoside liposome drug delivery system and mechanism of tumor-targeted therapy.

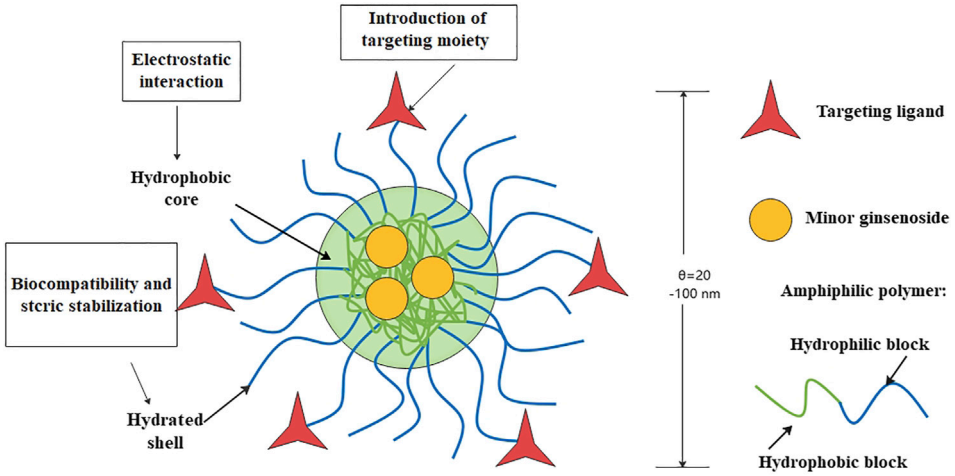

FIGURE 4
Structure and functions of micelles.

stronger ability of small-size nanoparticles permeate into the tumor and improves the anti-tumor potential.

Self microemulsion drug delivery system is a solid or liquid preparation composed of oil, surfactant and cosurfactant (Liu and Feng, 2015). Because of its small droplet size and large surface area, the bioavailability is improved (Bolko et al., 2014). Feifei Yang et al. (2017) encapsulated minor ginsenosides Rh1 and Rh2 into two self microemulsions (SME-1 and SME-2). The results showed that compared with unencapsulated drugs, encapsulated drugs enhanced intestinal cell uptake and oral utilization. This may be because the self microemulsions can disturb the cell membrane, reversing the opening of tight junctions (Wu et al., 2015), thereby improving cell uptake and bioavailability.

3.2.1.3 Pharmacological effects and mechanism of minor ginsenoside polymer micelle drug delivery system

Polymer micelles are colloidal dispersion systems formed by self-assembly of amphiphilic block copolymers in water (Pei et al., 2021), which can prevent drugs from being degraded (Wang et al.,

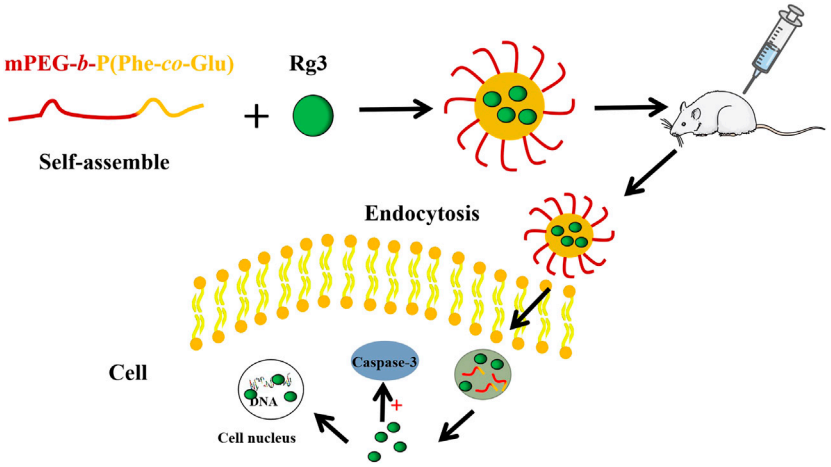

FIGURE 5
Preparation and action mechanism of Rg3-NPs.

2013). The hydrophobic core is used as the natural carrier for encapsulating hydrophobic drugs, while the hydrophilic shell stabilizes the particles in aqueous solution (Nasongkla et al., 2006) (Figure 4). Zhang et al. (2020) prepared micelles loaded with minor ginsenoside CK (APD-CK) with A54 peptide. Compared with CK alone, polymer micelles have enhanced antiproliferative effects on Huh-7 cells and HepG2 cells, and have better anticancer effects. This may because the A54 is a hepatoma-specific binding peptide, it can help the modified drug-loaded nanosystem specifically target hepatoma cells through cell surface receptors and be absorbed by these cells quickly. The release of CK in micelles is pH-dependent, which may be attributed to the electrostatic interaction between polymer-carriers and hydrophobic drugs. The sustained release may be due to the gradual separation of CK from the micellar carrier and release into the solution. And this prolongs the time of the drug in the blood, which is conducive to the targeted release and improves the bioavailability of minor ginsenosides.

3.2.1.4 Pharmacological effects and mechanism of minor ginsenoside polymer nano-drug delivery system

Polymer nanoparticles encapsulate drugs into the core formed by polymer materials and adsorb them onto particles (Liu and Feng, 2015), which can make drugs release continuously. Qiu et al. (2019) prepared self-assembled polymer nanoparticles of poly (ethylene glycol)-block-poly (L-glutamic acid-*co*-L-phenylalanine) [mPEG-*b*-P (Glu-*co*-Phe)]. Then the minor ginsenoside Rg3 was encapsulated into it to form mPEG-*b*-P (Glu-*co*-Phe) nanoparticles (Rg3-NPs). Compared with free Rg3, Rg3-NPs are more cytotoxic to colon cancer cells and can effectively inhibit the proliferation of tumor cells. The mechanism is that nanoparticles enter cells through endocytosis, and there is electrostatic interaction between drugs and polymers. The increase of acidity in the TME destroys the electrostatic interaction, which is conducive to the release of more drugs, enhancing the accumulation of drugs in tumors and achieving the effect of treating tumor cells (Lv et al., 2013). It is reported that the particle size of 100 nm is an appropriate particle size for selective accumulation in the tumor through EPR effect (Linqiang Xu et al., 2015). And it leads to apoptosis by enhancing the expression of caspase-3 (Figure 5).

3.2.1.5 Pharmacological effects and mechanism of minor ginsenoside biopolymer nano-drug delivery system

Biopolymer based nanocarriers include natural biopolymers derived from proteins and polysaccharides, as well as modified forms of these substances and derivatives (Pei et al., 2021). Zhang et al. (2018) prepared chitosan nanoparticles (CK-NPs) loaded with minor ginsenoside CK, with deoxycholic acid-O carboxymethyl chitosan as polymer carrier (Figure 6). The results showed that the prepared nanoparticles had uniform particle size distribution and good dispersion, and showed a significant anti-proliferation effect on HepG2 cells. This may be because the release of CK is pH-dependent, and CK release is significantly enhanced in a slightly acidic environment. CK-NPs may be absorbed by cells through endocytosis, and the encapsulated drugs are released in a slightly acidic environment, increasing the absorption of drugs by HepG2 cells. At pH 7.4, it will reduce the release, to decrease the toxic and side effects on normal tissues.

3.2.2 Inorganic nanocarrier drug delivery system

3.2.2.1 Pharmacological effects and mechanism of minor ginsenoside gold nano-drug delivery system

As a drug carrier, gold nanoparticles show biocompatibility and non-toxicity. Drugs are loaded through non-covalent

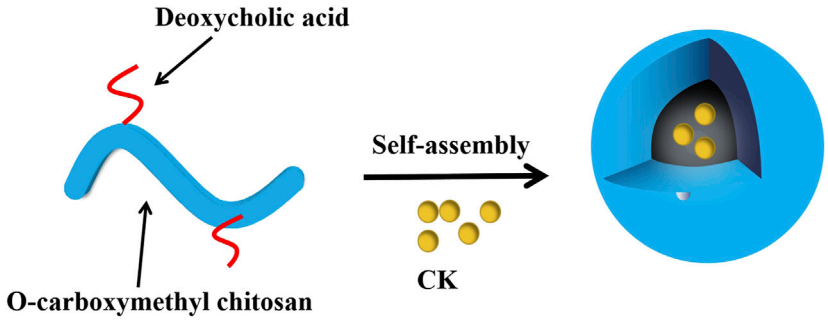

FIGURE 6
Self-assembly process of chitosan nanoparticles loaded with minor ginsenoside CK (Zhang et al., 2018).

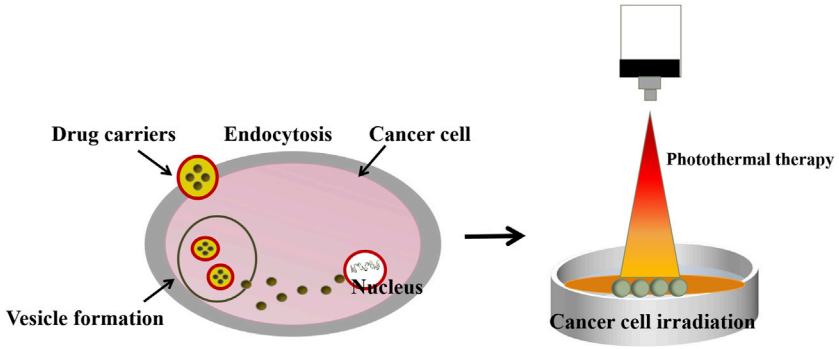

FIGURE 7
Schematic diagram of endocytosis mechanism and photothermal therapy (Kim et al., 2019).

interactions (Vigderman and Zubarev, 2013). Kim et al. (2019) prepared biosynthetic gold nanoparticles loaded with minor ginsenoside CK. Compared with free minor ginsenosides, gold nanoparticles showed slightly higher cytotoxicity to A549 cells and HT29 and were more likely to increase the apoptosis of cancer cells under light-induced hyperthermia. It is reported that as a drug carrier, gold nanoparticles can increase the absorption of drugs by tumor tissues stimulated by hyperthermia (Zhang et al., 2016). Nanoparticles bind to cells through endocytosis. And because the surface is cationic, nanoparticles can gather on the anionic surface of cancer cells. After photoinduced hyperthermia, they can quickly induce cell lysis and release the curative effect (Figure 7).

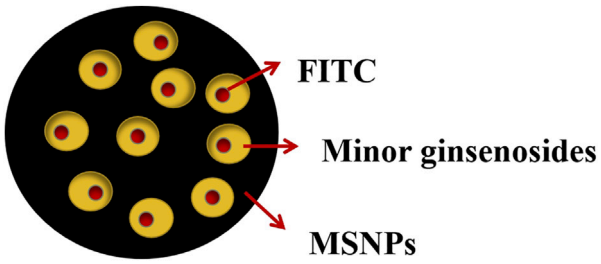

FIGURE 8
Structure of mesoporous silica nanoparticles (Singh et al., 2017c).

3.2.2.2 Pharmacological effects and mechanism of minor ginsenoside mesoporous silica nano-drug delivery system

Mesoporous silica nanoparticles with large surface area and pore volume have been reported as an effective drug delivery carrier due to their biocompatibility and high drug loading (Liu and Feng, 2015). Singh et al. (2017b) loaded minor ginsenoside CK and Rh2 onto 200 nm mesoporous silica nanoparticles (MSNPs) with pore size of 4 nm to

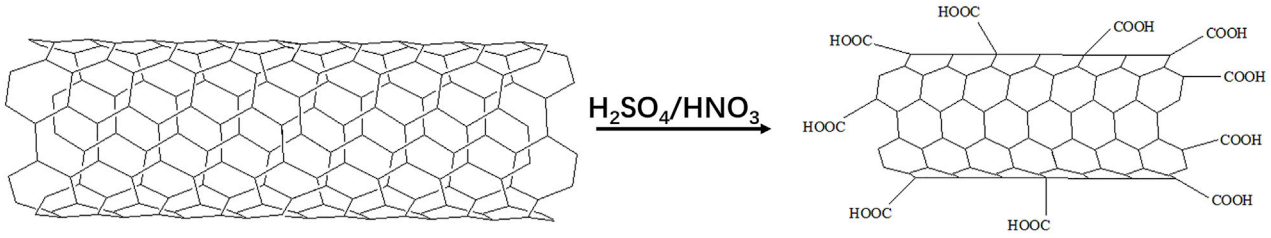

FIGURE 9
Functional principle of carbon nanotubes (Bianco et al., 2005).

prepare MSNPs-CK and MSNPs-Rh2 respectively. Fluorescein isothiocyanate (FITC) fluorescent dye was combined in MSNPs carrier system to track cell uptake and facilitating *in vitro* research (Figure 8). The results showed that compared with the unencapsulated CK and Rh2, the two nanoparticles had biocompatibility with HaCaT skin cells, and showed higher cytotoxicity in A549, HepG2, and HT29 cell lines. The anti-inflammatory effect was better in RAW264.7 cells. This may be because MSNPs are essentially immune to hydrolysis and enzymatic degradation, which can protect drugs from early release before reaching the point of action (Tang et al., 2012). Moreover, MSNPs have nanoscale pores, and the diameter of most enzymes is much larger than their pores, which prevents the entry of many enzymes, thus protecting the drugs from being hydrolyzed prematurely (Heidegger et al., 2016). Combined with its high drug loading, the curative effect of the drug is enhanced.

3.2.2.3 Pharmacological effects and mechanism of minor ginsenoside magnetic nano-drug delivery system

Magnetic nanoparticles are often used to obtain targeting and trigger drug release through the heat generated by the magnetic field (Pei et al., 2021). Zhao et al. (2018) coupled minor ginsenoside Rg3 with magnetic components to obtain magnetic nanoparticles. The results showed that the synthesized nanoparticles had good biocompatibility and stability, and had the ability of automatic targeting to mouse liver. Subsequent evaluation of important organs in mice showed that nanodrugs were non-toxic and safe.

3.2.2.4 Pharmacological effects and mechanism of minor ginsenoside nanotube drug delivery system

Two functionalization methods are widely used to modify carbon nanotubes (CNT). One is to use strong acid oxidation, and the other one is to react with amino acid derivatives and aldehydes to add solubilized parts around the outer surface. Functionalized carbon nanotubes can be connected to a variety of active molecules (Bianco et al., 2005). Luo et al. (2021) combined the minor ginsenoside Rg3 with CNT to obtain the conjugate CNT-loaded Rg3 (Rg3-CNT). Nitric acid and sulfuric acid were mixed to functionalize CNT. This method reduced the length, produced carboxyl groups and increased the dispersion in aqueous solution (Liu et al., 1998) (Figure 9). The results showed that the anti-cancer activity was enhanced compared with free Rg3. The reason is that Rg3-CNT can reduce the expression of PD-1 in activated T cells, thereby enhancing the anti-cancer effect of Rg3 on triple-negative breast cancer. Many experiments have proved that diverse mammalian cells absorb CNT or its conjugates, and CNT can overcome the cell barrier (Shi Kam et al., 2004), CNT-loaded glycopolymer can target breast cancer (Ozgen et al., 2020), so the enhancement of anticancer activity may be because CNT overcomes the cell barrier to release drugs in cells.

3.2.2.5 Pharmacological effects and mechanism of minor ginsenoside graphene drug delivery system

Graphene is a single layer of SP^2-hybridized carbon atoms arranged in a two-dimensional honeycomb lattice (Liu et al., 2013), with a high specific surface area and easy surface modification (Hong Wang et al., 2021). Zare-zardini et al. (2018a) studied several graphene nanosystems treated with minor ginsenoside Rh2, that is, Rh2 combined with lysine (Lys) treated high porous graphene (Gr) (Gr-Lys-Rh2), Rh2 combined with arginine (Arg) treated Gr (Gr-Arg-Rh2). The results showed that the functionalization of Gr composite Rh2, positively charged amino acids lysine and Gr showed higher antitumor activity. Compared with pure graphene, it reduces the toxicity to the coagulation system and heart tissue.

This may be due to the synergistic effect of minor ginsenoside and graphene, which show better antitumor effect and cytotoxic activity. In addition, there is stronger electrostatic absorption and interaction between positively charged amino acids and negative charged amino acids on certain biological surfaces and cancer cells, which may also be responsible for the enhanced biological activity.

3.2.3 Pharmacological effects and mechanism of minor ginsenoside composite nano-drug delivery system

Combining organic nanomaterials with inorganic nanomaterials to prepare composite nanocarriers can make the carrier absorbed adequately to improve curative effect (Zhou, 2020). Lee et al. (2014) developed a mixed composite nanocarrier based on hyaluronic acid-ceramide (HACE) and 1,2-distearoyl-*sn*-glycero-3-phosphoethanolamine-N-[methoxy (polyethyleneglycol)-2000] to load minor ginsenoside Rg3. The results showed that compared with HACE alone, the composite nanocarrier had higher cell uptake rate and enhanced circulation time in the blood stream. This may be due to the fact that lipid vesicles can bind to the cell surface and their lipid parts can fuse with the cell membrane, thus improving the cell uptake rate. The lipid fraction also provides spatial stability, thereby prolonging circulation in the blood stream. Therefore, composite nanocarriers can become a superior choice for drug delivery.

3.2.4 Pharmacological effects and mechanism of other new minor ginsenoside nano-drug delivery systems

Other novel nanocarriers for the delivery of drugs and active ingredients include nanocapsules, liquid crystals, polymer vesicles and nanofibers (Liu and Feng, 2015). Sun et al. (2014) used electrospun PLGA with three-dimensional nanofiber structure as drug carrier and coated it with chitosan to load minor ginsenoside Rg3. The results showed that PLGA-Rg3 surface coated chitosan had a better effect on inhibiting hypertrophic scar formation than materials and drugs alone. This may be because chitosan coating promotes wound healing and improves the hydrophilicity and biocompatibility of fiber membrane. The sustained release of Rg3 also helps to significantly inhibit the formation of hypertrophic scars.

4 Conclusion and prospects

Minor ginsenosides have attracted the attention of researchers due to their various pharmacological activities. However, because of poor water solubility and stability, the efficacy cannot be well guaranteed, which limits the clinical application. Nanocrystallization of minor ginsenosides can well solve this problem. At present, relevant researchers have explored and practiced in the preparation methods, pharmacological effects and mechanism of minor ginsenosides nanocrystallization, which provides a reference for the clinical application of minor ginsenoside nanoparticles.

Compared with nanocarriers, nanocrystals have the advantages of high drug load, simple preparation methods and not restricted by carrier materials. The preparation difficulty of nanocrystals is closely related to the choice of preparation methods and physicochemical properties of drugs. However, it is still difficult to shorten the preparation time and improve the stability of nanocrystals. The key factors affecting the preparation of nanocrystals and the content of targeted drug delivery need to be further studied. Compared with nanocrystals, nanocarriers can achieve targeted release and protect drugs from early release before reaching the endpoint. But there are also some shortcomings. In the preparation process, the research and development of nanocarrier technology requirements are high, and the preparation process is complex. The process is greatly affected by equipment, operating conditions, raw materials and process parameters. The subtle changes in the manufacturing process can cause large changes in the final product quality, resulting in high uncertainty and poor reproducibility in production. The tissue specificity of the targeted drug is not high, and most experiments are conducted *in vitro,* and intracorporeal environment is not easy to be detected. So the development of core technology of nano medicine needs to be further broken.

In summary, some achievements have been made in the research of minor ginsenoside nanoparticles. However, the research on the targeted release, mechanism and optimization of preparation of minor ginsenoside nanoparticles needs to be further strengthened. It is necessary to further explore the pharmacokinetics *in vivo* and pre-clinical safety evaluation and management of minor ginsenoside nano-drugs, in addition, to evaluate the side effects and adverse reactions of minor ginsenoside nano-drugs to patients and promote the clinical application of nano minor ginsenoside drugs. The development and improvement of new dosage forms of minor ginsenosides show great potential in minor ginsenoside drug treatment.

Author contributions

TW and LW contributed to design of the study. YK and LH responsible for document retrieval and manuscript writing. YS responsible for making illustrations and tables. TW, YK, LH, ZL, and LL contributed to manuscript revision. All authors read and approved the submitted version.

Conflict of interest

The authors declare that the research was conducted in the absence of any commercial or financial relationships that could be construed as a potential conflict of interest.

Publisher's note

References

Arneth, B. (2019). Tumor microenvironment. *Medicina* 56 (1), 15. doi:10.3390/medicina56010015

Bianco, A., Kostarelos, K., and Prato, M. (2005). Applications of carbon nanotubes in drug delivery. *Curr. Opin. Chem. Biol.* 9 (6), 674–679. doi:10.1016/j.cbpa.2005.10.005

Bolko, K., Zvonar, A., and Gašperlin, M. (2014). Mixed lipid phase SMEDDS as an innovative approach to enhance resveratrol solubility. *Drug Dev. Ind. Pharm.* 40 (1), 102–109. doi:10.3109/03639045.2012.749888

Cao, L. Q., Wang, S., Zhang, L. M., and Li, J. N. (2022). mPEG-bP (Glu-co-Phe) nanoparticles increase gastric retention time and gastric ulcer treatment efficacy of 20 (S)-ginsenoside Rg3. *Biomed. Pharmacother.* 146, 112608. doi:10.1016/j.biopha.2021.112608

Chen, D. Z., Wang, C. Z., Chen, W. Y., Li, X. D., Liu, L., Zhang, T., et al. (2013). Anti-proliferation effects of 20 (S)-ginsenoside Rg3 loaded human albumin nanoparticles (SPG-Rg3-HAS-NP) on human cervical cancer Hela cells *in vitro*. *Chin. J. Laboratory Diagnosis* 17 (8), 1394–1397. doi:10.3969/j.issn.1007-4287.2013.08.010

Chen, D. Q., Yu, H. Y., Mu, H. J., Li, G. S., and Shen, Y. (2014). Novel multicore niosomes based on double pH-sensitive mixed micelles for Ginsenoside Rh2 delivery. *Artif. Cells Nanomed. Biotechnol.* 42 (3), 205–209. doi:10.3109/21691401.2013.794358

Cheng, H. Y., and Zheng, D. R. (2014). Inhibitory effect of ginsenoside albumin nanoparticles on the growth of human lung adenocarcinoma cell A549. *Heilongjiang Med. J.* 38 (10), 1138–1140. doi:10.3969/j.issn.1004-5775.2014.10.008

Choi, J. H., Cho, S. H., Yun, J. J., Yu, Y. B., and Cho, C. W. (2015). Ethosomes and transfersomes for topical delivery of ginsenoside Rh1 from red ginseng: Characterization and *in vitro* evaluation. *J. Nanosci. Nanotechnol.* 15 (8), 5660–5662. doi:10.1166/jnn.2015.10462

Cui, Y. Q., Yang, P., Sun, P., Yan, Y. D., Jin, G. Y., Quan, J. S., et al. (2020). Preparation of PEGylated liposomal ginsenoside; formulation design and *in vitro* evaluation. *Indian J. Pharm. Sci.* 82 (1), 149–156. doi:10.36468/pharmaceutical-sciences.632

Dai, M. M., Zhang, Y. Y., Wang, S. H., and Sheng, H. G. (2019). Research progress in nanocrystal drug preparation technology. *China Powder Sci. Technol.* 25 (5), 56–62. doi:10.13732/j.issn.1008-5548.2019.05.010

Dong, X. X., Yang, C. R., Ping, Y., Liu, C. J., Lin, J., and Zhang, Y. H. (2017). Research advances on brain-targeted strategies of nanoscale drug delivery system. *Guangdong Chem. Ind.* 44 (7), 142–143. doi:10.3969/j.issn.1007-1865.2017.07.061

Dong, Y. N., Fu, R. Z., Yang, J., Ma, P., Liang, L. H., Mi, Y., et al. (2019). Folic acid-modified ginsenoside Rg5-loaded bovine serum albumin nanoparticles for targeted cancer therapy *in vitro* and *in vivo*. *Int. J. Nanomedicine* 14, 6971–6988. doi:10.2147/IJN.S210882

Feifei Yang, F. F., Zhou, J., Hu, X., Yu, S. K., Liu, C. Y., Pan, R. L., et al. (2017). Preparation and evaluation of self-microemulsions for improved bioavailability of ginsenoside-Rh1 and Rh2. *Drug Deliv. Transl. Res.* 7 (5), 731–737. doi:10.1007/s13346-017-0402-7

Fukuda, K., Utsumi, H., Shoji, J., and Hamada, A. (1985). Saponins can cause the agglutination of phospholipid vesicles. *Biochim. Biophys. Acta* 820 (2), 199–206. doi:10.1016/0005-2736(85)90113-0

Gao, L., Liu, G. Y., Ma, J. L., Wang, X. Q., Zhou, L., Li, X., et al. (2012). Drug nanocrystals: *In vivo* performances. *J. Control. Release* 160 (3), 418–430. doi:10.1016/j.jconrel.2012.03.013

Geng, L., Xing, S. L., Yu, J., Sun, W. M., Jin, X. Y., and Hua, B. J. (2014a). Research of 20(R)-ginsenoside Rg3 and PEG-PLGA-Rg3 nanoparticles on the angiogennesis of lung cancer *in vivo*. *China J. Traditional Chin. Med. Pharm.* 29 (2), 601–604.

Geng, L., Yang, C. L., Tian, T. D., Yu, J., Sun, W. M., Jin, X. Y., et al. (2014b). Influences of nanoparticles Rg3 and PEG-PLGA-Rg3 on endothelial cells invasion and tube formation. *J. Beijing Univ. Traditional Chin. Med.* 37 (9), 611–615. doi:10.3969/j.issn.1006-2157.2014.09.009

Geng, L., Fan, J., Gao, Q. L., Yu, J., and Hua, B. J. (2016). Preliminary study for the roles and mechanisms of 20(R)-ginsenoside Rg3 and PEG-PLGA-Rg3 nanoparticles in the Lewis lung cancer mice. *J. Peking Univ. Heal. Sci.* 48 (3), 496–501. doi:10.3969/j.issn.1671-167X.2016.03.021

Gu, Q., Zhou, J., Zhang, J. M., Shang, Z., Shen, T., Yang, X. J., et al. (2021). Preparation of ginsenoside Rh2-Loaded chitosan nanoparticles and its cytotoxicity to A549 cells. *Food Sci.* 42 (7), 162–168. doi:10.7506/spkx1002-6630-20200311-175

He, Y., Hu, Z. Y., Li, A. R., Zhu, Z. Z., Yang, N., Ying, Z. X., et al. (2019). Recent advances in biotransformation of saponins. *Molecules* 24 (13), E2365. doi:10.3390/molecules24132365

Heidegger, S., Gößl, D., Schmidt, A., Niedermayer, S., Argyo, C., Endres, S., et al. (2016). Immune response to functionalized mesoporous silica nanoparticles for targeted drug delivery. *Nanoscale* 8 (2), 938–948. doi:10.1039/c5nr06122a

Hong, C., Wang, D., Liang, J. M., Guo, Y. Z., Zhu, Y., Xia, J. X., et al. (2019). Novel ginsenoside-based multifunctional liposomal delivery system for combination therapy of gastric cancer. *Theranostics* 9 (15), 4437–4449. doi:10.7150/thno.34953

Hong, C., Liang, J. M., Xia, J. X., Zhu, Y., Guo, Y. Z., Wang, A. N., et al. (2020). One stone four birds: A novel liposomal delivery system multi-functionalized with ginsenoside Rh2 for tumor targeting therapy. *Nanomicro. Lett.* 12 (1), 129. doi:10.1007/s40820-020-00472-8

Hong Wang, H., Zheng, Y., Sun, Q., Zhang, Z., Zhao, M. N., Peng, C., et al. (2021). Ginsenosides emerging as both bifunctional drugs and nanocarriers for enhanced antitumor therapies. *J. Nanobiotechnology* 19 (1), 322. doi:10.1186/s12951-021-01062-5

Hou, P. P., Pu, F. L., Zou, H. Y., Diao, M. X., Zhao, C. H., Xi, C. Y., et al. (2019). Whey protein stabilized nanoemulsion: A potential delivery system for ginsenoside Rg3 whey protein stabilized nanoemulsion: Potential Rg3 delivery system. *Food Biosci.* 31, 100427. doi:10.1016/j.fbio.2019.100427

Hui, G., Zhao, Y., Zhang, J. Z., Liu, W., Li, H. D., Zhao, B., et al. (2014). Raman and DSC spectroscopic studies on the interaction between ginsenosides and DMPC bilayer membranes. *Spectrosc. Spectr. Analysis* 34 (2), 410–414. doi:10.3964/j.issn.1000-0593(2014)02-0410-05

Iyer, A. K., Khaled, G., Fang, J., and Maeda, H. (2006). Exploiting the enhanced permeability and retention effect for tumor targeting. *Drug Discov. Today* 11 (17-18), 812–818. doi:10.1016/j.drudis.2006.07.005

Jiang, J., Wu, C., Lu, M. M., and Qiu, Y. (2016). The research of mesoporous silica nanoparticles MCM-41 loading ginsenoside Rg3 for human lung cancer cells A549. *Chin. Pharm. J.* 51 (17), 1478–1482. doi:10.11669/cpj.2016.17.010

Jin, X., Zhou, J. P., Zhang, Z. H., and Lv, H. X. (2018). The combined administration of parthenolide and ginsenoside CK in long circulation liposomes with targeted tLyp-1 ligand induce mitochondria-mediated lung cancer apoptosis. *Artif. Cells Nanomed. Biotechnol.* 46 (3), S931–S942. doi:10.1080/21691401.2018.1518913

Kaehler, T. (1994). Nanotechnology: Basic concepts and definitions. *Clin. Chem.* 40 (9), 1797. doi:10.1093/clinchem/40.9.1797b

Kang, H., Hwang, Y. G., Lee, T. G., Jin, C. R., Cho, C. H., Jeong, H. Y., et al. (2016). Use of gold nanoparticle fertilizer enhances the ginsenoside contents and anti-inflammatory effects of red ginseng. *J. Microbiol. Biotechnol.* 26 (10), 1668–1674. doi:10.4014/jmb.1604.04034

Kim, Y. J., Perumalsamy, H., Markus, J., Balusamy, S. R., Wang, C., Kang, S. H., et al. (2019). Development of lactobacillus kimchicus dcy51t-mediated gold nanoparticles for delivery of ginsenoside compound K: *In vitro* photothermal effects and apoptosis detection in cancer cells. *Artif. Cells Nanomed. Biotechnol.* 47 (1), 30–44. doi:10.1080/21691401.2018.1541900

Lan Li, L., Ni, J. Y., Li, M., Chen, J. R., Han, L. F., Zhu, Y., et al. (2017). Ginsenoside Rg3 micelles mitigate doxorubicin-induced cardiotoxicity and enhance its anticancer efficacy. *Drug Deliv.* 24 (1), 1617–1630. doi:10.1080/10717544.2017.1391893

Lee, J. Y., Yang, H., Yoon, I. S., Kim, S. B., Ko, S. H., Shim, J. S., et al. (2014). Nanocomplexes based on amphiphilic hyaluronic acid derivative and polyethylene glycol–lipid for ginsenoside Rg3 delivery. *J. Pharm. Sci.* 103 (10), 3254–3262. doi:10.1002/jps.24111

Lei Yang, L., Zhang, Z. H., Hou, J., Jin, X., Ke, Z. C., Liu, D., et al. (2017). Targeted delivery of ginsenoside compound K using TPGS/PEG-PCL mixed micelles for effective treatment of lung cancer. *Int. J. Nanomedicine* 12, 7653–7667. doi:10.2147/IJN.S144305

Li, Y., Zhang, T. J., Liu, S. X., and Chen, C. Q. (2009). The cardioprotective effect of postconditioning is mediated by ARC through inhibiting mitochondrial apoptotic pathway. *Apoptosis.* 14 (1), 164–172. doi:10.1007/s10495-008-0296-4

Li, H., Hu, S. L., Wang, H. L., and Zhu, Z. T. (2014a). TF modified doxorubicin and Rg3 loaded liposome for gastric cancer targeting and therapy. *Chin. J. Biochem. Pharm.* 34 (1), 9–11, 15.

Li, J., Xu, H. L., and Hua, L. (2014b). Preparation and properties of RGD modified paclitaxel and Rg3 loaded liposome *in vitro*. *West China J. Pharm. Sci.* 29 (3), 251–253. doi:10.13375/j.cnki.wcjps.2014.03.007

Li, L., Wang, Y. L., Guo, R., Li, S., Ni, J. Y., Gao, S., et al. (2020). Ginsenoside Rg3-loaded, reactive oxygen species-responsive polymeric nanoparticles for alleviating myocardial ischemia-reperfusion injury. *J. Control. Release* 317, 259–272. doi:10.1016/j.jconrel.2019.11.032

Li, B., Zhang, C. B., Song, K., and Lu, W. Y. (2021a). Advances in biosynthesis of rare ginsenosides. *China Biotechnol.* 41 (6), 71–88. doi:10.13523/j.cb.2103036

Li, Y., Hao, T. N., and Yu, Z. H. (2021b). Preparation and evaluation of docetaxel and elacridar albumin nanoparticles. *West China J. Pharm. Sci.* 36 (1), 9–14. doi:10.13375/j.cnki.wcjps.2021.01.003

Linqiang Xu, L. Q., Yu, H., Yin, S. P., Zhang, R. X., Zhou, Y. D., Li, J., et al. (2015). Liposome-based delivery systems for ginsenoside Rh2: *In vitro* and *in vivo* comparisons. *J. Nanopart. Res.* 17 (10), 415. doi:10.1007/s11051-015-3214-z

Liu, J., Rinzler, A. G., Dai, H. J., Hafner, J. H., Bradley, R. K., Boul, P. J., et al. (1998). Fullerene pipes. *Science* 280 (5367), 1253–1256. doi:10.1126/science.280.5367.1253

Liu, C. B., Zhang, D., Li, D. G., Jiang, D., and Chen, X. (2008). Preparation and characterization of biodegradable polylactide (PLA) microspheres encapsulating ginsenoside Rg3. *Chem. Res. Chin. Univ.* 24 (5), 588–591. doi:10.1016/s1005-9040(08)60124-5

Liu, J. Q., Cui, L., and Losic, D. (2013). Graphene and graphene oxide as new nanocarriers for drug delivery applications. *Acta Biomater.* 9 (12), 9243–9257. doi:10.1016/j.actbio.2013.08.016

Liu, X. C., Zhang, R., and Yang, Y. S. (2014). The application of nanotechnology in traditional Chinese medicine. *J. Inn. Mong. Med. Univ.* 36 (5), 458–464. doi:10.16343/j.cnki.issn.2095-512x.2014.05.005

Liu, R., Xu, P. P., Li, S. L., and Zhang, W. (2019). Research progress in preparation of rare ginsenosides by biotransformation technology. *Special Wild Econ. Animal Plant Res.* 41 (2), 114–117. doi:10.16720/j.cnki.tcyj.2019.02.027

Liu, Y., and Feng, N. P. (2015). Nanocarriers for the delivery of active ingredients and fractions extracted from natural products used in traditional Chinese medicine (TCM). *Adv. Colloid Interface Sci.* 221, 60–76. doi:10.1016/j.cis.2015.04.006

Luo, X., Wang, H., and Ji, D. G. (2021). Carbon nanotubes (CNT)-loaded ginsenosides Rb3 suppresses the PD-1/PD-L1 pathway in triple-negative breast cancer. *Aging (Albany NY)* 13 (13), 17177–17189. doi:10.18632/aging.203131

Lv, S. X., Li, M. Q., Tang, Z. H., Song, W. T., Sun, H., Liu, H. Y., et al. (2013). Doxorubicin-loaded amphiphilic polypeptide-based nanoparticles as an efficient drug delivery system for cancer therapy. *Acta Biomater.* 9 (12), 9330–9342. doi:10.1016/j.actbio.2013.08.015

Ma, Q. M., Jin, Y. Q., Cao, J., Xi, L., and Sun, Y. (2021). Recent progress of self-assembly-based chitosan/phospholipid nanoparticles for advanced drug delivery. *Chin. J. Pharm.* 52 (5), 619–627. doi:10.16522/j.cnki.cjph.2021.05.004

Mathiyalagan, R., Subramaniyam, S., Kim, Y. J., Kim, Y. C., and Yang, D. C. (2014). Ginsenoside compound K-bearing glycol chitosan conjugates: Synthesis, physicochemical characterization, and *in vitro* biological studies. *Carbohydr. Polym.* 112, 359–366. doi:10.1016/j.carbpol.2014.05.098

Mathiyalagan, R., Wang, C., Kim, Y. J., Castro-Aceituno, V., Ahn, S., Subramaniyam, S., et al. (2019). Preparation of polyethylene glycol-ginsenoside Rh1 and Rh2 conjugates and their efficacy against lung cancer and inflammation. *Molecules* 24 (23), E4367. doi:10.3390/molecules24234367

Moein Moghimi, S., Hamad, I., Bünger, R., Andresen, T. L., Jørgensen, K., Christy Hunter, A., et al. (2006). Activation of the human complement system by cholesterol-rich and pegylated liposomes—Modulation of cholesterol-rich liposome-mediated complement activation by elevated serum ldl and hdl levels. *J. Liposome Res.* 16 (3), 167–174. doi:10.1080/08982100600848801

Nag, S. A., Qin, J. J., Wang, W., Wang, M. H., Wang, H., Zhang, R. W., et al. (2012). Ginsenosides as anticancer agents: *In vitro* and *in vivo* activities, structure-activity relationships, and molecular mechanisms of action. *Front. Pharmacol.* 3, 25. doi:10.3389/fphar.2012.00025

Nasongkla, N., Bey, E., Ren, J., Ai, H., Khemtong, C., Guthi, J. S., et al. (2006). Multifunctional polymeric micelles as cancer-targeted, MRI-ultrasensitive drug delivery systems. *Nano Lett.* 6 (11), 2427–2430. doi:10.1021/nl061412u

Ozgen, P. S. O., Atasoy, S., Kurt, B. Z., Durmus, Z., Yigit, G., Dag, A., et al. (2020). Glycopolymer decorated multiwalled carbon nanotubes for dual targeted breast cancer therapy. *J. Mat. Chem. B* 8 (15), 3123–3137. doi:10.1039/c9tb02711d

Pan, C. S., Wang, F. H., Guo, J. W., Sang, W., and Wang, Y. (2015). Optimization of formulation and preparation of ginsenoside Rg3 PLGA nanoparticles. *Cent. South Pharm.* 13 (11), 1132–1136. doi:10.7539/j.issn.1672-2981.2015.11.004

Park, J. D., Rhee, D. K., and Lee, Y. H. (2005). Biological activities and chemistry of saponins from *Panax ginseng* CA Meyer. *Phytochem. Rev.* 4 (2), 159–175. doi:10.1007/s11101-005-2835-8

Park, Y. M., Im, A., Joo, E. J., Lee, J. H., Park, H. G., Kang, Y. H., et al. (2011). Conjugation of ginsenoside Rg3 with gold nanoparticles. *Bull. Korean Chem. Soc.* 32 (1), 286–290. doi:10.5012/bkcs.2011.32.1.286

Pei, Z. R., Li, F. Y., Gong, J. N., Zou, L. E., Ding, L. Q., and Qiu, F. (2021). Research progress on nano-drug delivery systems for antitumor active components of traditional Chinese medicine. *Chin. Traditional Herb. Drugs* 52 (24), 7658–7667. doi:10.7501/j.issn.0253-2670.2021.24.029

Peng Li, P., Zhou, X. Y., Qu, D., Guo, M. F., Fan, C. Y., Zhou, T., et al. (2017). Preliminary study on fabrication, characterization and synergistic anti-lung cancer effects of self-assembled micelles of covalently conjugated celastrol–polyethylene glycol–ginsenoside Rh2. *Drug Deliv.* 24 (1), 834–845. doi:10.1080/10717544.2017.1326540

Qiu, J., Huang, L. J., and Zhang, L. X. (2004). Nanomedicine and nanocarrier systems. *China Pharm.* 13 (3), 28–29. doi:10.3969/j.issn.1006-4931.2004.03.021

Qiu, R. N., Qian, F., Wang, X. F., Li, H. J., and Wang, L. Z. (2019). Targeted delivery of 20 (S)-ginsenoside Rg3-based polypeptide nanoparticles to treat colon cancer. *Biomed. Microdevices* 21 (1), 18. doi:10.1007/s10544-019-0374-0

Qu, D., Guo, M. F., Qin, Y., Wang, L. X., Zong, B., Chen, Y. Y., et al. (2017a). A multicomponent microemulsion using rational combination strategy improves lung cancer treatment through synergistic effects and deep tumor penetration. *Drug Deliv.* 24 (1), 1179–1190. doi:10.1080/10717544.2017.1365394

Qu, D., Wang, L. X., Liu, M., Shen, S. Y., Li, T., Liu, Y. P., et al. (2017b). Oral nanomedicine based on multicomponent microemulsions for drug-resistant breast cancer treatment. *Biomacromolecules* 18 (4), 1268–1280. doi:10.1021/acs.biomac.7b00011

Sahay, G., Alakhova, D. Y., and Kabanov, A. V. (2010). Endocytosis of nanomedicines. *J. Control. Release* 145 (3), 182–195. doi:10.1016/j.jconrel.2010.01.036

Shaozhi Zhang, S. Z., Liu, J. W., Ge, B. J., Du, M. L., Fu, L., Fu, Y. S., et al. (2017). Enhanced antitumor activity in A431 cells via encapsulation of 20 (R)-ginsenoside Rg3 in PLGA nanoparticles. *Drug Dev. Ind. Pharm.* 43 (10), 1734–1741. doi:10.1080/03639045.2017.1339079

Shen, S. W., Wang, Y., Zhu, B. B., Tian, J., and Wang, J. D. (2014). Developments of ultrafine powder preparation techniques. *Environ. Eng.* 32 (9), 102–105. doi:10.13205/j.hjgc.201409023

Shen, C. Y., Hu, F., Zhu, J. J., Li, X. F., Shen, B. D., Yuan, H. L., et al. (2021). Advances in formation and application of self-assembled nanoparticles from traditional Chinese medicine. *China J. Chin. Materia Medica* 46 (19), 4875–4880. doi:10.19540/j.cnki.cjcmm.20210528.603

Shi Kam, N. W., Jessop, T. C., Wender, P. A., and Dai, H. (2004). Nanotube molecular transporters: Internalization of carbon nanotube–protein conjugates into mammalian cells. *J. Am. Chem. Soc.* 126 (22), 6850–6851. doi:10.1021/ja0486059

Singh, P., Kim, Y. J., Singh, H., Ahn, S., Castro-Aceituno, V., Yang, D. C., et al. (2017a). *In situ* preparation of water-soluble ginsenoside Rh2-entrapped bovine serum albumin nanoparticles: *In vitro* cytocompatibility studies. *Int. J. Nanomedicine* 12, 4073–4084. doi:10.2147/IJN.S125154

Singh, P., Singh, H., Castro-Aceituno, V., Ahn, S., Kim, Y. J., Yang, D., et al. (2017b). Bovine serum albumin as a nanocarrier for the efficient delivery of ginsenoside compound K: Preparation, physicochemical characterizations and *in vitro* biological studies. *RSC Adv.* 7 (25), 15397–15407. doi:10.1039/c6ra25264h

Singh, P., Singh, H., Castro-Aceituno, V., Ahn, S., Kim, Y. J., Farh, M. E. A., et al. (2017c). Engineering of mesoporous silica nanoparticles for release of ginsenoside CK and Rh2 to enhance their anticancer and anti-inflammatory efficacy: *In vitro* studies. *J. Nanopart. Res.* 19 (7), 257. doi:10.1007/s11051-017-3949-9

Sinha, B., Müller, R. H., and Möschwitzer, J. P. (2013). Bottom-up approaches for preparing drug nanocrystals: Formulations and factors affecting particle size. *Int. J. Pharm.* 453 (1), 126–141. doi:10.1016/j.ijpharm.2013.01.019

Su, X. M., Zhang, D. S., Zhang, H. W., Zhao, K. Y., and Hou, W. S. (2020). Preparation and characterization of angiopep-2 functionalized ginsenoside-Rg3 loaded nanoparticles and the effect on C6 glioma cells. *Pharm. Dev. Technol.* 25 (3), 385–395. doi:10.1080/10837450.2018.1551901

Sun, X. M., Cheng, L. Y., Zhu, W. K., Hu, C. M., Jin, R., Sun, B. S., et al. (2014). Use of ginsenoside Rg3-loaded electrospun PLGA fibrous membranes as wound cover induces healing and inhibits hypertrophic scar formation of the skin. *Colloids Surf. B Biointerfaces* 115, 61–70. doi:10.1016/j.colsurfb.2013.11.030

Talegaonkar, S., Azeem, A., Ahmad, F. J., Khar, R. K., Pathan, S. A., Khan, Z. I., et al. (2008). Microemulsions: A novel approach to enhanced drug delivery. *Recent Pat. Drug Deliv. Formul.* 2 (3), 238–257. doi:10.2174/187221108786241679

Tang, F. Q., Li, L. L., and Chen, D. (2012). Mesoporous silica nanoparticles: Synthesis, biocompatibility and drug delivery. *Adv. Mat.* 24 (12), 1504–1534. doi:10.1002/adma.201104763

Tao, C., Zhang, J. J., Wang, J. X., and Le, Y. (2018). Ginsenoside drug nanocomposites prepared by the aerosol solvent extraction system for enhancing drug solubility and stability. *Pharmaceutics* 10 (3), 95. doi:10.3390/pharmaceutics10030095

Torchilin, V. P. (2010). Passive and active drug targeting: Drug delivery to tumors as an example. *Drug Deliv. (Lond).* 197, 3–53. doi:10.1007/978-3-642-00477-3_1

Vigderman, L., and Zubarev, E. R. (2013). Therapeutic platforms based on gold nanoparticles and their covalent conjugates with drug molecules. *Adv. Drug Deliv. Rev.* 65 (5), 663–676. doi:10.1016/j.addr.2012.05.004

Wang, B. L., Shen, Y. M., Zhang, Q. W., Li, Y. L., Luo, M., Liu, Z., et al. (2013). Codelivery of curcumin and doxorubicin by MPEG-PCL results in improved efficacy of systemically administered chemotherapy in mice with lung cancer. *Int. J. Nanomedicine* 8, 3521–3531. doi:10.2147/IJN.S45250

Wang, L. Q., Rong, X. Y., Liu, K., Hu, Y., Gao, Q., Zhao, S. C., et al. (2014). Preparation technologies and applications of drug nanocrystals. *J. Hebei Univ. Sci. Technol.* 35 (4), 339–348. doi:10.7535/hbkd.2014yx04006

Wang, X. H., Zhang, X., Fan, L. L., He, H., Zhao, X. F., Zhang, Y. Y., et al. (2018). Influence of polymeric carrier on the disposition and retention of 20 (R)-ginsenoside-rg3-loaded swellable microparticles in the lung. *Drug Deliv. Transl. Res.* 8 (1), 252–265. doi:10.1007/s13346-017-0456-6

Wei, Z. F., Bi, L. L., and Bao, C. Y. (2014). Study of transferrin conjugated paclitaxel and Rg3loaded liposome for tumor targeting and therapy *in vitro* and *in vivo*. *Chin. J. Cancer Prev. Treat.* 21 (16), 1227–1231. doi:10.16073/j.cnki.cjcpt.2014.16.001

Wei Zhang, W., Wang, X. Y., Zhang, M., Xu, M., Tang, W. Y., Zhang, Y., et al. (2017). Intranasal delivery of microspheres loaded with 20 (R)-ginsenoside Rg3 enhances anti-fatigue effect in mice. *Curr. Drug Deliv.* 14 (6), 867–874. doi:10.2174/1567201814666161109121151

Weiguo Xu, W. G., Ding, J. X., Xiao, C. S., Li, L. Y., Zhuang, X. L., Chen, X. S., et al. (2015). Versatile preparation of intracellular-acidity-sensitive oxime-linked polysaccharide-doxorubicin conjugate for malignancy therapeutic. *Biomaterials* 54, 72–86. doi:10.1016/j.biomaterials.2015.03.021

Wu, L., Qiao, Y. L., Wang, L. N., Guo, J. H., Wang, G. C., He, W., et al. (2015). A self-microemulsifying drug delivery system (SMEDDS) for a novel medicative compound against depression: A preparation and bioavailability study in rats. *AAPS PharmSciTech* 16 (5), 1051–1058. doi:10.1208/s12249-014-0280-y

Xia, X. J., Tao, J., Ji, Z. W., Long, C. C., Hu, Y., Zhao, Z. Y., et al. (2020). Increased antitumor efficacy of ginsenoside Rh2 via mixed micelles: *In vivo* and *in vitro* evaluation. *Drug Deliv.* 27 (1), 1369–1377. doi:10.1080/10717544.2020.1825542

Xie, Y. J., Yu, T., and Lou, W. (2016). Preparation and assessment of the antitumor effect of ginsenoside Rg3 nanocrystals. *Her. Med.* 35 (11), 1186–1189. doi:10.3870/j.issn.1004-0781.2016.11.007

Xu, Y., Li, X., Gong, W., Hung, H. B., Zhu, B. W., Hu, J. N., et al. (2020). Construction of ginsenoside nanoparticles with pH/reduction dual response for enhancement of their cytotoxicity toward HepG2 cells. *J. Agric. Food Chem.* 68 (32), 8545–8556. doi:10.1021/acs.jafc.0c03698

Xu, Y., Zhu, B. W., Li, X., Li, Y. F., Ye, X. M., Hu, J. N., et al. (2022). Glycogen-based pH and redox sensitive nanoparticles with ginsenoside Rh2 for effective treatment of ulcerative colitis. *Biomaterials* 280, 121077. doi:10.1016/j.biomaterials.2021.121077

Xue Wang, X., Zheng, W. W., Shen, Q., Wang, Y. H., Tseng, Y. J., Luo, Z. G., et al. (2021). Identification and construction of a novel biomimetic delivery system of paclitaxel and its targeting therapy for cancer. *Signal Transduct. Target. Ther.* 6 (1), 33. doi:10.1038/s41392-020-00390-6

Yang, X. L., Xu, H. B., Wu, J. Z., and Xie, C. S. (2000). Application of nano-technology in the research of traditional Chinese medicine. *J. Huazhong Univ. Sci. Technol.* 28 (12), 104–105. doi:10.3321/j.issn:1671-4512.2000.12.038

Yang, R., Chen, D. Z., Li, M. F., Miao, F. Q., Liu, P. D., Tang, Q. S., et al. (2014). 20 (s)-ginsenoside Rg3-loaded magnetic human serum albumin nanospheres applied to HeLa cervical cancer cells *in vitro*. *Biomed. Mat. Eng.* 24 (6), 1991–1998. doi:10.3233/BME-141008

Yang, L., Xin, J., Zhang, Z. H., Yan, H. M., Wang, J., Sun, E., et al. (2016). TPGS-Modified liposomes for the delivery of ginsenoside compound K against non-small cell lung cancer: Formulation design and its evaluation *in vitro* and *in vivo*. *J. Pharm. Pharmacol.* 68 (9), 1109–1118. doi:10.1111/jphp.12590

Ye, F. F., Dai, Y., Xu, H., Li, Y., Yu, X., Hu, M. N., et al. (2014). Preparation and characterization of ginsenosides Rg3 liposomes and their inhibitory effect on melanoma cells. *Chin. J. New Drugs* 23 (21), 2542–2546.

Yoo, J. M., Yang, J. H., Yang, H. J., Cho, W. K., and Ma, J. Y. (2016). Inhibitory effect of fermented Arctium lappa fruit extract on the IgE-mediated allergic response in RBL-2H3 cells. *Int. J. Mol. Med.* 37 (2), 501–508. doi:10.3892/ijmm.2015.2447

Youwen Zhang, Y. W., Tong, D. Y., Che, D. B., Pei, B., Xia, X. D., Yuan, G. F., et al. (2017). Ascorbyl palmitate/d-α-tocopheryl polyethylene glycol 1000 succinate monoester mixed micelles for prolonged circulation and targeted delivery of compound K for antilung cancer therapy *in vitro* and *in vivo*. *Int. J. Nanomedicine* 12, 605–614. doi:10.2147/IJN.S119226

Yu, W. L., Zhao, Y. P., and Zhang, H. J. (2006). Preparation of PLA microparticles by ASES technique. *CIESC J.* 57 (7), 1694–1698. doi:10.3321/j.issn:0438-1157.2006.07.035

Yu, H., Teng, L. R., Meng, Q. F., Li, Y. H., Sun, X. C., Lu, J. H., et al. (2013). Development of liposomal ginsenoside Rg3: Formulation optimization and evaluation of its anticancer effects. *Int. J. Pharm.* 450 (1-2), 250–258. doi:10.1016/j.ijpharm.2013.04.065

Yu, X., Xu, H., Hu, M. N., Luan, X. J., Wang, K. Q., Fu, Y. S., et al. (2015). Ginsenoside Rg3 bile salt-phosphatidylcholine-based mixed micelles: Design, characterization, and evaluation. *Chem. Pharm. Bull.* 63 (5), 361–368. doi:10.1248/cpb.c15-00045

Zare-Zardini, H., Taheri-Kafrani, A., Amiri, A., and Bordbar, A. K. (2018a). New generation of drug delivery systems based on ginsenoside Rh2-Lysine-and Arginine-treated highly porous graphene for improving anticancer activity. *Sci. Rep.* 8 (1), 586. doi:10.1038/s41598-017-18938-y

Zare-Zardini, H., Taheri-Kafrani, A., Ordooei, M., Amiri, A., and Karimi-Zarchi, M. (2018b). Evaluation of toxicity of functionalized graphene oxide with ginsenoside Rh2, lysine and arginine on blood cancer cells (K562), red blood cells, blood coagulation and cardiovascular tissue: *In vitro* and *in vivo* studies. *J. Taiwan Inst. Chem. Eng.* 93, 70–78. doi:10.1016/j.jtice.2018.08.010

Zare-Zardini, H., Alemi, A., Taheri-Kafrani, A., Hosseini, S. A., Soltaninejad, H., Hamidieh, A. A., et al. (2020). Assessment of a new ginsenoside Rh2 nanoniosomal formulation for enhanced antitumor efficacy on prostate cancer: An *in vitro* study. *Drug Des. devel. Ther.* 14, 3315–3324. doi:10.2147/DDDT.S261027

Zhang, A. W., Guo, W. H., Qi, Y. F., Wang, J. Z., Ma, X. X., Yu, D. X., et al. (2016). Synergistic effects of gold nanocages in hyperthermia and radiotherapy treatment. *Nanoscale Res. Lett.* 11 (1), 279. doi:10.1186/s11671-016-1501-y

Zhang, J. M., Wang, Y. J., Jiang, Y. Y., Liu, T. W., Luo, Y. Y., Diao, E. J., et al. (2018). Enhanced cytotoxic and apoptotic potential in hepatic carcinoma cells of chitosan nanoparticles loaded with ginsenoside compound K. *Carbohydr. Polym.* 198, 537–545. doi:10.1016/j.carbpol.2018.06.121

Zhang, L. J., Hui, J. F., Ma, P., Mi, Y., Fan, D. D., Zhu, C. H., et al. (2019). PEGylation of ginsenoside rg3-entrapped bovine serum albumin nanoparticles: Preparation, characterization, and *in vitro* biological studies. *J. Nanomater.*, 1–13. doi:10.1155/2019/3959037

Zhang, J. M., Jiang, Y. Y., Li, Y. P., Li, W. B., Zhou, J., Chen, J. W., et al. (2020). Micelles modified with a chitosan-derived homing peptide for targeted intracellular delivery of ginsenoside compound K to liver cancer cells. *Carbohydr. Polym.* 230, 115576. doi:10.1016/j.carbpol.2019.115576

Zhang, J. M., Zhou, J. Y., Yuan, Q. Y., Zhan, C. Y., Shang, Z., Gu, Q., et al. (2021). Characterization of ginsenoside compound K loaded ionically cross-linked carboxymethyl chitosan–calcium nanoparticles and its cytotoxic potential against prostate cancer cells. *J. Ginseng Res.* 45 (2), 228–235. doi:10.1016/j.jgr.2020.01.007

Zhang W N, W. N., Xu, Y., and Yu, M. (2017). Preparation of ginsenoside Rg3 thermo-sensitive nanoparticles and their inhibitory effect on hepatoma cells. *Pract. Pharm. Clin. Remedies* 20 (11), 1231–1235. doi:10.14053/j.cnki.ppcr.201711001

Zhao, H. J., Zhao, W. Y., and Hong, Z. H. (2016). Preparation and characterization of self-assemble micelles based on a novel polymer designed as polyethylene glycol-modified ginsenoside Rh2 and etoposide. *Chin. J. NewDrugs* 25 (17), 2027–2035.

Zhao, X. X., Wang, J. M., Song, Y. J., and Chen, X. H. (2018). Synthesis of nanomedicines by nanohybrids conjugating ginsenosides with auto-targeting and enhanced MRI contrast for liver cancer therapy. *Drug Dev. Ind. Pharm.* 44 (8), 1307–1316. doi:10.1080/03639045.2018.1449853

Zheng, A. P., and Shi, J. (2012). Research progress in nanocrystal drugs. *J. Int. Pharm. Res.* 39 (3), 177–183. doi:10.3969/j.issn.1674-0440.2012.03.001

Zheng, L., and Song, H. T. (2012). Research progress of nanomedicine preparation technology. *Pharm. J. Chin. People's Liberation Army* 28 (6), 537–540. doi:10.3969/j.issn.1008-9926.2012.06.21

Zhou, B. S., Yang, N., Li, Y. M., Wang, Y. R., Liu, J. P., Zhang, Z. D., et al. (2017). Advances in research of biological activities of ginsenoside Rg2. *Special Wild Econ. Animal Plant Res.* 39 (2), 67–70. doi:10.16720/j.cnki.tcyj.2017.02.015

Zhou, J. P. (2020). Application and prospect of nanotechnology in drug delivery system. *J. China Pharm. Univ.* 51 (4), 379–382. doi:10.11665/j.issn.1000-5048.20200401

Zhu, Y., Liang, J. M., Gao, C. F., Wang, A. N., Xia, J. X., Hong, C., et al. (2021). Multifunctional ginsenoside Rg3-based liposomes for glioma targeting therapy. *J. Control. Release* 330, 641–657. doi:10.1016/j.jconrel.2020.12.036

Zou, L., Fu, J., Li, W., Yu, T., Guo, X. H., Yang, L., et al. (2016). [Preparation and characterization of ginsenoside-Rh$_2$ lipid nanoparticles and synergistic effect with borneol in resisting tumor activity]. *China J. Chin. Materia Medica* 41 (7), 1235–1240. doi:10.4268/cjcmm20160713

frontiers | Frontiers in Pharmacology

TYPE Systematic Review
PUBLISHED 10 August 2022
DOI 10.3389/fphar.2022.946554

OPEN ACCESS

EDITED BY
Bing Chun Yan,
Yangzhou University, China

REVIEWED BY
Nasra Ayuob,
Damietta University, Egypt
Renping Liu,
Nanchang University, China
Di Qi,
Chongqing Medical University, China

*CORRESPONDENCE
Han Liu,
liuhan@jlu.edu.cn
Lei Song,
lsong@jlu.edu.cn

SPECIALTY SECTION
This article was submitted to Experimental Pharmacology and Drug Discovery, a section of the journal Frontiers in Pharmacology

RECEIVED 17 May 2022
ACCEPTED 27 June 2022
PUBLISHED 10 August 2022

CITATION
Wang S, Luo SX, Jie J, Li D, Liu H and Song L (2022), Efficacy of terpenoids in attenuating pulmonary edema in acute lung injury: A meta-analysis of animal studies.
Front. Pharmacol. 13:946554.
doi: 10.3389/fphar.2022.946554

Efficacy of terpenoids in attenuating pulmonary edema in acute lung injury: A meta-analysis of animal studies

Shuai Wang[1], Sean X. Luo[1], Jing Jie[2], Dan Li[2], Han Liu[2]* and Lei Song[2]*

[1]Department of Vascular Surgery, General Surgery Center, The First Hospital of Jilin University, Chasngchun, JL, China, [2]Center for Pathogen Biology and Infectious Diseases, Key Laboratory of Organ Regeneration and Transplantation of the Ministry of Education, Department of Respiratory Medicine, State Key Laboratory for Zoonotic Diseases, The First Hospital of Jilin University, Changchun, China

Background: The clinical efficiency of terpenoids in treating human acute lung injury (ALI) is yet to be determined. The lipopolysaccharide-induced rat model of ALI is a well-established and widely used experimental model for studying terpenoids' effects on ALI. Using a systematic review and meta-analysis, the therapeutic efficiency of terpenoid administration on the lung wet-to-dry weight ratio in rats was investigated.

Methods: Using the Cochrane Library, Embase, and PubMed databases, a comprehensive literature search for studies evaluating the therapeutic efficacy of terpenoids on ALI in rats was conducted. The lung wet-to-dry weight ratio was extracted as the main outcome. The quality of the included studies was assessed using the Systematic Review Center for Laboratory Animal Experimentation's risk of bias tool.

Results: In total, 16 studies were included in this meta-analysis. In general, terpenoids significantly lowered the lung wet-to-dry weight ratio when compared with the control vehicle (p = 0.0002; standardized mean difference (SMD): −0.16; 95% confidence interval (CI): −0.24, −0.08). Subgroup analysis revealed that low dose (≤10 μmol/kg) (p < 0.0001; SMD: −0.68; 95% CI: −1.02, −0.34), intraperitoneal injection (p = 0.0002; SMD: −0.43; 95% CI: −0.66, −0.20), diterpenoid (p = 0.004; SMD: −0.13; 95% CI: −0.23, −0.04), and triterpenoid (p = 0.04; SMD: −0.28; 95% CI: −0.54, −0.01) significantly lowered the lung wet-to-dry weight ratio when compared with the control vehicle.

Conclusion: A low dose of diterpenoid and triterpenoid administered intraperitoneally is effective in alleviating ALI. This systematic review and meta-analysis provides a valuable mirror for clinical research aiming at the advancement of terpenoids for preventive and therapeutic use.

Systematic Review Registration: CRD42022326779

KEYWORDS

acute lung injury, terpenoids, lipopolysaccharide, lung wet-to-dry weight ratio, animal model

Introduction

Acute lung injury (ALI) is an acute inflammatory disease that disrupts the lung's endothelial and epithelial barriers (Manicone, 2009). It is associated with systemic inflammatory response syndrome and multiple organ dysfunction syndrome (Wu et al., 2021). ALI, which is characterized by pulmonary edema and severe hypoxia, has also been regarded as the leading cause of death in patients with sepsis, imposing an enormous health burden worldwide each year (Schingnitz et al., 2010).

Although the pathophysiology of ALI has been extensively studied, effective clinical treatments for ALI remain limited. Therefore, there is an urgent need for the development of additional medications to treat ALI. Several natural compounds, such as terpenoids, alkaloids, and flavonoids, have been used over the last few years to treat ALI (Ren et al., 2019; Zhang et al., 2019; Zhao et al., 2021). Terpenoids, also known as isoprenoids, are the most abundant and structurally diverse natural compounds found in numerous plant species. They are a diverse and large group of naturally occurring organic chemicals derived from the 5-carbon compound isoprene. In addition, they are known to have diverse pharmacological properties, including antiatherosclerotic, antitumor, anti-inflammatory, antinociceptive, and antimalarial activities (Liu et al., 2019; Yuan et al., 2020; El-Baba et al., 2021; Sankhuan et al., 2022). The majority of research on terpenoids' anti-ALI effects has focused on diterpenoids; however, there is no consensus on other terpenoids (Yang et al., 2011; Yang et al., 2014; Li et al., 2018a).

Endotoxin can enter humans' airways through inhalation of contaminated dust or aerosol particles in hospital, occupational, agricultural, and domestic environments. Lipopolysaccharide (LPS), which is a major endotoxin component of Gram-negative bacteria, is regarded as the most important pathogen responsible for the development of ALI in sepsis (Li et al., 2014a; Park et al., 2018). Animal studies allow for the investigation of the efficacy and safety of novel therapies, linking basic research and clinical trials. LPS is thought to be a significant inducer of lung injury. Because of its widespread use and accessibility, LPS-induced lung injury is the most commonly used animal model of ALI for replicating the pathophysiological process (Li et al., 2018a). In this present meta-analysis, we investigated the effects of terpenoid administration on the wet-to-dry weight (W/D) ratio of the lungs in rats with LPS-induced ALI to better understand the preventive and therapeutic potential of terpenoids on ALI.

Materials and methods

Reporting standards

The systematic review protocol for animal intervention studies was prepared in accordance with the Preferred Reporting Items for Systematic Reviews and Meta-Analyses guideline and the Systematic Review Center for Laboratory Animal Experimentation (SYRCLE) format (Hooijmans and Ritskes-Hoitinga, 2013; De Vries et al., 2015).

Search strategy

A comprehensive search was conducted by a competent information specialist (SW) in the Cochrane Library, Embase, and PubMed databases between January 2000 and March 2022 using the terms "acute lung injury," "ALI," "terpenoid," "lipopolysaccharide," "LPS," and "rat." The search terms are as follows: (acute lung injury or ALI) and (diterpenoid or hemiterpenoid or monoterpenoid or polyterpenoid or sesquiterpenoid or sesterterpenoid or terpenoid or tetraterpenoid or triterpenoid) and (lipopolysaccharide or LPS) and (rat or rats). Following a manual screening, further relevant studies were identified from the datasheet of included and reviewed articles.

Inclusion and exclusion criteria

The inclusion criteria are as follows: (a) original research, (b) terpenoid intervention, and (c) rat with LPS-induced ALI research model. The exclusion criteria were as follows: (a) reviews, abstracts, case reports, comments, and editorials; (b) missing data; (c) duplicate and/or overlapping datasets; and (d) publications that were not written in English.

Study selection

To collect qualified studies, the abstracts and titles of the articles identified by the comprehensive search were independently reviewed by three investigators (SW, JJ, and HL). The full text of potentially eligible studies was thereafter reviewed and checked by three investigators (SL, DL, and LS) to determine if the studies met the inclusion and exclusion criteria. Disagreements as regards the study's selection were resolved through discussion and compromise.

Data extraction

The characteristic data were extracted from qualified studies independently by three investigators (SL, LS, and HL), such as publication year, first author name, sample size of control and terpenoid groups, age, gender, rat strain and weight, diet type, terpenoid dosage, the interval between LPS administration and sacrifice, route and duration of LPS and terpenoid administration, lung wet-to-dry weight ratio, and dryer parameter. The statistics displayed graphically in the original publications were extracted using Adobe Photoshop (Ps v7.0). The main outcome was the lung wet-to-dry weight ratio, which is measured as a numerical value. Disagreements as regards data extraction were resolved through discussion and compromise.

Quality assessment

The quality of the included studies was assessed by two investigators (SW and JJ) using SYRCLE's risk of bias tool. The allocation concealment, incomplete outcome data, randomization, blinding and selective outcome assessments, baseline characteristics, random housing, domains evaluating sequence generation, and other sources of bias were included in the SYRCLE's risk of bias tool (Hooijmans et al., 2014). Publication bias was assessed through visual inspection of funnel plots. Disagreements about quality assessment were resolved through discussion and compromise.

Data synthesis and statistical analysis

All statistical analyses were conducted using the Review Manager (RevMan v5.3) software. The effects of control vehicle and terpenoids on lung wet-to-dry weight ratio were assessed using the mean differences with 95% confidence intervals (CI). A fixed effects model was used to pool studies, and the inconsistency index was used to calculate heterogeneity as high ($I^2 \geq 50\%$) or moderate ($I^2 \geq 30\%$).

In one study, datasets with more than three independent groups, namely, a control group, a low terpenoid dosage group, and a high terpenoid dosage group, were defined. A single control group was compared with various groups that investigated different terpenoid dosages in eight studies (Yang et al., 2011; Chen et al., 2014; Yang et al., 2014; Wei and Wang, 2017; Li et al., 2018a; Ren et al., 2019; Wang et al., 2021; Wu et al., 2021). To avoid a redundant expansion in the meta-analysis sample size, the number of samples in the control group in each study was divided by those in the matched groups. Subanalyses of the effects of different terpenoid routes and doses on lung wet-to-dry weight ratio were conducted. A sensitivity analysis was conducted to assess the robustness of the results. A p-value of <0.05 was considered statistically significant.

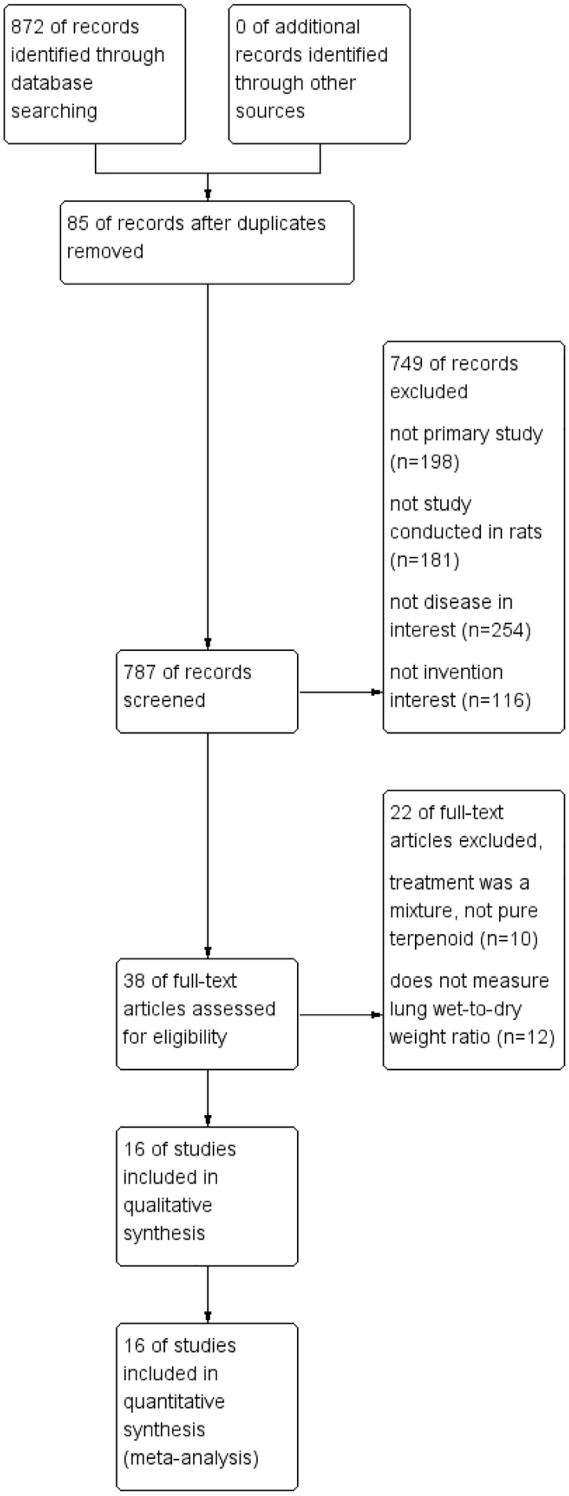

FIGURE 1
The flow diagram of the study identification and selection process.

TABLE 1 The characteristics of included studies.

Study	Terpenoid	Gender	Age	Strain	Weight	Route of LPS	Dose of LPS	Dose of terpenoid	Interval between LPS administration and sacrifice	Route of terpenoid	Parameter of dryer	Groups and sample size
Ali F, 2021 (Ali et al., 2021)	Aescin, triterpenoid	Male	8 w	Wistar	180–200 g	i.t.	8 mg/kg	4.42 μmol/kg	24 h	i.g.	80°C	Control = 10
											24 h	Triterpenoid = 10
Chen J, 2014 (Chen et al., 2014)	Triptolid, diterpenoid	Male	?	Sprague Dawley	200–250 g	i.v.	5 mg/kg	0.28 μmol/kg	12 h	i.p.	?	Control = 5
								0.14 μmol/kg				Diterpenoid high = 5
								0.08 μmol/kg				Diterpenoid medium = 5
												Diterpenoid low = 5
Dikmen N, 2021 (Dikmen et al., 2021)	Oleuropein, monoterpenoid	Male	8–10 w	Wistar	180–250 g	i.t.	5 mg/kg	370 μmol/kg	20 h	i.g.	60°C	Control = 8
											72 h	Monoterpenoid = 8
Li J, 2017 (Li et al., 2018a)	Tanshinone IIA, diterpenoid	Male	10 w	Wistar	250–300 g	i.v.	5 mg/kg		24 h	i.v.		Control = 24
								34 μmol/kg			70 °C	Diterpenoid high = 24
								20 μmol/kg			72 h	Diterpenoid medium = 15
								10 μmol/kg				Diterpenoid low = 15
Li L, 2018 (Li et al., 2018b)	Tanshinone IIA, diterpenoid	Male	8 w	Sprague Dawley	200–220 g	i.p.	10 mg/kg	1 μmol/kg	8 d	i.p.	?	Control = 10
												Diterpenoid = 10
Li S, 2021 (Li et al., 2021)	Retinoic acid, diterpenoid	Male	8–10 w	Sprague Dawley	220–270 g	i.v.	5 mg/kg	17 μmol/kg	48 h	i.p.	70°C	Control = 10
											72 h	Diterpenoid = 10
Luo X, 2019 (Luo et al., 2019)	Genipin, monoterpenoid	Male	8 w	Sprague Dawley	180–220 g	i.t.	5 mg/kg	22 μmol/kg	12 h	i.t.	80°C	Control = 6
											48 h	Monoterpenoid = 6
Shi XM, 2007 (Shi et al., 2007)	Tanshinone IIA, diterpenoid	?	?	Sprague Dawley	240–280 g	i.v.	5 mg/kg	17 μmol/kg	6 h	i.p.	80°C	Control = 8
											20 h	Sesquiterpenoid = 8
Wang YJ, 2020 (Wang et al., 2021)	Zaluzanin D, sesquiterpenoid	Male	6–8 w	Sprague Dawley	?	i.t.	3 mg/kg		7 d	i.v.		Control = 6
								347 μmol/kg			60°C	Sesquiterpenoid high = 6
								174 μmol/kg			48 h	

(Continued on following page)

10.3389/fphar.2022.946554

TABLE 1 (*Continued*) The characteristics of included studies.

Study	Terpenoid	Gender	Age	Strain	Weight	Route of LPS	Dose of LPS	Dose of terpenoid	Interval between LPS administration and sacrifice	Route of terpenoid	Parameter of dryer	Groups and sample size
												Sesquiterpenoid medium = 6
								69 μmol/kg				Sesquiterpenoid low = 6
Wei Y, 2017 (Wei and Wang, 2017)	Celastrol, triterpenoid	Male	?	Wistar	180–220 g	i.t.	2 mg/kg		24 h	i.g.		Control = 8
								44 μmol/kg			80°C	Triterpenoid high = 8
								11 μmol/kg			72 h	Triterpenoid medium = 8
								1.1 μmol/kg				Triterpenoid low = 8
Wu Y, 2021 (Wu et al., 2021)	Platycodin D, triterpenoid	?	6 w	Sprague Dawley	90–110 g	i.t.	5 mg/kg		?	i.p.		Control = 7
								20 μmol/kg			60°C	Triterpenoid high = 7
								10 μmol/kg			48 h	Triterpenoid low = 7
Yang N, 2014 (Yang et al., 2014)	Andrographolide, diterpenoid	Male	8 w	Sprague Dawley	180–220 g	i.v.	5 mg/kg		6 h	i.g.		Control = 43
								128 μmol/kg			80°C	Diterpenoid high = 43
								13 μmol/kg			72 h	Diterpenoid low = 43
Yang W, 2011 (Yang et al., 2011)	Isoforskolin, diterpenoid	Male	12 w	Sprague Dawley	260–300 g	i.v.	6 mg/kg		3 h	i.p.		Control = 8
								49 μmol/kg			80 °C	Diterpenoid high = 8
								24 μmol/kg			48 h	Diterpenoid medium = 8
								12 μmol/kg				Diterpenoid low = 8
Yuan Q, 2014 (Yuan et al., 2014)	Ginsenoside Rb1, triterpenoid	Male	?	Wistar	300–350 g	i.v.	0.1 mg/kg	4.5 μmol/kg	?	i.v.	80°C	Control = 10
											48 h	Triterpenoid = 10
Zhang E, 2020 (Zhang et al., 2020)	Artesunate, sesquiterpenoid	?	?	Sprague Dawley	220–250 g	i.t	5 mg/kg	5.2 μmol/kg	24 h	i.p.	?	Control = 8
												Sesquiterpenoid = 8
Zhang Z, 2019 (Zhang et al., 2019)	Genipin, monoterpenoid	Male	8 w	Sprague Dawley	180–220 g	i.t.	5 mg/kg		12 h	i.p.		Control = 6
								22 μmol/kg			80°C	Monoterpenoid high = 6
								8.8 μmol/kg			48 h	Monoterpenoid low = 6

Note: i.v., intravenous injection; i.t., intratracheal administration; i.p., intraperitoneal injection; i.g., intragastric administration;? = not reported.

10.3389/fphar.2022.946554

Results

Study selection

Through the search strategy, 872 articles were identified. The investigators extracted the abstracts and titles and identified 38 studies that met the inclusion criteria. After reviewing all of the publications, 10 studies were excluded because of missing outcome data (Ehrhart et al., 2000; Tawadros et al., 2007; Nader and Baraka, 2012; An et al., 2014; Wang et al., 2015; Liu and Chen, 2016; Shen et al., 2017; Ni et al., 2019; Wang et al., 2019; Yang et al., 2019), and another 12 studies were excluded because multiple interventions were investigated (Murakami et al., 2000; Lin et al., 2011; Li et al., 2014b; Li et al., 2016a; Li et al., 2016b; Baradaran Rahimi et al., 2019; Ye et al., 2019; Duan et al., 2020; Yue et al., 2020; Choi et al., 2021; Zhang et al., 2021; Liu et al., 2022). In conclusion, 16 studies were included in this meta-analysis, as described below (Shi et al., 2007; Yang et al., 2011; Chen et al., 2014; Yang et al., 2014; Yuan et al., 2014; Wei and Wang, 2017; Li et al., 2018a; Li et al., 2018b; Luo et al., 2019; Ren et al., 2019; Zhang et al., 2020; Ali et al., 2021; Dikmen et al., 2021; Li et al., 2021; Wang et al., 2021; Wu et al., 2021) (Figure 1).

Study characteristics

From the 16 included studies, 29 datasets and 499 rats were extracted. The characteristics of these studies are shown in Table 1. Rats ranged in age from 6 to 8 weeks and in weight from 90 to 350 g. In terms of intervention, diterpenoid, monoterpenoid, sesquiterpenoid, and triterpenoid were used in seven studies (Shi et al., 2007; Yang et al., 2011; Yang et al., 2014; Wei and Wang, 2017; Li et al., 2018a; Li et al., 2018b; Luo et al., 2019), three studies (Yuan et al., 2014; Ren et al., 2019; Li et al., 2021), two studies (Ali et al., 2021; Wang et al., 2021), and four studies (Chen et al., 2014; Zhang et al., 2020; Dikmen et al., 2021; Wu et al., 2021), respectively. In addition, 13 studies used male rats (Shi et al., 2007; Yang et al., 2011; Chen et al., 2014; Yang et al., 2014; Yuan et al., 2014; Wei and Wang, 2017; Li et al., 2018a; Luo et al., 2019; Ren et al., 2019; Zhang et al., 2020; Dikmen et al., 2021; Li et al., 2021; Wang et al., 2021), whereas three studies did not report gender (Li et al., 2018b; Ali et al., 2021; Wu et al., 2021). Sprague Dawley rats were used in 11 studies (Shi et al., 2007; Yang et al., 2014; Wei and Wang, 2017; Li et al., 2018a; Li et al., 2018b; Luo et al., 2019; Ren et al., 2019; Ali et al., 2021; Li et al., 2021; Wang et al., 2021; Wu et al., 2021) and Wistar rats in five studies (Yang et al., 2011; Chen et al., 2014; Yuan et al., 2014; Zhang et al., 2020; Dikmen et al., 2021).

LPS was administered intravenously in seven studies (Yang et al., 2011; Yang et al., 2014; Wei and Wang, 2017; Li et al., 2018a; Li et al., 2018b; Luo et al., 2019; Dikmen et al., 2021), intraperitoneally in one study (Shi et al., 2007), and intratracheally in eight studies (Chen et al., 2014; Yuan et al., 2014; Ren et al., 2019; Zhang et al., 2020; Ali et al., 2021; Li et al., 2021; Wang et al., 2021; Wu et al., 2021). The LPS dosage ranged from 0.1 to 10 mg/kg. Terpenoid was administered intragastrically in four studies (Chen et al., 2014; Yang et al., 2014; Yuan et al., 2014; Zhang et al., 2020), intravenously in three studies (Yang et al., 2011; Dikmen et al., 2021; Wang et al., 2021), intraperitoneally in eight studies (Shi et al., 2007; Wei and Wang, 2017; Li et al., 2018a; Li et al., 2018b; Luo et al., 2019; Ren et al., 2019; Ali et al., 2021; Wu et al., 2021), and intratracheally in one study (Li et al., 2021). The terpenoid dosage ranged from 0.08 to 370 μmol/kg. The terpenoid was given prior to LPS in eight studies (Chen et al., 2014; Yang et al., 2014; Yuan et al., 2014; Li et al., 2018a; Luo et al., 2019; Ren et al., 2019; Zhang et al., 2020; Li et al., 2021), after LPS in seven studies (Shi et al., 2007; Yang et al., 2011; Wei and Wang, 2017; Li et al., 2018b; Ali et al., 2021; Dikmen et al., 2021; Wang et al., 2021), and undetermined in one study (Wu et al., 2021). The interval between LPS administration and sacrifice ranged from 3 h to 8 days. The drying time ranged from 20 to 72 h, and the temperature ranged from 60 to 80°C.

Quality assessment

The quality assessment of these studies is shown in Figure 2. In total, 12 studies were randomized, with eight studies demonstrating unclear risks of bias in blinding and allocation concealment. All studies' outcomes were reported, with six studies demonstrating an unclear risk of selective outcome reporting. Overall, the risk of bias from other sources was low. The potential publication bias was evaluated through visual inspection of a funnel plot (Figure 3).

Effect of terpenoids on lung wet-to-dry weight ratio

The effect of terpenoids on lung wet-to-dry weight ratio was presented for 29 datasets acquired from 16 studies (rats given terpenoids [n = 317] vs. rats given a control vehicle [n = 182]). Overall, terpenoids significantly reduced the lung wet-to-dry weight ratio when compared with the control vehicle (p = 0.0002; standardized mean difference (SMD): −0.16; 95% CI: −0.24, −0.08), with no evidence of heterogeneity among studies (I^2 = 0%) (Figure 4).

Subgroup analyses were conducted to assess the effects of diterpenoid, monoterpenoid, sesquiterpenoid, and triterpenoid on the lung wet-to-dry weight ratio. Monoterpenoid (rats given a monoterpenoid [n = 26] vs. rats given a control vehicle [n = 20]; p = 0.22; SMD: −0.21; 95% CI: −0.55, 0.13) and sesquiterpenoid (rats given a sesquiterpenoid [n = 26] vs. rats given a control vehicle [n = 14]; p = 0.22; SMD: −0.26; 95% CI: −0.69, 0.16) did not significantly lower the lung wet-to-dry weight ratio when

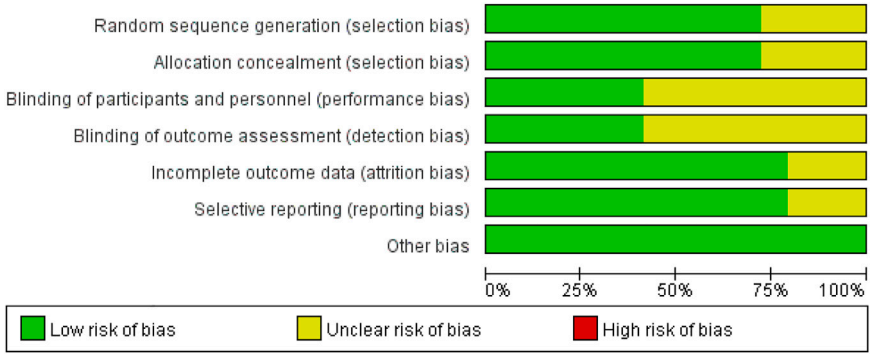

FIGURE 2
The risk of bias and quality evaluation score (%) per risk of bias item.

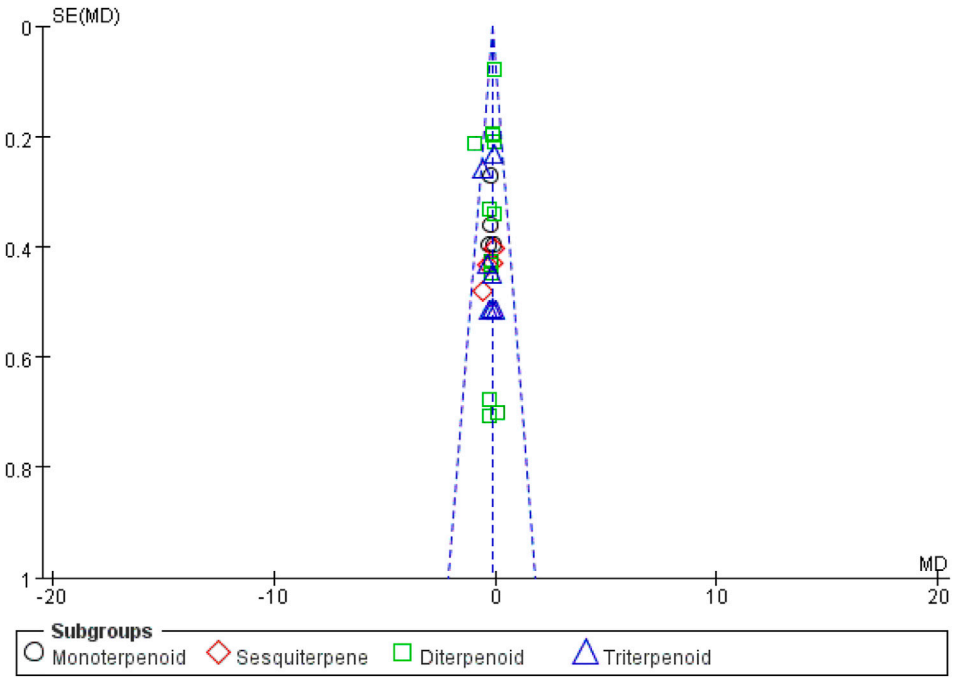

FIGURE 3
The funnel plot for accessing publication bias.

compared with the control vehicle, with no evidence of heterogeneity among studies (I^2 = 0%). Diterpenoid (rats given a diterpenoid [n = 207] vs. rats given a control vehicle [n = 111]) significantly reduced the lung wet-to-dry weight ratio when compared with the control vehicle (p = 0.004; SMD: −0.13; 95% CI: −0.23, −0.04), with evidence of low heterogeneity among studies (I^2 = 20%). Triterpenoid (rats given a triterpenoid [n = 58] vs. rats given a control vehicle [n = 37]) significantly decreased the lung wet-to-dry weight ratio when compared with the control vehicle (p = 0.04; SMD: −0.28; 95% CI: −0.54, −0.01), with no evidence of heterogeneity among studies (I^2 = 0%) (Figure 4). The sensitivity analysis, which substituted the random effects model for the fixed effects model, had no effect on the overall outcome (SMD: −0.16, CI: −0.24, −0.08 vs. SMD: −0.36, CI: −0.55, −0.17).

In terms of the administration route, subgroup analyses revealed that intraperitoneal injection of terpenoid (rats given

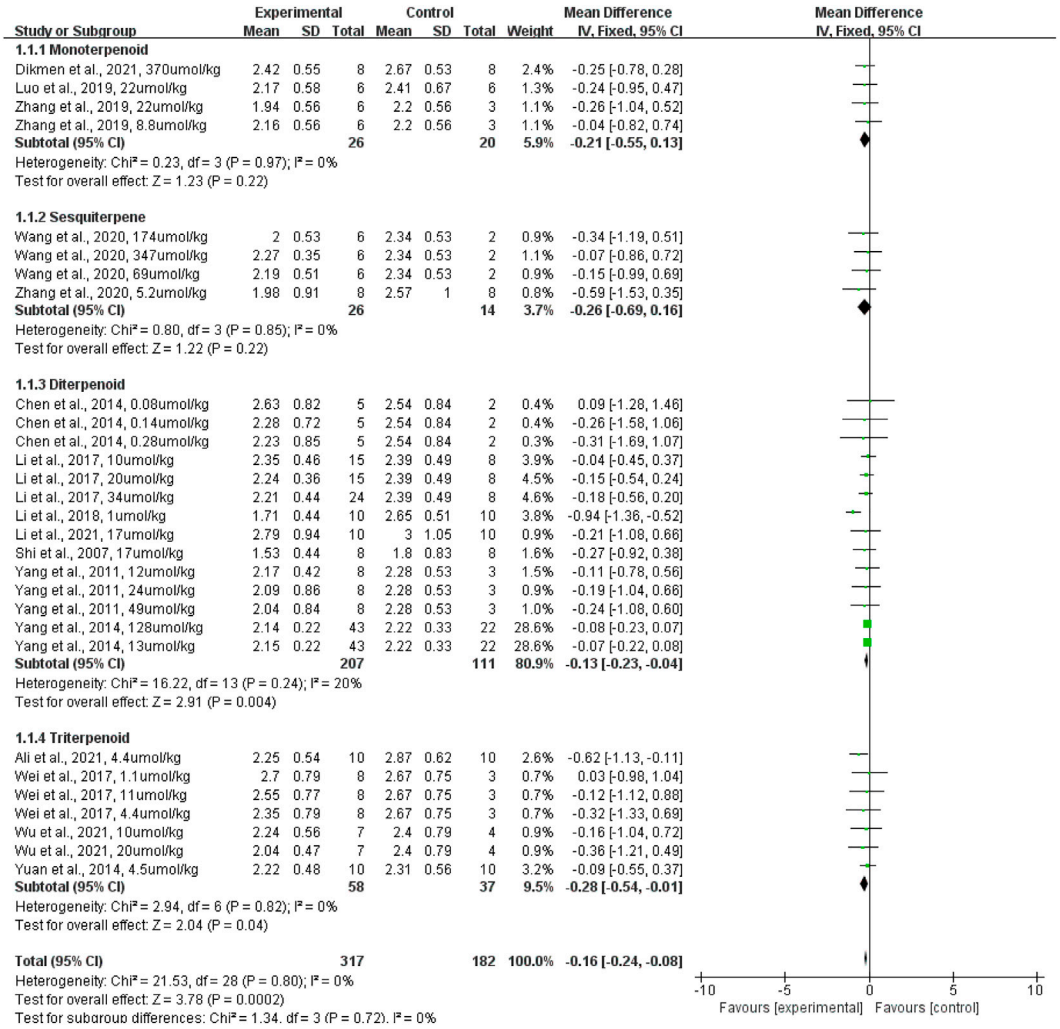

FIGURE 4
The forest plot of therapeutic efficiency of terpenoids on lung wet-to-dry weight ratio. Subgroup analyses investigated the therapeutic efficiency of monoterpenoid, sesquiterpene, diterpenoid, and triterpenoid. CI, confidence interval; IV, inverse variance; Std, standard; SD, standard deviation.

a terpenoid [n = 81] vs. rats given a control vehicle [n = 51]) significantly reduced the lung wet-to-dry weight ratio when compared with the control vehicle (p = 0.0002; SMD: −0.43; 95% CI: −0.66, −0.20), with no evidence of heterogeneity among studies (I^2 = 0%). However, intravenous injection of terpenoid (rats given a terpenoid [n = 64] vs. rats given a control vehicle [n = 34]) did not significantly lower the lung wet-to-dry weight ratio when compared with the control vehicle (p = 0.25; SMD: −0.12; 95% CI: −0.32, −0.08), with no evidence of heterogeneity among studies (I^2 = 0%). Likewise, intragastric administration of terpenoid (rats given a terpenoid [n = 96] vs. rats given a control vehicle [n = 54]) did not significantly lower the lung wet-to-dry weight ratio when compared with the control vehicle (p = 0.06; SMD: −0.10; 95% CI: −0.20, −0.00), with no evidence of heterogeneity among studies (I^2 = 0%) (Figure 5). The sensitivity analysis, which substituted the random effects model for the fixed effects model, had no effect on the overall outcome (SMD: −0.15, CI: −0.24, −0.06 vs. SMD: −0.36, CI: −0.57, −0.15).

In terms of terpenoid dosage, subgroup analyses revealed that low doses of terpenoid administered intraperitoneally (rats given terpenoid at a dose of 10 μmol/kg or lower [n = 32] vs. rats given a control vehicle [n = 20]) significantly lowered the lung wet-to-dry weight ratio when compared with the control vehicle (p < 0.0001; SMD: −0.68; 95% CI: −1.02, −0.34), with no evidence of heterogeneity among studies (I^2 = 0%). However, the high dose (rats given terpenoid at a dose greater than 10 μmol/kg [n = 49] vs. rats given a control vehicle [n = 31]) did not

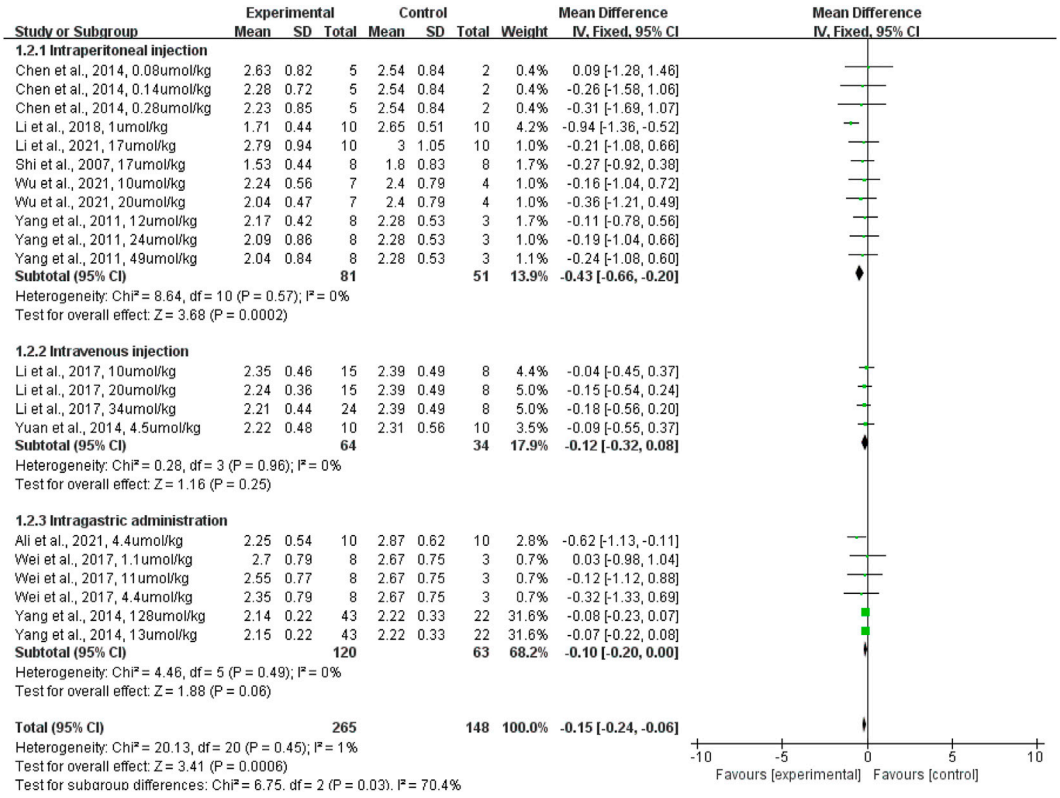

FIGURE 5
The forest plot of therapeutic efficiency of the route of terpenoid administration on lung wet-to-dry weight ratio. Subgroup analyses evaluated the therapeutic efficiency of intraperitoneal injection, intravenous injection, and intragastric administration. CI, confidence interval; IV, inverse variance; Std, standard; SD, standard deviation.

significantly lower the lung wet-to-dry weight ratio when compared with the control vehicle (p = 0.16; SMD: −0.22; 95% CI: −0.54, −0.09), with no evidence of heterogeneity among studies (I^2 = 0%) (Figure 6). The sensitivity analysis, which substituted the random effects model for the fixed effects model, had no effect on the overall outcome (SMD: −0.43, CI: −0.66, −0.20 vs. SMD: −0.46, CI: −0.83, −0.09).

Discussion

Despite significant advances in pharmacotherapy agents for ALI, such as antibiotics, N-acetylcysteine, β-agonists, corticosteroids, surfactants, and statins, an efficient approach to lowering ALI morbidity and mortality is yet to be identified (Lewis et al., 2019). Because diterpenoids were found to be promising in treating ALI in some studies (Yang et al., 2011; Yang et al., 2014; Li et al., 2018a), it was necessary to investigate the pharmacological effects of terpenoids on ALI. The use of animal models provides a valuable gateway for preclinical research, identifying novel therapeutic strategies for disease and developing new drugs. An ideal animal model should be able to replicate the consequences and mechanisms of human disease, including pathological and physiological hallmarks. LPS is a component of Gram-negative bacterial cell walls. LPS-induced animal models, by inhalation or systemic (intravenous and intraperitoneal) administration, reproduce acute damage to the lung epithelial and endothelial barriers, as well as acute inflammatory responses, in a short period of time (typically <48 h) (Matute-Bello et al., 2008). LPS-induced injury is a valuable *in vivo* experimental model that is similar to ALI and acute respiratory distress syndrome in humans. LPS is easy to use, and its outcomes are often replicable in experiments. Although mouse models of human disease are widely used because of the availability of specific reagents and the development of transgenic mice that can be administered to assess the physiological function of specific genes, animal size remains an important consideration when choosing an animal model for ALI. Because there is no difference between rats and mice in ALI animal models (Matute-Bello et al., 2008), rats were used as experimental animals in this study.

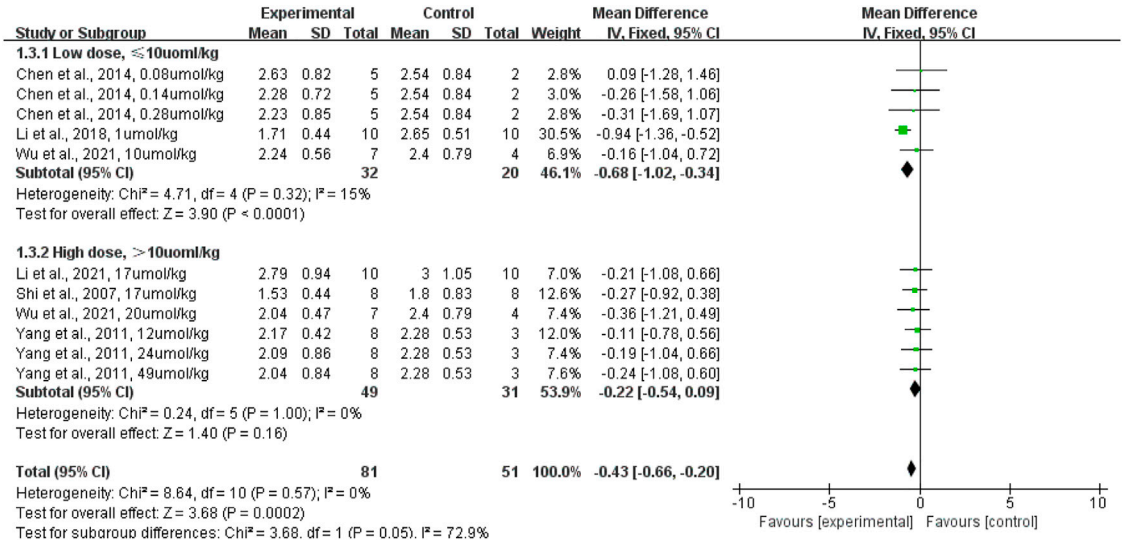

FIGURE 6
The forest plot of therapeutic efficiency of terpenoid dose on lung wet-to-dry weight ratio. Subgroup analyses investigated therapeutic efficiency of high dose (>10 μmol/kg) and low dose (≤10 μmol/kg). CI, confidence interval; IV, inverse variance; Std, standard; SD, standard deviation.

Previous animal experiments suggest that natural terpenoids may have therapeutic effects on ALI. However, study parameters such as sample size, animal strain and age, and treatment and follow-up duration were noted to differ among studies. A quantitative and comprehensive analysis of these heterogeneous sources of animal model data can provide insights into the benefits of terpenoids in the treatment of ALI. Therefore, we conducted a systematic review and meta-analysis to investigate the effects of terpenoids on lung wet-to-dry weight ratio in rats with LPS-induced ALI. The findings revealed that the use of terpenoids significantly reduced the lung wet-to-dry weight ratio and alleviated pulmonary edema when compared with the control group.

The terpenoid family includes monoterpenoid, sesquiterpenoid, diterpenoid, triterpenoid, and tetraterpenoid (Christianson, 2017). In a subgroup analysis, the number of isoprene groups, monoterpenoid and sesquiterpenoid, did not drastically lower the lung wet-to-dry weight ratio. By contrast, diterpenoid and triterpenoid attenuated pulmonary edema and ameliorated ALI in LPS-induced ALI rats compared with the control vehicle. We presumed that the differences among the groups might be induced by the sample size gap and underlying publication bias. Of course, more studies are needed to confirm this speculation. Moreover, a low dose (≤10 μmol/kg) of diterpenoid and triterpenoid via intraperitoneal injection showed a significant outcome for decreasing lung wet-to-dry weight ratio. To our knowledge, this meta-analysis is an initial assessment of the therapeutic efficiency of terpenoids on LPS-induced ALI in rats. The total outcomes might offer a valuable reference to the future preventive and therapeutic use of terpenoids in human ALI.

In the overall analysis, there was no heterogeneity among studies. However, among studies in the subgroups of diterpenoid and low-dose terpenoid, it had a low degree of heterogeneity. Possible origin of heterogeneity contained strain of rat, route of LPS, and interval between LPS administration and sacrifice, each of which can influence the progression of ALI (Chen et al., 2010).

The meta-analysis is coupled with some restrictions. First, the correlation between the outcomes and humans is restrained by the differences between species in the development of pulmonary edema. The LPS-induced ALI animal model is well reputable, and the main characteristics and development of pulmonary edema in humans and rats emerge similar, but to a certain extent, it is different in pathogenesis (Tomashefski, 2000). We realize that an LPS-induced ALI animal model duplicates a lot of pathological features, but it is still relatively simple and rapid to reproduce the pathologic processes of humans (Matute-Bello et al., 2008). Second, other animal models of ALI were not included in this meta-analysis, such as pigs and sheep, which are easier to be induced by LPS because they have a more sensitive pulmonary hypertensive response and a higher speed circulation than rats (Warner et al., 1988; Schmidhammer et al., 2006). Third, only the lung wet-to-dry weight ratio was extracted to investigate the effects of terpenoids on ALI. Other parameters, such as proinflammatory cytokines, including tumor necrosis factor and interleukin, lung injury score, and lung-to-body weight ratio, were not considered (Eastwood et al., 2015; Butt et al., 2016). Fourth, hemiterpenoids, sesterterpenoids, and other terpenoids were not investigated in the analysis. In addition,

more studies based on a huge number of samples and large-scale animal models are still necessary for determining whether terpenoids are effective for attenuating ALI in humans.

This meta-analysis showed that terpenoid is beneficial for alleviating ALI in rats. In particular, low-dose (≤10 μmol/kg) diterpenoid and triterpenoid significantly decrease lung wet-to-dry weight ratio in rats via intraperitoneal injection. We need more well-designed, prospective, and extensive animal model research to expand our understanding of the mechanisms of terpenoids in ALI treatment. We still need randomized controlled trials in humans to demonstrate the clinical benefit of terpenoids in the prevention and therapy of ALI.

Data availability statement

The original contributions presented in the study are included in the article/supplementary material; further inquiries can be directed to the corresponding authors.

Author contributions

SW conducted the analysis, JJ and DL collected and performed a preliminary analysis of references, HL and SL wrote the manuscript, and LS designed and revised the manuscript.

Funding

This work was supported by the Office of Science and Technology in Jilin Province (No. 20210204114YY and 20210101325JC).

Acknowledgments

We would like to thank Enago Academy for the revisions to the manuscript in terms of language and grammar.

Conflict of interest

The authors declare that the research was conducted in the absence of any commercial or financial relationships that could be construed as potential conflicts of interest.

Publisher's note

All claims expressed in this article are solely those of the authors and do not necessarily represent those of their affiliated organizations, or those of the publisher, the editors, and the reviewers. Any product that may be evaluated in this article, or claim that may be made by its manufacturer, is not guaranteed or endorsed by the publisher.

References

Ali, F. E. M., Ahmed, S. F., Eltrawy, A. H., Yousef, R. S., Ali, H. S., Mahmoud, A. R., et al. (2021). Pretreatment with coenzyme Q10 combined with aescin protects against sepsis-induced acute lung injury. *Cells Tissues Organs* 210 (3), 195–217. doi:10.1159/000516192

An, J. F., Sun, Y., Zhang, Q. L., Zhang, F. L., and Zhang, J. L. (2014). The effects of germacrone on lipopolysaccharide-induced acute lung injury in neonatal rats. *Cell Mol. Biol. (Noisy-le-grand)* 60 (4), 8–12.

Baradaran Rahimi, V., Rakhshandeh, H., Raucci, F., Buono, B., Shirazinia, R., Samzadeh Kermani, A., et al. (2019). Anti-inflammatory and anti-oxidant activity of portulaca oleracea extract on LPS-induced rat lung injury. *Molecules* 24 (1), 139. doi:10.3390/molecules24010139

Butt, Y., Kurdowska, A., and Allen, T. C. (2016). Acute lung injury: A clinical and molecular review. *Arch. Pathol. Lab. Med.* 140 (4), 345–350. doi:10.5858/arpa.2015-0519-RA

Chen, H., Bai, C., and Wang, X. (2010). The value of the lipopolysaccharide-induced acute lung injury model in respiratory medicine. *Expert Rev. Respir. Med.* 4 (6), 773–783. doi:10.1586/ers.10.71

Chen, J., Gao, J., Yang, J., Zhang, Y., and Wang, L. (2014). Effect of triptolide on the regulation of ATP-binding cassette transporter A1 expression in lipopolysaccharide-induced acute lung injury of rats. *Mol. Med. Rep.* 10 (6), 3015–3020. doi:10.3892/mmr.2014.2636

Choi, M., Thuy, L. T., Lee, Y., Piao, C., Choi, J. S., and Lee, M. (2021). Dual-functional dendrimer micelles with glycyrrhizic acid for anti-inflammatory therapy of acute lung injury. *ACS Appl. Mater Interfaces* 13 (40), 47313–47326. doi:10.1021/acsami.1c08107

Christianson, D. W. (2017). Structural and chemical Biology of terpenoid cyclases. *Chem. Rev.* 117 (17), 11570–11648. doi:10.1021/acs.chemrev.7b00287

De Vries, R. B. M., Hooijmans, C. R., Langendam, M. W., and Luijk, J. V. (2015). A protocol format for the preparation, registration and publication of systematic reviews of animal intervention studies. *Evid. Based Preclin. Med.* 2, 1–9. doi:10.1002/ebm2.7

Dikmen, N., Cellat, M., Etyemez, M., İşler, C. T., Uyar, A., Aydın, T., et al. (2021). Ameliorative effects of oleuropein on lipopolysaccharide-induced acute lung injury model in rats. *Inflammation* 44 (6), 2246–2259. doi:10.1007/s10753-021-01496-x

Duan, Q., Jia, Y., Qin, Y., Jin, Y., Hu, H., and Chen, J. (2020). Narciclasine attenuates LPS-induced acute lung injury in neonatal rats through suppressing inflammation and oxidative stress. *Bioengineered* 11 (1), 801–810. doi:10.1080/21655979.2020.1795424

Eastwood, M. P., Russo, F. M., Toelen, J., and Deprest, J. (2015). Medical interventions to reverse pulmonary hypoplasia in the animal model of congenital diaphragmatic hernia: A systematic review. *Pediatr. Pulmonol.* 50 (8), 820–838. doi:10.1002/ppul.23206

Ehrhart, I. C., Zou, L., Theodorakis, M. J., Parkerson, J. B., Gu, X., Caldwell, R. B., et al. (2000). Effect of nitrite on endothelial function in isolated lung. *Gen. Pharmacol.* 34 (6), 401–408. doi:10.1016/s0306-3623(01)00077-5

El-Baba, C., Baassiri, A., Kiriako, G., Dia, B., Fadlallah, S., Moodad, S., et al. (2021). Terpenoids' anti-cancer effects: Focus on autophagy. *Apoptosis* 26 (9-10), 491–511. doi:10.1007/s10495-021-01684-y

Hooijmans, C. R., and Ritskes-Hoitinga, M. (2013). Progress in using systematic reviews of animal studies to improve translational research. *PLoS Med.* 10 (7), e1001482. doi:10.1371/journal.pmed.1001482

Hooijmans, C. R., Rovers, M. M., de Vries, R. B., Leenaars, M., Ritskes-Hoitinga, M., and Langendam, M. W. (2014). SYRCLE's risk of bias tool for animal studies. *BMC Med. Res. Methodol.* 14, 43. doi:10.1186/1471-2288-14-43

Lewis, S. R., Pritchard, M. W., Thomas, C. M., and Smith, A. F. (2019). Pharmacological agents for adults with acute respiratory distress syndrome. *Cochrane Database Syst. Rev.* 7 (7), CD004477. doi:10.1002/14651858.CD004477.pub3

Li, G., Zhou, C. L., Zhou, Q. S., and Zou, H. D. (2016). Galantamine protects against lipopolysaccharide-induced acute lung injury in rats. *Braz J. Med. Biol. Res.* 49 (2), e5008. doi:10.1590/1414-431X20155008

Li, J., Zheng, Y., Li, M. X., Yang, C. W., and Liu, Y. F. (2018). Tanshinone IIA alleviates lipopolysaccharide-induced acute lung injury by downregulating TRPM7 and pro-inflammatory factors. *J. Cell Mol. Med.* 22 (1), 646–654. doi:10.1111/jcmm.13350

Li, K. C., Ho, Y. L., Chen, C. Y., Hsieh, W. T., Chang, Y. S., and Huang, G. J. (2016). Lobeline improves acute lung injury via nuclear factor-κB-signaling pathway and oxidative stress. *Respir. Physiol. Neurobiol.* 225, 19–30. doi:10.1016/j.resp.2015.12.003

Li, L., Zhang, Y. G., Tan, Y. F., Zhao, J. J., Zhang, H. R., and Zhao, B. (2018). Tanshinone II is a potent candidate for treatment of lipopolysaccharide-induced acute lung injury in rat model. *Oncol. Lett.* 15 (2), 2550–2554. doi:10.3892/ol.2017.7581

Li, S., Lei, Y., Lei, J., and Li, H. (2021). All-trans retinoic acid promotes macrophage phagocytosis and decreases inflammation via inhibiting CD14/TLR4 in acute lung injury. *Mol. Med. Rep.* 24 (6), 868. doi:10.3892/mmr.2021.12508

Li, T., Liu, Y., Li, G., Wang, X., Zeng, Z., Cai, S., et al. (2014). Polydatin attenuates ipopolysaccharide-induced acute lung injury in rats. *Int. J. Clin. Exp. Pathol.* 7, 8401–8410.

Li, W., Huang, H., Niu, X., Fan, T., Hu, H., Li, Y., et al. (2014). Tetrahydrocoptisine protects rats from LPS-induced acute lung injury. *Inflammation* 37 (6), 2106–2115. doi:10.1007/s10753-014-9945-7

Lin, Y., Zhu, X., Yao, W. Z., and Yang, Y. L., (2011). Yohimbine protects against endotoxin-induced acute lung injury by blockade of alpha 2A adrenergic receptor in rats. *Chin. Med. J. Engl.* 124 (7), 1069–1074.

Liu, H., Zhang, Y., Sun, S., and Wang, S. (2019). Efficacy of terpenoid in attenuating aortic atherosclerosis in apolipoprotein-E deficient mice: A meta-analysis of animal studies. *Biomed. Res. Int.* 2019, 2931831. doi:10.1155/2019/2931831

Liu, P., Hao, J., Zhao, J., Zou, R., Han, J., Tian, J., et al. (2022). Integrated network Pharmacology and experimental validation approach to investigate the therapeutic effects of capsaicin on lipopolysaccharide-induced acute lung injury. *Mediat. Inflamm.* 2022, 9272896. doi:10.1155/2022/9272896

Liu, T. Y., and Chen, S. B. (2016). Sarcandra glabra combined with lycopene protect rats from lipopolysaccharide induced acute lung injury via reducing inflammatory response. *Biomed. Pharmacother.* 84, 34–41. doi:10.1016/j.biopha.2016.09.009

Luo, X., Lin, B., Gao, Y., Lei, X., Wang, X., Li, Y., et al. (2019). Genipin attenuates mitochondrial-dependent apoptosis, endoplasmic reticulum stress, and inflammation via the PI3K/AKT pathway in acute lung injury. *Int. Immunopharmacol.* 76, 105842. doi:10.1016/j.intimp.2019.105842

Manicone, A. M. (2009). Role of the pulmonary epithelium and inflammatory signals in acute lung injury. *Expert Rev. Clin. Immunol.* 5 (1), 63–75. doi:10.1586/177666X.5.1.63

Matute-Bello, G., Frevert, C. W., and Martin, T. R. (2008). Animal models of acute lung injury. *Am. J. Physiol. Lung Cell. Mol. Physiol.* 295 (3), L379–L399. doi:10.1152/ajplung.00010.2008

Murakami, K., Okajima, K., and Uchiba, M. (2000). The prevention of lipopolysaccharide-induced pulmonary vascular injury by pretreatment with cepharanthine in rats. *Am. J. Respir. Crit. Care Med.* 161 (1), 57–63. doi:10.1164/ajrccm.161.1.9808142

Nader, M. A., and Baraka, H. N. (2012). Effect of betulinic acid on neutrophil recruitment and inflammatory mediator expression in lipopolysaccharide-induced lung inflammation in rats. *Eur. J. Pharm. Sci.* 46 (1-2), 106–113. doi:10.1016/j.ejps.2012.02.015

Ni, Y. L., Shen, H. T., Su, C. H., Chen, W. Y., Huang-Liu, R., Chen, C. J., et al. (2019). Nerolidol suppresses the inflammatory response during lipopolysaccharide-induced acute lung injury via the modulation of antioxidant enzymes and the AMPK/Nrf-2/HO-1 pathway. *Oxid. Med. Cell Longev.* 2019, 9605980. doi:10.1155/2019/9605980

Park, J., Chen, Y., Zheng, M., Ryu, J., Cho, G. J., Surh, Y. J., et al. (2018). Pterostilbene 4'-β-Glucoside attenuates LPS-induced acute lung injury via induction of heme oxygenase-1. *Oxid. Med. Cell Longev.* 2018, 2747018. doi:10.1155/2018/2747018

Ren, J., Lu, Y., Qian, Y., Chen, B., Wu, T., and Ji, G. (2019). Recent progress regarding kaempferol for the treatment of various diseases. *Exp. Ther. Med.* 18 (4), 2759–2776. doi:10.3892/etm.2019.7886

Sankhuan, D., Niramolyanun, G., Kangwanrangsan, N., Nakano, M., and Supaibulwatana, K. (2022). Variation in terpenoids in leaves of Artemisia annua grown under different LED spectra resulting in diverse antimalarial activities against Plasmodium falciparum. *BMC Plant Biol.* 22 (1), 128. doi:10.1186/s12870-022-03528-6

Schingnitz, U., Hartmann, K., Macmanus, C. F., Eckle, T., Zug, S., Colgan, S. P., et al. (2010). Signaling through the A2B adenosine receptor dampens endotoxin-induced acute lung injury. *J. Immunol.* 184 (9), 5271–5279. doi:10.4049/jimmunol.0903035

Schmidhammer, R., Wassermann, E., Germann, P., Redl, H., and Ullrich, R. (2006). Infusion of increasing doses of endotoxin induces progressive acute lung injury but prevents early pulmonary hypertension in pigs. *Shock* 25 (4), 389–394. doi:10.1097/01.shk.0000209529.43367.00

Shen, B., Zhao, C., Chen, C., Li, Z., Li, Y., Tian, Y., et al. (2017). Picroside II protects rat lung and A549 cell against LPS-induced inflammation by the NF-κB pathway. *Inflammation* 40 (3), 752–761. doi:10.1007/s10753-017-0519-3

Shi, X. M., Huang, L., Xiong, S. D., and Zhong, X. Y. (2007). Protective effect of tanshinone II A on lipopolysaccharide-induced lung injury in rats. *Chin. J. Integr. Med.* 13 (2), 137–140. doi:10.1007/s11655-007-0137-2

Tawadros, P. S., Powers, K. A., Yang, I., Becker, D. A., Ginsberg, M. D., Szaszi, K., et al. (2007). Stilbazulenyl nitrone decreases oxidative stress and reduces lung injury after hemorrhagic shock/resuscitation and LPS. *Antioxid. Redox Signal* 9 (11), 1971–1977. doi:10.1089/ars.2007.1765

Tomashefski, J. F., Jr. (2000). Pulmonary pathology of acute respiratory distress syndrome. *Clin. Chest Med.* 21 (3), 435–466. doi:10.1016/s0272-5231(05)70158-1

Wang, Y. M., Ji, R., Chen, W. W., Huang, S. W., Zheng, Y. J., Yang, Z. T., et al. (2019). Paclitaxel alleviated sepsis-induced acute lung injury by activating MUC1 and suppressing TLR-4/NF-κB pathway. *Drug Des. Devel Ther.* 13, 3391–3404. doi:10.2147/DDDT.S222296

Wang, Y. Y., Qiu, X. G., and Ren, H. L. (2015). Inhibition of acute lung injury by rubriflordilactone in LPS-induced rat model through suppression of inflammatory factor expression. *Int. J. Clin. Exp. Pathol.* 8 (12), 15954–15959.

Wang, Y., Zhang, J., Gao, X., Li, Q., and Sun, D. (2021). *In vitro* and *in vivo* anti-inflammatory effect of Zaluzanin D isolated from Achillea acuminate. *Int. Immunopharmacol.* 90, 107130. doi:10.1016/j.intimp.2020.107130

Warner, A. E., DeCamp, M. M., Jr, Molina, R. M., and Brain, J. D. (1988). Pulmonary removal of circulating endotoxin results in acute lung injury in sheep. *Lab. Invest* 59 (2), 219–230.

Wei, Y., and Wang, Y. (2017). Celastrol attenuates impairments associated with lipopolysaccharide-induced acute respiratory distress syndrome (ARDS) in rats. *J. Immunotoxicol.* 14 (1), 228–234. doi:10.1080/1547691X.2017.1394933

Wu, Y., Huang, D., Wang, X., Pei, C., Xiao, W., Wang, F., et al. (2021). Suppression of NLRP3 inflammasome by Platycodin D via the TLR4/MyD88/NF-κB pathway contributes to attenuation of lipopolysaccharide induced acute lung injury in rats. *Int. Immunopharmacol.* 96, 107621. doi:10.1016/j.intimp.2021.107621

Yang, H., Lv, H., Li, H., Ci, X., and Peng, L. (2019). Oridonin protects LPS-induced acute lung injury by modulating Nrf2-mediated oxidative stress and Nrf2-independent NLRP3 and NF-κB pathways. *Cell Commun. Signal* 17 (1), 62. doi:10.1186/s12964-019-0366-y

Yang, N., Liu, Y. Y., Pan, C. S., Sun, K., Wei, X. H., Mao, X. W., et al. (2014). Pretreatment with andrographolide pills(®) attenuates lipopolysaccharide-induced pulmonary microcirculatory disturbance and acute lung injury in rats. *Microcirculation* 21 (8), 703–716. doi:10.1111/micc.12152

Yang, W., Qiang, D., Zhang, M., Ma, L., Zhang, Y., Qing, C., et al. (2011). Isoforskolin pretreatment attenuates lipopolysaccharide-induced acute lung injury in animal models. *Int. Immunopharmacol.* 11 (6), 683–692. doi:10.1016/j.intimp.2011.01.011

Ye, J., Guan, M., Lu, Y., Zhang, D., Li, C., and Zhou, C. (2019). Arbutin attenuates LPS-induced lung injury via Sirt1/Nrf2/NF-κBp65 pathway. *Pulm. Pharmacol. Ther.* 54, 53–59. doi:10.1016/j.pupt.2018.12.001

Yuan, H. L., Zhao, Y. L., Ding, C. F., Zhu, P. F., Jin, Q., Liu, Y. P., et al. (2020). Anti-inflammatory and antinociceptive effects of Curcuma kwangsiensis and its bioactive terpenoids *in vivo* and *in vitro*. *J. Ethnopharmacol.* 259, 112935. doi:10.1016/j.jep.2020.112935

Yuan, Q., Jiang, Y. W., Ma, T. T., Fang, Q. H., and Pan, L. (2014). Attenuating effect of Ginsenoside Rb1 on LPS-induced lung injury in rats. *J. Inflamm. (Lond)* 11 (1), 40. doi:10.1186/s12950-014-0040-5

Yue, Q., Liu, T., and Cheng, Z. (2020). Protective effect of colchicine on LPS-induced lung injury in rats via inhibition of P-38, ERK1/2, and JNK activation. *Pharmacology* 105 (11-12), 639–644. doi:10.1159/000504759

Zhang, C., Wang, X., Wang, C., He, C., Ma, Q., Li, J., et al. (2021). Qingwenzhike prescription alleviates acute lung injury induced by LPS via inhibiting TLR4/NF-kB pathway and NLRP3 inflammasome activation. *Front. Pharmacol.* 12, 790072. doi:10.3389/fphar.2021.790072

Zhang, E., Wang, J., Chen, Q., Wang, Z., Li, D., Jiang, N., et al. (2020). Artesunate ameliorates sepsis-induced acute lung injury by activating the mTOR/AKT/PI3K axis. *Gene* 759, 144969. doi:10.1016/j.gene.2020.144969

Zhang, Z., Wang, X., Ma, C., Li, Z., Chen, H., Zhang, Z., et al. (2019). Genipin protects rats against lipopolysaccharide-induced acute lung injury by reinforcing autophagy. *Int. Immunopharmacol.* 72, 21–30. doi:10.1016/j.intimp.2019.03.052

Zhao, R., Wang, B., Wang, D., Wu, B., Ji, P., and Tan, D. (2021). Oxyberberine prevented lipopolysaccharide-induced acute lung injury through inhibition of mitophagy. *Oxid. Med. Cell Longev.* 2021, 6675264. doi:10.1155/2021/6675264

frontiers | Frontiers in Pharmacology

TYPE Original Research
PUBLISHED 31 August 2022
DOI 10.3389/fphar.2022.953871

OPEN ACCESS

EDITED BY
Weicheng Hu,
Huaiyin Normal University, China

REVIEWED BY
Di Wang,
Jilin Agriculture University, China
Jianmei Zhang,
Sungkyunkwan University, South Korea

*CORRESPONDENCE
Ying-Hua Jin,
yhjin@jlu.edu.cn

SPECIALTY SECTION
This article was submitted to Inflammation Pharmacology, a section of the journal Frontiers in Pharmacology

RECEIVED 26 May 2022
ACCEPTED 14 July 2022
PUBLISHED 31 August 2022

CITATION
To K-I, Zhu Z-X, Wang Y-N, Li G-A, Sun Y-M, Li Y and Jin Y-H (2022), Integrative network pharmacology and experimental verification to reveal the anti-inflammatory mechanism of ginsenoside Rh4.
Front. Pharmacol. 13:953871.
doi: 10.3389/fphar.2022.953871

Integrative network pharmacology and experimental verification to reveal the anti-inflammatory mechanism of ginsenoside Rh4

Kwang-Il To, Zhen-Xing Zhu, Ya-Ni Wang, Gang-Ao Li, Yu-Meng Sun, Yang Li and Ying-Hua Jin*

Key Laboratory for Molecular Enzymology and Engineering of the Ministry of Education, School of Life Sciences, Jilin University, Changchun, China

Inflammation is an innate immune response to infection, and it is the main factor causing bodily injury and other complications in the pathological process. Ginsenoside Rh4 (G-Rh4), a minor ginsenoside of Panax ginseng C. A. Meyer and Panax notoginseng, has excellent pharmacological properties. However, many of its major pharmacological mechanisms, including anti-inflammatory actions, remain unrevealed. In this study, network pharmacology and an experimental approach were employed to elucidate the drug target and pathways of G-Rh4 in treating inflammation. The potential targets of G-Rh4 were selected from the multi-source databases, and 58 overlapping gene symbols related to G-Rh4 and inflammation were obtained for generating a protein–protein interaction (PPI) network. Molecular docking revealed the high affinities between key proteins and G-Rh4. Gene ontology (GO) and pathway enrichment analyses were used to analyze the screened core targets and explore the target–pathway networks. It was found that the JAK-STAT signaling pathway, TNF signaling pathway, NF-κB signaling pathway, and PI3K-Akt signaling pathway may be the key and main pathways of G-Rh4 to treat inflammation. Additionally, the potential molecular mechanisms of G-Rh4 predicted from network pharmacology analysis were validated in RAW264.7 cells. RT-PCR, Western blot, and ELISA analysis indicated that G-Rh4 significantly inhibited the production of pro-inflammatory cytokines such as TNF-α, IL-6, and IL-1β, as well as inflammation-related enzymes in lipopolysaccharide (LPS)-stimulated RAW264.7 cells. Moreover, *in vitro* experiments evaluated that Ginsenoside Rh4 exerts anti-inflammatory effects *via* the NF-κB and STAT3 signaling pathways. It is believed that our study will provide the basic scientific evidence that G-Rh4 has potential anti-inflammatory effects for further clinical studies.

KEYWORDS

network pharmacology, ginsenoside, inflammation, proinflamamtory cytokines, pharmacological mechanism

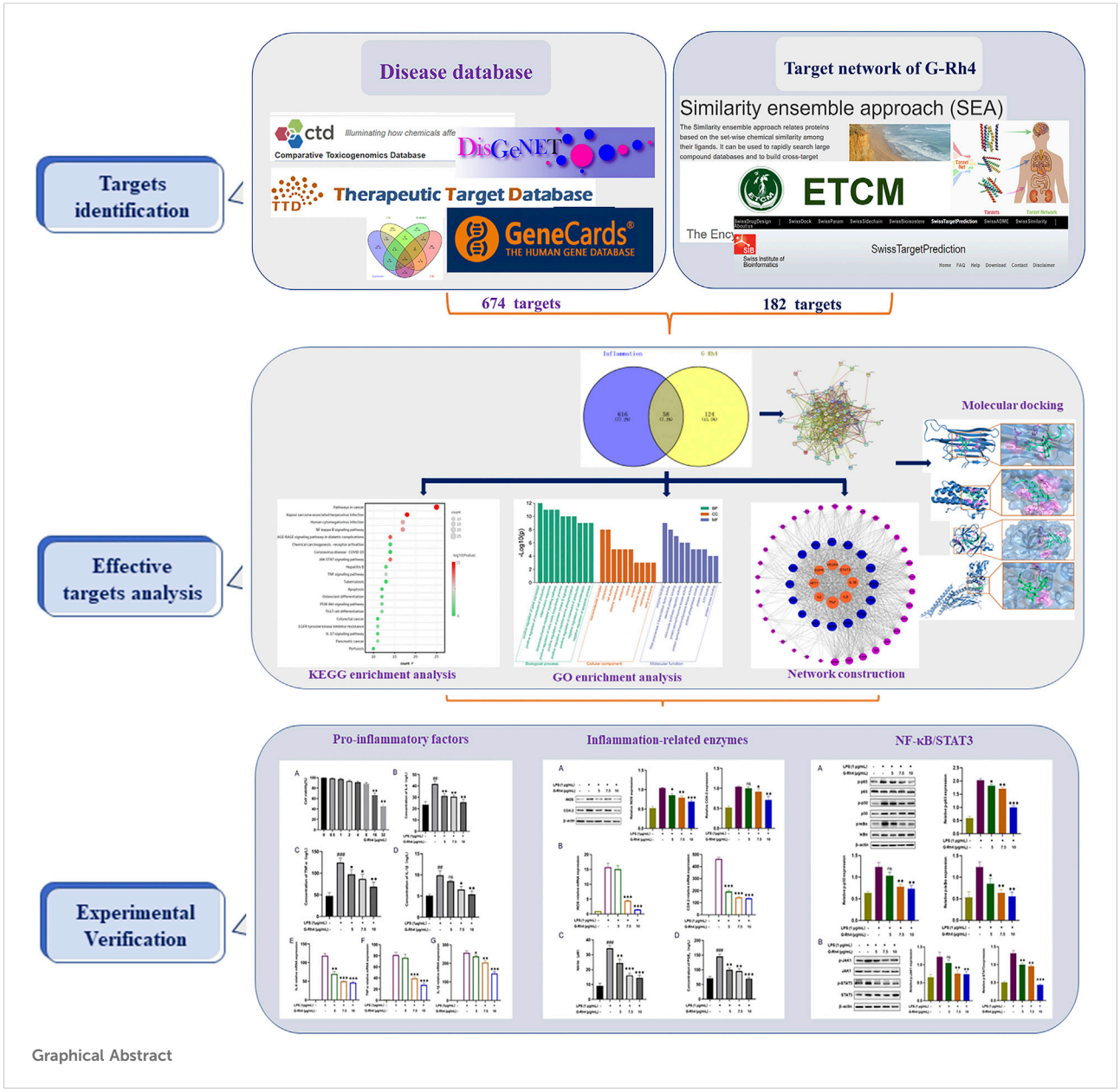

Graphical Abstract

Introduction

The occurrence of self-limited inflammation is critical for survival during physical injury and infection; however, the persistence of inflammation leads to several pivotal diseases that collectively represent the leading causes of disability and mortality worldwide (Furman et al., 2019; Panigrahy et al., 2020). Recent research has revealed that chronic inflammatory diseases have been recognized as the most important cause of death in the world today (Libby, 2021), and more than 50% of deaths are attributed to inflammation-related diseases such as ischemic heart disease, cancer, non-alcoholic fatty liver disease (NAFLD), and diabetes mellitus (GBD 2017 Causes of Death Collaborators, 2018). In addition, it was reported that typical biomarkers of acute inflammation can predict the incidence rate and mortality of various diseases (Arai et al., 2015), but this approach also has limitations. To address the limitations of assessment with a few selected inflammatory biomarkers, researchers have adopted a multi-dimensional approach, including analyzing a large number of inflammatory markers and then combining these markers into more reliable indicators representing high inflammatory activity (Morrisette-Thomas et al., 2014). The anti-inflammatory drugs, including non-steroidal anti-inflammatory drugs, have been developed and applied in

clinics, but studies have shown that these drugs frequently cause adverse effects such as liver injury (Schmeltzer et al., 2016). Looking for more effective and safe anti-inflammatory drugs is an urgent issue in the global medical community.

Ginsenoside is the main active ingredient of ginseng, which displayed a broad spectrum of activities, such as cancer cell toxicity, anti-inflammation, and enhancing immunity. G-Rh4 is a trace saponin in white ginseng, and it became the most abundant triol-type ginsenoside after the heating process. Compared with other saponins, G-Rh4 has relatively better water solubility (Wang et al., 2022), suggesting its potential clinical applications. However, due to its low content in fresh or white ginseng and consequent preparation difficulty, there are few studies on the pharmacological effects of G-Rh4; especially, its anti-inflammatory activity and underlying mechanism are largely unknown.

Network pharmacology is the construction and analysis of biological networks based on network database retrieval and computer simulation calculation to study the mechanism of drug action. In particular, in determining the pharmacological mechanism and safety of Chinese medicine, the application of network analysis is a new paradigm for traditional Chinese medicine, from empirical medicine to evidence-based medicine (Wang et al., 2021). Therefore, network pharmacology research, as a new interdisciplinary approach, is of great value to the research and development of modern Chinese medicine (Sun et al., 2020; Wang et al., 2021). In this study, we clarified the drug target and multiple pathways of G-Rh4 in the treatment of inflammation by network pharmacology and the experimental approach.

Methods

Prediction of G-Rh4-related targets

The PubChem database (https://pubchem.ncbi.nlm.nih.gov/) was searched to obtain the two-dimensional structure diagram in SDF format and the canonical smiles of G-Rh4 (Figure 1A). The main potential targets of ginsenoside-Rh4 were identified using the Swiss Target Prediction (http://swisstargetprediction.ch/), the TargetNet (http://targetnet.scbdd.com/), the Similarity Ensemble Approach (SEA) (https://sea.bkslab.org/), and the Encyclopedia of Traditional Chinese Medicine (ETCM) (http://www.tcmip.cn/ETCM/index.php/Home/Index/) database.

Acquisition of gene targets for inflammation

The genes related to inflammation were selected from the Therapeutic Target Database (TTD, http://db.idrblab.net/ttd/) (Wang Y. et al., 2019), the GeneCards (https://www.genecards.org/) (Rappaport et al., 2017), DisGeNET (https://www.disgenet.org/search) (Piñero et al., 2019), and the Comparative Toxicogenomics Database (CTD, http://ctdbase.org/search/) (Davis et al., 2021), where the database was searched using "inflammation" and "inflammatory" as the keywords.

Screening of potential therapeutic targets

The target genes of G-Rh4 and the target information of inflammation were uploaded to Venny 2.1 (https://bioinfogp.cnb.csic.es/tools/venny/index.html) to obtain the target information of G-Rh4 intersecting with inflammation, and it is considered as the potential target of Rh4 in the treatment of inflammation.

Network diagram of drug–disease PPI

The protein–protein interaction (PPI) network diagram was obtained through the STRING database (https://string-db.org/) (Szklarczyk et al., 2021). The TSV-format file was downloaded from the STRING database and imported into Cytoscape 3.8.0 for core target screening.

Gene Ontology and KEGG enrichment analysis

The candidate targets were identified by using the DAVID v6.8 (https://david.ncifcrf.gov/) (Huang et al., 2009) to conduct GO and Kyoto Encyclopedia of Genes and Genomes (KEGG) enrichment analysis on the target of G-Rh4 in the treatment of inflammation. A threshold of $p < 0.05$ was used to identify key GO and KEGG pathways; GraphPad Prism 8 0.1 software was used to visualize the analysis results.

Diagram of core drug targets

Using the software Cytoscape 3 8.0, the relationship network diagram of core drug targets was constructed and topological analysis was performed, after which the importance of targets was analyzed according to the degree value (Rahimmanesh and Fatehi, 2020).

Molecular docking verification

First, PDB format of the key target proteins and MOL2 format of Ginsenoside Rh4 were obtained through the RCSR protein database (https://www.rcsb.org/) and the NCBI PubChem Compound database, and PyMOL software was employed to remove the water and ligands. After that,

molecular docking was conducted between the treated proteins and active components by using AutoDock Vina software, and the binding energy was evaluated, where the value of <0 indicated that the receptors and compounds can bind by themselves (Liang et al., 2021), while the value of <−5.0 kcal/mol meant that they had good binding activities. The lower the binding energy, the greater the probability of binding and the more credible the result.

Cell lines and culture

RAW264.7 cells were purchased from the Chinese Academy of Sciences Stem Cell Bank. DMEM containing 10% FBS and double antibodies (penicillin 100 U/mL and streptomycin 100 μg/ml) was used as a culture medium, and cells were cultured in an incubator at 37°C and 5% CO_2.

Assay to measure cell viability

The logarithmic period RAW264.7 cells (1 × 104 cells/well) were inoculated on 96-well plates and cultured for 24 h. After treatment with different concentrations of G-Rh4 in serum-free DMEM for 24 h, 20 μL of MTT (5 mg/ml; Sigma, USA) solution was added. After incubation for another 4 h, the culture medium was discarded and 150 μL DMSO (Sigma, USA) was added to each well. The absorbance at 550 nm was measured using a TECAN microplate reader (Maennedorf, Switzerland).

Real-time quantitative polymerase chain Reaction

RAW264.7cells (2 × 105 cells/mL) were inoculated in 100-mm dishes and cultured for 24 h. LPS (1 μg/ml) was pretreated for 4 h and further treated with different concentrations (5, 7.5, and 10 μg/ml) of G-Rh4 for another 16 h. At the end of treatments, the total RNA of RAW264.7 cells was isolated with TRIzol (Invitrogen, Grand Island, NY, USA), and 5 μg total RNA was proceeded for cDNA synthesis with a High Capacity cDNA Reverse Transcription Kit (4368814, Applied Biosystems, Foster City, CA, USA). Real-time quantitative experiments were conducted according to the instructions of the 7,500 Real-time PCR system (Applied Biosystems, Foster City, CA, USA) to determine the mRNA expression. The primer sequences are shown in Supplementary Table S1.

Determination of levels of IL-6, TNF-α, IL-1β, and PGE_2 by ELISAs

RAW264.7 cells (2.5 × 105 cells/mL) were inoculated in 12-well plates and cultured for 24 h. LPS (1 μg/ml) was pretreated for 4 h and different concentrations of G-Rh4 were treated for 16 h. The levels of IL-6, TNF-α, IL-1β, and PGE2 in the supernatant were measured, respectively, according to the operation instructions of the ELISA kit (CLOUD-CLONE CORP., Wuhan, Hubei).

Nitrite assay

The logarithmic period RAW264.7 cells (1 × 104 cells/well) were inoculated on 96-well plates and cultured for 24 h. The cells were pretreated with LPS (1 μg/ml) for 4 h and then treated with different concentrations of G-Rh4 for 16 h. Nitrite levels in the cell culture supernatants were measured using Griess assay. Subsequently, 50 μL of the culture medium were mixed with 50 μL reagents of Griess A and Griess B, followed by incubation for 10 min at room temperature (light protected). A wavelength of 540 nm was selected to detect the absorbance values using a microplate reader, and nitrite levels were measured using a standard curve prepared from sodium nitrite (Park et al., 2005).

Western blot analysis

RAW264.7cells (7×10^5 cells/well) were seeded in 6-well plates and cultured for 24 h. The cells were pretreated with LPS (1 μg/ml) for 4 h and treated with different concentrations of G-Rh4 for 16 h. At the end of treatments, the cells were collected in a 1.5-ml centrifuge tube and then centrifuged at 10,000 r/min (rpm) for 5 min at 4°C, and the supernatant was discarded. The supernatant was washed with PBS and centrifuged at 10,000 rpm for 5 min, after which the cells were lysed with the RIPA cell lysate supplemented with 1% PMSF for 50 min and centrifuged at 12,000 rpm for 15 min to collect the supernatant. The protein concentrations were detected using BSA (bovine serum albumin, Sigma) as a standard. Equal amounts of protein (30 μg) were taken and subjected to SDS-PAGE electrophoresis. Then, the protein was transferred to the PVDF membrane and sealed with 5% (w/v) skim milk in Tris-buffered saline containing 0.1% Tween 20 (TBST). The primary antibody was incubated overnight at 4°C. After washing with TBST buffer, the membranes were incubated with the secondary antibody at room temperature for 1 h. The protein bands were quantitatively analyzed by ECL chromogenic exposure in a dark chamber.

Statistical analysis

The experimental data were obtained from independent triple-replicated experiments and were expressed as the mean ± SD. Statistical analyses were processed using

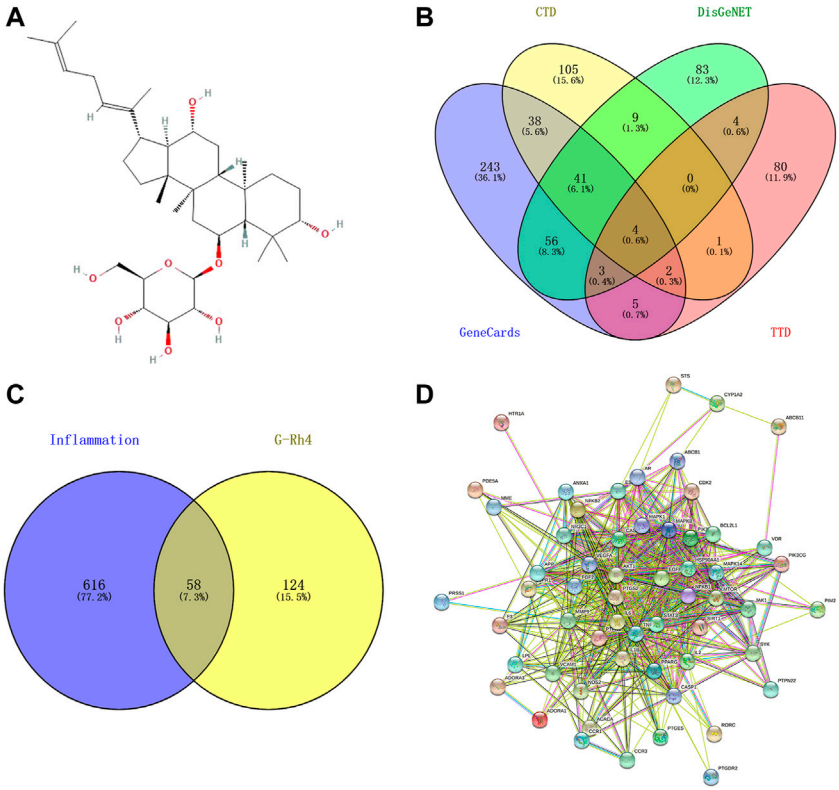

FIGURE 1
Targets screening involved in G-Rh4 for treating inflammation. **(A)** Molecule structure of G-Rh4. **(B)**Venn diagram of the potential inflammation-specific targets. **(C)** Fifty-eight overlapping target proteins between inflammation-related proteins and targets of G-Rh4. **(D)** Protein–protein networks of overlapping 58 target proteins. Edges: Interactions between protein(s) and protein(s).

GraphPad Prism 8.0, and the Student's *t*-test statistical analysis method was used to compare groups. $p < 0.05$ showed that the difference was statistically significant.

Results

Prediction of G-Rh4 potential target

In this experiment, network pharmacology and an experimental approach were employed to elucidate the drug target and pathways of G-Rh4 against inflammation (Figure 1). A total of 182 potential targets of ginsenoside Rh4 (G-Rh4) were collected from the databases such as Swiss Target Prediction, TargetNet, SEA, and ETCM, and 674 inflammation-related targets were screened through databases including GeneCards, DisGeNET, Therapeutic Target Database (TTD), and Comparative Toxicogenomics Database (CTD) (Figure 1B). The potential targets of G-Rh4 were intersected with inflammation-related genes, and as a result, 58 intersected genes were obtained. The Venn diagram is drawn in Figure 1C, and the names of intersection genes are listed in Supplementary Table S2.

Identification of G-Rh4 core targets against inflammation

A total of 58 intersected target genes of G-Rh4 against inflammation were uploaded to the String database. Organization was set as *Homo sapiens*, and obtained the key targets (Figure 1D). The PPI data were imported into Cytoscape software, and the target node degree is taken as an important parameter of topology analysis to screen out the key nodes in the network, which are shown in Figure 2, where the size of the ellipse represents the major degree of the target genes.

Gene Ontology and KEGG pathway enrichment analysis of the target genes of G-Rh4 against inflammation

To further understand the biological processes involved in the screened key candidate targets above and their correlation with "inflammation," we conducted analyses of GO and KEGG signaling pathways. The DAVID database was used to classify and count the GO function of 58 intersected genes of G-Rh4 in

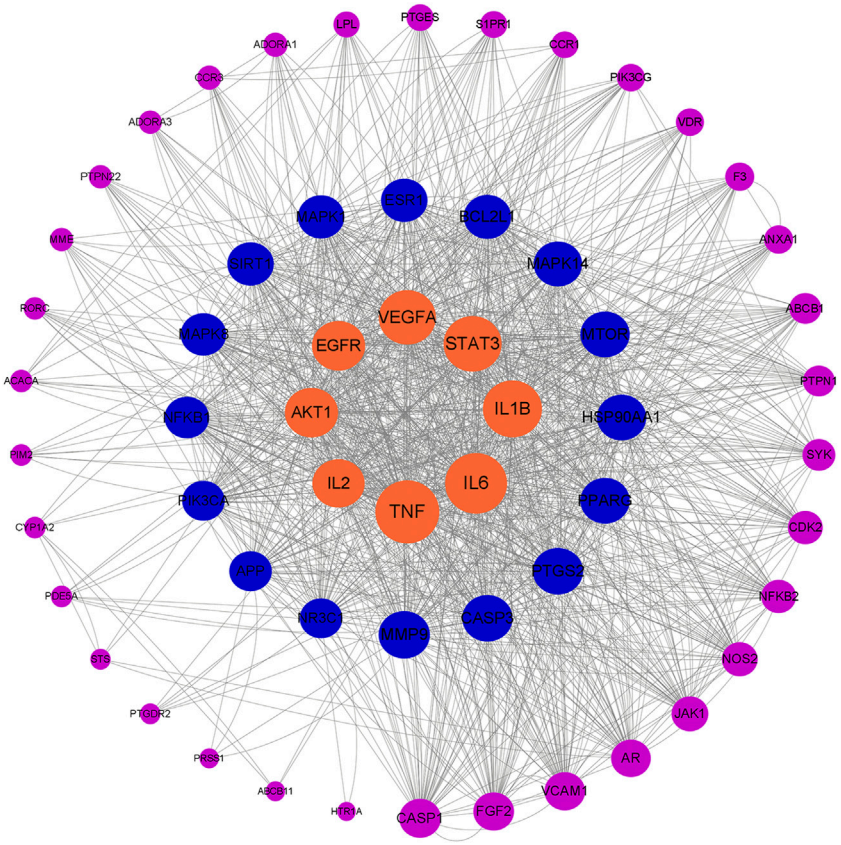

FIGURE 2
Network topology analysis of G-Rh4 treating inflammation; the target genes are sorted according to degree.

the treatment of inflammation (Supplementary Table S3). The pathways were visually analyzed to understand the functional distribution characteristics of different genes. The histogram for the pathway enrichment analysis was shown in Figure 3A. The GO analysis results indicated that the biological process (BP) terms were mainly associated with the positive regulation of the nitric oxide biosynthetic process, inflammatory response, positive regulation of interleukin-6 production, the lipopolysaccharide-mediated signaling pathway, and negative regulation of cell proliferation; the main cellular component (CC) terms were the macromolecular complex, cytoplasm, cell surface, plasma membrane, and endosome. Their primary molecular function (MF) was concentrated on enzyme binding, RNA polymerase II transcription factor activity, identical protein binding, nitric-oxide synthase regulator activity, and protein serine/threonine kinase activity.

In addition, to clarify the underlying involved pathway of inflammation targets treated by G-Rh4, the pathway enrichment analysis on target genes was conducted through the KEGG public database (Supplementary Table S4). A total of 58 intersected genes were imported into the DAVID database for KEGG pathway annotation analysis, after which the top 20 pathways were visually analyzed to obtain the pathway enrichment analysis bubble diagram (Figure 3B). It could be seen that common targets were mainly concentrated in the JAK-STAT signaling pathway, TNF signaling pathway, NF-κB signaling pathway, and PI3K-Akt signaling pathway.

Molecular docking simulation

According to hub gene analysis, TNF-α, IL-6, IL-1β, and STAT3 are the key targets of G-Rh4 in the treatment of inflammation. Molecular docking simulation was applied to predict the binding ability between G-Rh4 and hub targets. The molecular docking of G-Rh4 with key targets was performed using AutoDock Vina software, and the binding energy was evaluated. The binding energy between G-Rh4 and TNF-α and IL-6 was −6.79 and −7.25 kcal/mol, respectively. The binding energy between G-Rh4 and IL-1β and STAT3 was −7.99 and −5.15 kcal/mol, respectively, suggesting that they have good binding activities (Table 1). The docking results were visualized using PyMOL software, as shown in Figures 3C–F.

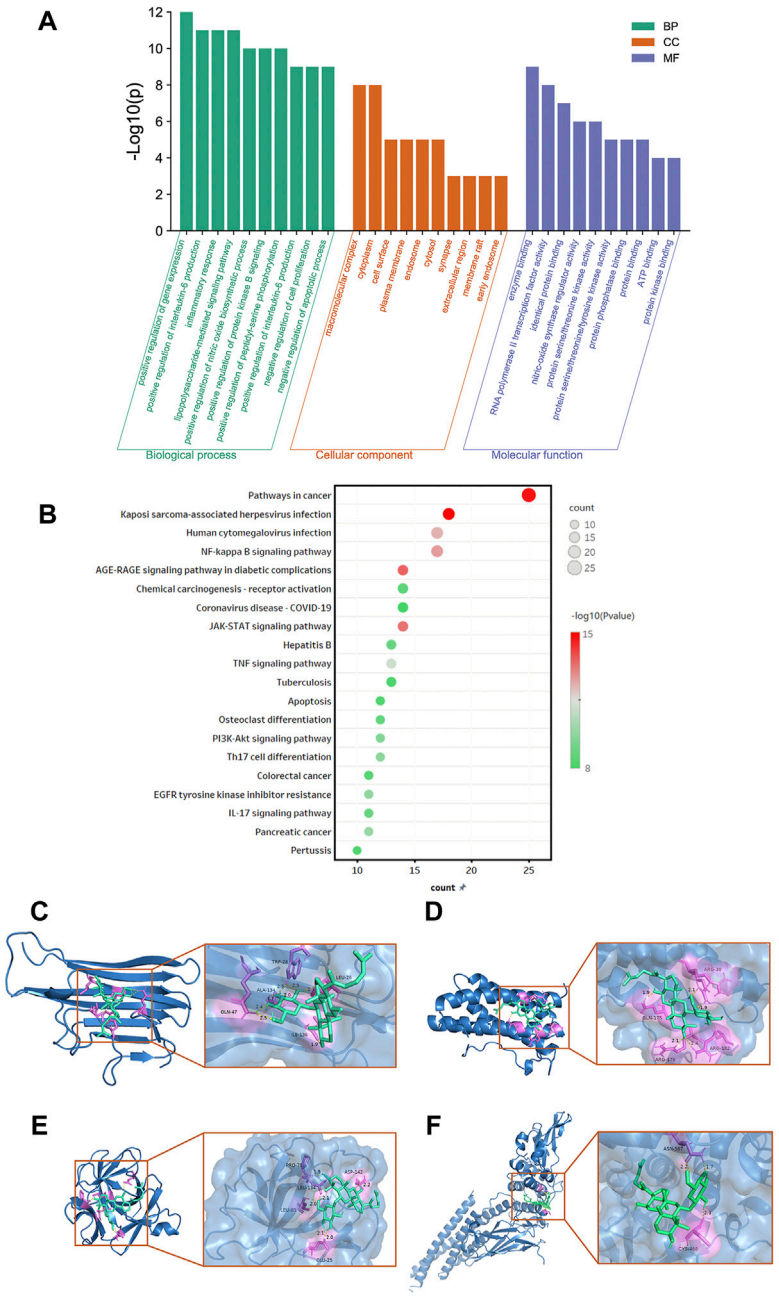

FIGURE 3
Functional enrichment analysis and docking simulation. Gene Ontology**(A)** and KEGG pathway enrichment **(B)** analysis of the target genes of G-Rh4 against inflammation. **(C–F)** The docking mode of G-Rh4 binding with target proteins; **(C)** TNF-α, **(D)** IL-6, **(E)** IL-1β, and **(F)** STAT3.

Effect of G-Rh4 on the viability of RAW264.7 cells

To study the effect of G-Rh4 on the viability of RAW264.7 macrophages, cells were treated with different concentrations of G-Rh4 for 24 h, and the cell activity was detected by MTT assay. As shown in Figure 4A, compared with the control group, G-Rh4 treatment showed no significant effect on the viability of macrophages at the concentration of 0.5–8 μg/ml ($p > 0.05$), indicating that G-Rh4 has no toxicity to RAW264.7 cells at this concentration.

TABLE 1 Result of molecular docking.

Targets	PDB	Binding energy (kcal/mol)
TNF-α	5M2J	−6.79
IL-6	1ALU	−7.25
IL-1β	2I1B	−7.99
STAT3	6NJS	−5.15

The production of IL-6, TNF-α, and IL-1β was inhibited by G-Rh4 treatment

LPS is a component of the cell wall of gram-negative bacteria, which can stimulate the activation of immune cells such as macrophages and cause a systemic inflammatory response. To study the effect of G-Rh4 on major inflammatory factors, the protein and mRNA levels of IL-6, TNF-α, and IL-1β in LPS-stimulated RAW264.7 cells were evaluated by ELISAs and RT-PCR. The results are shown in Figures 4B–D. The contents of TNF–α, IL-6, and IL-1β in LPS-stimulated RAW264.7 were significantly higher than those in the normal group ($p < 0.01$, $p < 0.001$), but after G-Rh4 treatment, they decreased significantly in a concentration-dependent manner ($p < 0.05$, $p < 0.01$). Also, the increased mRNA expression of the main target factor after stimulation of LPS decreased significantly with the addition of G-Rh4 (Figures 4E–G), which seems to support the experimental results of ELISAs.

Effect of G-Rh4 on expression of iNOS/COX-2 and NO/PGE_2 production in RAW264.7 cells

The expression levels of iNOS and COX-2 in RAW264.7 cells were detected by Western blot and RT-PCR analysis. Compared

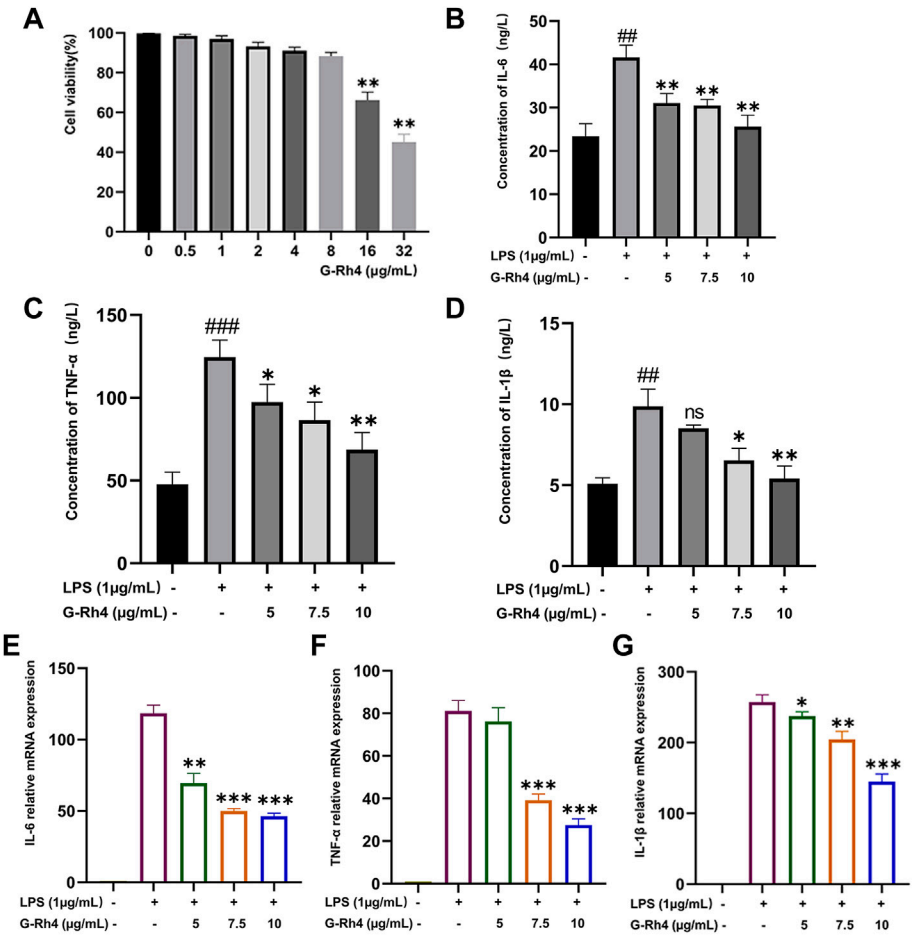

FIGURE 4
Effect of G-Rh4 on RAW264.7 cells. **(A)** Effect of G-Rh4 on cell viability. Cells were treated with different concentrations of G-Rh4 for 24 h. **(B–D)** Production of IL-6, TNF-α, and IL-1β in LPS-stimulated RAW264.7 cells was determined by ELISAs. **(E–G)** Effect of G-Rh4 on TNF-α, IL-6, and IL-1β mRNA levels in RAW264.7 cells. Data were presented as the mean ± SD values performed in triplicate ($^{\#\#}p < 0.01$ and $^{\#\#\#}p < 0.001$ vs. control group, $^{*}p < 0.05$, $^{**}p < 0.01$, $^{***}p < 0.001$ vs. LPS group).

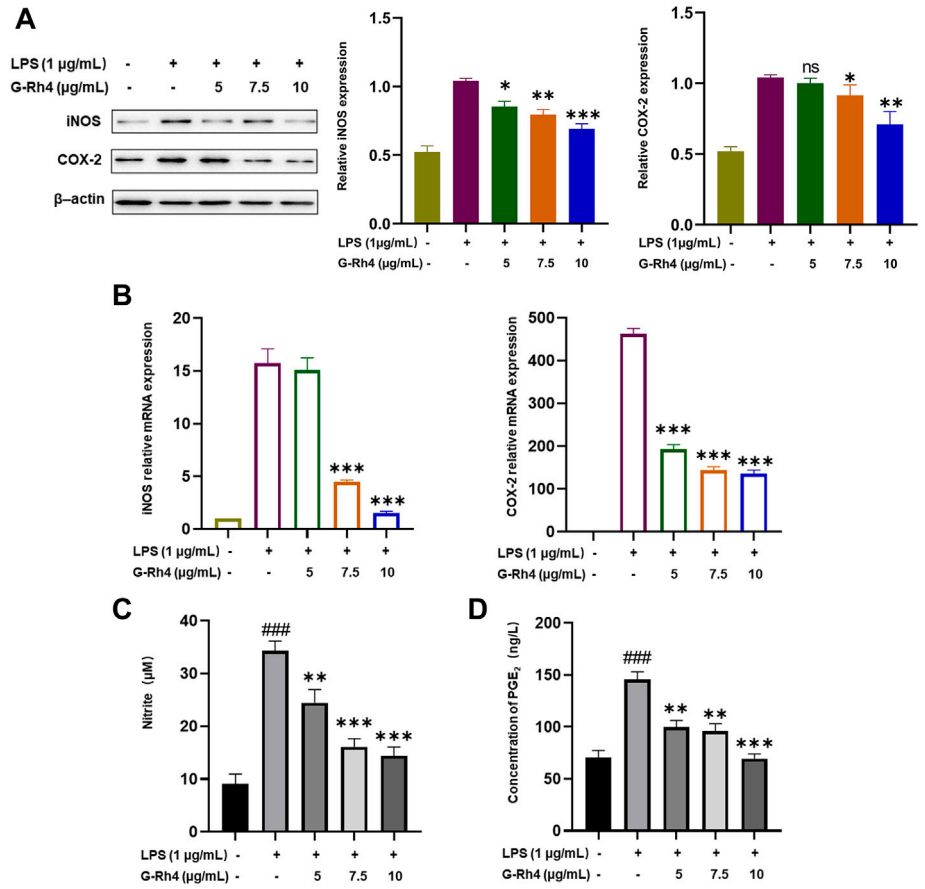

FIGURE 5
Inhibitory effects of G-Rh4 on NO/PGE_2 production and iNOS/COX-2 expression in LPS-stimulated RAW264.7 cells. **(A)** Effect of G-Rh4 on iNOS and COX-2 protein levels in RAW264.7 cells. **(B)** Determination of iNOS and COX-2 mRNA levels in LPS-stimulated RAW264.7 cells. **(C)** NO levels in the culture medium evaluated by Griess reagent. **(D)** Effect of G-Rh4 on the release of PGE_2 in RAW264.7 cells. Data were presented as the mean ± SD values performed in triplicate ($^{\#\#}p < 0.01$ and $^{\#\#\#}p < 0.001$ vs. control group, $^{*}p < 0.05$, $^{**}p < 0.01$, $^{***}p < 0.001$ vs. LPS group).

with the LPS treatment group, a 5 μg/ml dose of G-Rh4 had no significant difference in inhibiting the expression of COX-2. But it decreased significantly at a dose of 7.5 μg/ml and iNOS levels were markedly reduced from those at the 5 μg/ml dose of G-Rh4 (Figure 5A). The mRNA expressions of iNOS and COX-2 were also decreased significantly at the 7.5 μg/ml dose of G-Rh4 compared with those in the LPS treatment group ($p < 0.001$) (Figure 5B). These results showed that G-Rh4 meaningfully inhibited the expression of inflammatory promoting enzymes in the inflammatory response. iNOS and COX-2 are the key enzymes involved in the synthesis of NO and PGE_2, which are also the key factors causing inflammatory responses and individual pathological status. We investigated whether G-Rh4 regulates NO and PGE_2 synthesis in LPS-stimulated RAW264.7 cells. LPS stimulation increased the production of NO and PGE_2, and the release of NO and PGE_2 was significantly reduced in a dose-dependent manner upon G-Rh4 treatment (Figures 5C,D).

G-Rh4 inhibited the LPS-induced NF-κB and STAT3 activation in RAW264.7 macrophages

NF-κB and STAT3 are transcriptional regulators involved in a series of critical signaling pathways, which plays a key role in the inflammatory response. Nuclear translocation of the NF-κB p50-p65 heterodimer is essential for NF-κB signaling. To further reveal the action mechanisms of G-Rh4, we investigated the effect of G-Rh4 on the expression and activation of p50-p65 and IκBα by Western blot analysis (Figure 6A). The results showed that G-Rh4 effectively inhibited LPS-induced phosphorylation of p50, p65, and IκBα in RAW264.7 cells. According to our network pharmacological analysis, STAT3 is also the main hub gene of G-Rh4 against inflammation, like the main inflammatory factors previously investigated. The Western blot analysis showed that the levels of p-JAK1/JAK1 and p-STAT3/STAT3 were significantly downregulated with the treatment of G-Rh4

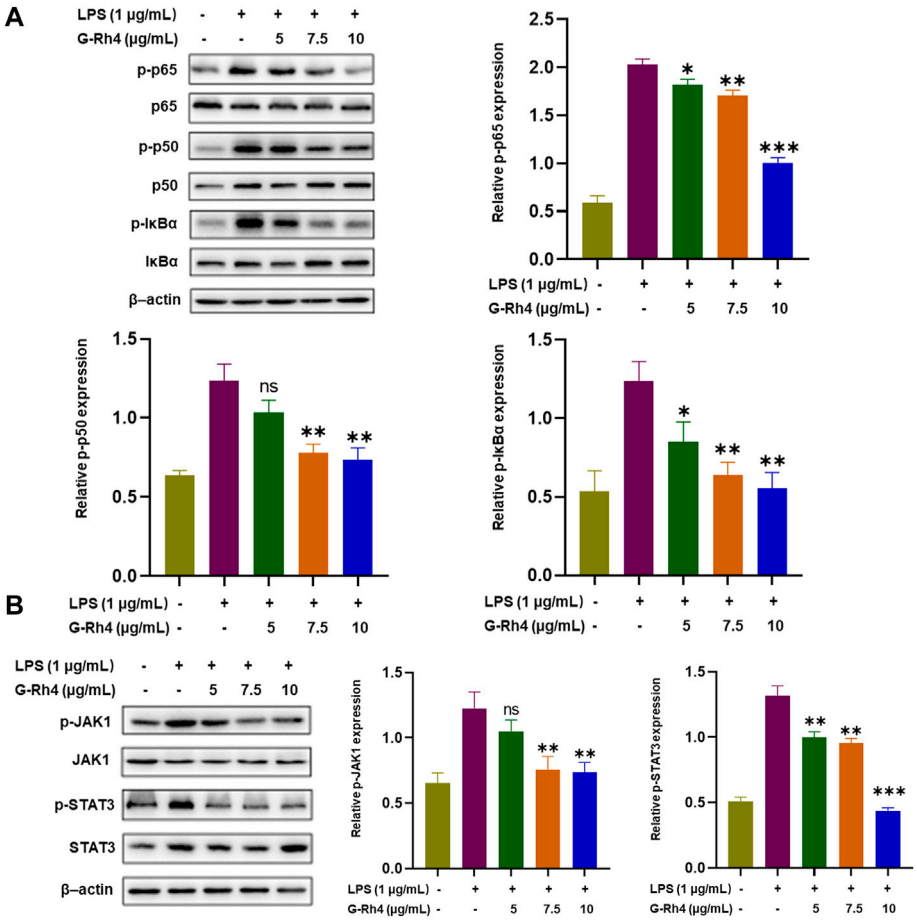

FIGURE 6
Effect of G-Rh4 on the NF-κB and STAT-3 activation in RAW264.7 cells. **(A)** Determination of the p-IκBα (Ser32), p-p65 (ser536), and p-p50 (ser337) protein using Western blot analysis. **(B)** Effect of G-Rh4 on the STAT-3 activation in RAW264.7 cells. Data were presented as the mean ± SD values performed in triplicate (*$p < 0.05$, **$p < 0.01$, ***$p < 0.001$ vs. LPS group).

(Figure 6B). With the increase of G-Rh4 concentration (5, 7.5, and 10 μg/ml), the phosphorylation levels of JAK1 and STAT3 protein decreased evidently ($p < 0.01$, $p < 0.001$). These results suggest that the anti-inflammatory effect of G-Rh4 can be mediated by the regulation of the NF-kB and STAT3 pathway.

Discussion

Inflammation is a specific defense response to physical injury or infection. The persistence of inflammation, however, leads to the occurrence and development of several refractory diseases, such as cardiovascular disease, cancer, diabetes mellitus, chronic kidney disease, non-alcoholic fatty liver disease, and autoimmune and neurodegenerative disorders. Therefore, the extensive study of the inflammation pathways and the development of effective inflammation-modulating drugs are the most challenging area in the field of life science and pharmacology. At present, traditional Chinese medicine has become an emerging candidate for the treatment of inflammation because of its potent efficacy and fewer side effects (Fan et al., 2021).

Network pharmacology, from the perspective of system-level and biological networks, analyzes the molecular relationship between drugs and targets, reveals the systematic pharmacological mechanism of drugs, and guides the development of new drugs and clinical diagnosis and treatment. It is reported that the existing differences in data collection and target prediction in network pharmacology analysis result in the loss of some target genes (Luo et al., 2021). Since some target genes may not be included in the public database, we explored multiple databases for G-Rh4 and inflammation-related target genes. A total of 58 anti-inflammatory common targets of G-Rh4 were

collected to analyze these common targets by hub gene analysis and GO and KEGG enrichment analysis. Our results showed that the anti-inflammatory effect of G-Rh4 was deeply related to the main target factors including TNF-α, IL-6, IL-1β, and STAT-3 and their related metabolic pathways, and the molecular docking analysis confirmed that G-Rh4 had a high binding possibility with these target factors. VEGFA is also the main target factor related to the anti-inflammatory effect in the network pharmacological analysis, but the possibility of binding with G-Rh4 was not recognized in molecular docking simulation (the experimental result has not shown).

It is reported that a prolonged inflammatory state is harmful to health, and long-term macrophages in tissues activate the abnormal expression of inflammatory factors such as TNF-α, IL-6, IL-1β, NO, and Prostaglandin E2, which can stimulate the inflammatory signaling pathway, eventually leading to chronic low-grade inflammation (Huang et al., 2017). These mediators stimulate the innate immune response, but their overexpression may cause endotoxemia, leading to tissue injury, organ failure, shock, and even death. Regulating the expression of these inflammatory mediators plays a key role in the treatment of inflammatory diseases (Joh et al., 2011). We confirmed the inhibitory effect of G-Rh4 on the expression of the primary target factors through LPS-stimulated mouse RAW264.7 cells. The *in vitro* inflammatory response model established by LPS-stimulated RAW264.7 macrophages is a widely used cell model for screening anti-inflammatory drugs. LPS mainly induces the synthesis and release of a variety of inflammatory mediators through the activation of nuclear transcription factors κB (NF-κB), JAK/STAT, MAPKs, phosphorylated ERK, phosphorylated JNK, and phosphorylated p38 signaling pathways (Liu et al., 2019). Our results indicated that LPS significantly increased mRNA and protein levels of TNF-α, IL-6, and IL-1β. In addition, we also confirmed using ELISAs and RT-PCR methods that G-Rh4 brings about the anti-inflammatory effects by decreasing TNF-α, IL-6, and IL-1β expression levels in LPS-activated RAW264.7 cells.

As reported previously, NO is an important inflammatory signal molecule in the pathogenesis of inflammation, which reacts with superoxide free radicals to produce peroxynitrite ions, resulting in various inflammatory states (Theofilis et al., 2021). Inducible nitric oxide synthase (iNOS) is a regulator of NO synthesis, and it plays a regulatory role in the production of proinflammatory mediators. In addition, inflammation is directly related to arachidonic acid metabolism (Wang T. et al., 2019), under the action of COX-2, and arachidonic acid is transformed into prostaglandin E2(PGE 2) through several enzymatic reactions. PGE_2 can not only induce the inflammatory cells to release the chemokines and recruit the inflammatory cell movement but also cooperate with lipopolysaccharide to induce the expression of IL-6 and IL-1 in macrophages (Oshima et al., 2011). It can also cooperate with IL-12 to promote the differentiation of naive T cells into helper T cell 1 (Yao et al., 2009). Since COX-2 can quickly respond to a series of proinflammatory mediators and cytokines, it has been considered for a long time to play an important role in the pathological process of inflammation. Moreover, GO analysis of network pharmacology revealed that the target genes of G-Rh4 against inflammation were involved in the "nitric oxide synthase regulator activity" in both biological process (BP) analysis and Molecular Function (MF) analysis. The results in LPS-activated RAW264.7 cells showed that G-Rh4 significantly reduced the release of NO and PGE_2 as well as the expression of elevated iNOS and COX-2, indicating that network pharmacology might be an effective approach to identify the key target and action pathway of G-Rh4 against inflammation.

In addition, KEGG pathway enrichment analysis pointed out that the intersection target genes of G-Rh4 and inflammation were closely related to the NF-κB and JAK-STAT signaling pathways, the including TNF signaling pathway. Nuclear factor-kappa B(NF-κB) is a protein complex responsible for DNA transcription, cytokine secretion, and cell survival (Wu et al., 2016), and its abnormal signaling pathway is associated with some chronic inflammatory diseases such as inflammatory bowel disease, sepsis, arthritis, and atherosclerosis (Theofilis et al., 2021). NF-κB (p50-p65) is constitutively present in the cytoplasm of RAW264.7cells and is sequestered by inhibitory protein IκBα. In the inflammatory state, the activation phosphorylation of p65 (ser536) and p50 (ser337) leads to the activation of NF-κB and the expression of a series of downstream inflammatory factors, such as IL-1β and IL-6. STAT3 (signal transducer and activator of transcription 3) is a key regulator of the inflammatory response induced by lipopolysaccharide (LPS) (Li et al., 2021), and the JAK-STAT (Janus kinase-signal transducer and activator of transcription) pathway is one of the important inflammatory signal transduction pathways, which can mediate the immune response (Zhao et al., 2021). Taken together, this study reveals that G-Rh4 might exert its anti-inflammatory effects through both NF-κB and STAT3 pathways.

Our study clarified, for the first time, the targets and working pathways of G-Rh4 in the inflammation process through network pharmacological analysis and experimental approaches and puts forward that G-Rh4 can directly bind with key pro-inflammatory cytokines including TNF-α, IL-6, and IL-1β to execute its anti-inflammatory activity. The further study is necessary to evaluate the effectiveness of G-Rh4 and explore the extensive working mechanism of *in vivo* inflammation models. This study provides a scientific basis for further pharmacological research on ginsenoside Rh4, as well as the development of novel anti-inflammatory drugs with high efficacy and few side effects and clinical application.

Data availability statement

The datasets presented in this study can be found in online repositories. The names of the repository/repositories and

accession number(s) can be found in the article/Supplementary Material.

Author contributions

Study design: Y-HJ and K-IT; network pharmacology analysis: Z-XZ and K-IT; RAW264.7 cell culture: G-AL and Y-MS; molecular docking: Y-NW; drafting the manuscript: K-IT; revision of the manuscript: YL and K-IT; supervision: Y-HJ; project administration: Y-HJ; funding acquisition: Y-HJ; All authors have read and agreed to the published version of the manuscript.

Funding

This research was supported by the Specific Funding of Development and Reform Commission of Jilin Province (2021FGWCXNLJSSZ01) and Science and Technology Development Program of Jilin Province (YDZJ202101ZYTS087).

Conflict of interest

The authors declare that the research was conducted in the absence of any commercial or financial relationships that could be construed as a potential conflict of interest.

Publisher's note

All claims expressed in this article are solely those of the authors and do not necessarily represent those of their affiliated organizations, or those of the publisher, the editors, and the reviewers. Any product that may be evaluated in this article, or claim that may be made by its manufacturer, is not guaranteed or endorsed by the publisher.

Supplementary material

The Supplementary Material for this article can be found online at: https://www.frontiersin.org/articles/10.3389/fphar.2022.953871/full#supplementary-material

References

Arai, Y., Martin-Ruiz, C. M., Takayama, M., Abe, Y., Takebayashi, T., Koyasu, S., et al. (2015). Inflammation, but not telomere length, predicts successful ageing at extreme old age: A longitudinal study of semi-supercentenarians. *EBioMedicine* 2, 1549–1558. doi:10.1016/j.ebiom.2015.07.029

Davis, A. P., Grondin, C. J., Johnson, R. J., Sciaky, D., Wiegers, J., Wiegers, T. C., et al. (2021). Comparative Toxicogenomics database (CTD): Update 2021. *Nucleic Acids Res.* 49, D1138–D1143. doi:10.1093/nar/gkaa891

Fan, Y., Wang, Y., Yu, S., Chang, J., Yan, Y., Wang, Y., et al. (2021). Natural products provide a new perspective for anti-complement treatment of severe COVID-19: A review. *Chin. Med.* 16, 67. doi:10.1186/s13020-021-00478-3

Furman, D., Campisi, J., Verdin, E., Carrera-Bastos, P., Targ, S., Franceschi, C., et al. (2019). Chronic inflammation in the etiology of disease across the life span. *Nat. Med.* 25, 1822–1832. doi:10.1038/s41591-019-0675-0

GBD 2017 Causes of Death Collaborators (2018). Global, regional, and national age-sex-specific mortality for 282 causes of death in 195 countries and territories, 1980-2017: A systematic analysis for the global burden of disease study 2017. *Lancet* 392, 1736–1788. doi:10.1016/S0140-6736(18)32203-7

Huang, D. W., Sherman, B. T., and Lempicki, R. A. (2009). Systematic and integrative analysis of large gene lists using DAVID bioinformatics resources. *Nat. Protoc.* 4, 44–57. doi:10.1038/nprot.2008.211

Huang, Q., Wang, T., and Wang, H. (2017). Ginsenoside Rb2 enhances the anti-inflammatory effect of ω-3 fatty acid in LPS-stimulated RAW264.7 macrophages by upregulating GPR120 expression. *Acta Pharmacol. Sin.* 38, 192–200. doi:10.1038/aps.2016.135

Joh, E.-H., Lee, I.-A., Jung, I.-H., and Kim, D.-H. (2011). Ginsenoside Rb1 and its metabolite compound K inhibit IRAK-1 activation—the key step of inflammation. *Biochem. Pharmacol.* 82, 278–286. doi:10.1016/j.bcp.2011.05.003

Li, S., Hu, K., Li, L., Shen, Y., Huang, J., Tang, L., et al. (2021). Stattic alleviates acute hepatic damage induced by LPS/ d -galactosamine in mice. *Innate Immun.* 27, 201–209. doi:10.1177/1753425920988330

Liang, Y., Liang, B., Chen, W., Wu, X.-R., Liu-Huo, W.-S., Zhao, L.-Z., et al. (2021). Potential mechanism of dingji fumai decoction against atrial fibrillation based on network pharmacology, molecular docking, and experimental verification integration strategy. *Front. Cardiovasc. Med.* 8, 712398. doi:10.3389/fcvm.2021.712398

Libby, P. (2021). The changing landscape of atherosclerosis. *Nature* 592, 524–533. doi:10.1038/s41586-021-03392-8

Liu, M., Fang, G., Yin, S., Zhao, X., Zhang, C., Li, J., et al. (2019). Caffeic acid prevented LPS-induced injury of primary bovine mammary epithelial cells through inhibiting NF- κ B and MAPK activation. *Mediat. Inflamm.* 2019, 1897820. doi:10.1155/2019/1897820

Luo, Z., Liu, W., Sun, P., Wang, F., and Feng, X. (2021). Pan-cancer analyses reveal regulation and clinical outcome association of the shelterin complex in cancer. *Brief. Bioinform.* 22, bbaa441. doi:10.1093/bib/bbaa441

Morrisette-Thomas, V., Cohen, A. A., Fülöp, T., Riesco, É., Legault, V., Li, Q., et al. (2014). Inflamm-aging does not simply reflect increases in pro-inflammatory markers. *Mech. Ageing Dev.* 139, 49–57. doi:10.1016/j.mad.2014.06.005

Oshima, H., Hioki, K., Popivanova, B. K., Oguma, K., Van Rooijen, N., Ishikawa, T., et al. (2011). Prostaglandin E2 signaling and bacterial infection recruit tumor-promoting macrophages to mouse gastric tumors. *Gastroenterology* 140, 596–607. e7. doi:10.1053/j.gastro.2010.11.007

Panigrahy, D., Gilligan, M. M., Huang, S., Gartung, A., Cortés-Puch, I., Sime, P. J., et al. (2020). Inflammation resolution: A dual-pronged approach to averting cytokine storms in COVID-19? *Cancer Metastasis Rev.* 39, 337–340. doi:10.1007/s10555-020-09889-4

Park, E.-K., Shin, Y.-W., Lee, H.-U., Kim, S.-S., Lee, Y.-C., Lee, B.-Y., et al. (2005). Inhibitory effect of ginsenoside Rb1 and compound K on NO and prostaglandin E2 biosyntheses of RAW264.7 cells induced by lipopolysaccharide. *Biol. Pharm. Bull.* 28, 652–656. doi:10.1248/bpb.28.652

Piñero, J., Ramírez-Anguita, J. M., Saüch-Pitarch, J., Ronzano, F., Centeno, E., Sanz, F., et al. (2019). The DisGeNET knowledge platform for disease genomics: 2019 update. *Nucleic Acids Res.* 48, D845–D855. gkz1021. doi:10.1093/nar/gkz1021

Rahimmanesh, I., and Fatehi, R. (2020). Systems biology approaches toward autosomal dominant polycystic kidney disease (ADPKD). *Clin. Transl. Med.* 9, 1. doi:10.1186/s40169-019-0254-5

Rappaport, N., Twik, M., Plaschkes, I., Nudel, R., Iny Stein, T., Levitt, J., et al. (2017). MalaCards: An amalgamated human disease compendium with diverse clinical and genetic annotation and structured search. *Nucleic Acids Res.* 45, D877–D887. doi:10.1093/nar/gkw1012

Schmeltzer, P. A., Kosinski, A. S., Kleiner, D. E., Hoofnagle, J. H., Stolz, A., Fontana, R. J., et al. (2016). Liver injury from nonsteroidal anti-inflammatory drugs in the United States. *Liver Int.* 36, 603–609. doi:10.1111/liv.13032

Sun, J. H., Sun, F., Yan, B., Li, J. Y., and Xin, D. L. (2020). Data mining and systematic pharmacology to reveal the mechanisms of traditional Chinese medicine

in Mycoplasma pneumoniae pneumonia treatment. *Biomed. Pharmacother.* 125, 109900. doi:10.1016/j.biopha.2020.109900

Szklarczyk, D., Gable, A. L., Nastou, K. C., Lyon, D., Kirsch, R., Pyysalo, S., et al. (2021). The STRING database in 2021: Customizable protein–protein networks, and functional characterization of user-uploaded gene/measurement sets. *Nucleic Acids Res.* 49, D605–D612. doi:10.1093/nar/gkaa1074

Theofilis, P., Sagris, M., Oikonomou, E., Antonopoulos, A. S., Siasos, G., Tsioufis, C., et al. (2021). Inflammatory mechanisms contributing to endothelial dysfunction. *Biomedicines* 9, 781. doi:10.3390/biomedicines9070781

Wang, C., Pang, X., Zhu, T., Ma, S., Liang, Y., Zhang, Y., et al. (2022). Rapid discovery of potential ADR compounds from injection of total saponins from Panax notoginseng using data-independent acquisition untargeted metabolomics. *Anal. Bioanal. Chem.* 414, 1081–1093. doi:10.1007/s00216-021-03734-5

Wang T, T., Fu, X., Chen, Q., Patra, J. K., Wang, D., Wang, Z., et al. (2019). Arachidonic acid metabolism and kidney inflammation. *Int. J. Mol. Sci.* 20, 3683. doi:10.3390/ijms20153683

Wang, Y., Yang, H., Chen, L., Jafari, M., and Tang, J. (2021). Network-based modeling of herb combinations in traditional Chinese medicine. *Brief. Bioinform.* 22, bbab106. doi:10.1093/bib/bbab106

Wang Y, Y., Zhang, S., Li, F., Zhou, Y., Zhang, Y., Wang, Z., et al. (2019). Therapeutic target database 2020: Enriched resource for facilitating research and early development of targeted therapeutics. *Nucleic Acids Res.* 48, D1031–D1041. gkz981. doi:10.1093/nar/gkz981

Wu, J., Yang, H., Zhao, Q., Zhang, X., and Lou, Y. (2016). Ginsenoside Rg1 exerts a protective effect against Aβ25–35-induced toxicity in primary cultured rat cortical neurons through the NF-κB/NO pathway. *Int. J. Mol. Med.* 37, 781–788. doi:10.3892/ijmm.2016.2485

Yao, C., Sakata, D., Esaki, Y., Li, Y., Matsuoka, T., Kuroiwa, K., et al. (2009). Prostaglandin E2–EP4 signaling promotes immune inflammation through TH1 cell differentiation and TH17 cell expansion. *Nat. Med.* 15, 633–640. doi:10.1038/nm.1968

Zhao, H., Wu, L., Yan, G., Chen, Y., Zhou, M., Wu, Y., et al. (2021). Inflammation and tumor progression: Signaling pathways and targeted intervention. *Signal Transduct. Target. Ther.* 6, 263. doi:10.1038/s41392-021-00658-5

frontiers | Frontiers in Pharmacology

TYPE Original Research
PUBLISHED 27 September 2022
DOI 10.3389/fphar.2022.991597

OPEN ACCESS

EDITED BY
Yunyao Jiang,
Tsinghua University, China

REVIEWED BY
Damao Wang,
Southwest University, China
Arpita Roy,
Sharda University, India
Trần Quang Đôn,
Chungnam National University, South Korea

*CORRESPONDENCE
Zili Lei,
3182683090@qq.com,
Jiao Guo,
gyguoyz@163.com

†These authors have contributed equally to this work

SPECIALTY SECTION
This article was submitted to Experimental Pharmacology and Drug Discovery, a section of the journal Frontiers in Pharmacology

RECEIVED 11 July 2022
ACCEPTED 07 September 2022
PUBLISHED 27 September 2022

CITATION
Lei Z, Chen L, Hu Q, Yang Y, Tong F, Li K, Lin T, Nie Y, Rong H, Yu S, Song Q and Guo J (2022), Ginsenoside Rb1 improves intestinal aging via regulating the expression of sirtuins in the intestinal epithelium and modulating the gut microbiota of mice. *Front. Pharmacol.* 13:991597. doi: 10.3389/fphar.2022.991597

Ginsenoside Rb1 improves intestinal aging *via* regulating the expression of sirtuins in the intestinal epithelium and modulating the gut microbiota of mice

Zili Lei[1*†], Lei Chen[1†], Qing Hu[1†], Yanhong Yang[2†], Fengxue Tong[1], Keying Li[1], Ting Lin[1], Ya Nie[1,3], Hedong Rong[1,3], Siping Yu[1,3], Qi Song[1] and Jiao Guo[1*]

[1]Guangdong Metabolic Diseases Research Center of Integrated Chinese and Western Medicine, Guangdong Pharmaceutical University, Guangzhou, China, [2]The First Affiliated Hospital (School of Clinical Medicine), Guangdong Pharmaceutical University, Guangzhou, China, [3]School of Traditional Chinese Medicine, Guangdong Pharmaceutical University, Guangzhou Higher Education Mega Center, Guangzhou, China

Intestinal aging seriously affects the absorption of nutrients of the aged people. Ginsenoside Rb1 (GRb1) which has multiple functions on treating gastrointestinal disorders is one of the important ingredients from Ginseng, the famous herb in tradition Chinese medicine. However, it is still unclear if GRb1 could improve intestinal aging. To investigate the function and mechanism of GRb1 on improving intestinal aging, GRb1 was administrated to 104-week-old C57BL/6 mice for 6 weeks. The jejunum, colon and feces were collected for morphology, histology, gene expression and gut microbiota tests using H&E staining, X-gal staining, qPCR, Western blot, immunofluorescence staining, and 16S rDNA sequencing technologies. The numbers of cells reduced and the accumulation of senescent cells increased in the intestinal crypts of old mice, and administration of GRb1 could reverse them. The protein levels of CLDN 2, 3, 7, and 15 were all decreased in the jejunum of old mice, and administration of GRb1 could significantly increase them. The expression levels of *Tert*, *Lgr5*, *mKi67*, and *c-Myc* were all significantly reduced in the small intestines of old mice, and GRb1 significantly increased them at transcriptional or posttranscriptional levels. The protein levels of SIRT1, SIRT3,

Abbreviations: ANOSIM, Analysis of similarity; Ascl2, achaete-scute family bHLH transcription factor 2; CLDN, Claudin; CMC-Na, CarboxyMethylCellulose-Na; EpCAM, epithelial cell adhesion molecule; ER, endoplasmic reticulum; H&E, hematoxylin and eosin; HRP, horseradish peroxidase; GRb1, Ginsenoside Rb1; KEGG, Kyoto Encyclopedia of Genes and Genomes; Lgr5, leucine rich repeat containing G protein-coupled receptor 5; mKi67, antigen identified by monoclonal antibody Ki 67; Myc, MYC proto-oncogene, bHLH transcription factor; OCT, optimal cutting temperature compound; Olfm4, olfactomedin 4; PCoA, principle coordinates analysis; qRT-PCR, quantitative real-time PCR; Rnf43, ring finger protein 43; RSV, resveratrol; Sirt, sirtuin; Sp5, Sp5 transcription factor; SPF, specific pathogen-free; Tert, telomerase reverse transcriptase; TGGR, total ginsenosides; TJ, tight junction; X-gal, beta-galactosidase.

and SIRT6 were all reduced in the jejunum of old mice, and GRb1 could increase the protein levels of them. The 16S rDNA sequencing results demonstrated the dysbiosis of the gut microbiota of old mice, and GRb1 changed the composition and functions of the gut microbiota in the old mice. In conclusion, GRb1 could improve the intestinal aging *via* regulating the expression of Sirtuins family and modulating the gut microbiota in the aged mice.

KEYWORDS

Ginsenoside Rb1, gut microbiota, intestinal aging, sirtuin, intestinal integrity

Introduction

The growing of aging societies is one of the major challenges for today's medical science (Friedrich, 2019). The nutrients absorption ability of the intestines becomes impaired with age (Pénzes, 1984) and causes the vulnerability to disease and the physical weakness of the elderly peoples (Ben Othman et al., 2020). It was also found that the morphology of jejunum changed in old rats (Hassan et al., 2017). Therefore, it would be meaningful to develop drugs for improving intestinal aging.

Ginsenoside Rb1 (GRb1) is the important ingredient from *Panax ginseng* Meyer which is the famous herb in traditional Chinese medicine (Lin et al., 2022). The *Panax ginseng* has been widely used to treat many kinds of disease. Recent study showed that the doxorubicin-induced early cancer therapeutics-related cardiac dysfunction and early decline in left ventricular ejection fraction in breast cancer patients can be protected through prophylactic Panax ginseng supplementation (Hamidian et al., 2022). The lifespan of *Drosophila* is extended with the treatment of total ginsenosides (TGGR), the main active components in Panax ginseng (Zhao et al., 2022b). Many types of ginsenosides have been demonstrated to have neuroprotective effects (Zhao et al., 2022a). There are around 200 ginsenosides have been detected from ginseng and GRb1 is one type of major ginsenosides (Zhao et al., 2022a; Hyun et al., 2022).

GRb1 has been reported to have multiple functions in various diseases. It can be used to treat obesity, hyperglycemia and diabetes through multi-targets (Zhou et al., 2019; Xiong et al., 2010). GRb1 also can ameliorate diabetic kidney podocyte injury *via* inhibiting the activity of aldose reductase (He et al., 2022). It was also found that GRb1 can reduce the myocardial ischemia/reperfusion injury *via* inhibiting cardiomyocyte autophagy through the PI3K/AKT/mTOR pathway (Qin et al., 2021). GRb1 also has anti-aging effect (Cheng et al., 2005), but the related mechanism is unclear. GRb1 can be used to treat many kinds of gastrointestinal disorders. It improves colitis in mice *via* alleviating endoplasmic reticulum (ER) stress through activating Hrd1 signaling pathway (Dong et al., 2021). GRb1 also can reduce ischemia/reperfusion-induced intestinal injury *via* activating PI3K/AKT/Nrf2 pathway (Chen et al., 2019). It was also found that GRb1 can promote the intestinal epithelial would healing of rats *via* activating ERK and Rho signaling (Toyokawa et al., 2019). GRb1 can protect the peritoneal air exposure caused intestinal mucosa damage in rats (Zhou et al., 2016). However, it is still unclear if GRb1can improve intestinal aging.

There are many genes have been reported to be related to the aging of intestines and other tissues. Stem cell exhaustion is one of the hallmarks of aging (López-Otín et al., 2013). Lgr5 is the mark gene of intestinal stem cells (Lei et al., 2012; Baghdadi et al., 2022). Telomerase plays important role in the intestinal stem cells and TERT is the important telomerase subunit (Hoffmeyer et al., 2012). Sirtuins, including Sirt1-7 in mammals, have been demonstrated to play important roles in maintaining the longevity of various tissues (Gámez-García and Vazquez, 2021; Yang et al., 2021a; Watroba and Szukiewicz, 2021). Hence, it would be very meaningful to explore if GRb1 could regulate the expression of these genes in the intestines of aging mice.

Many studies have demonstrated the changes of the composition and functions of gut microbiota with aging (Ishaq et al., 2021; Niu et al., 2021; Ruiz-Gonzalez et al., 2022). It was reported that specific bacterial community pattern and signature taxa are related to longevity of people (Ren et al., 2021). The dysbiosis of gut microbiota is also associated with age-related disorders (Sharma, 2022). Relationships between gut microbiota and age-related macular degeneration have been found (Lima-Fontes et al., 2021). Gut microbiota-derived pro-inflammatory neurotoxins have been detected in brain cells and tissues of aged people with Alzheimer's disease (Lukiw et al., 2021; Zhao et al., 2021). Gut microbiota dysbiosis has also been found to promote the age-related atrial fibrillation *via* activating NLRP3-inflammasome (Zhang et al., 2021). GRb1 can improve glucose and lipid metabolic disorders through regulating gut microbiota of high fat diet induced obesity mice (Yang et al., 2021b; Bai et al., 2021). GRb1 also can be converted into compound K by the gut microbiota to prevent inflammatory-associated colorectal cancer (Yao et al., 2018). However, it still needs to explore whether GRb1 could improve intestinal aging *via* modulating gut microbiota.

In the present study, we reported the function and mechanisms of GRb1 on improving the intestinal aging of old mice. Our work encouraged the exploration of drugs for prevention and treatment of age-related diseases.

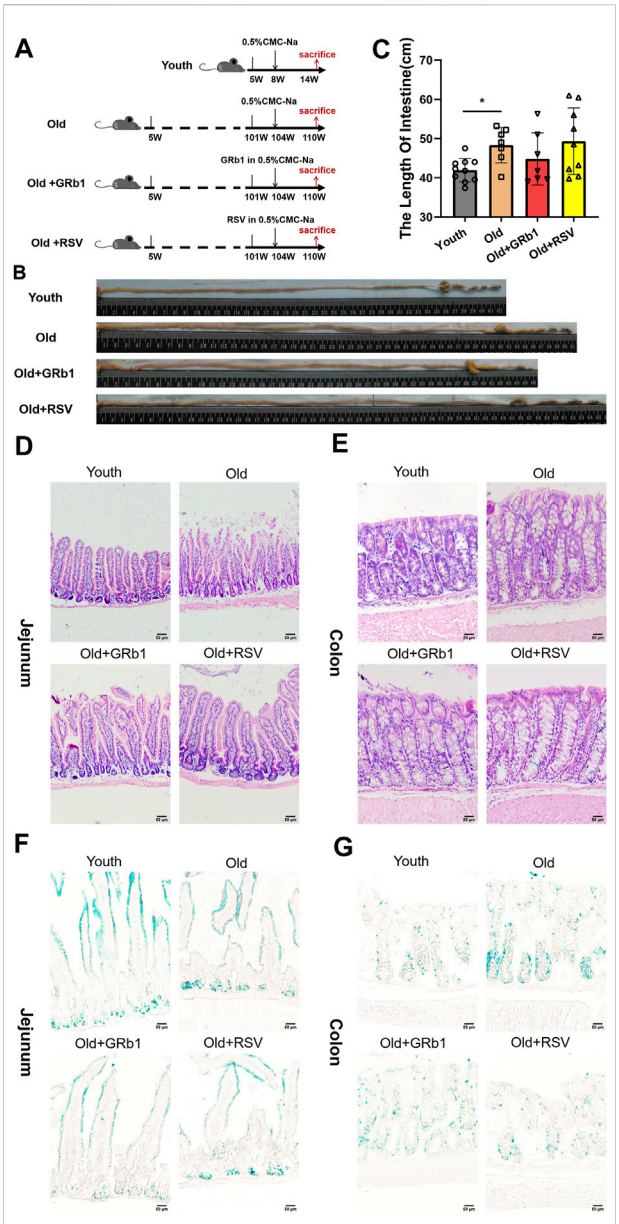

FIGURE 1
GRb1 showed the potential of improving intestinal aging of old mice. **(A)** The scheme of the experimental design. **(B)** Representative images of the intestines of mice from Youth, Old, Old + GRb1 and Old + RSV groups. **(C)** The length of intestines from each group. **(D,E)** Representative images of **(D)** jejunal and **(E)** colonal sections of H&E staining. **(F,G)** Representative images of **(F)** jejunal and **(E)** colonal sections of beta-galactosidase staining. *$p < 0.05$ compared with the Youth group. Scale bar, 50 μm. W, weeks of age; GRb1, Ginsenoside Rb1; RSV, Resveratrol.

Materials and methods

Mice

All animal experimental procedures were approved by the Experimental Animal Ethics Committee of Guangdong Pharmaceutical University. Female C57BL/6 mice (5-week-old) purchased from Hunan Lex Jingda Laboratory Animal Co., Ltd. (Changsha, Hunan Province, China), were housed in the specific pathogen-free (SPF) animal facility, at 25°C, 60%–65% humidity, 12 h light-dark cycle, with free access to water and food. At the age of 104-week-old, the mice were randomly divided into three groups, 10 mice in each group. The Old + GRb1 group was administrated with GRb1 (50mg/kg; Meilunbio, Dalian, China; MB6856-1) intragastrically once a day. The GRb1 was diluted in 0.5% CarboxyMethylCellulose-Na (CMC-Na) (Tianjin Zhiyuan Chemical Reagent Co., Ltd., Tianjin, China). The Old group was administrated with the corresponding volume of 0.5% CMC-Na intragastrically once a day. Resveratrol (RSV; Meilunbio, Dalian, China; MB5267-1) was used as the positive drug. The Old + RSV group was intragastrically administrated with RSV (50 mg/kg) diluted in 0.5% CMC-Na once a day. The 8-week-old mice in Youth group was used as control, and they were also administrated with the corresponding volume of 0.5% CMC-Na intragastrically once a day. After 6 weeks of administration, the intestines were collected (Figure 1A).

H&E staining and X-gal staining

The H&E staining was performed as previously (Lei et al., 2021b). Briefly, intestinal tissues were fixed in 4% paraformaldehyde at 4°C for overnight, then dehydrated, embedded in paraffin and sectioned. 4-μm-thick sections were stained with hematoxylin (H9627, Sigma-Aldrich) for 3 min, and then followed with eosin (E4009, Sigma-Aldrich) for 20 s at room temperature.

For X-gal staining, intestinal tissues were embedded in optimal cutting temperature compound (OCT) (Sakura Finetek) and sectioned. 7-μm-thick frozen sections were stained according to the manufacturer's protocols for Senescence Detection Kit (Abcam, ab65351).

Images for H&E staining and X-gal staining were got using the Olympus DP74 microscope.

Immunofluorescence staining

The immunofluorescence staining was performed as previously (Lei et al., 2021b). The intestinal tissues were fixed in 4% paraformaldehyde at 4°C for overnight, then dehydrated, embedded in OCT compound and sectioned. 7-μm-thick frozen sections were first boiled in 10 mM citric acid (Merck) at pH 6.0 for 5 min, then exposed in goat serum blocking buffer (ZSGB-BIO, ZLI- 9056) to block nonspecific sites for 1h at room temperature, following incubated with primary antibodies in blocking buffer at 4° C for overnight, and then with secondary antibodies for 1h at room temperature. The primary and

secondary antibodies were listed in Supplementary Table 1. Images were got by using Olympus confocal microscope.

qRT-PCR

Total RNA was extracted from each jejunal and colonal tissue using Trizol reagent (T9108, Takara Bio, Inc.), then subjected to reverse transcription *via* the PrimeScript™ RT Reagent kit (RR047A, Takara Bio, Inc.) at 37°C for 15 min and then 85°C for 5 s. The qPCR was conducted through the SYBR Premix Ex Taq kit (RR820A, Takara Bio, Inc.) *via* the LightCycler 480II System (Roche, Inc.). The processes of cycling were: 95°C for 30 s; followed 40 cycles of 95°C for 5 s, then 60°C for 20 s and 65°C for 15 s. Mouse GAPDH was used as the internal reference. All primers were listed in Supplementary Table 2.

Western blot

Jejunal and colonal tissues of mice were lysed using the Radio-Immunoprecipitation Assay lysis buffer (MA0151, Dalian Meilun Biotechnology co., Ltd., Dalian, China), centrifuged at 13,680 x g, 4°C, for 30 min, then the supernatant was collected. Protein concentration was measured by the BCA kit (P0011, Beyotime, Shanghai, China). Equal amounts of protein (40 μg) were separated through the SDS-PAGE, subsequently transferred to a PVDF membrane. The PVDF membrane was blocked using the 5% skimmed milk (0040895, Biosharp, Hefei, China) in TBST buffer at room temperature for 1 h, incubated with primary antibodies in 4°C for overnight, and then incubated with HRP (horseradish peroxidase)-labeled secondary antibodies, the signals were detected *via* the enhanced chemiluminescence reagent. The primary and secondary antibodies were listed in Supplementary Table 3. The quantification of western blot bands was analyzed using the Lane 1d software (version 5.1.0.0; SageCreation).

The 16S rRNA gene analysis

Fecal samples were quickly collected and frozen in the liquid nitrogen and stored at −80°C. The extraction of fecal bacterial DNA, PCR amplification of 16S rRNA genes, sequencing, and analysis were performed by the Gene *Denovo* Biotechnology Company (Guangzhou, China). The experimental procedures were performed as previously (Lei et al., 2021a).

Statistical analysis

Statistical differences were determined *via* the SPSS software (version 25.0; IBM Corp.). Mean ± SE was used to express data. One-way ANOVA was performed between two groups. p-value<0.05 was considered to be significant.

Results

GRb1 improved the aging state of intestines of old mice

After 6 weeks of the administration of GRb1 or RSV, 7 (70%) mice survived in each of Old and Old + GRb1 groups, 9 (90%) mice survived in Old + RSV group, and all the mice survived in the Youth group. The intestines of old mice were significantly longer than the Youth group, and they are shorter but not significant in mice of the Old + GRb1 group compared to the Old group (Figures 1B,C). The numbers of cells in crypts of jejunum from old mice decreased compared to the Youth group, and it was increased after administration of GRb1 or RSV (Figure 1D). The numbers of cells in crypts of the colon of old mice were also lower than that of yang mice, and the administration of GRb1 or RSV could also improve it (Figure 1E).

The increase of cellular senescence is another hallmark of aging (López-Otín et al., 2013). Therefore, senescence-associated beta-galactosidase (X-gal) staining was next performed. The accumulation of senescent cells increased in crypts of jejunum from the Old group compared to young mice, and GRb1 or RSV could reduce them (Figure 1F; Supplementary Figure 1A). The senescence-associated signal was stronger in the colon of old mice than the Youth group, and it became weak and reduced after administration of GRb1 or RSV (Figure 1G; Supplementary Figure 1B). The intestinal stem and progenitor cells are localized in the crypts of the intestines. So, the increase of the numbers of the X-gal stained cells in the crypts of the intestines indicated the aging of the intestinal stem and progenitor cells of the old mice. Hence, the administration of GRb1 or RSV could improve the aging of the intestinal stem and progenitor cells of these mice. These results demonstrated that GRb1 could improve the aging state of intestines from old mice.

GRb1 improved the intestinal integrity of old mice

The increase of the permeability of the intestinal barrier has been reported in both aged human and animals (Tran and Greenwood-Van Meerveld, 2013; Parrish, 2017; Li et al., 2021), indicating the impaired intestinal integrity with aging. Hence, the protein levels of CLDN 1, 2, 3, 7, and 15 which are abundant components of tight junctions (TJs) in the intestinal epithelium (Lei et al., 2012; Lei et al., 2020) were first checked. CLDN 3, 7, and 15 were all significantly reduced in the jejunum of Old group compared to young mice, and the administration of

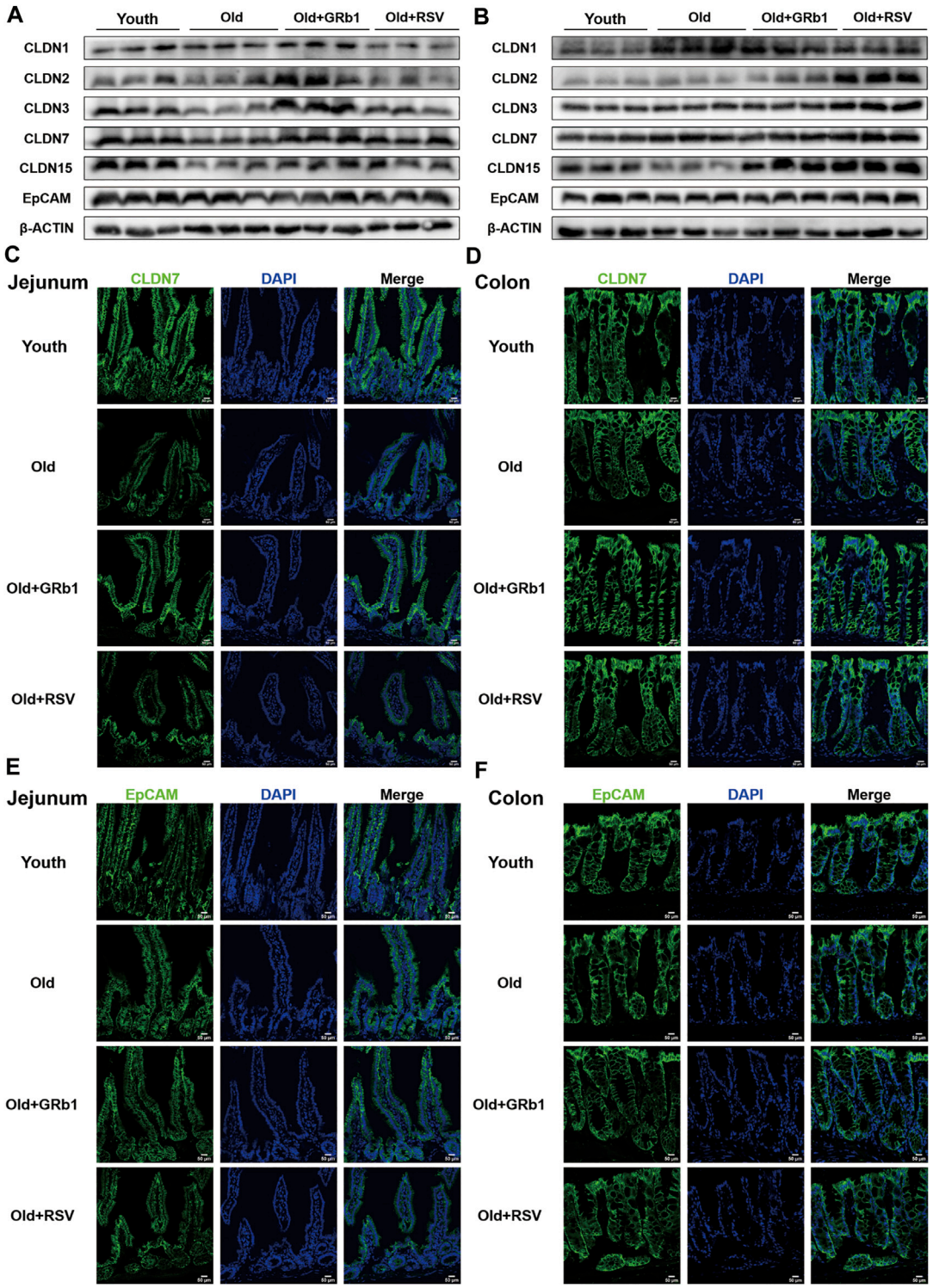

FIGURE 2
GRb1 improved the expression and localization of junctional proteins in the intestines of old mice. **(A,B)** Images of Western blot bands of CLDN 1, 2, 3, 7,15, and EpCAM in the **(A)** jejunum and **(B)** colon. **(C,D)** Representative images of immunofluorescence staining with antibodies to CLDN 7 of frozen sections of **(C)** jejunum and **(D)** colon. **(E,F)** Representative images of immunofluorescence staining with antibodies to EpCAM of frozen sections of **(E)** jejunum and **(F)** colon. Scale bar, 50 μm.

GRb1 increased the expression of them (Figure 2A; Supplementary Figures 2C–E). CLDN 2 was also reduced in the jejunum of old mice, and it was also increased after GRb1 administration, although these changes were not significant (Figure 2A; Supplementary Figure 2B). RSV also could improve the expression of CLDN 3, 7, and 15, but the level of CLDN 2 had no significant change in the Old + RSV group (Figure 2A; Supplementary Figures 2B–E). Immunofluorescence staining results showed that the localization of CLDN 7 was still normal in the jejunum from Old group, but the expression level of it was significantly lower in Old group than the Youth, Old + GRb1 and Old + RSV groups (Figure 2C). The protein level of CLDN 1 had no significant difference in the jejunum of mice among the Youth, Old, Old + GRb1 and Old + RSV groups (Figure 2A; Supplementary Figure 2A). The protein level of EpCAM which is essential to maintain the functional tight junctions in the intestinal epithelium *via* recruiting proteins of Claudins (Lei et al., 2012; Wu et al., 2013) was significantly lower in the jejunum of Old group than the Youth group, and administration of GRb1 could not improve it (Figure 2A; Supplementary Figure 2F). The administration of RSV could significantly increase the protein level of EpCAM in the jejunum of old mice (Figure 2A; Supplementary Figure 2F). However, the localization of EpCAM had no significant difference in the jejunum of mice among the four groups (Figure 2E).

CLDN 15 was also lower in the colon of Old group than the Youth group, although the decrease was not significant (Figure 2B; Supplementary Figure 3E). The administration of GRb1 or RSV could significantly increase the protein level of CLDN 15 in the colon of old mice (Figure 2B; Supplementary Figure 3E). CLDN 1 and 2 were all increased in the colon of Old group compared to the Youth group, and CLDN 2 was significantly increased in the Old + GRb1 and Old + RSV groups (Figure 2B; Supplementary Figures 3A,B). CLDN 3 and 7 were all significantly increased in the colon of old mice compared to the Youth group, and RSV could also increase them in the colon of old mice but not significantly (Figure 2B; Supplementary Figures 3C, D). The immunofluorescence staining results confirmed that the localization of CLDN 7 had no significant difference in the colon among the four groups (Figure 2D). The expression and localization of EpCAM had no significant difference in the colon among the Youth, Old, Old + GRb1 and Old + RSV groups (Figures 2B,F; Supplementary Figure 3F). These results demonstrated that GRb1 could improve the integrity of intestinal epithelium of old mice.

GRb1 improved the function of intestinal stem and progenitor cells of old mice

Tert was significantly reduced in the jejunum of old mice at both mRNA and protein levels compared to the Youth group (Figures 3A,B; Supplementary Figure 4A). The administration of GRb1 or RSV could not change the transcription of Tert in the jejunum of old mice (Figure 3A). However, both GRb1 and RSV could evidently increase the reduced TERT protein in the jejunum of old mice (Figure 3B; Supplementary Figure 4A). The protein level of TERT was also significantly lower in the colon of Old group than the Youth group, but GRb1 and RSV could not improve it (Figure 3C; Supplementary Figure 4B). The transcriptional level of *Lgr5* was significantly reduced in the jejunum of old mice compared to the young mice, and it was increased in the Old + GRb1 group although the increase was not significant ($p = 0.061$) (Figure 3A). RSV could not increase the mRNA level of *Lgr5* in the jejunum of old mice (Figure 3A). The transcriptional levels of other intestinal stem cell related genes, including *Olfm4*, *Ascl2, Rnf43*, and *Sp5*, showed no significant difference in the jejunum from Old and Youth groups (Figure 3A). However, RSV could increase *Ascl2* and *Sp5* in the jejunum of old mice (Figure 3A).

The proliferative ability of intestinal stem and progenitor cells was checked *via* testing the expression of mKi67 in the intestines of mice. Compared to the young mice, the mRNA level of *mKi67* was significantly reduced in the jejunum of the Old group, but GRb1 or RSV could not improve it (Figure 3A). The protein level of Ki67 was also significantly decreased in the jejunum of the Old group compared to the Youth group, and GRb1 could evidently increase it (Figure 3D; Supplementary Figure 4C). GRb1 increased the numbers of Ki67 positive cells in crypts of jejunum of the old mice (Supplementary Figure 5A). The administration of GRb1 also increased the reduced Ki67 protein in the colon of old mice, although the increase was not significant ($p = 0.06$) (Figure 3E; Supplementary Figures 4E, 5B). The protein level of c-Myc which is responsible for the transcription of pro-proliferative genes (Ruan et al., 2021) was significantly reduced in the jejunum of old mice, and GRb1 could significantly improve it (Figure 3D; Supplementary Figure 4D). The protein level of c-Myc was evidently higher in the colon of old mice than the Youth group, and it was decreased in the colon of Old + GRb1 and Old + RSV groups but not significantly (Figure 3E; Supplementary Figure 4F). These results indicated that GRb1 could improve the function of intestinal stem and progenitor cells.

GRb1 regulated the expression of sirtuins in the intestines of old mice

The mRNA levels of *Sirt4* and *Sirt6* were all significantly decreased in the jejunum of old mice compared to the Youth group, and GRb1 or RSV could significantly increase the transcription of *Sirt6* but not *Sirt4* in old mice (Figure 4A). There was no significant difference of the transcriptional levels of *Sirt1*, *Sirt2*, *Sirt3*, *Sirt5*, and *Sirt7* between young and old mice (Figure 4A). However, the mRNA levels of *Sirt2* and *Sirt7* were all

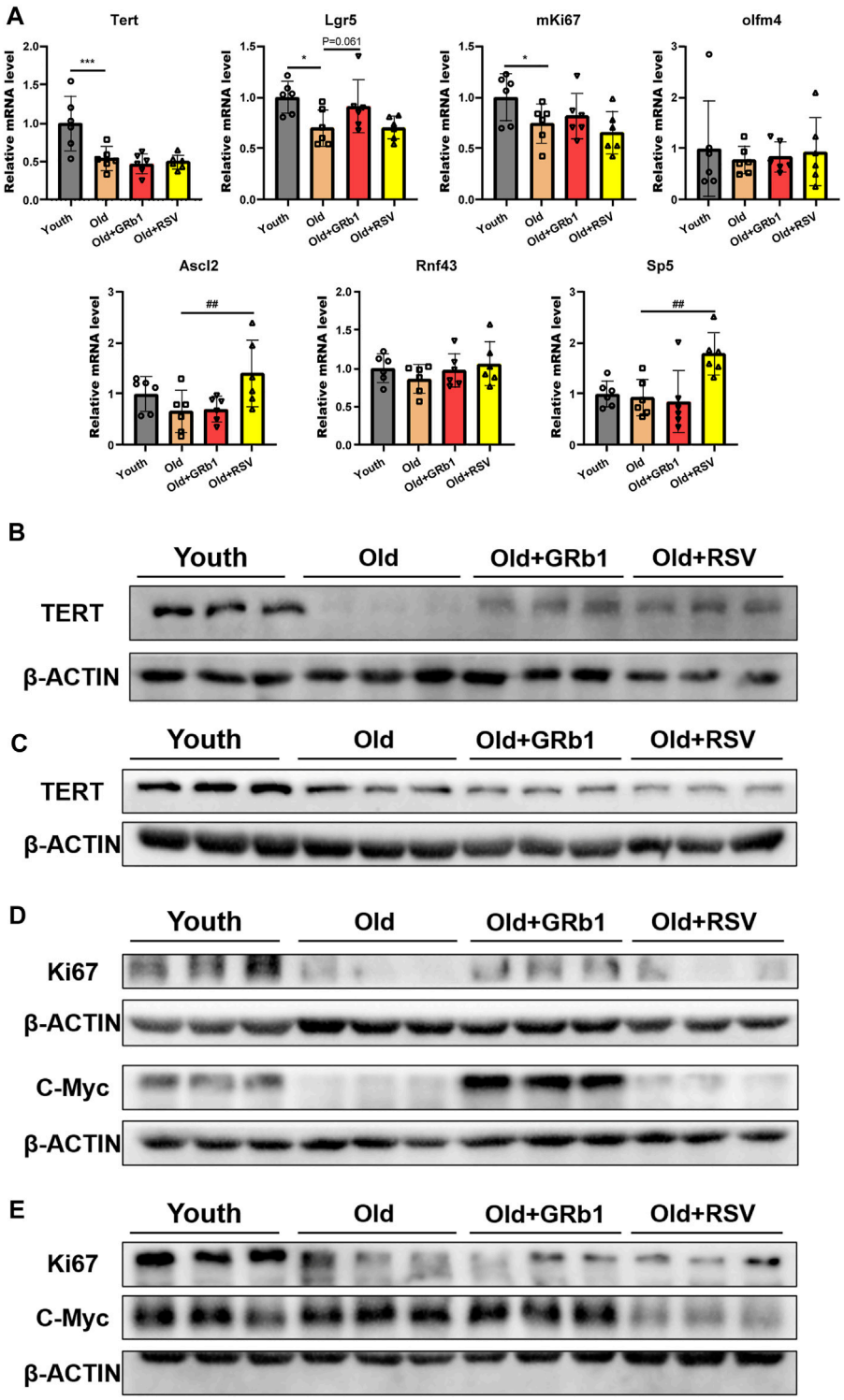

FIGURE 3
GRb1 was effective to improve the function of intestinal stem cells of old mice. **(A)** Relative mRNA expression levels of *Tert*, *Lgr5*, *mKi67*, *Olfm4*, *Ascl2*, *Rnf43*, and *Sp5* in the small intestines. **(B,C)** Images of western blot bands of TERT in the **(B)** jejunum and **(C)** colon. **(D,E)** Western blot results of Ki67 and c-Myc from the **(D)** jejunum and **(E)** colon. $^{*}p < 0.05$, $^{***}p < 0.001$, compared with the Youth group; $^{\#\#}p < 0.01$, compared with the Old group.

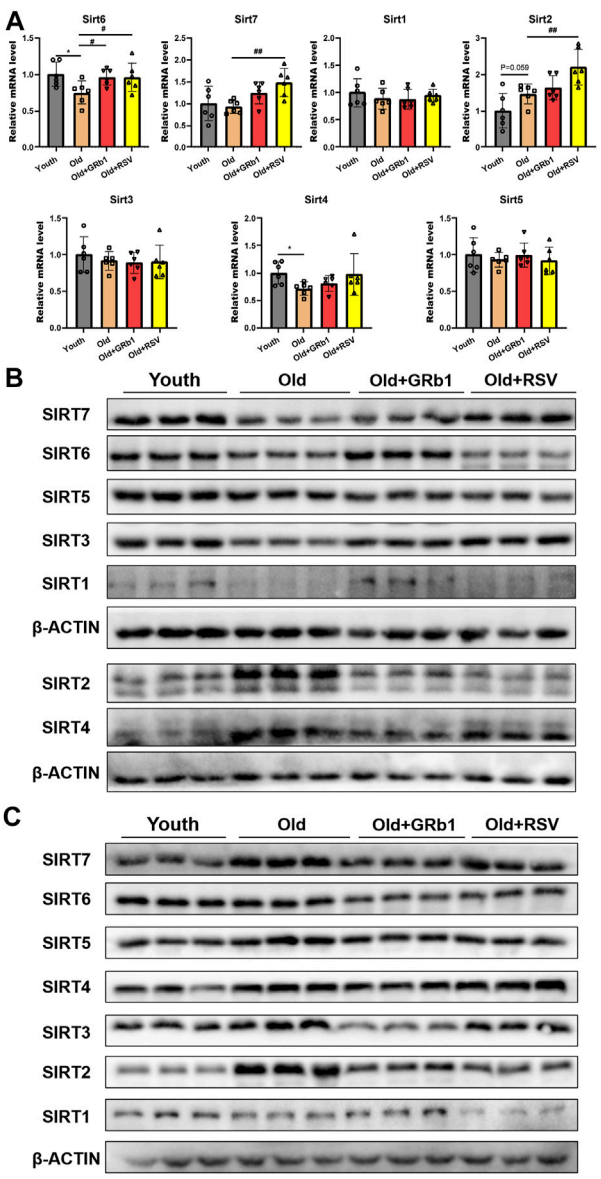

FIGURE 4
GRb1 improved the expression of Sirtuins in the intestines of old mice. **(A)** Relative mRNA expression levels of *Sirt 1-7* in the jejunum. **(B,C)** Images of Western blot bands of SIRT 1-7 in the (C) jejunum and (D) colon. $^{*}p < 0.05$, compared with the Youth group; $^{\#}p < 0.05$, $^{\#\#}p < 0.01$, compared with the Old group.

significantly increased in the jejunum of Old + RSV group compared to the Old group (Figure 4A). The protein levels of SIRT1, SIRT3, SIRT5, and SIRT6 were all lower in the jejunum of old mice than the Youth group, and GRb1 could rescue SIRT1 and SIRT6 in the jejunum of old mice (Figure 4B; Supplementary Figures 6A,C,E,F). The administration of GRb1 or RSV could also increase the expression of SIRT3 and SIRT7 in the jejunum of old mice, but the increase was not significant (Figure 4B; Supplementary Figures 6C,G). SIRT2 and SIRT4 were significantly increased in the jejunum of Old mice, but the protein level of SIRT4 was significantly reduced after administration of GRb1 or RSV (Figure 4B; Supplementary Figures 6B,D). However, the administration of GRb1 or RSV could not reduce the protein level of SIRT2 in the jejunum of old mice (Figure 4B; Supplementary Figure 6B).

The protein levels of SIRT1 and SIRT7 showed no significant difference among the Youth, Old, Old + GRb1 and Old + RSV groups (Figure 4C; Supplementary Figures 7A,G). The protein levels of SIRT2, SIRT3, SIRT4, SIRT5, and SIRT6 were all significantly increased in the colon of old mice compared to the Youth group, and administration of GRb1 or RSV could reduce SIRT2 in the colon of old mice (Figure 4C; Supplementary Figures 7B–F). These results indicated that GRb1 might improve the aging of intestines *via* regulating the expression sirtuins at both transcriptional and post-transcriptional levels.

GRb1 changed the composition and function of gut microbiota of old mice

The 16S rRNA gene sequence was performed to analyze the composition and functions of the gut microbiota in mice (https://www.ncbi.nlm.nih.gov/sra/PRJNA856886). The Shannon rarefaction curves for every group had reached the saturated platform (Figure 5A), and the principle coordinates analysis (PCoA) showed that the Youth and the Old groups could be clearly distinguished (Figure 5B). Analysis of similarity (ANOSIM) showed that the rank of the Old group was lower than the Youth group, and the rank of the Old + GRb1 and Old + RSV groups was higher than the Old group (Figure 5C). At the phylum level, the abundance of *Firmicutes* and *Tenericutes* was significantly increased in the Old group compared to the Youth group, and the abundance of *Firmicutes* was significantly reduced after administration of GRb1 (Figures 5D,E). The abundance of *Bacteroidetes* and *Verrucomicrobia* was significantly reduced in the Old group compared to the Youth group (Figures 5D,E). The abundance of *Proteobacteria* was significantly increased in the Old + GRb1 group compared to the Old group (Figures 5D,E).

LEFse analysis showed there were 79 bacterial taxa differed in abundance between the Youth and Old groups, with 32 predominant for the Youth group and 47 predominant for the Old group (Supplementary Figures 8A,B). There were 57 bacterial taxa differed in abundance between the Old + GRb1 group and the Old group, with 21 predominant for the Old + GRb1 group and 36 predominant for the Old group (Supplementary Figures 8A,B). There were 24 bacterial taxa differed in abundance between the Old + RSV group and the Old group, with 12 predominant for the Old + RSV group and 12 predominant for the Old group (Supplementary Figures 10A,B). Compared to the Old group, there were three bacterial taxa predominant in all the three groups of the Youth, Old +

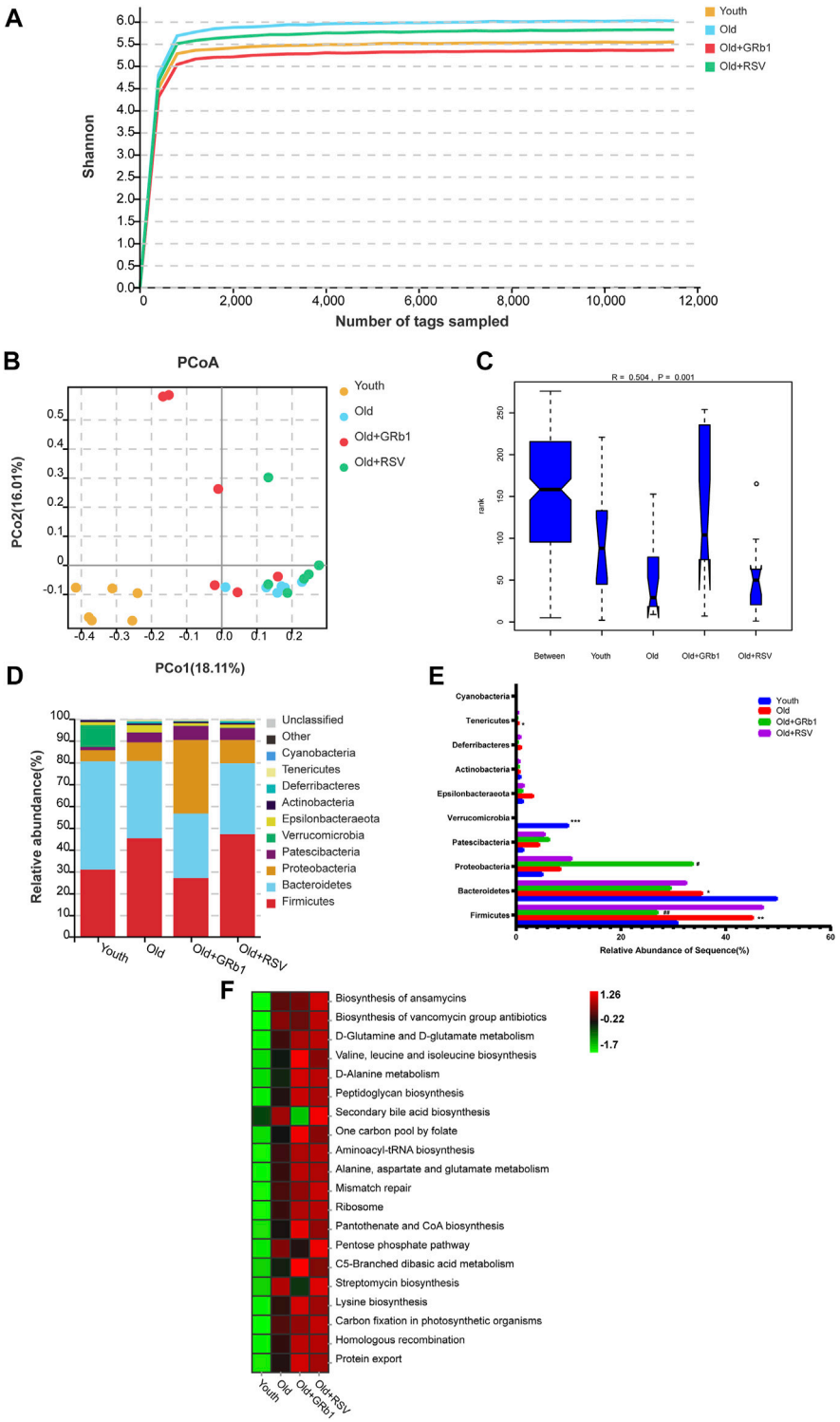

FIGURE 5
GRb1 changed the relative abundance and functions of gut microbiota of old mice. **(A)** Shannon rarefaction curves for each group. **(B)** The PCo analysis of the gut microbiota. **(C)** Analysis of similarity (ANOSIM) of the gut microbiota. **(D)** Relative abundance of the gut microbiota at phylum levels in mice. Different colors illustrated different flora. **(E)** Bar chart of proportional abundance of the gut microbiota at phylum levels in mice. **(F)** KEGG analysis showed the top 20 altered pathways of the gut microbiota. $^{*}p < 0.05$, $^{**}p < 0.01$, $^{***}p < 0.001$, compared with the Youth group; $^{\#}p < 0.05$, $^{\#\#}p < 0.01$, compared with the Old group. PCo, Principle coordinates.

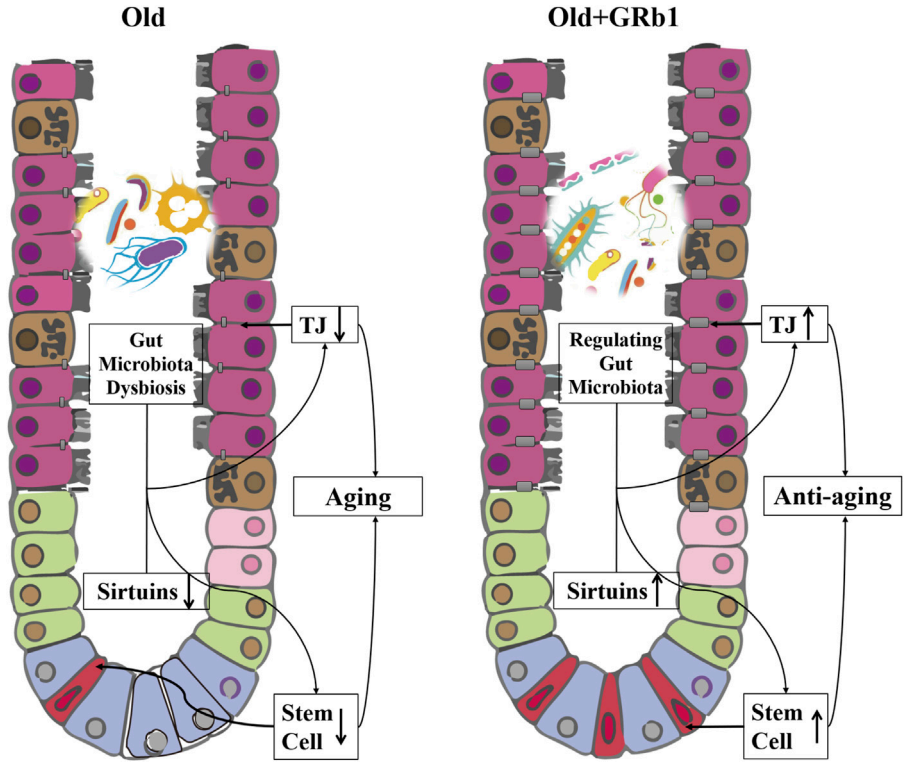

FIGURE 6
GRb1 improves the intestinal aging *via* up-regulating the expression sirtuins and modulating the gut microbiota. The downregulation of the members of sirtuins in the intestinal epithelium, especially in the small intestines, and the dysbiosis of the gut microbiota in the old mice are the two important mechanisms on inducing the aging of intestines. The integrity of the intestinal epithelium is affected because of the downregulation of tight junction components with the aging of intestines, and the stem and progenitor cells of the intestines is also reduced in the aged mice. GRb1 can upregulate the members of sirtuins family in the small intestines at transcriptional or post-transcriptional levels. At the same time, GRb1 can improve the dysbiosis of the gut microbiota in the old mice. Therefore, GRb1 might improve the aging of the intestinal epithelium via regulating the expression sirtuins and modulating the gut microbiota of the old mice.

GRb1 and Old + RSV, including Class *Actinobacteria*, Order *Corynebacteriales* and Family Corynebacteriaceae, and the Family Corynebacteriaceae belongs to the Order *Corynebacteriales*, the Order *Corynebacteriales* belongs to the Class *Actinobacteria* (Supplementary Figures 8A,B; Supplementary Figures 9A,B; Supplementary Figures 10A,B).

The top 20 altered pathways in the Kyoto Encyclopedia of Genes and Genomes (KEGG) pathway analysis were shown in Figure 5F. All the 20 pathways increased in the Old group, and GRb1 reduced four of them including "Biosynthesis of vancomycin group antibiotics," "Pentose phosphate pathway," "Streptomycin biosynthesis" and "Secondary bile acid biosynthesis," although RSV could not reduce them. The other 16 pathways all increased after administration of GRb1 or RSV. These results indicated that the composition and functions of gut microbiota changed in old mice, and GRb1 might improve the intestinal aging partly through regulating the gut microbiota in old mice.

Discussion

We uncovered a new role of GRb1 on improving the intestinal aging of old mice (Figure 6). First, administration of GRb1 could increase the numbers of cells and reduce the accumulation of senescent cells in crypts of both small and large intestines from old mice. Then, GRb1 could improve the integrity of the intestinal epithelium *via* increasing the protein levels of the intestinal abundant Claudins in the intestinal epithelium of old mice. GRb1 could improve the function of intestinal stem and progenitor cells *via* upregulating the expression of Tert, Lgr5, mKi67, and c-Myc at transcriptional or posttranscriptional level in the small intestines of old mice. Then, it was demonstrated that GRb1 might improve intestinal aging through modulating the expression of members of Sirtuin family at both transcriptional and posttranscriptional levels in the intestines of old mice. Finally, 16S rDNA sequence results showed that

GRb1 could modulate the composition and functions of gut microbiota in old mice, and it might be one of the mechanisms of GRb1 on improving intestinal aging of old mice.

Intestinal barrier defects are one of the hallmarks of intestinal aging (Arnold et al., 2021). It was reported that the serum LPS level is significantly higher in old mice than the young control mice (Shin et al., 2020), indicating the gut leaky of the old mice. In the present study, CLDN 2, 3, 7 and 15 all decreased in the small intestines of old mice and CLDN 15 also decreased in the large intestines of old mice. We speculated that the reduction of these intestinal abundance Claudins might be the important reason for the defects of the intestinal barrier of the old mice. Tight junction proteins, such as ZO-1, Occludin and CLDN 1, has also been found reduced in the ileum of aged rats (Ren et al., 2018). CLDN 2 and 15 have been reported to have important functions on regulating the paracellular flow of Na^+ from the intestinal submucosa to dominate the absorption of glucose, amino acids and fats (Tamura et al., 2011; Wada et al., 2013). Therefore, the decrease of CLDN 2 and 15 in the small intestines of old mice might affect the absorption of nutrients. GRb1 might promote the nutrients absorption of aged mice *via* increasing the levels of CLDN 2 and 15 in the small intestines of them.

Previous study showed that GRb1 can promote the differentiation of muscle stem cells (Go et al., 2020). Neural stem cells in rats of Alzheimer's disease models are also improved by GRb1 (Zhao et al., 2018). In the present study, GRb1 could improve the function of intestinal stem and progenitor cells *via* upregulating the expression of *Tert*, *Lgr5*, *mKi67*, and *c-Myc* in the small intestines of old mice. *Tert* has been confirmed to specifically express in the intestinal stem cells (Breault et al., 2008; Itzkovitz et al., 2011; Montgomery et al., 2011; Muñoz et al., 2012). Overexpression of TERT improves the fitness of intestinal barriers and produces a system delay in aging of mice (Tomás-Loba et al., 2008). GRb1 enhanced the protein level of TERT in the small intestines of old mice indicating its effects on anti-aging of intestinal stem cells. Ki67 has been used as the cell proliferation marker in both normal and cancer tissues (Chakritbudsabong et al., 2021; Silva et al., 2022). The increase of Ki67 in both small and large intestines of old mice after administration of GRb1 demonstrated that the number of proliferative cells increased in the intestinal crypts of them. We speculated the increase of the proliferative cells should be the direct mechanism on the increase of cells in crypts of intestines of the GRb1 treated mice.

Members of sirtuin family play the key role in aging and age-related disease (Kaitsuka et al., 2021). In the present study, GRb1 could increase the protein levels of SIRT1, SIRT3, SIRT6, and SIRT7 in the small intestines of old mice. SIRT1 becomes a target for the prevention and treatment of age-related cardiovascular and cerebrovascular diseases since it has been confirmed to have important function on preventing vascular aging (Begum et al., 2021). Recent study reported that LARP7 can ameliorate cellular senescence and aging through enhancing the activity of SIRT1 (Yan et al., 2021). The increase of the expression or activity of SIRT3 can extend the life span of human (Silaghi et al., 2021; Rose et al., 2003). Recently, it was found that reduced SIRT3 abundance in mice can exacerbate age-related periodontal disease (Chen et al., 2021). The level and activation of SIRT6 have been found to be reduced in the aging brain (Stein et al., 2021). The overexpression of SIRT6 can extend the life span of both mice and *Drosophila melanogaster* (Roichman et al., 2021; Taylor et al., 2022). SIRT7 has been found to antagonize stem cell aging *via* stabilizing heterochromatin (Sun and Dang, 2020; Bi et al., 2020). Therefore, the upregulation of SIRTs should be considered as one of the important mechanisms on improving the small intestinal aging of old mice.

In the present study, the composition and functions of gut microbiota changed in the old mice after administration of GRb1. At the phylum level of gut microbiota, the ratio of *Bacteroidetes*/*Firmicutes* decreased in the Old group compared to the Youth group, and administration of GRb1 could improve it. Many studies confirmed the decrease of the ratio of *Bacteroidetes*/*Firmicutes* in ob/ob mice compared with normal control mice (Turnbaugh et al., 2006; Abenavoli et al., 2019). The dysbiosis of the gut microbiota can increase the intestinal permeability (Zhang et al., 2010). Therefore, GRb1 might enhance the integrity of the intestinal epithelium *via* improving the dysbiosis of the gut microbiota in old mice. Compared to the Old group, the Class *Actinobacteria* was predominant in the Youth, Old + GRb1 and Old + RSV groups. *Actinobacteria* have been confirmed to be the biosynthetic factories which produce various bioactive metabolites, and many of these bioactive metabolites can be developed as drugs for human (Azman et al., 2019; Hussain et al., 2020; Jose et al., 2021). The pathways for "Valine, leucine and isoleucine biosynthesis" and "Lysine biosynthesis" significantly increased in old mice after administration with GRb1. Lysine, valine, leucine and isoleucine are essential amino acids for human, so the increase of the biosynthesis of them should be good for the health of the old mice. Hence, we speculated that the regulating of the gut microbiota might be another important mechanism of GRb1 on improving the intestinal aging of the old mice.

Conclusion

In conclusion, GRb1 could improve the intestinal aging *via* regulating the expression of members of Sirtuin family in the intestinal epithelium at transcriptional or posttranscriptional levels and modulating the composition and functions of gut microbiota in the old mice (Figure 6).

Data availability statement

The datasets presented in this study can be found in online repositories. The names of the repository/repositories and accession number(s) can be found below: https://www.ncbi.nlm.nih.gov/sra/PRJNA856886.

Ethics statement

The animal study was reviewed and approved by the Experimental Animal Ethics Committee of Guangdong Pharmaceutical University.

Author contributions

Conceptualization, ZL and YY; methodology, LC, KL, and HR; validation, LC, QH. TL and YY; formal analysis, YY, SY, and QS; investigation, ZL, LC, and QH; resources, JG; data curation, FT and YN; writing—original draft preparation, ZL, LC, and YY; writing—review and editing, ZL, LC, and YY; visualization, LC and FT; supervision, ZL and JG; project administration, ZL and JG; funding acquisition, YY, ZL, and JG. All authors have read and agreed to the published version of the manuscript.

Funding

This work was supported by the National Natural Science Foundation of China (No. 81830113, No. 82171855); National key R and D plan "Research on modernization of traditional Chinese medicine" (2018YFC1704200); Major basic and applied basic research projects of Guangdong Province of China (2019B030302005); the Guangdong Basic and Applied Basic Research Foundation (2021A1515012383); the Opening Foundation of the Key Laboratory of Regenerative Biology, Guangzhou Institutes of Biomedicine and Health, Chinese Academy of Sciences (KLRB201807); the Science and Technology Planning Project of Guangzhou City (No. 201803010069).

Acknowledgments

The authors thank Miss Zitong Peng and Miss Lulu Liu from Guangdong Pharmaceutical University for technical assistance.

Conflict of interest

The authors declare that the research was conducted in the absence of any commercial or financial relationships that could be construed as a potential conflict of interest.

Publisher's note

All claims expressed in this article are solely those of the authors and do not necessarily represent those of their affiliated organizations, or those of the publisher, the editors and the reviewers. Any product that may be evaluated in this article, or claim that may be made by its manufacturer, is not guaranteed or endorsed by the publisher.

Supplementary material

The Supplementary Material for this article can be found online at: https://www.frontiersin.org/articles/10.3389/fphar.2022.991597/full#supplementary-material

References

Abenavoli, L., Scarpellini, E., Colica, C., Boccuto, L., Salehi, B., Sharifi-Rad, J., et al. (2019). Gut microbiota and obesity: A role for probiotics. *Nutrients* 11, E2690. doi:10.3390/nu11112690

Arnold, J. W., Roach, J., Fabela, S., Moorfield, E., Ding, S., Blue, E., et al. (2021). The pleiotropic effects of prebiotic galacto-oligosaccharides on the aging gut. *Microbiome* 9, 31. doi:10.1186/s40168-020-00980-0

Azman, A. S., Mawang, C. I., Khairat, J. E., and Abubakar, S. (2019). Actinobacteria-a promising natural source of anti-biofilm agents. *Int. Microbiol.* 22, 403–409. doi:10.1007/s10123-019-00066-4

Baghdadi, M. B., Ayyaz, A., Coquenlorge, S., Chu, B., Kumar, S., Streutker, C., et al. (2022). Enteric glial cell heterogeneity regulates intestinal stem cell niches. *Cell Stem Cell* 29, 86–100.e6. doi:10.1016/j.stem.2021.10.004

Bai, Y., Bao, X., Mu, Q., Fang, X., Zhu, R., Liu, C., et al. (2021). Ginsenoside Rb1, salvianolic acid B and their combination modulate gut microbiota and improve glucolipid metabolism in high-fat diet induced obese mice. *PeerJ* 9, e10598. doi:10.7717/peerj.10598

Begum, M. K., Konja, D., Singh, S., Chlopicki, S., and Wang, Y. (2021). Endothelial SIRT1 as a target for the prevention of arterial aging: Promises and challenges. *J. Cardiovasc. Pharmacol.* 78, S63–s77. doi:10.1097/FJC.0000000000001154

Ben Othman, S., Ido, K., Masuda, R., Gotoh, S., Hosoda-Yabe, R., Kitaguchi, K., et al. (2020). Senescence-accelerated mouse prone 8 mice exhibit specific morphological changes in the small intestine during senescence and after pectin supplemented diet. *Exp. Gerontol.* 142, 111099. doi:10.1016/j.exger.2020.111099

Bi, S., Liu, Z., Wu, Z., Wang, Z., Liu, X., Wang, S., et al. (2020). SIRT7 antagonizes human stem cell aging as a heterochromatin stabilizer. *Protein Cell* 11, 483–504. doi:10.1007/s13238-020-00728-4

Breault, D. T., Min, I. M., Carlone, D. L., Farilla, L. G., Ambruzs, D. M., Henderson, D. E., et al. (2008). Generation of mTert-GFP mice as a model to identify and study tissue progenitor cells. *Proc. Natl. Acad. Sci. U. S. A.* 105, 10420–10425. doi:10.1073/pnas.0804800105

Chakritbudsabong, W., Sariya, L., Jantahiran, P., Chaisilp, N., Chaiwattanarungruengpaisan, S., Rungsiwiwut, R., et al. (2021). Generation of

porcine induced neural stem cells using the sendai virus. *Front. Vet. Sci.* 8, 806785. doi:10.3389/fvets.2021.806785

Chen, J., Zhang, Y., Gao, J., Li, T., Gan, X., and Yu, H. (2021). Sirtuin 3 deficiency exacerbates age-related periodontal disease. *J. Periodontal Res.* 56, 1163–1173. doi:10.1111/jre.12930

Chen, S., Li, X., Wang, Y., Mu, P., Chen, C., Huang, P., et al. (2019). Ginsenoside Rb1 attenuates intestinal ischemia/reperfusion-induced inflammation and oxidative stress via activation of the PI3K/Akt/Nrf2 signaling pathway. *Mol. Med. Rep.* 19, 3633–3641. doi:10.3892/mmr.2019.10018

Cheng, Y., Shen, L. H., and Zhang, J. T. (2005). Anti-amnestic and anti-aging effects of ginsenoside Rg1 and Rb1 and its mechanism of action. *Acta Pharmacol. Sin.* 26, 143–149. doi:10.1111/j.1745-7254.2005.00034.x

Dong, J. Y., Xia, K. J., Liang, W., Liu, L. L., Yang, F., Fang, X. S., et al. (2021). Ginsenoside Rb1 alleviates colitis in mice via activation of endoplasmic reticulum-resident E3 ubiquitin ligase Hrd1 signaling pathway. *Acta Pharmacol. Sin.* 42, 1461–1471. doi:10.1038/s41401-020-00561-9

Friedrich, A. W. (2019). Control of hospital acquired infections and antimicrobial resistance in europe: The way to go. *Wien. Med. Wochenschr.* 169, 25–30. doi:10.1007/s10354-018-0676-5

Gámez-García, A., and Vazquez, B. N. (2021). Nuclear sirtuins and the aging of the immune system. *Genes (Basel)* 12, 1856. doi:10.3390/genes12121856

Go, G. Y., Jo, A., Seo, D. W., Kim, W. Y., Kim, Y. K., So, E. Y., et al. (2020). Ginsenoside Rb1 and Rb2 upregulate Akt/mTOR signaling-mediated muscular hypertrophy and myoblast differentiation. *J. Ginseng Res.* 44, 435–441. doi:10.1016/j.jgr.2019.01.007

Hamidian, M., Foroughinia, F., Haghighat, S., Attar, A., and Haem, E. (2022). Protective effects of Panax ginseng against doxorubicin-induced cardiac toxicity in patients with non-metastatic breast cancer: A randomized, double-blind, placebo-controlled clinical trial. *J. Oncol. Pharm. Pract.* 2022, 107815522211185. doi:10.1177/10781552221118530

Hassan, Z. A., Zauszkiewicz-Pawlak, A., Abdelrahman, S. A., Algaidi, S., Desouky, M., and Shalaby, S. M. (2017). Morphological alterations in the jejunal mucosa of aged rats and the possible protective role of green tea. *Folia histochem. Cytobiol.* 55, 124–139. doi:10.5603/FHC.a2017.0012

He, J. Y., Hong, Q., Chen, B. X., Cui, S. Y., Liu, R., Cai, G. Y., et al. (2022). Ginsenoside Rb1 alleviates diabetic kidney podocyte injury by inhibiting aldose reductase activity. *Acta Pharmacol. Sin.* 43, 342–353. doi:10.1038/s41401-021-00788-0

Hoffmeyer, K., Raggioli, A., Rudloff, S., Anton, R., Hierholzer, A., Del Valle, I., et al. (2012). Wnt/β-catenin signaling regulates telomerase in stem cells and cancer cells. *Science* 336, 1549–1554. doi:10.1126/science.1218370

Hussain, A., Hassan, Q. P., and Shouche, Y. S. (2020). New approaches for antituberculosis leads from Actinobacteria. *Drug Discov. Today* 25, 2335–2342. doi:10.1016/j.drudis.2020.10.005

Hyun, S. H., Bhilare, K. D., Park, C. K., and Kim, J. H. (2022). Effects of Panax ginseng and ginsenosides on oxidative stress and cardiovascular diseases: Pharmacological and therapeutic roles. *J. Ginseng Res.* 46, 33–38. doi:10.1016/j.jgr.2021.07.007

Ishaq, M., Khan, A., Bacha, A. S., Shah, T., Hanif, A., Ahmad, A. A., et al. (2021). Microbiota targeted interventions of probiotic lactobacillus as an anti-ageing approach: A review. *Antioxidants (Basel)* 10, 1930. doi:10.3390/antiox10121930

Itzkovitz, S., Lyubimova, A., Blat, I. C., Maynard, M., Van Es, J., Lees, J., et al. (2011). Single-molecule transcript counting of stem-cell markers in the mouse intestine. *Nat. Cell Biol.* 14, 106–114. doi:10.1038/ncb2384

Jose, P. A., Maharshi, A., and Jha, B. (2021). Actinobacteria in natural products research: Progress and prospects. *Microbiol. Res.* 246, 126708. doi:10.1016/j.micres.2021.126708

Kaitsuka, T., Matsushita, M., and Matsushita, N. (2021). Regulation of hypoxic signaling and oxidative stress via the MicroRNA-SIRT2 Axis and its relationship with aging-related diseases. *Cells* 10, 3316. doi:10.3390/cells10123316

Lei, Z., Maeda, T., Tamura, A., Nakamura, T., Yamazaki, Y., Shiratori, H., et al. (2012). EpCAM contributes to formation of functional tight junction in the intestinal epithelium by recruiting claudin proteins. *Dev. Biol.* 371, 136–145. doi:10.1016/j.ydbio.2012.07.005

Lei, Z., Wu, H., Yang, Y., Hu, Q., Lei, Y., Liu, W., et al. (2021a). Ovariectomy impaired hepatic glucose and lipid homeostasis and altered the gut microbiota in mice with different diets. *Front. Endocrinol.* 12, 708838. doi:10.3389/fendo.2021.708838

Lei, Z., Yang, L., Lei, Y., Yang, Y., Zhang, X., Song, Q., et al. (2021b). High dose lithium chloride causes colitis through activating F4/80 positive macrophages and inhibiting expression of Pigr and Claudin-15 in the colon of mice. *Toxicology* 457, 152799. doi:10.1016/j.tox.2021.152799

Lei, Z., Yang, Y., Liu, S., Lei, Y., Yang, L., Zhang, X., et al. (2020). Dihydroartemisinin ameliorates dextran sulfate sodium induced inflammatory bowel diseases in mice. *Bioorg. Chem.* 100, 103915. doi:10.1016/j.bioorg.2020.103915

Li, X., Khan, I., Xia, W., Huang, G., Liu, L., Law, B. Y. K., et al. (2021). Icariin enhances youth-like features by attenuating the declined gut microbiota in the aged mice. *Pharmacol. Res.* 168, 105587. doi:10.1016/j.phrs.2021.105587

Lima-Fontes, M., Meira, L., Barata, P., Falcão, M., and Carneiro, Â. (2021). Gut microbiota and age-related macular degeneration: A growing partnership. *Surv. Ophthalmol.* 67, 883. doi:10.1016/j.survophthal.2021.11.009

Lin, Z., Xie, R., Zhong, C., Huang, J., Shi, P., and Yao, H. (2022). Recent progress (2015-2020) in the investigation of the pharmacological effects and mechanisms of ginsenoside Rb(1), a main active ingredient in Panax ginseng Meyer. *J. Ginseng Res.* 46, 39–53. doi:10.1016/j.jgr.2021.07.008

López-Otín, C., Blasco, M. A., Partridge, L., Serrano, M., and Kroemer, G. (2013). The hallmarks of aging. *Cell* 153, 1194–1217. doi:10.1016/j.cell.2013.05.039

Lukiw, W. J., Arceneaux, L., Li, W., Bond, T., and Zhao, Y. (2021). Gastrointestinal (GI)-Tract microbiome derived neurotoxins and their potential contribution to inflammatory neurodegeneration in Alzheimer's disease (AD). *J. Alzheimers Dis. Park.* 11, 525. doi:10.4172/2161-0460.1000525

Montgomery, R. K., Carlone, D. L., Richmond, C. A., Farilla, L., Kranendonk, M. E., Henderson, D. E., et al. (2011). Mouse telomerase reverse transcriptase (mTert) expression marks slowly cycling intestinal stem cells. *Proc. Natl. Acad. Sci. U. S. A.* 108, 179–184. doi:10.1073/pnas.1013004108

Muñoz, J., Stange, D. E., Schepers, A. G., Van De Wetering, M., Koo, B. K., Itzkovitz, S., et al. (2012). The Lgr5 intestinal stem cell signature: Robust expression of proposed quiescent '+4' cell markers. *Embo J.* 31, 3079–3091. doi:10.1038/emboj.2012.166

Niu, K. M., Bao, T., Gao, L., Ru, M., Li, Y., Jiang, L., et al. (2021). The impacts of short-term NMN supplementation on serum metabolism, fecal microbiota, and telomere length in pre-aging phase. *Front. Nutr.* 8, 756243. doi:10.3389/fnut.2021.756243

Parrish, A. R. (2017). The impact of aging on epithelial barriers. *Tissue Barriers* 5, e1343172. doi:10.1080/21688370.2017.1343172

Pénzes, L. (1984). Intestinal response in aging: Changes in reserve capacity. *Acta Med. hung.* 41, 263–277.

Qin, G. W., Lu, P., Peng, L., and Jiang, W. (2021). Ginsenoside Rb1 inhibits cardiomyocyte autophagy via PI3K/Akt/mTOR signaling pathway and reduces myocardial ischemia/reperfusion injury. *Am. J. Chin. Med.* 49, 1913–1927. doi:10.1142/S0192415X21500907

Ren, M., Li, H., Fu, Z., and Li, Q. (2021). Succession analysis of gut microbiota structure of participants from long-lived families in hechi, guangxi, China. *Microorganisms* 9, 2524. doi:10.3390/microorganisms9122524

Ren, W., Wu, J., Li, L., Lu, Y., Shao, Y., Qi, Y., et al. (2018). Glucagon-Like peptide-2 improve intestinal mucosal barrier function in aged rats. *J. Nutr. Health Aging* 22, 731–738. doi:10.1007/s12603-018-1022-8

Roichman, A., Elhanati, S., Aon, M. A., Abramovich, I., Di Francesco, A., Shahar, Y., et al. (2021). Restoration of energy homeostasis by SIRT6 extends healthy lifespan. *Nat. Commun.* 12, 3208. doi:10.1038/s41467-021-23545-7

Rose, G., Dato, S., Altomare, K., Bellizzi, D., Garasto, S., Greco, V., et al. (2003). Variability of the SIRT3 gene, human silent information regulator Sir2 homologue, and survivorship in the elderly. *Exp. Gerontol.* 38, 1065–1070. doi:10.1016/s0531-5565(03)00209-2

Ruan, Y., Kim, H. N., Ogana, H. A., Wan, Z., Hurwitz, S., Nichols, C., et al. (2021). Preclinical evaluation of a novel dual targeting PI3kδ/BRD4 inhibitor, SF2535, in B-cell acute lymphoblastic leukemia. *Front. Oncol.* 11, 766888. doi:10.3389/fonc.2021.766888

Ruiz-Gonzalez, C., Cardona, D., Rodriguez-Arrastia, M., Ropero-Padilla, C., Rueda-Ruzafa, L., Carvajal, F., et al. (2022). Effects of probiotics on cognitive and emotional functions in healthy older adults: Protocol for a double-blind randomized placebo-controlled crossover trial. *Res. Nurs. Health* 45, 274–286. doi:10.1002/nur.22209

Sharma, R. (2022). Emerging interrelationship between the gut microbiome and cellular senescence in the context of aging and disease: Perspectives and therapeutic opportunities. *Probiotics Antimicrob. Proteins* 14, 648–663. doi:10.1007/s12602-021-09903-3

Shin, H. E., Kwak, S. E., Zhang, D. D., Lee, J., Yoon, K. J., Cho, H. S., et al. (2020). Effects of treadmill exercise on the regulation of tight junction proteins in aged mice. *Exp. Gerontol.* 141, 111077. doi:10.1016/j.exger.2020.111077

Silaghi, C. N., Farcaș, M., and Crăciun, A. M. (2021). Sirtuin 3 (SIRT3) pathways in age-related cardiovascular and neurodegenerative diseases. *Biomedicines* 9, 1574. doi:10.3390/biomedicines9111574

Silva, L. C., Faustino, I. S. P., Cantadori, G. R., Santos-Silva, A. R., Vargas, P. A., and Lopes, M. A. (2022). Adenocarcinoma not otherwise specified (NOS) arising in the sublingual gland: Rare case report and follow-up. *Oral Oncol.* 126, 105754. doi:10.1016/j.oraloncology.2022.105754

Stein, D., Mizrahi, A., Golova, A., Saretzky, A., Venzor, A. G., Slobodnik, Z., et al. (2021). Aging and pathological aging signatures of the brain: Through the focusing lens of SIRT6. *Aging (Albany NY)* 13, 6420–6441. doi:10.18632/aging.202755

Sun, L., and Dang, W. (2020). SIRT7 slows down stem cell aging by preserving heterochromatin: A perspective on the new discovery. *Protein Cell* 11, 469–471. doi:10.1007/s13238-020-00735-5

Tamura, A., Hayashi, H., Imasato, M., Yamazaki, Y., Hagiwara, A., Wada, M., et al. (2011). Loss of claudin-15, but not claudin-2, causes Na+ deficiency and glucose malabsorption in mouse small intestine. *Gastroenterology* 140, 913–923. doi:10.1053/j.gastro.2010.08.006

Taylor, J. R., Wood, J. G., Mizerak, E., Hinthorn, S., Liu, J., Finn, M., et al. (2022). Sirt6 regulates lifespan in *Drosophila melanogaster*. *Proc. Natl. Acad. Sci. U. S. A.* 119, e2111176119. doi:10.1073/pnas.2111176119

Tomás-Loba, A., Flores, I., Fernández-Marcos, P. J., Cayuela, M. L., Maraver, A., Tejera, A., et al. (2008). Telomerase reverse transcriptase delays aging in cancer-resistant mice. *Cell* 135, 609–622. doi:10.1016/j.cell.2008.09.034

Toyokawa, Y., Takagi, T., Uchiyama, K., Mizushima, K., Inoue, K., Ushiroda, C., et al. (2019). Ginsenoside Rb1 promotes intestinal epithelial wound healing through extracellular signal-regulated kinase and Rho signaling. *J. Gastroenterol. Hepatol.* 34, 1193–1200. doi:10.1111/jgh.14532

Tran, L., and Greenwood-Van Meerveld, B. (2013). Age-associated remodeling of the intestinal epithelial barrier. *J. Gerontol. A Biol. Sci. Med. Sci.* 68, 1045–1056. doi:10.1093/gerona/glt106

Turnbaugh, P. J., Ley, R. E., Mahowald, M. A., Magrini, V., Mardis, E. R., and Gordon, J. I. (2006). An obesity-associated gut microbiome with increased capacity for energy harvest. *Nature* 444, 1027–1031. doi:10.1038/nature05414

Wada, M., Tamura, A., Takahashi, N., and Tsukita, S. (2013). Loss of claudins 2 and 15 from mice causes defects in paracellular Na+ flow and nutrient transport in gut and leads to death from malnutrition. *Gastroenterology* 144, 369–380. doi:10.1053/j.gastro.2012.10.035

Watroba, M., and Szukiewicz, D. (2021). Sirtuins at the service of healthy longevity. *Front. Physiol.* 12, 724506. doi:10.3389/fphys.2021.724506

Wu, C. J., Mannan, P., Lu, M., and Udey, M. C. (2013). Epithelial cell adhesion molecule (EpCAM) regulates claudin dynamics and tight junctions. *J. Biol. Chem.* 288, 12253–12268. doi:10.1074/jbc.M113.457499

Xiong, Y., Shen, L., Liu, K. J., Tso, P., Xiong, Y., Wang, G., et al. (2010). Antiobesity and antihyperglycemic effects of ginsenoside Rb1 in rats. *Diabetes* 59, 2505–2512. doi:10.2337/db10-0315

Yan, P., Li, Z., Xiong, J., Geng, Z., Wei, W., Zhang, Y., et al. (2021). LARP7 ameliorates cellular senescence and aging by allosterically enhancing SIRT1 deacetylase activity. *Cell Rep.* 37, 110038. doi:10.1016/j.celrep.2021.110038

Yang, C., Wang, W., Deng, P., Li, C., Zhao, L., and Gao, H. (2021a). Fibroblast growth factor 21 modulates microglial polarization that attenuates neurodegeneration in mice and cellular models of Parkinson's disease. *Front. Aging Neurosci.* 13, 778527. doi:10.3389/fnagi.2021.778527

Yang, X., Dong, B., An, L., Zhang, Q., Chen, Y., Wang, H., et al. (2021b). Ginsenoside Rb1 ameliorates glycemic disorder in mice with high fat diet-induced obesity via regulating gut microbiota and amino acid metabolism. *Front. Pharmacol.* 12, 756491. doi:10.3389/fphar.2021.756491

Yao, H., Wan, J. Y., Zeng, J., Huang, W. H., Sava-Segal, C., Li, L., et al. (2018). Effects of compound K, an enteric microbiome metabolite of ginseng, in the treatment of inflammation associated colon cancer. *Oncol. Lett.* 15, 8339–8348. doi:10.3892/ol.2018.8414

Zhang, W., Gu, Y., Chen, Y., Deng, H., Chen, L., Chen, S., et al. (2010). Intestinal flora imbalance results in altered bacterial translocation and liver function in rats with experimental cirrhosis. *Eur. J. Gastroenterol. Hepatol.* 22, 1481–1486. doi:10.1097/MEG.0b013e32833eb8b0

Zhang, Y., Zhang, S., Li, B., Luo, Y., Gong, Y., Jin, X., et al. (2021). Gut microbiota dysbiosis promotes age-related atrial fibrillation by lipopolysaccharide and glucose-induced activation of NLRP3-inflammasome. *Cardiovasc. Res.* 118, 785–797. doi:10.1093/cvr/cvab114

Zhao, A., Liu, N., Yao, M., Zhang, Y., Yao, Z., Feng, Y., et al. (2022a). A review of neuroprotective effects and mechanisms of ginsenosides from Panax ginseng in treating ischemic stroke. *Front. Pharmacol.* 13, 946752. doi:10.3389/fphar.2022.946752

Zhao, J., Lu, S., Yu, H., Duan, S., and Zhao, J. (2018). Baicalin and ginsenoside Rb1 promote the proliferation and differentiation of neural stem cells in Alzheimer's disease model rats. *Brain Res.* 1678, 187–194. doi:10.1016/j.brainres.2017.10.003

Zhao, Q., Liu, Y., Zhang, S., Zhao, Y., Wang, C., Li, K., et al. (2022b). Studies on the regulation and molecular mechanism of Panax ginseng saponins on senescence and related behaviors of *Drosophila melanogaster*. *Front. Aging Neurosci.* 14, 870326. doi:10.3389/fnagi.2022.870326

Zhao, Y., Jaber, V., and Lukiw, W. J. (2021). Gastrointestinal tract microbiome-derived pro-inflammatory neurotoxins in Alzheimer's disease. *J. Aging Sci.* 9, 002. doi:10.35248/2329-8847.21.s5.002

Zhou, F., Zhang, P., Chen, X., Yan, J., Yao, J., Yu, Z., et al. (2016). Ginsenoside Rb1 protects the intestinal mucosal barrier following peritoneal air exposure. *Exp. Ther. Med.* 12, 2563–2567. doi:10.3892/etm.2016.3639

Zhou, P., Xie, W., He, S., Sun, Y., Meng, X., Sun, G., et al. (2019). Ginsenoside Rb1 as an anti-diabetic agent and its underlying mechanism analysis. *Cells* 8, E204. doi:10.3390/cells8030204

frontiers | Frontiers in Pharmacology

TYPE Original Research
PUBLISHED 29 September 2022
DOI 10.3389/fphar.2022.977539

OPEN ACCESS

EDITED BY
Weicheng Hu,
Huaiyin Normal University, China

REVIEWED BY
Hongxin Wang,
Jinzhou Medical University, China
Penke Vijaya Babu,
CURIA INDIA PVT LTD, India
Edson Roberto Silva,
University of São Paulo, Brazil

*CORRESPONDENCE
Hui Ao,
aohui2005@126.com

SPECIALTY SECTION
This article was submitted to Inflammation Pharmacology, a section of the journal Frontiers in Pharmacology

RECEIVED 24 June 2022
ACCEPTED 15 September 2022
PUBLISHED 29 September 2022

CITATION
Wan Y, Liu D, Xia J, Xu J-F, Zhang L, Yang Y, Wu J-J and Ao H (2022), Ginsenoside CK, rather than Rb1, possesses potential chemopreventive activities in human gastric cancer via regulating PI3K/AKT/NF-κB signal pathway.
Front. Pharmacol. 13:977539.
doi: 10.3389/fphar.2022.977539

Ginsenoside CK, rather than Rb1, possesses potential chemopreventive activities in human gastric cancer *via* regulating PI3K/AKT/NF-κB signal pathway

Yan Wan[1], Dong Liu[1], Jia Xia[1], Jin-Feng Xu[1], Li Zhang[1], Yu Yang[1], Jiao-Jiao Wu[1] and Hui Ao[1,2]*

[1]State Key Laboratory of Southwestern Chinese Medicine Resources, Chengdu University of Traditional Chinese Medicine, Chengdu, China, [2]Innovative Institute of Chinese Medicine and Pharmacy, Chengdu University of Traditional Chinese Medicine, Chengdu, China

Ginsenoside Rb1, a main component of ginseng, is often transformed into ginsenoside CK by intestinal flora to exert various pharmacological activity. However, it remains unclear whether ginsenoside CK is responsible for the anti-gastric cancer effect of ginsenoside Rb1 *in vivo*. In this study, network pharmacology was applied to predict the key signal pathways of ginsenoside Rb1 and ginsenoside CK when treating gastric cancer. The anti-proliferative effects of ginsenoside Rb1 and ginsenoside CK and the underlying mechanism in gastric cancer cells were explored by MTT, Hoechst3328 staining, ELISA, RT-qPCR and Western blotting. The results showed that PI3K-AKT/NF-κB signal pathway was the common important pathway of ginsenoside Rb1 and CK in the treatment of gastric cancer. The results of MTT assay showed that ginsenoside Rb1 could hardly inhibit the proliferation of HGC-27 cells, whereas ginsenoside CK could inhibit the proliferation of HGC-27 cells. Hoechst3328 staining showed that cells in the ginsenoside CK group were densely stained bright blue and nuclear fragmented, indicating that apoptosis occurred. ELISA results showed that ginsenoside CK could effectively downregulate the levels of cyclin CyclinB1 and CyclinD1, but ginsenoside Rb1 had no significant effect. Also, the results of Western blot and RT-qPCR showed that ginsenoside CK inhibited the expressions of anti-apoptosis-related protein Bcl-2 and apoptosis-related pathway PI3K/AKT/NF-κB, and promoted the expression of pro-apoptosis proteins Bax and Caspase 3, whereas ginsenoside Rb1 exerted no effect. In short, ginsenoside Rb1 had no anti-gastric cancer cell activity *in vitro*, but ginsenoside CK could effectively inhibit cell proliferation and induce cell apoptosis in HGC-27 cells. The mechanism might relate to the inhibitory effect of ginsenoside CK on the PI3K/AKT/NF-κB pathway. These results suggest that ginsenoside CK might be the *in vivo* material basis for the anti-gastric cancer activity of ginsenosides.

KEYWORDS

ginsenoside Rb1, ginsenoside CK, gastric cancer, network pharmacology, apoptosis, gut microbiota

1 Introduction

Gastric cancer is the fourth most common male cancer diagnosis in the world, after lung, prostate and colorectal cancer, and the fifth among women, after breast cancer, colorectal cancer, cervical cancer, and lung cancer. The pathogenesis of gastric cancer involves multi-steps, multi-factors and multi-targets. It is estimated that the fatality rate of gastric cancer is about 70%, which is much higher than other epidemic diseases (Sung et al., 2021). At present, the main treatment of gastric cancer is the combination of neoadjuvant radiotherapy and chemotherapy, molecular targeted therapy and immunotherapy (Song et al., 2017). However, these methods have defects that cannot be ignored. For example, although radiotherapy and chemotherapy are effective treatments, serious side effects (loss of appetite, indigestion, burning sensation, nausea, vomiting, etc.) seriously affect the efficiency of treatment (Bae et al., 2017). Natural products, which are extracted from the plant kingdom with the characteristics of low toxicity and few side effects, are multiple targeted (Wan et al., 2021). Therefore, it is of great importance to discover natural drugs with anti-gastric cancer effects.

Ginseng is known as the "King of Herbs," which has the effect of nourishing vitality, strengthening the body and eliminating evil, according to Traditional Chinese Medicine. As the main active ingredients of ginseng, ginsenosides play a pivotal role in the pharmacological effects of ginseng. Current studies have shown that total ginsenosides have a certain anti-gastric cancer activity, whereas ginsenoside Rb1, one of the main prototype components of total ginsenosides, also plays an important role in anti-gastric precancerous lesions, indicating that ginsenoside Rb1 may have anti-gastric cancer potential (Xu et al., 2018a). Notably, ginsenoside compound K (CK) is the gut microbiota-derived product of ginsenoside Rb1. Recently, a growing number of studies demonstrated that CK, the microbial transformed metabolites of Rb1, showed greater therapeutic activities compared with its parent compound Rb1, either *in vivo* or *in vitro*. For example, *in vitro* models of breast and colon cancer, ginsenoside CK has better anticancer activity than ginsenoside Rb1 (Wang et al., 2012; Yao et al., 2018). Therefore, it is worth studying whether ginsenoside CK has stronger anti-gastric cancer activity than ginsenoside Rb1.

Also, the anti-cancer mechanism of ginsenoside Rb1 and CK is worth studying. However, the pathogenesis of gastric cancer is complex, involving multiple pathways and targets, which brings difficulties to the discovery of the anti-cancer drugs. As a systematic and comprehensive discipline, network pharmacology can easily obtain relevant targets for drug treatment of diseases, and select appropriate signaling targets for mechanism analysis. However, the network pharmacology results are only predictions and often need to be verified by the experiments. Therefore, it is undoubtedly a promising approach to study the anti-gastric cancer mechanism of ginsenoside Rb1 and CK based on the results of network pharmacology.

This study is designed to resolve the above problems according to the corresponding experimental scheme. The network pharmacology was applied to speculate the common signaling pathway responsible for the anti-gastric cancer effects of ginsenoside Rb1 and CK, and its pharmacological effect and the underlying mechanism were verified by the *in vitro* experiments. The purpose of this study is to compare the anti-gastric cancer activity of ginsenoside Rb1 and CK, and in turn explore the material basis and mechanism the anti-gastric cancer effect of ginsenosides *in vivo*, providing scientific basis for the clinical application of ginsenosides.

2 Materials

Ginsenoside Rb1 and ginsenoside CK were purchased from Chengdu Mansite Biotechnology Co., Ltd., and the purity was higher than 98%. (Chengdu, China). Human gastric cancer cell line HGC-27 was purchased from Shanghai Fuheng Biotechnology Co., Ltd. (Shanghai, China). DMEM, penicillin and streptomycin were purchased from Shanghai Biyuntian Biology Co., Ltd. (Shanghai, China). Fetal bovine serum was purchased from Zhejiang Tianhang Biotechnology Co., Ltd. (Zhejiang, China). MTT is purchased from Biosharp Company (Guangzhou, China). HumanCyclin-B1ELISAKIT and HumanCyclin-D1ELISAKIT are purchased from Ruixin Biotechnology Co., Ltd. (Fujian, China). 5X All-In-One MasterMix was purchased from abm (Canada). Bcl-2 antibody (AF6139), Bax antibody (AF0120), Phospho-I κB alpha antibody (AF 2002), Phospho-PI3K P85 alpha antibody (AF3241), Phospho-pan-AKT1/2/3 antibody (AF0016) and pan-AKT1/2/3 antibody (AF6261) were purchased from Affinity (Jiangsu, China). IκB alpha antibody (#9242), NF- κB p65 antibody (#8242) and Caspase-3 antibody (#14220) were purchased from Cell Signaling Technology (United States). PI3K p85alpha antibodies (TA6241) were purchased from Abimat Biomedical Co., Ltd. (Shanghai, China). Goat anti-rabbit IgG-HRP (Cat. No. 05-4030- 05) were purchased from Multi Sciences (LIANKE) Biotech Co., Ltd. (Hangzhou, China). Animal Total RNA Isolation Kit (R210801), RT EasyTM II (210401) and Real Time PCR EasyTM-SYBR Green I (P210501) were purchased from Chengdu Fuji Biotechnology Co., Ltd. (Chengdu, China). Hoechst33258 (C0020) was purchased from Beijing Solebo Technology Co., Ltd. (Beijing, China).

3 Methods

3.1 Study on the mechanism of ginsenoside Rb1 and its intestinal bacterial transformant-ginsenoside CK in the treatment of gastric cancer based on network pharmacology

3.1.1 Target prediction of ginsenoside Rb1 and CK

The Herb Ingredients' Targets (HIT) database is made up of more than 3,250 articles manually (Liang et al., 2019). In addition to more than 1,300 kinds of Chinese herbal medicine and 586 kinds of traditional Chinese medicine compounds, there are 1,301 protein targets. Compared with the traditional database, the information obtained by HIT database is calibrated by manual standardization. Therefore, the potential targets of ginsenoside Rb1 and CK were obtained by HIT (http://lifecenter.biosino.org/) database.

3.1.2 Target prediction of gastric cancer

Using "gastric cancer" as the key word, the target of gastric cancer was obtained in disgenet (http://www.disgenet.org/), malacards (http://www.malacards.org/) and OMIM (https://omim.org/) database, and the obtained target was de-repeated to get the potential target of the disease.

3.1.3 Core target "fishing" and protein-protein interaction network construction

BisoGenet aims to evaluate the prominence of functional relationships between genes or proteomes from proteomics or genomics experiments. A more comprehensive set of PPI networks can be obtained by expanding and analyzing the input targets through the internal integration database of Bisogenet. In the Cytoscape 3.8.2 software (Wang and Yuan, 2022), input the potential targets of ginsenoside CK, Rb1 and gastric cancer into the Bisogenet plug-in, click "Geneidentifiersonly" to enter the next step "DataSettings," check the "ProteinProteinInteraction" option, and click OK to construct the PPI network of ginsenoside F2, Rd and gastric cancer, respectively. Then the PPI networks of ginsenoside Rb1 and CK were intersected with the PPI network of gastric cancer by Merged tool to obtain the PPI network of ginsenoside Rb1 for gastric cancer and the PPI network of ginsenoside CK for gastric cancer. Use the CytoNCA plug-in to calculate the attribute values of two groups of PPI networks. In the PPI network of ginsenoside Rb1 in the treatment of gastric cancer, the double median of Degree value was used to screen once, and then Degree, Betweenness and Clossness were used to screen twice to obtain the core target of ginsenoside Rb1 in the treatment of gastric cancer. In the PPI network of ginsenoside CK in the treatment of gastric cancer, the core target of ginsenoside CK in the treatment of gastric cancer was obtained by twice screening the median of Degree, Betweenness and Clossness.

3.1.4 Gene ontology and pathway enrichment analysis

The core targets of ginsenoside Rb1 in the treatment of gastric cancer and ginsenoside CK in the treatment of gastric cancer were imported into the Metascape (http://metascape.org/) database, the species selection "*Homo sapiens*," and click Costom Analysis to proceed to the next step. On the Enrichment page, select GO Biological Processes option for gene ontology (Gene Ontology, GO) biological process analysis, and check KEGG Pathway option for KEGG analysis. The results of GO analysis and KEGG enrichment were obtained.

3.2 Demonstration of the anti-gastric cancer mechanism of ginsenoside Rb1 and its intestinal bacterial transformant-ginsenoside CK regulating PI3K/AKT/NF-κB apoptosis pathway based on *in vitro* experiments.

3.2.1 Cell culture

HGC-27 cells were cultured in DMEM enriched with 10% fetal bovine serum and 1% penicillin/streptomycin. The culture environment is an incubator under the conditions of 5% carbon dioxide and 37°.

3.2.2 Cell viability assay

HGC-27 cell suspension (100 μl) in logarithmic growth phase was inoculated in 96-well plate at the rate of 5×10^{-5} per well. The cells were cultured for 24 h and then added with drug-containing medium. Experimental groups: Rb1 or CK (10, 20, 30, 40, 50, and 60 μM) acted on HGC-27 cells, the control group (with cells) added the same amount of drug carrier solvent (DMSO content <0.3%), and the blank group (no cells) only added the same amount of medium. Five multiple holes were set up for each dose, and cultured for 24, 48, and 72 h after adding the drug, then the medium was absorbed, and each well was added with MTT (5 mg/ml) 20 and 100 μl basic medium, and continued to culture for 4 h. The supernatant was absorbed, and 100 μl of DMSO was added to each hole to avoid light and oscillate 10 min, so that the crystal could be fully dissolved. The absorbance (OD) of each hole at 490 nm was measured by enzyme-linked immunosorbent assay (ElISA), the cell survival rate of each group (%) was calculated, the line chart was drawn, and the IC_{50} of the inhibitory effect of drugs on cells was calculated. The cell survival rate (%) was calculated according to the following formula: cell survival rate (%) = (OD value of administration group-OD value of blank group)/(OD value of control group-OD value of blank group) × 100%.

TABLE 1 Primer information.

Gene	Primer	Reverse
PI3K	Forward	GGTTTGGCCTGCTTTTGGAG
	Reverse	CCATTGCCTCGACTTGCCTA
AKT	Forward	GGACAAGGACGGGCACATTA
	Reverse	CGACCGCACATCATCTCGTA
NF-κB	Forward	AATGGGCTACACCGAAGCAA
	Reverse	TTGCGGAAGGATGTCTCCAC
NF-κB P65	Forward	TCCTATAGAAGAGCAGCGTGG
	Reverse	GCCAGAGTTTCGGTTCACTC
βactin	Forward	CCTTCCTGGGCATGGAGTC
	Reverse	TGATCTTCATTGTGCTGGGTG

3.2.3 Cell morphology observation

In order to observe the effect of drugs on cell morphology, HGC-27 cells were evenly inoculated in five petri dishes. After the cells grew to 70% Mel 80%, the cells were treated with different concentrations of ginsenoside CK (20, 40, and 60 μM) and ginsenoside Rb1 (60 μM) for 16 h, and the cell morphology of each group was observed under ×200 microscope.

3.2.4 Apoptosis observation

HGC-27 is administered as described in Section 3.2.3. Then the cells were fixed with cell fixation solution, washed and removed properly after 30 min, and Hoechst33258 staining solution was added to cover the sample. Then the Hoechst33258 staining solution was removed and washed with PBS for 2-3 times. Finally, observed directly under the fluorescence microscope, if the cells are densely stained bright blue and show nuclear fragmentation, it indicates the occurrence of apoptosis.

3.2.5 Enzyme-linked immunosorbent assay

HGC-27 is administered as described in Section 3.2.3. Then the supernatant of cell was collected and CyclinB1 and CyclinD1 were detected by enzyme linked immunosorbent assay (Elisa) kit.

3.2.6 Real time quantitative PCR assay

Extract the total RNA by using Cell Total RNA Isolation Kit, according to the manufacturer's instructions. The total RNA was reverse transcribed into cDNA with 5X All-in-One Master Mix. Quantitative PCR was carried out on the applied biological system 7900HT FAST system using SYBR Green PCR Master Mix. The RT-qPCR reaction conditions are as follows: 95°C for 10 min, 40 cycles of 95°C for 15 s, and 60°C for 30 s. The relative mRNA expression level was calculated by $2^{-\Delta\Delta CT}$ method. The sequence of primers used by RT-qPC is shown in Table 1.

3.2.7 Western blot assay

Treat the cells as described in Section 3.2.3. Then split it with RIPA cleavage solution on the ice. According to the manufacturer's instructions, the BCA protein assay kit is used to quantify the protein concentration of each sample. After quantification, the protein sample buffer was added and heated at 100°C for 5 min. Then, each group of equal amount of protein was loaded into 10% SDS-PAGE and transferred to PVDF membrane. Then, the membrane and the primary antibodies (β-actin, PI3K, Akt, phospho-PI3K, phospho-AKT, p65, IκBα, p-IκBα, Bax, Bcl2, and caspase 3; 1:1,000) were used overnight at 4°C and the secondary antibodies (Goat anti-Rabbit IgG-HRP; 1:5,000) was used at 37°C for another 2 h. Finally, the protein bands were visualized by ECL Kit, and the immunoblotting signals were quantitatively analyzed by ImageJ software.

3.2.8 Statistical analysis

All the results were statistically analyzed and plotted by GraphPadPrism 9.0.0. One-way ANOVA was used to compare multiple groups of samples, and then Tukey method was used to compare any two groups of data. p value ($p < 0.05$) showed that the difference was statistically significant. The IC_{50} values were calculated by GraphPadPrism 9.0.0 and the results of nonlinear regression of IC_{50} were plotted.

4 Results

4.1 Results of network pharmacology

4.1.1 Potential targets of ginsenosides Rb1, CK, and gastric cancer

According to the HIT database, 22 targets of ginsenoside Rb1 and 2 targets of ginsenoside CK were obtained. 34, 32, and 140 gastric cancer-related targets were obtained from the disgenet, malacards, and OMIM databases, respectively. The above search results were combined and duplicates were deleted, and a total of 189 gastric cancer-related targets were obtained (Supplementary Table S1).

4.1.2 Screening of key targets of ginsenoside Rb1 and CK in the treatment of gastric cancer

The PPI network of ginsenoside Rb1 targets was constructed, including 2,083 nodes and 49,806 relationships between nodes; a PPI network of gastric cancer disease-related targets was constructed, including 5,804 nodes and 149,080 relationships between nodes. Then, using the Merge plug-in, the intersection targets of ginsenoside Rb1 in the treatment of gastric cancer were extracted, and then the key targets of ginsenoside Rb1 in the treatment of diseases were screened, such as Neurotrophic receptor tyrosine kinase 1 (NTRK1), Fibronectin 1 (FN1), Minichromosome maintenance complex component 2

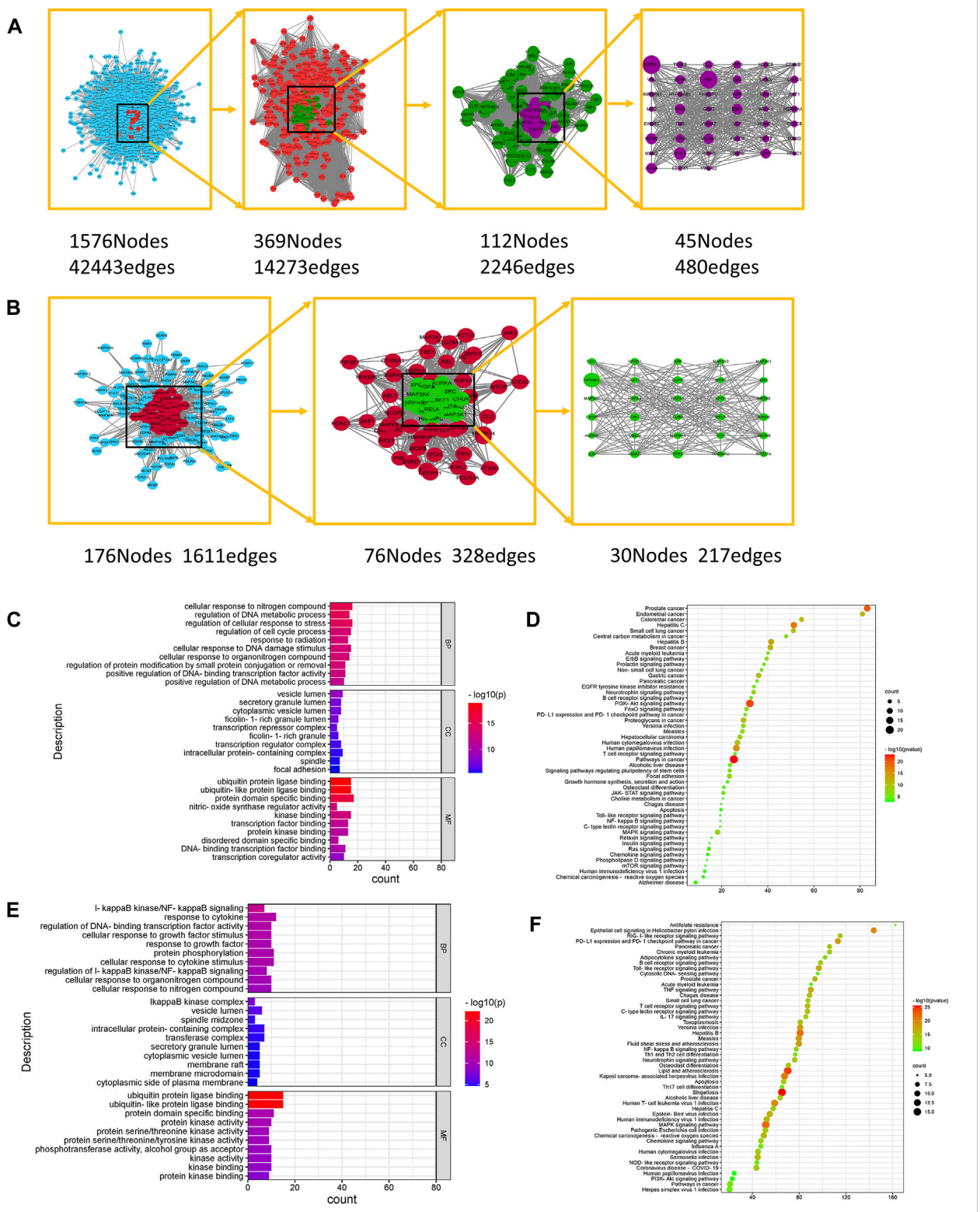

FIGURE 1
Network Pharmacological Analysis of Ginsenoside Rb1 and CK. **(A)** Topological network of key targets of ginsenoside Rb1 in the treatment of gastric cancer. **(B)** Topological network of key targets of ginsenoside CK in the treatment of gastric cancer. **(C)** GO biological function enrichment analysis of key targets of ginsenoside Rb1 in the treatment of gastric cancer. **(D)** KEGG pathway enrichment analysis of key targets of ginsenoside Rb1 in the treatment of gastric cancer. **(E)** GO biological function enrichment analysis of key targets of ginsenoside CK in the treatment of gastric cancer. **(F)** KEGG pathway enrichment analysis of key targets of ginsenoside CK in the treatment of gastric cancer.

(MCM2), Inhibitor of nuclear factor kappa B kinase subunit gamma (IKBKG), AKT serine/threonine kinase 1 (AKT1) and other 45 targets, as shown in Figure 1A.

The PPI network of the targets of ginsenoside CK was constructed, including 223 nodes and 1912 interrelationships between nodes; the PPI network of gastric cancer disease-related targets was constructed, including 5,804 nodes and 149080 interrelationships between nodes. Then the Merge plug-in to extract the intersection targets of ginsenoside CK in the treatment of gastric cancer was applied, and the key targets of ginsenoside CK in the treatment of diseases were screened, such as Heterogeneous nuclear ribonucleoprotein U (HNRNPU), Aurora kinase A (AURKA), IKBKB, AKT1 and so on, as shown in Figure 1B.

4.1.3 Gene ontology and kyoto encyclopedia of genes and genomes analysis of key targets of ginsenoside Rb1 and CK

The key targets of ginsenoside Rb1 were analyzed by Gene Ontology (GO) using Metascape database, including 632 biological processes (BP), 53 cellular components (CC) and 72 molecular functions (MF). The enriched top 10 BP, CC, and MF are visualized as shown in Figure 1C. Among them, the biological process includes the regulation of cell cycle process, cell response to nitrogen compounds, regulation of DNA metabolism process, cell response to DNA damage stimulation, regulation of protein modification through small protein binding or removal, etc. Cell components involve cytoplasmic vesicle cavity, transcriptional inhibitory complex, intracellular protein complex, spindle and adhesion spot, etc. Molecular functions include protein domain specific binding, kinase binding, protein kinase binding, disordered domain specific binding, DNA binding transcription factor binding, transcription coregulator activity and so on. The results of Kyoto Encyclopedia of Genes and Genomes (KEGG) analysis of ginsenoside Rb1 key targets showed that the key targets of ginsenoside Rb1 were enriched to make a bubble map (Figure 1D), including Phosphatidylinositol 3-kinase/Protein kinases B (PI3K-AKT), FoxO signal pathway, ErbB s, JAK-STAT Ras signal pathway, Mammalian target of rapamycin (mTOR), Mitogen activated protein kinases (MAPK), Nuclear factor kappa-B (NF-κB), Toll-like receptor, and Wnt signal pathways.

The key targets of ginsenoside CK were analyzed by GO using Metascape database, which included 403 biological processes, 47 cellular components and 41 molecular functions. The enriched top 10 BP, CC, and MF are visualized as shown in Figure 1E. Among them, the biological process includes IκB kinase/NF-κB signal transduction, cell response to growth factor stimulation, protein phosphorylation, IκB kinase/NF-κB signal regulation, cell response to organic nitrogen compounds, etc. Cell components involve IκB kinase complex, vesicular cavity, spindle middle region, intracellular protein complex, membrane microdomain, etc. Molecular functions include ubiquitin protein ligase binding, protein kinase activity, protein serine/threonine kinase activity, phosphotransferase activity of alcohol group as receptor, kinase activity, kinase binding and so on. The KEGG analysis results of the key targets of ginsenoside CK are shown in Figure 1F, including PI3K-AKT signal pathway, MAPK signal pathway, NF-κB signal pathway, Toll-like receptor signal pathway, Wnt signal pathway, Rap1 signal pathway and so on.

As the purpose of this study was to compare the efficacy of ginsenoside Rb1 and CK in the treatment of gastric cancer, the common potential pathways of ginsenoside Rb1 and ginsenoside CK obtained from network pharmacology were studied. After the non-common pathway and non-cancer-related pathway were removed, the PI3K-AKT signal pathway, MAPK signal pathway, NF-κB signal pathway, Toll-like receptor signal pathway, TNF signal pathway, Wnt signal pathway, NOD-like receptor signal pathway, IL-17 signal pathway, HIF-1 signal pathway and so on were screened out. According to the GO analysis, the biological process involved in the anti-gastric cancer effects of ginsenoside Rb1 included the regulation of cell cycle process, the regulation of DNA metabolic process and the response of cells to DNA damage stimulation, which were related to cell apoptosis and proliferation. The biological process of ginsenoside CK was related to IκB kinase/NF-κB signal transduction, protein phosphorylation and the regulation of IκB kinase/NF-κB signal, which meant that the anti-gastric cancer effect of ginsenoside CK might be closely related to the IκB kinase/NF-κB signal pathway. Therefore, based on the biological process characteristics of ginsenoside Rb1 and CK obtained from GO analysis, it was found that PI3K/AKT/NF-κB might play an important role in the anti-gastric cancer effects of ginsenoside Rb1 and CK.

4.2 The results of the anti-cancer effects and mechanisms of ginsenoside Rb1 and CK

4.2.1 Ginsenoside CK, rather than ginsenoside Rb1, inhibited the proliferation of gastric cancer cell line HGC-27

As was shown in Figures 2A,B, ginsenoside Rb1 had almost no inhibitory effect on the proliferation of HGC-27 cells. In contrast, ginsenoside CK had an inhibitory effect on the proliferation of HGC-27 cells. The inhibitory effect of ginsenoside CK on HGC-27 cells was concentration- and time-dependent. In addition, IC_{50} of ginsenoside CK in HGC-27 cells at 24, 48, and 72 h were 46.29, 36.93, and 24.95 μM as illustrated in the Figures 2C–E, respectively.

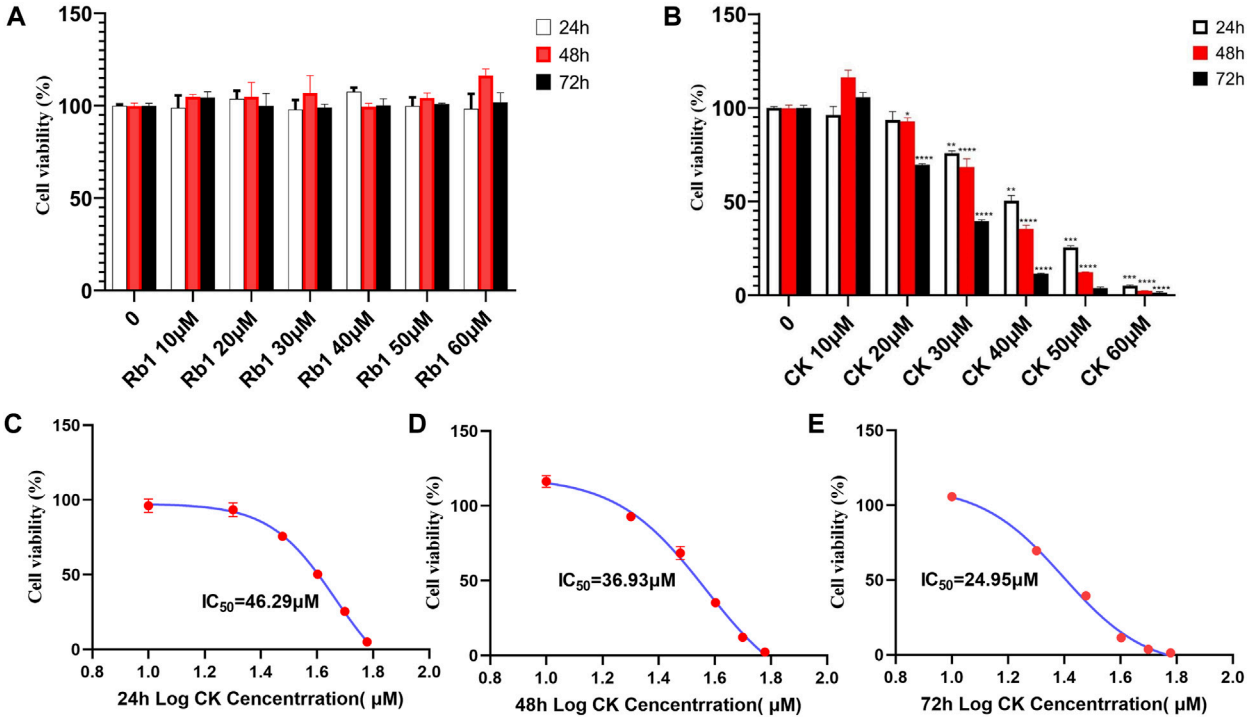

FIGURE 2
Effects of ginsenoside Rb1 and CK on Proliferation of Human Gastric cancer cells. **(A)** Effects of different concentrations of ginsenoside Rb1 and CK on the growth inhibition rate of human gastric cancer cells HGC-27 under different action times. **(B)** Effects of different concentrations of ginsenoside CK on the growth and survival rate of human gastric cancer cells HGC-27 under different action times. **(C)** Nonlinear regression results of IC_{50} after 24 h of CK treatment. **(D)** Nonlinear regression results of IC_{50} after 48 h of CK treatment. **(E)** Nonlinear regression results of IC_{50} after 72 h of CK treatment.

4.2.2 Ginsenoside CK, rather than ginsenoside Rb1, reversed the morphological injury of HGC-27 cells

The normal adherent growth of cells in the blank group was observed under ×200 microscope, and the 60 μM ginsenoside Rb1 group and 20 μM ginsenoside CK group also grew well and distributed evenly without excessive inhibition as illustrated in the Figure 3A. However, the proliferation of cells in 40 μM ginsenoside CK and 60 μM ginsenoside CK was significantly inhibited, and the number of cells was lower than that in normal group. Not only that, the morphology of the two groups of cells also changed, showing shrinkage and clumps, and even obvious cell death. And with the increase of the dose of ginsenoside CK, the morphological abnormality was more obvious.

4.2.3 Ginsenoside CK, rather than ginsenoside Rb1, induced apoptosis in HGC-27 cells

According to Figure 3B, Hoechst33258 staining results showed that the cells in the blank group and 60 μM ginsenoside Rb1 were light blue, and the distribution of chromatin is relatively uniform. After treated by 20, 40, and 60 μM ginsenoside CK, some cells were densely stained bright blue and showed nuclear fragmentation (red arrow), indicating the occurrence of apoptosis. And with the increase of the dose of ginsenoside CK, the number of normal cells decreased, and the characteristics of apoptosis were more obvious.

4.2.4 Ginsenoside CK, rather than ginsenoside Rb1, inhibits the levels of cell cycle related proteins cyclinB1 and cyclinD1

The results of Enzyme-linked immunosorbent assay (ELISA) (Figures 4A,B) showed that although ginsenoside Rb1 could downregulate cyclin CyclinB1, there was no significant difference between the control group and the control group. Ginsenoside CK could effectively downregulate the level of cyclin CyclinB1. Among them, 20, 40, and 60 μM CK significantly decreased the expression of CyclinB1 ($p < 0.05$).

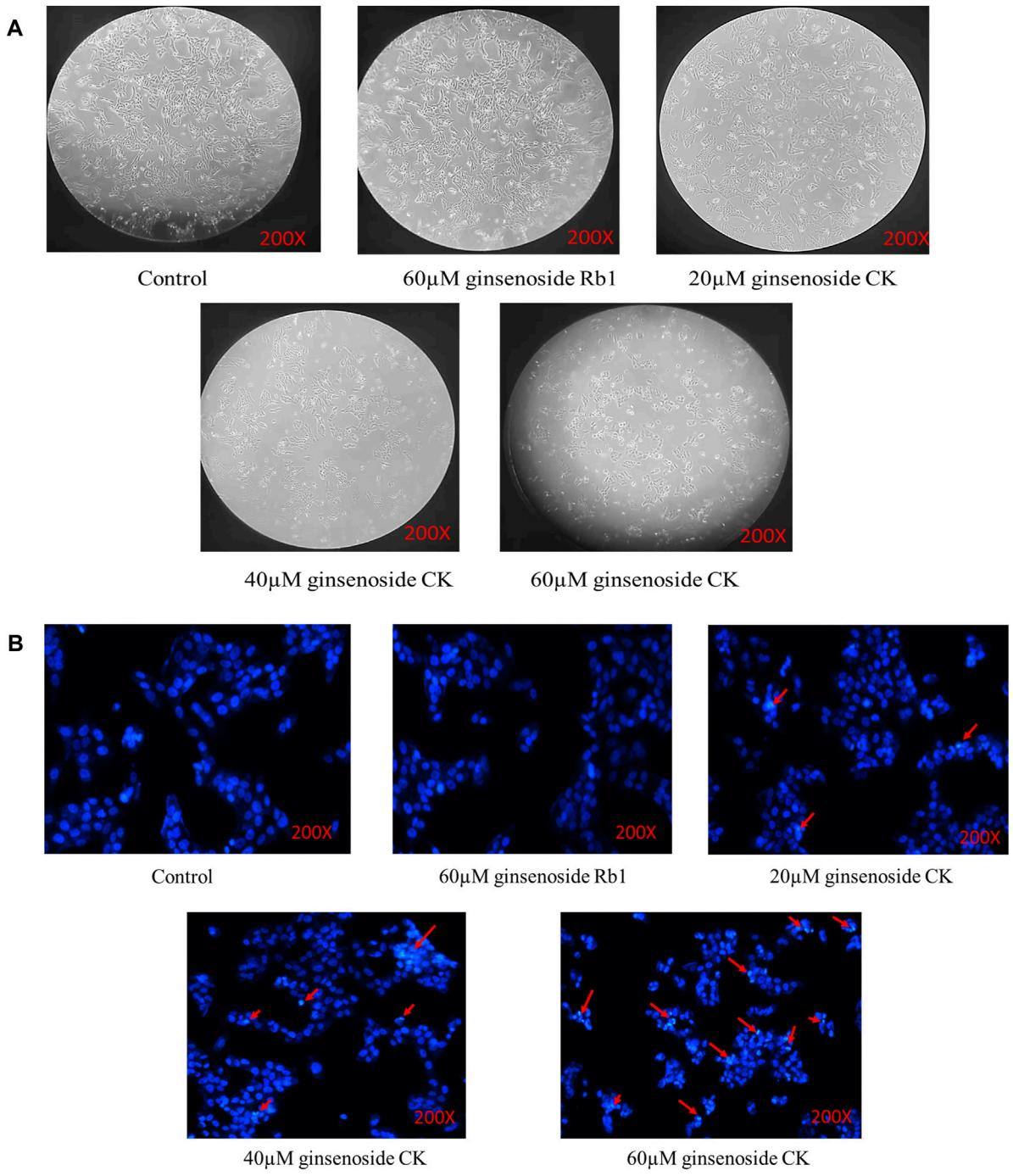

FIGURE 3
Effects of ginsenoside Rb1 and CK on the morphology and apoptosis of HGC-27 cells **(A)** Changes of cell morphology in each group after drug treatment. **(B)** Hoechst33258 staining results.

In addition, compared with the blank group, ginsenoside Rb1 could only regulate cyclin CyclinD1 level in a down trend without significance ($p > 0.05$). Ginsenoside CK could effectively downregulate the level of cyclin CyclinD1 ($p < 0.05$). Among them, 40 and 60 μM CK significantly decreased the expression of CyclinD1 ($p < 0.05$).

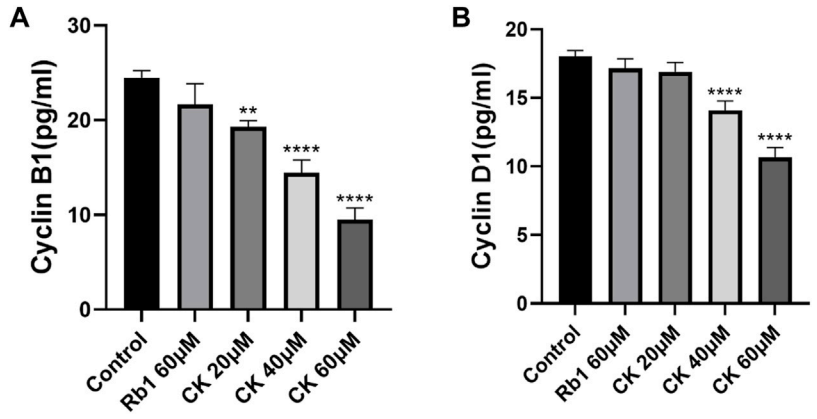

FIGURE 4
Effects of Ginsenoside Rb1 and Ginsenoside CK on Cyclin in HGC-27 **(A)** Histogram comparing the expression of CyclinB1 in each group. **(B)** Histogram comparing the expression of CyclinD1 in each group.

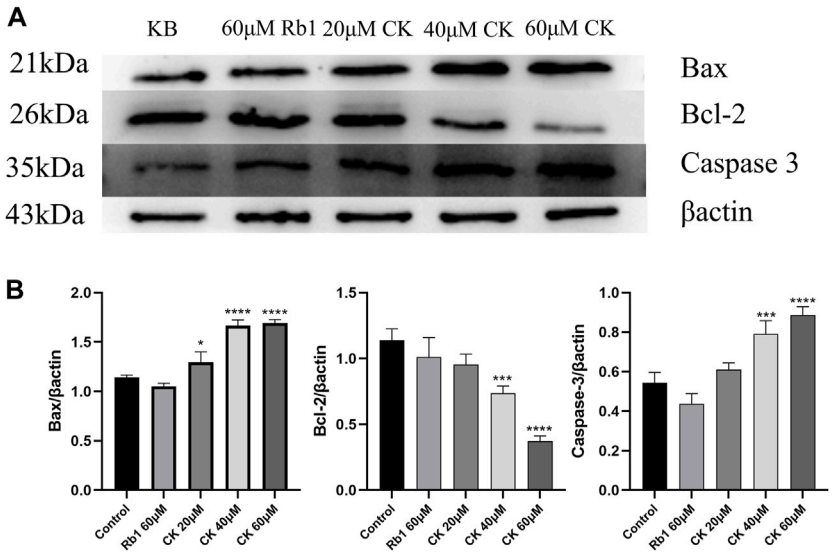

FIGURE 5
Effects of Ginsenoside Rb1 and Ginsenoside CK on Apoptosis-related Proteins in HGC-27 **(A)** Apoptosis-related proteins Bax, Bcl-2, Caspase 3 bands. **(B)** Histogram comparing the expressions of apoptosis-related proteins Bax, Bcl-2, and Caspase 3.

4.2.5 Ginsenoside CK, rather than ginsenoside Rb1, inhibited the expression of anti-apoptosis related protein Bcl-2 and promoted the expression of pro-apoptosis proteins Bax and Caspase 3 in HGC-27 cells

As can be seen from Figures 5A,B, ginsenoside Rb1 did not increase the expression of pro-apoptotic proteins Bcl-2 Associated X Protein (Bax) and Caspase 3 compared with the blank group. In addition, compared with the blank group, ginsenoside Rb1 could only downregulate the expression of anti-apoptotic protein B-cell lymphoma-2 (Bcl-2) in a down trend, without significant significance ($p > 0.05$). In contrast, ginsenoside CK could effectively increase the expressions of pro-apoptotic proteins ($p < 0.05$). Among them, 40 and 60 μM ginsenoside CK could significantly increase the expression of Caspase 3 ($p < 0.05$), and 20, 40, and 60 μM ginsenoside CK

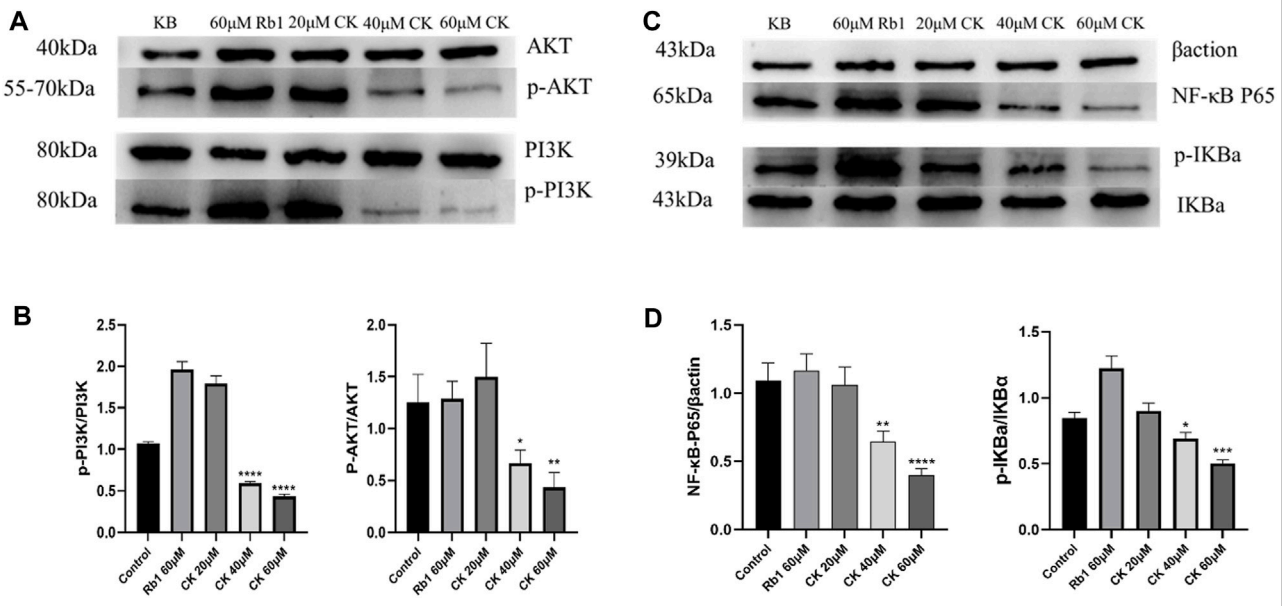

FIGURE 6
Effects of Ginsenoside Rb1 and Ginsenoside CK on Apoptosis-related Pathways Proteins in HGC-27 **(A)** Apoptosis-related pathways PI3K, p-PI3K, AKT, p-AKT bands. **(B)** Histogram comparing the expression of p-PI3K and p-AKT proteins in apoptosis-related pathways. **(C)** Apoptosis-related pathways NF-κB P65, Inhibitor α of NF-κb (IκBα), p-IκBα bands. **(D)** Histogram comparing the expression of NF-κB P65 and p-IκBα in apoptosis-related pathways.

significantly increased the expression of Bax ($p < 0.05$). In addition, ginsenoside CK decreased the expression of Bcl-2, especially at the concentration of 40 and 60 μM ($p < 0.05$).

4.2.6 Ginsenoside CK, rather than ginsenoside Rb1, inhibited the protein expression of PI3K/AKT/NF-κB in HGC-27 cells

As illustrated in Figures 6A,B, ginsenoside Rb1 did not reduce the expressions of p-PI3K and p-AKT proteins compared with the blank group. In contrast, 40 and 60 μM ginsenoside CK significantly decreased the expressions of p-PI3K and p-AKT protein, indicating that middle and high doses of ginsenoside CK inhibited the activation of PI3K/AKT pathway.

Additionally, as shown in Figures 6C,D, compared with the blank group, ginsenoside Rb1 could not reduce the protein expressions of NF-κB p65 and p-I κBα, but promoted the protein expressions of NF-κB p65 and p-IκB α. In contrast, 40 and 60 μM ginsenoside CK significantly decreased the expressions of NF- κB p65 and p-I κB α protein, which suggested that middle and high doses of ginsenoside CK inhibited the activation of NF-κB pathway.

4.2.7 Ginsenoside CK, rather than ginsenoside Rb1, decreased the mRNA level of PI3K/AKT/NF-κB

Compared with the blank group, ginsenoside Rb1 did not significantly downregulate the mRNA expressions of PI3K and AKT as shown in Figures 7A,B. In contrast, ginsenoside CK at 40 and 60 μM could significantly reduce the mRNA expressions of PI3K and AKT, which further confirmed that middle and high doses of ginsenoside CK could also inhibit PI3K/AKT pathway at the gene levels.

As indicated in Figures 7C,D, compared with the blank group, ginsenoside Rb1 could only downregulate the mRNA expressions of NF-κB p65 and NF-κB in a down trend, without significant significance ($p > 0.05$). In contrast, 40, 60 μM ginsenoside K could significantly reduce the mRNA expressions of NF-κB p65 and NF-κB, which further confirmed that middle and high doses of ginsenoside CK could also inhibit NF-κB pathway at the transcriptional level.

5 Discussion

Like most herbal medicines, ginseng is generally consumed orally. When ginseng is administrated orally, its bioavailability is low due to incomplete parent compound absorption and conversion to metabolites. In the intestine, the main metabolic pathway consists of the deglycosylation of ginsenosides (including ginsenoside Rb1) in the intestinal microbiota by progressive cleavage of the sugar fraction (Tawab et al., 2003; Hasegawa, 2004; Liu et al., 2009). Previous studies showed that after ginseng ingestion, Rb1 is converted in the intestine to CK, which is the main metabolite absorbed into the body circulation (Tawab et al., 2003; Qi et al.,

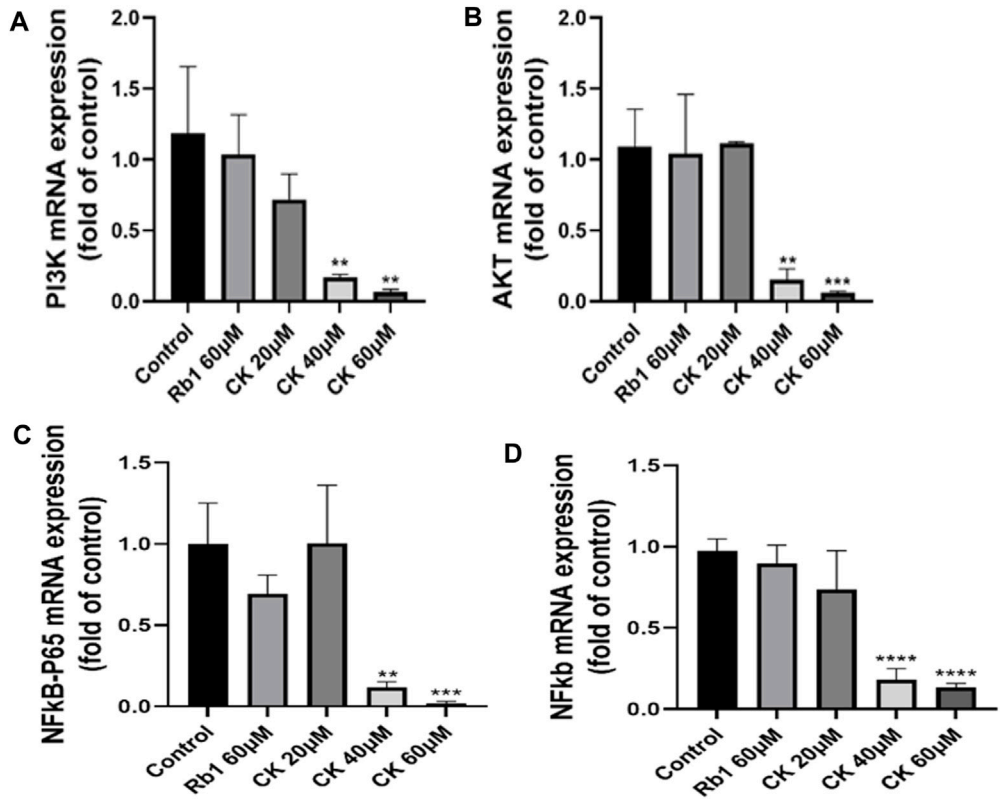

FIGURE 7
Effects of Ginsenoside Rb1 and Ginsenoside CK on apoptosis-related pathways mRNA in HGC-27 **(A)** Histograms comparing the expressions of PI3K mRNA in apoptosis-related pathways. **(B)** Histograms comparing the expressions of AKT mRNA in apoptosis-related pathways. **(C)** Histograms comparing the expressions of NF-κB p65 mRNA in apoptosis-related pathways. **(D)** Histograms comparing the expressions of NF-κB mRNA in apoptosis-related pathways.

2011). As a parent compound, ginsenoside Rb1 itself does not have significant anticancer effects. In contract, ginsenoside CK showed significant anti-proliferative effects in gastric cancer cells (Hu et al., 2012). However, comparative studies on the anti-proliferative effects of ginsenoside CK and Rb1 in human gastric cancer cell lines have not been reported. Therefore, in this study, ginsenoside CK, instead of Rb1, had significant anti-gastric cancer proliferative activity, which was consistent with that of the cell morphological observations. Additionally, hoechst33258 staining results showed that ginsenoside CK induced cell apoptosis in gastric cancer cells treated by ginsenoside CK. ELISA results indicated that ginsenoside CK could effectively downregulate the levels of cyclinB1 and cyclinD1, and western blot results showed that CK inhibited the expression of anti-apoptosis-related protein Bcl-2 and promoted the expression of pro-apoptotic proteins Bax and Caspase 3. The above results tentatively confirmed that ginsenoside CK, the intestinal flora transformant of Rb1, had significant anti-gastric cancer activity but Rb1 showed no any effects, which was similar to the results of Rb1 and CK in colorectal cancer assays (Wang et al., 2012).Network pharmacology was a new discipline based on the theory of systems biology, which analyzed the network of biological systems and selected specific signal nodes for multi-target drug molecular design (Zhang et al., 2019; Wang et al., 2021). In this study, network pharmacology was used to predict the related targets of ginsenoside Rb1 and ginsenoside CK in the treatment of gastric cancer. The biological process of ginsenoside Rb1 obtained by GO analysis was close to cell apoptosis and proliferation. The biological process of ginsenoside CK was closely related to IκB kinase/NF-κB signal pathway. KEGG results showed that the common potential pathways of ginsenoside Rb1 and ginsenoside CK included PI3K-AKT signal pathway, MAPK signal pathway, NF-κB signal pathway, Toll-like receptor signal pathway, TNF signal pathway, Wnt signal pathway and so on. Inhibition of PI3K/AKT/NF-κB pathway was a potential target for cancer treatment (Sha et al., 2014; Pickard et al., 2017; Mao et al., 2019; Lian et al., 2020; Ling et al., 2020; Sun et al., 2020; Zhang et al., 2020). In the study of gastric cancer apoptosis induced by traditional Chinese medicine or compound prescription of traditional Chinese medicine, PI3K/AKT/NF-κB signal pathway axis of apoptosis-related pathway played an important role in the occurrence and development of gastric cancer (Sha et al., 2014).

PI3K/AKT pathway is a classic pathway for activating NF-κB. It has been found in most tumors and used as a target for drug therapy. Studies on gastric cancer cells have shown that after regulation of AKT signal pathway, the expressions of Bax and Bcl-2 proteins can be regulated and apoptosis occurs (Wu et al., 2013; Gou et al., 2015; Wang et al., 2015; Niapour and Seyedasli, 2022). NF-κB plays an important role in regulating cellular response because it is a "fast acting" primary transcription factor that can be activated without new protein synthesis. When NF-κB is activated by corresponding stimulators, expressions of Bax, caspase-3 increased and Bcl-2 are decreased, showing a role in promoting apoptosis (Sun et al., 2014; Li et al., 2015; Rui et al., 2016; Xu et al., 2018b; Shang et al., 2019). Therefore, the authors believed that ginsenoside Rb1 and CK might play a role in the treatment of gastric cancer by inhibiting PI3K/AKT/NF-κB pathway and inducing apoptosis of gastric cancer cells. However, the current network pharmacology results were only conjectures and still needed to be validated by experiments, especially *in vitro* experiments. Therefore, according to the results of network pharmacology, the effect of ginsenoside Rb1 and CK on apoptosis-related pathway PI3K/AKT/NF-κB were investigated. In this study, the levels of NF-κB and PI3K/AKT related proteins were detected by Western blotting and RT-qPCR methods. The results showed that ginsenoside CK could inhibit the PI3K/AKT and NF-κB pathways in both of transcriptional and translational levels, whereas ginsenoside Rb1 had no obvious inhibitory effect.

To sum up, this experiment combines network pharmacology with *in vitro* cell experiment to study the drug action mechanism from the point of view of multi-target, optimizes the complex process of multi-target drug design. The results indicated that ginsenoside Rb1 had no anti-gastric cancer activity, while the intestinal microbiota metabolite of ginsenoside Rb1, ginsenoside CK could effectively exert its anti-gastric cancer activity *in vitro*. Moreover, ginsenoside CK, rather than ginsenoside Rb1, could induce cell apoptosis, and regulate expressions of apoptosis related proteins and cycle-related factors. The underlying mechanism may be attributed to its inhibition of the P13K/Akt/NF-κB signaling pathway. Therefore, ginsenoside CK may be the *in vivo* material basis for the anti-gastric cancer activity of ginsenosides. In conclusion, our study provides a scientific basis for the rational clinical application of ginsenosides, and sheds light on the studies of oral traditional Chinese medicines with low bioavailability and excellent therapeutic effect.

Data availability statement

The original contributions presented in the study are included in the article/Supplementary Material, further inquiries can be directed to the corresponding author.

Author contributions

YW contributed to the drafting of the manuscript. HA obtained funding, designed, conceived and supervised process, and revised the manuscript. Others were involved in searching, screening the search results, translation, and data collection. All the authors have read and approved the final manuscript.

Funding

This work was supported by the Program of National Natural Science Foundation of China (81503272, 81630101), Application Foundation Research Project of Sichuan Provincial Department of Science and Technology (2017JY0188), Xinglin Scholar Research Premotion Project of Chengdu University of TCM (2018016), the National Natural Science Foundation of China (81891012), the Regional Joint Fund of the National Natural Science Foundation of China: Study on the Geoherbalism of Medicinal Materials from Sichuan Tract (U19A2010), National Interdisciplinary Innovation Team of Traditional Chinese Medicine: Multi-dimensional evaluation and multi-disciplinary cross-innovation team of traditional Chinese medicine resources with Southwest characteristics (ZYYCXTD-D-202209), Sichuan Traditional Chinese Medicine Technology Industry Innovation Team: Multidimensional Evaluation of Characteristic Traditional Chinese Medicine Resources and Product Development Innovation Team (2022C001). Sichuan Provincial Administration of Traditional Chinese Medicine Project (2020JC0031).

Conflict of interest

The authors declare that the research was conducted in the absence of any commercial or financial relationships that could be construed as a potential conflict of interest.

Publisher's note

Supplementary material

The Supplementary Material for this article can be found online at: https://www.frontiersin.org/articles/10.3389/fphar.2022.977539/full#supplementary-material

References

Bae, S. H., Kim, D. W., Kim, M. S., Shin, M. H., Park, H. C., and Lim, D. H. (2017). Radiotherapy for gastric mucosa-associated lymphoid tissue lymphoma: Dosimetric comparison and risk assessment of solid secondary cancer. *Radiat. Oncol. J.* 35 (1), 78–89. doi:10.3857/roj.2016.01942

Gou, W. F., Shen, D. F., Yang, X. F., Zhao, S., Liu, Y. P., Sun, H. Z., et al. (2015). ING5 suppresses proliferation, apoptosis, migration and invasion, and induces autophagy and differentiation of gastric cancer cells: A good marker for carcinogenesis and subsequent progression. *Oncotarget* 6 (23), 19552–19579. doi:10.18632/oncotarget.3735

Hasegawa, H. (2004). Proof of the mysterious efficacy of ginseng: Basic and clinical trials: Metabolic activation of ginsenoside: Deglycosylation by intestinal bacteria and esterification with fatty acid. *J. Pharmacol. Sci.* 95 (2), 153–157. doi:10.1254/jphs.fmj04001x4

Hu, C., Song, G., Zhang, B., Liu, Z., Chen, R., Zhang, H., et al. (2012). Intestinal metabolite compound K of panaxoside inhibits the growth of gastric carcinoma by augmenting apoptosis via Bid-mediated mitochondrial pathway. *J. Cell. Mol. Med.* 16 (1), 96–106. doi:10.1111/j.1582-4934.2011.01278.x

Li, W., Fan, M., Chen, Y., Zhao, Q., Song, C., Yan, Y., et al. (2015). Melatonin induces cell apoptosis in AGS cells through the activation of JNK and P38 MAPK and the suppression of nuclear factor-kappa B: A novel therapeutic implication for gastric cancer. *Cell. Physiol. biochem.* 37 (6), 2323–2338. doi:10.1159/000438587

Lian, J., Zou, Y., Huang, L., Cheng, H., Huang, K., Zeng, J., et al. (2020). Hepatitis B virus upregulates cellular inhibitor of apoptosis protein 2 expression via the PI3K/AKT/NF-κB signaling pathway in liver cancer. *Oncol. Lett.* 19 (3), 2043–2052. doi:10.3892/ol.2020.11267

Liang, X. Z., Li, R., Xu, B., Luo, D., Liu, G. B., Peng, J., et al. (2019). Systematic evaluation of the mechanisms of zoledronic acid based on network pharmacology. *Comput. Biol. Chem.* 83, 107097. doi:10.1016/j.compbiolchem.2019.107097

Ling, D., Zhao, Y., Zhang, Z., Li, J., Zhu, C., and Wang, Z. (2020). Morphine inhibits the promotion of inflammatory microenvironment on chronic tibial cancer pain through the PI3K-Akt-NF-κB pathway. *Am. J. Transl. Res.* 12 (10), 6868–6878. PMID: 33194078; PMCID: PMC7653610.

Liu, H., Yang, J., Du, F., Gao, X., Ma, X., Huang, Y., et al. (2009). Absorption and disposition of ginsenosides after oral administration of Panax notoginseng extract to rats. *Drug Metab. Dispos.* 37 (12), 2290–2298. doi:10.1124/dmd.109.029819

Mao, M., Chen, Y., Jia, Y., Yang, J., Wei, Q., Li, Z., et al. (2019). PLCA8 suppresses breast cancer apoptosis by activating the PI3k/AKT/NF-κB pathway. *J. Cell. Mol. Med.* 23 (10), 6930–6941. doi:10.1111/jcmm.14578

Niapour, A., and Seyedasli, N. (2022). Acquisition of paclitaxel resistance modulates the biological traits of gastric cancer AGS cells and facilitates epithelial to mesenchymal transition and angiogenesis. *Naunyn. Schmiedeb. Arch. Pharmacol.* 395 (5), 515–533. doi:10.1007/s00210-022-02217-3

Pickard, J. M., Zeng, M. Y., Caruso, R., and Núñez, G. (2017). Gut microbiota: Role in pathogen colonization, immune responses, and inflammatory disease. *Immunol. Rev.* 279 (1), 70–89. doi:10.1111/imr.12567

Qi, L. W., Wang, C. Z., and Yuan, C. S. (2011). Isolation and analysis of ginseng: Advances and challenges. *Nat. Prod. Rep.* 28 (3), 467–495. doi:10.1039/c0np00057d

Rui, L. X., Shu, S. Y., Jun, W. J., Mo, C. Z., Wu, S. Z., Min, L. S., et al. (2016). The dual induction of apoptosis and autophagy by SZC014, a synthetic oleanolic acid derivative, in gastric cancer cells via NF-κB pathway. *Tumour Biol.* 37 (4), 5133–5144. doi:10.1007/s13277-015-4293-2

Sha, M., Ye, J., Zhang, L. X., Luan, Z. Y., Chen, Y. B., and Huang, J. X. (2014). Celastrol induces apoptosis of gastric cancer cells by miR-21 inhibiting PI3K/Akt-NF-κB signaling pathway. *Pharmacology* 93 (1-2), 39–46. doi:10.1159/000357683

Shang, H., Cao, Z., Zhao, J., Guan, J., Liu, J., Peng, J., et al. (2019). Babao Dan induces gastric cancer cell apoptosis via regulating MAPK and NF-κB signaling pathways. *J. Int. Med. Res.* 47 (10), 5106–5119. doi:10.1177/0300060519867502

Song, Z., Wu, Y., Yang, J., Yang, D., and Fang, X. (2017). Progress in the treatment of advanced gastric cancer. *Tumour Biol.* 39 (7), 1010428317714626. doi:10.1177/1010428317714626

Sun, G., Zheng, C., Deng, Z., Huang, C., and Huang, J. (2020). TRAF5 promotes the occurrence and development of colon cancer via the activation of PI3K/AKT/NF-κB signaling pathways. *J. Biol. Regul. Homeost. Agents* 34 (4), 1257–1268. doi:10.23812/19-520-A

Sun, Y., Zhao, Y., Hou, L., Zhang, X., Zhang, Z., and Wu, K. (2014). RRR-α-tocopheryl succinate induces apoptosis in human gastric cancer cells via the NF-κB signaling pathway. *Oncol. Rep.* 32 (3), 1243–1248. doi:10.3892/or.2014.3282

Sung, H., Ferlay, J., Siegel, R. L., Laversanne, M., Soerjomataram, I., Jemal, A., et al. (2021). Global cancer statistics 2020: GLOBOCAN estimates of incidence and mortality worldwide for 36 cancers in 185 countries. *Ca. Cancer J. Clin.* 71 (3), 209–249. doi:10.3322/caac.21660

Tawab, M. A., Bahr, U., Karas, M., Wurglics, M., and Schubert-Zsilavecz, M. (2003). Degradation of ginsenosides in humans after oral administration. *Drug Metab. Dispos.* 31 (8), 1065–1071. doi:10.1124/dmd.31.8.1065

Wan, Y., Wang, J., Xu, J. F., Tang, F., Chen, L., Tan, Y. Z., et al. (2021). Panax ginseng and its ginsenosides: Potential candidates for the prevention and treatment of chemotherapy-induced side effects. *J. Ginseng Res.* 45 (6), 617–630. doi:10.1016/j.jgr.2021.03.001

Wang, C. Z., Du, G. J., Zhang, Z., Wen, X. D., Calway, T., Zhen, Z., et al. (2012). Ginsenoside compound K, not Rb1, possesses potential chemopreventive activities in human colorectal cancer. *Int. J. Oncol.* 40 (6), 1970–1976. doi:10.3892/ijo.2012.1399

Wang, L., and Yuan, L. (2022). Analysis of ginseng in the treatment of Interstitial Cystitis/Bladder Pain Syndrome based on network pharmacology. *Eur. Rev. Med. Pharmacol. Sci.* 26 (13), 4709–4720. doi:10.26355/eurrev_202207_29196

Wang, X., Wang, Z. Y., Zheng, J. H., and Li, S. (2021). TCM network pharmacology: A new trend towards combining computational, experimental and clinical approaches. *Chin. J. Nat. Med.* 19 (1), 1–11. doi:10.1016/S1875-5364(21)60001-8

Wang, Y. H., Zhou, Z. B., Guo, C. A., Zhai, J., Qi, F. M., and Li, H. L. (2015). Role of mimic of manganese superoxide dismutase in proliferation and apoptosis of gastric carcinoma BGC-823 cells *in vitro* and *in vivo*. *Int. Immunopharmacol.* 26 (2), 277–285. doi:10.1016/j.intimp.2015.04.003

Wu, M., Chen, Y., Jiang, L., Li, Y., Lan, T., Wang, Y., et al. (2013). Type II cGMP-dependent protein kinase inhibits epidermal growth factor-induced phosphatidylinositol-3-kinase/Akt signal transduction in gastric cancer cells. *Oncol. Lett.* 6 (6), 1723–1728. doi:10.3892/ol.2013.1630

Xu, J., Shen, W., Pei, B., Wang, X., Sun, D., Li, Y., et al. (2018b). Xiao Tan He Wei Decoction reverses MNNG-induced precancerous lesions of gastric carcinoma *in vivo* and vitro: Regulation of apoptosis through NF-κB pathway. *Biomed. Pharmacother.* 108, 95–102. doi:10.1016/j.biopha.2018.09.012

Xu, L., Xiao, S., Yuan, W., Cui, J., Su, G., and Zhao, Y. (2018a). Synthesis and anticancer activity evaluation of hydrolyzed derivatives of panaxnotoginseng saponins. *Molecules* 23 (11), 3021. doi:10.3390/molecules23113021

Yao, H., Wan, J. Y., Zeng, J., Huang, W. H., Sava-Segal, C., Li, L., et al. (2018). Effects of compound K, an enteric microbiome metabolite of ginseng, in the treatment of inflammation associated colon cancer. *Oncol. Lett.* 15 (6), 8339–8348. doi:10.3892/ol.2018.8414

Zhang, B., Zhang, Y. F., Li, R., Zhao, L., Qin, S. G., Pan, L. F., et al. (2020). MiR-217 inhibits apoptosis of atherosclerotic endothelial cells via the TLR4/PI3K/Akt/NF-κB pathway. *Eur. Rev. Med. Pharmacol. Sci.* 24 (24), 12867–12877. doi:10.26355/eurrev_202012_24190

Zhang, R., Zhu, X., Bai, H., and Ning, K. (2019). Network pharmacology databases for traditional Chinese medicine: Review and assessment. *Front. Pharmacol.* 10, 123. doi:10.3389/fphar.2019.00123

frontiers | Frontiers in Pharmacology

TYPE Original Research
PUBLISHED 01 December 2022
DOI 10.3389/fphar.2022.999192

OPEN ACCESS

EDITED BY
Guangbo Fu,
Huaian No.1 People's Hospital Nanjing Medical University, China

REVIEWED BY
Dong Bai,
Institute of Basic Theory for Chinese Medicine, China Academy of Chinese Medical Science, China
Nailiang Zhu,
Xinyang Agriculture and Forestry University, China

*CORRESPONDENCE
Deok Chun Yang,
dcyang@khu.ac.kr
Se Chan Kang,
sckang@khu.ac.kr

†These authors have contributed equally to this work and share first authorship

SPECIALTY SECTION
This article was submitted to Experimental Pharmacology and Drug Discovery, a section of the journal Frontiers in Pharmacology

RECEIVED 20 July 2022
ACCEPTED 31 October 2022
PUBLISHED 01 December 2022

CITATION
Ahn JC, Mathiyalagan R, Nahar J, Ramadhania ZM, Kong BM, Lee D-W, Choi SK, Lee CS, Boopathi V, Yang DU, Kim BY, Park H, Yang DC and Kang SC (2022), Transcriptome expression profile of compound-K-enriched red ginseng extract (DDK-401) in Korean volunteers and its apoptotic properties. *Front. Pharmacol.* 13:999192. doi: 10.3389/fphar.2022.999192

Transcriptome expression profile of compound-K-enriched red ginseng extract (DDK-401) in Korean volunteers and its apoptotic properties

Jong Chan Ahn[1†], Ramya Mathiyalagan[1†], Jinnatun Nahar[1], Zelika Mega Ramadhania[1], Byoung Man Kong[2], Dong-Wook Lee[3], Sung Keun Choi[4], Chang Soon Lee[4], Vinothini Boopathi[1], Dong Uk Yang[3], Bo Yeon Kim[5], Hyon Park[5], Deok Chun Yang[1,2]* and Se Chan Kang[1]*

[1]Graduate School of Biotechnology, College of Life Sciences, Kyung Hee University, Yongin-si, South Korea, [2]Department of Oriental Medicinal Biotechnology, College of Life Science, Kyung Hee University, Yongin-si, South Korea, [3]Hanbangbio Inc., Yongin-si, South Korea, [4]Daedong Korea Ginseng Co., Ltd., Geumsan-gun, South Korea, [5]Exercise Nutrition & Biochemistry Lab, Kyung Hee University, Yongin-si, South Korea

Ginseng and ginsenosides have been reported to have various pharmacological effects, but their efficacies depend on intestinal absorption. Compound K (CK) is gaining prominence for its biological and pharmaceutical properties. In this study, CK-enriched fermented red ginseng extract (DDK-401) was prepared by enzymatic reactions. To examine its pharmacokinetics, a randomized, single-dose, two-sequence, crossover study was performed with eleven healthy Korean male and female volunteers. The volunteers were assigned to take a single oral dose of one of two extracts, DDK-401 or common red ginseng extract (DDK-204), during the initial period. After a 7-day washout, they received the other extract. The pharmacokinetics of DDK-401 showed that its maximum plasma concentration (Cmax) occurred at 184.8 ± 39.64 ng/mL, Tmax was at 2.4 h, and AUC_{0-12h} was 920.3 ± 194.70 ng h/mL, which were all better than those of DDK-204. The maximum CK absorption in the female volunteers was higher than that in the male volunteers. The differentially expressed genes from the male and female groups were subjected to a KEGG pathway analysis, which showed results in the cell death pathway, such as apoptosis and necroptosis. In cytotoxicity tests, DDK-401 and DDK-204 were not particularly toxic to normal (HaCaT) cells, but at a concentration of 250 μg/mL, DDK-401 had a much higher toxicity to human lung cancer (A549) cells than DDK-204. DDK-401 also showed a stronger antioxidant capacity than DDK-204 in both the DPPH and potassium ferricyanide reducing power assays. DDK-401 reduced the reactive oxygen species production in HaCaT cells with induced oxidative stress and led to apoptosis in the A549 cells. In the mRNA sequence analysis, a signaling pathway with selected marker genes was assessed by RT-PCR. In the HaCaT cells, DDK-401 and DDK-204 did not regulate FOXO3, TLR4, MMP-9, or p38 expression;

however, in the A549 cells, DDK-401 downregulated the expressions of MMP9 and TLR4 as well as upregulated the expressions of the p38 and caspase-8 genes compared to DDK-204. These results suggest that DDK-401 could act as a molecular switch for these two cellular processes in response to cell damage signaling and that it could be a potential candidate for further evaluations in health promotion studies.

KEYWORDS

fermented red ginseng, compound K (CK), pharmacokinetics, clinical trial, mRNA sequence, antioxidant, cancer, inflammation

Introduction

Traditional Chinese medicine (TCM) is the oldest medicinal practice in history, and its basic rule is to incorporate the principles of Yin and Yang in all of its therapeutics. Various other medical systems, particularly oriental medicine rooted in Chinese medicine, are still considered valid (Borman and Kim, 1966). Given that ginseng is mentioned as a medicinal herb in the Classic Herbal of Shennong, which was written around 100 CE, it is apparent that the therapeutic history of ginseng began in the ancient times (Dharmananda, 2002). Ginseng is a common name for plants in the Panax family. In Chinese, "gin" refers to man, and "seng" means essence; it was known as a gift to man from the deity of the mountains in ancient times. It is also known as a plant made of crystals of the essence needed to cure human diseases (Hu, 1976). In addition to historical references, fossil evidence shows that plants from the Araliaceous family existed 65 million years ago, and the Panax species are about 38 million years old (Court, 2000). The book of Shanghan Lun, written in 220 CE, mentions the medical applications of and methods to measure 107 formulas, of which 21 contain ginseng. Even today, most people practicing TCM follow the formulations of Shanghan Lun. Dharmananda (2002) documented the medical history of ginseng from 220 CE to the 20th century. Experts in various fields, such as oncology (Majeed et al., 2018; Nakhjavani et al., 2019; Yu-hang et al., 2019), central nervous system (Radad et al., 2011), energy metabolism (Zhang et al., 2017), stroke (Liu et al., 2019), depression (Jin et al., 2019), infectious diseases (Nguyen and Nguyen, 2019), neurology (Huang et al., 2019), skin disorders (Kim and Kim, 2018), Parkinson's disease (González-Burgos et al., 2015), autophagy (Wu et al., 2019), inflammation (Ramadhania et al., 2022), diabetes (Zhou et al., 2019), hepatology (Gao et al., 2017), obesity (Li and Ji, 2018), mitochondrial activity (Zhou et al., 2019c), cardiology (Zheng et al., 2012), antimicrobials (Kachur and Suntres, 2016), immune functions (Kang and Min, 2012; Riaz et al., 2019), and molecular signaling pathways (Mohanan et al., 2018), have reviewed the continuous details of ginseng's efficacy to understand how the ginsenosides disrupt diseases as well as their related mechanisms. Ginseng is generally classified into white, red, and black ginseng according to different stages of processing, and all of these ginseng products are available in the market. Depending on the stage of processing, the therapeutic metabolite content varies widely. The different therapeutic functions attributed to products from different steps have been classified previously (Jin et al., 2015; Shin et al., 2019; Zhu et al., 2019). The dried fresh roots are called white ginseng. The process of obtaining red ginseng begins by washing the fresh ginseng roots in water to remove soil particles; then, they are steamed at 90–98 °C for 1–3 h. This process is repeated once or twice more to achieve appropriate gelatinization of the ginseng starch; the product is then dried until the root has a moisture content of 15–18%. This processing method has been used since 1123 CE, although it has been optimized in various ways (Lee et al., 2015). The value of the resulting formulation depends upon the key chemical ingredient, i.e., tri-terpenoid saponins called ginsenosides, which are the key metabolites of ginseng (Christensen, 2008; Liu, 2012; Boopathi et al., 2020). Ginsenosides are classified into major and minor based on their molecular weights. Naturally biosynthesized ginsenosides in plants are called major ginsenosides, and the converted forms are called minor ginsenosides. The conversion method involves hydrolysis of the glycose molecules in the backbone moiety using physical (heat, microwave, and puffing), chemical (acid and alkali), or enzymatic (various glycosidase enzymes, genetic engineering, lactic acid bacteria) techniques. The bioavailability of the major and minor ginsenosides are the key issue in promoting ginsenosides as drug candidates. Ginsenoside compound K (CK) is one of the major metabolites that reaches systemic circulation, where it has its various pharmacological effects (Sharma and Lee, 2020; Murugesan et al., 2022). Recently, the benefits of fermented functional food products (i.e., probiotics) that enhance human gut health and immunity have gained attention for their potential in treating various chronic diseases. The ginseng functional food industry has also risen to leverage the efficacy of ginseng. Another current trend focuses on the advantages of drug combinations over individual drugs, with primarily enhanced efficacy in slowing or reversing disease progression and reduced side effects (Liu et al., 2020). However, choosing effective combinations through trial and error is both tedious and expensive. Therefore, a principle similar to that long used in TCM is suggested to moderate the various side effects without requiring systematic evaluations of the extract formulations (Posadzki et al., 2013). However, such a system needs to

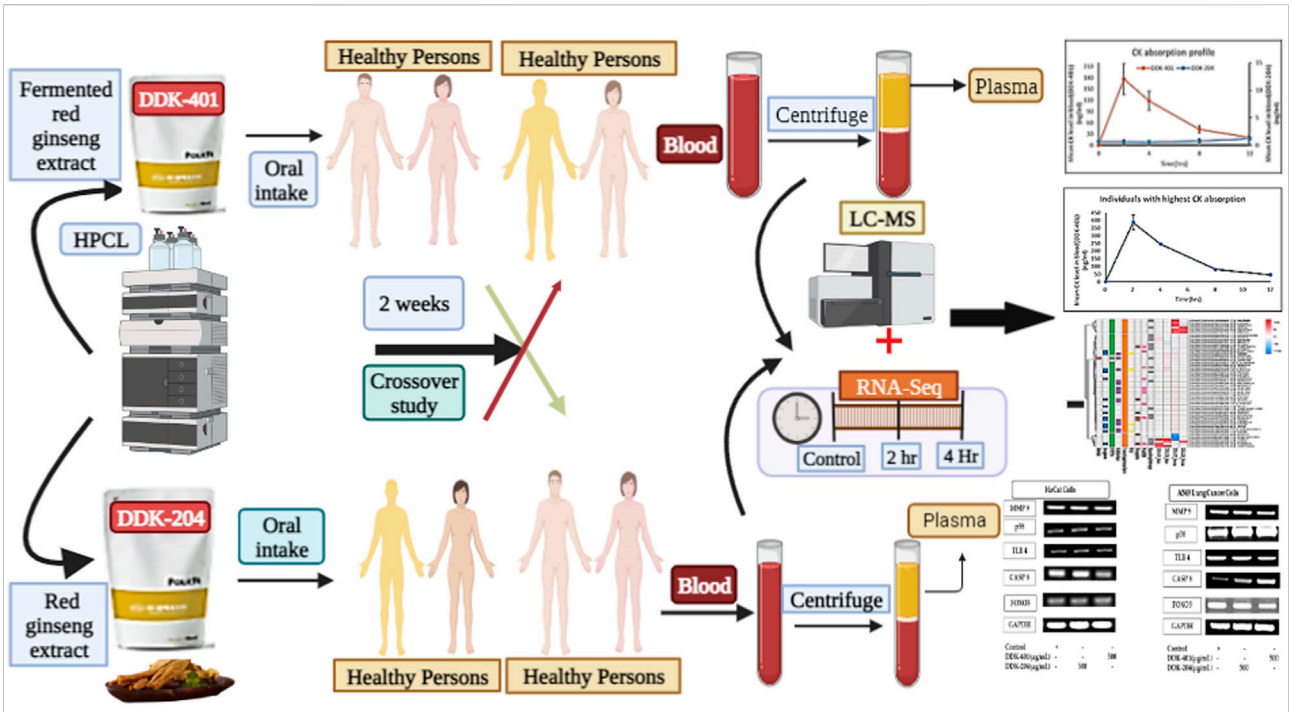

FIGURE 1
Graphical illustration of the fermented red ginseng extract (DDK-401) and red ginseng extract (DDK-204) analyzed by Korean volunteers.

accommodate modern medicine by offering valid evidence when identifying novel drug combinations practically (Shin et al., 2021). Therefore, various studies have been conducted to assess the therapeutic effects of individual ginsenosides as well as crude, red, or fermented red ginseng extracts in animal models and human trials (Lee et al., 2012; Jung et al., 2013; Kim, 2013; Sohn et al., 2013; Choi et al., 2016; Choi et al., 2018; Ban et al., 2021; Panossian et al., 2021), but these datasets are insufficient to conclusively demonstrate the effectiveness of ginseng/ginsenosides at the molecular level. In the present study, we examine a CK-enriched fermented ginseng extract DDK-401 in a human trial with a healthy population to understand its effects on various signaling pathways (Figure 1). Moreover, we elucidate its effects on the functional and therapeutic markers already approved for treating various diseases.

Materials and methods

Ethical committee and study design

A randomized, open-label, single-dose, two-period, two-sequence, crossover study was performed with healthy Korean male and female subjects. This study was performed in accordance with the principles of the Declaration of Helsinki and Korean Good Clinical Practice guidelines. Informed written consent was obtained from each subject in advance. The study was approved by the Institutional Review Board of Kyung Hee University Hospital (KHGIRB-21-419). Eleven healthy male and female Koreans were enrolled in this study, and their age details are shown in Supplementary Table S1. We expected to find large individual variability in the pharmacokinetic profile of CK. To reduce the individual variability in pharmacokinetics caused by sex, we combined and calculated the means of the pharmacokinetic data from the male and female groups separately. The exclusion criteria were any significant clinical illness within 2 weeks before the study, i.e., history of high blood pressure, diabetes, and cardiovascular, hepatic, renal, hematological, gastrointestinal, neurologic, or psychiatric disease; blood donation within 8 weeks before the study; and use of any medications, including prescription and over-the-counter drugs, within 2 weeks before the study. In addition, subjects who previously experienced adverse reactions to ginseng were excluded.

The enrolled subjects were assigned to receive a single oral dose of one of two extracts, DDK-401 (100 mL spout pouch, combination of well-known representative ginsenosides Rg1, Rb1, and Rg3 at 21.51 mg and ginsenoside CK at 31.19 mg) or DDK-204 (100 mL spout pouch, ginsenosides Rg1, Rb1, and Rg3 at 11.29 mg and ginsenoside CK at 0 mg) during the first period. After a 7-day washout, each subject received the other extract. The dose for oral administration was chosen based on

the recommended total daily intake of each investigational product.

DDK-401 and DDK-204 extract preparations

CK-enriched fermented ginseng extract (DDK-401) and common red ginseng extract (DDK-204) were supplied by Deadong Korea Ginseng Co., Ltd. (Geumsan, Korea). First, the red ginseng powder was dissolved in a mixture of water and food-grade alcohol and extracted at 75 ± 5 °C. This extraction procedure was repeated 4 times. Then, the supernatant was collected and evaporated at 60 ± 5 °C with 500–760 mmHg vacuum until the sugar content was 65 brix and solid content was ≥60%. Finally, the sample was sterilized at 80–85 °C for 30–40 min and aged at 60 ± 5 °C for 24–75 h; this product was named DDK-204 and used as the control.

Second, the red ginseng concentrate (60 brix) was diluted in water until the solid content was 5%. Then, an enzyme mixture (pectinase and β-glucosidase) was added to the diluted red ginseng concentrate at a concentration of 3% and reacted at 60 ± 2 °C for 114–168 h at 3000 rpm. Thereafter, the enzyme was inactivated at 90 °C for 30 min. Next, the sample was evaporated at 55 ± 5 °C and 500–760 mmHg vacuum until the solid content reached 40%. Then the sample was dissolved in 80% food-grade alcohol and incubated for 1–2 h. Following this, centrifugation was performed at 0.5 m^3/h for 5–6 h, and the supernatant was collected. A second evaporation was then performed at 55 ± 5 °C and 500–760 mmHg vacuum until the sugar content was 65 brix and solid content was ≥60%. The concentrate was then fermented with a mixture of *Lactobacillus* species at 1% concentration and 37 °C for one day. The resulting CK-enriched red ginseng concentrate was named DDK-401 and stored in the refrigerator until it was used for the analysis and bioassays.

Chromatographic conditions for analyzing the ginsenoside profiles of DDK-401 and DDK-204

One g each of DDK-401 and DDK-204 were dissolved in 50 mL of 70% methanol and filtered with a 0.45 μm membrane filter. The samples were then injected into an Ultimate 3000 HPLC system with a PRONTOSIL 120-5-C18 ACE-EPS (250 × 4.6 mm i.d., 5 μm particle size) (Bischoff Chromatography, Leonberg, Germany). The mobile phase consisted of water (solvent A) and acetonitrile (solvent B) in the following gradients: 0–10 min, 20% B; 10–42 min, 29% B; 42–67 min, 41% B; 67–70 min, 47% B; 70–90 min, 71% B; 90–95 min, 71% B. The flow rate of the mobile phase was 1.0 mL/min, and an injection volume of 10 μL was used in the quantitative analysis. The column temperature was maintained constant at 40 °C. The ginsenoside profiles were determined at 203 nm.

Preparation of standard solution for quantitative calibration

A standard stock solution of 10% was prepared by dissolving accurately weighed quantities of the standard for each ginsenoside in high-performance liquid chromatography (HPLC)-grade methanol. These stock solutions were then diluted with HPLC-grade methanol to 200, 100, 50, 25, and 12.5 μg/mL concentrations as working solutions for the quantitative calibrations. The calibration curves and quantitative evaluations were then obtained at 203 nm.

Pharmacokinetic assessment

The quantitative determination of CK concentration in the plasma was achieved using 2 mL of intravenous blood collected from each volunteer before administration and at 2, 4, 8, and 12 h after dosing during each period. The blood samples were centrifuged at 3000 rpm for 10 min, and the supernatant was separated and frozen at -80 °C until analysis. The plasma concentrations of ginsenoside CK were determined by PCAM KOREA Co., Ltd. (Daejeon, Korea) using a HPLC–tandem mass spectrometry system. The chromatographic analysis was performed using a Waters I-class (Waters, USA), with Berberine (Dr. Ehrenstorfer GmbH, Germany) as the internal standard. Chromatographic separation was achieved with an Acquity UPLC BEH C18 column (100 mm × 2.1 mm, 1.7 μm; Waters, USA) maintained at 45 °C. The mobile phase was a gradient of 0.1% formic acid in water and 100% acetonitrile. Mass spectrometry was performed in the positive mode on an API Xevo TQ-XS instrument (Waters, USA) equipped with an electrospray ionization probe. The temperature of the ion source was set to 150 °C, and the voltage of the ion spray was 3 kV. The quantifications were performed by multiple reaction monitoring of the transitions at 645.2–203 nm for ions of ginsenoside CK, with a dwell time of 11.28 min. To validate the quantitative data in terms of linearity, the limit of detection (LOD) and limit of quantification metrics were calculated (Supplementary Table S2).

RNA-sequencing and analysis

The total mRNA was extracted from each blood plasma sample to build the mRNA-seq libraries that were generated using a TruSeq stranded mRNA LT sample prep kit (Illumina, San Diego, CA, USA) following manufacturer protocols and

sequenced using a Novaseq 6000 sequencing system (Illumina). The reads were trimmed with Trimmomatic (Bolger et al., 2014) to remove any adapters and low-quality reads, resulting in clean reads for improved paired-end mapping. The trimmed reads were mapped to the *Homo sapiens* reference genome (GRCm38) transcriptome using Salmon software version 1.3.0 (Patro et al., 2017). Differential gene expressions among the three experimental groups were evaluated using edgeR (version 3.30.3) software (McCarthy et al., 2012). The differentially expressed genes were identified based on a cutoff threshold of $p < 0.05$ and log-fold change >1 before being subjected to further analyses.

Functional annotations

Functional annotations for each gene were made using the drug discovery protocol. The seven datasets used are included in Supplementary Table S3: DrugBank (Wishart et al., 2018), Human Protein Atlas (Uhlén et al., 2015), STITCH (Szklarczyk et al., 2016), Surfaceome (Bausch-Fluck et al., 2018), Tumor Suppressor Gene Database v2.0 (TSGene) (Zhao et al., 2016), pepBDB (Wen et al., 2019), and Comparative Toxicogenomics Database (Grondin et al., 2021). First, entered the DrugBank ID for each gene to navigate the details of known drugs from the complete database xml file. Second, downloaded the FDA-approved potential drug candidate list from the Human Protein Atlas database. Third, searched STITCH to observe small-molecule drug interactions. Fourth, used Surfaceome to understand the cell surface proteins. Fifth, used TSGene to obtain the cancer therapeutic gene candidates. Sixth, observed the peptide-binding protein interactions.

Cell cytotoxicity assay

Cell cultures

Immortalized human epidermal keratinocyte (HaCaT) and murine macrophage RAW 264.7 cells were cultured in Dulbecco's modified Eagle's medium (DMEM) supplemented with 10% fetal bovine serum (FBS) and 1% penicillin-streptomycin. Generally, 89% Roswell Park Memorial Institute (RPMI) 1640 with 10% FBS and 1% penicillin-streptomycin were used to culture the human lung carcinoma cells (A549). All three cell lines were allowed to adhere and develop for 24 h before being treated with different samples in a humidified 37 °C incubator with a 5% CO_2 atmosphere.

Cell cytotoxicity assay

We evaluated the cytotoxicities of DDK-401 and DDK-204 on the HaCaT and RAW 264.7 cells using an MTT colorimetric assay, which was performed in 96-well plates (Mathiyalagan et al., 2019; Pu et al., 2021). Seeding was performed at 5×10^4 cells/well (HaCaT) and 1×10^4 cells/well (RAW 264.7), and the 96-well plates were incubated at 37 °C in a humidified atmosphere of 5% CO_2 for 24 h (Ramadhania et al., 2022). Subsequently, the cells were treated with various concentrations of DDK-401 or DDK-204 in serum-free-medium at 62.5, 125, 250, and 500 μg/mL for the HaCaT cells and at 25, 50, 100, 250, and 500 μg/mL for the RAW 264.7 and A549 cells, followed by incubation for 24 h. Then, 20 μL of MTT (5 mg/mL, phosphate-buffered saline (PBS), Life Technologies, Eugene, OR, USA) were added to the cells at 37 °C for 4 h. The insoluble formazan was dissolved by placing 100 μL of dimethylsiloxane (DMSO) in each well and absorbance was measured at 570 nm using an enzyme-linked immunosorbent assay (ELISA) microplate reader (Bio-Tek, Instruments, Inc., Winooski, VT, USA).

Antioxidant assay

In vitro DPPH assay

The 2,2-diphenyl-1-picryl-hydrazyl (DPPH) method was used with a slight modification to estimate the free-radical scavenging activities of the samples (Subbiah et al., 2020). DPPH (0.2 mM) was dissolved with ethanol (pro-analysis grade) to obtain a DPPH radical solution. Then, 20 μL of the sample extract and 180 μL of the DPPH solution were added to a 96-well plate and incubated at 25 °C for 30 min in the dark, followed by absorbance measurement at 517 nm. Vitamin C (ascorbic acid) standard curves with concentrations from 0 to 100 μg/mL were used to determine the DPPH radical scavenging activity, which is expressed in milligrams of ascorbic acid equivalent per gram (mg AAE/g) of the extract.

Reducing power assay

The reducing capacity of a compound indicates its potential antioxidant activity. To conduct this assay (Akter et al., 2021), 100 μL of various concentrations of the samples were mixed with 250 μL of 0.2 mM phosphate buffer (pH 6.6) and 250 μL of 1% potassium ferricyanide. The mixtures were then incubated at 50 °C for 20 min. After cooling, 250 μL of 10% trichloroacetic acid was added to the mixtures and centrifuged at 3000 rpm for 10 min. Then, 50 μL of the upper layer of each mixed solution was transferred and mixed with 50 μL of distilled water and 250 μL of 0.1% ferric chloride solution in a 96-well plate. The absorbance was then measured at 700 nm using a UV spectrometer microplate reader (Bio-Tek, Instruments, Inc., Winooski, VT, USA). Vitamin C was used as the standard, and a blank solution was prepared by omitting the sample; the results are expressed as mg AAE/g of extract.

Reactive oxygen species generation assays in HaCaT and lung cancer cells

Effects of DDK-401 on reactive oxygen species production in HaCaT cells under oxidative stress

Intracellular reactive oxygen species (ROS) were determined using the 2′,7′-dichlorodihydro-fluorescein diacetate (DCFH-DA) reagent, as described by Pu et al. (2021), with a slight modification. Briefly, HaCaT cells (5×10^4 cells/well) were seeded in a 96-well plate (Nest Inc., Corning, NY, USA) and incubated for 24 h at 37 °C and 5% CO_2. To assess the antioxidant activity, the cells were treated with H_2O_2 (500 μmol/L) for 2 h, and the supernatant was aspirated. The cells were then either treated or not treated with different concentrations of the samples for 24 h. Vitamin C was used as the positive control. After washing the cells twice with PBS, we added 20 μM DCFH-DA in PBS and incubated them for another 20 min. The supernatant was next removed by washing the cells with PBS twice, and a multimodal plate reader was used to measure the fluorescence intensity at an excitation wavelength of 485 nm and emission wavelength of 528 nm.

Effects of DDK-401 on reactive oxygen species production in A549 cells under oxidative stress

To detect the ROS intensity of human lung cancer cells (A549), we used the DCFH-DA reagent with fluorescent image capture technique. We plated the cells at a density of 1×10^4 cells/well in 96-well culture plates, allowed them to adhere, and then placed them in an incubator overnight to achieve 100% confluency. The A549 cells were then treated with various concentrations of DDK-401 or DDK-204 (0, 25, 50, 100, 250, and 500 μg/mL) for 24 h. The next day, the cells were stained by adding 100 μL of DCFH-DA solution (10 μM) to each well and incubated in the dark for 30 min. The old media were discarded, and the cells were washed twice with 1× PBS (100 μL/well). A multimodal plate reader (spectrofluorometer) was used to determine the fluorescence intensity caused by ROS production at an excitation wavelength of 485 nm and emission wavelength of 528 nm.

Inflammation inhibition assay

The detection of nitric oxide (NO) levels has been described previously (Ramadhania et al., 2022). The RAW 264.7 cells (1×10^4) were placed in 24-well culture plates and incubated for 24 h at 37 °C in a humidified environment with 5% CO_2. Then, they were treated with different concentrations of DDK-401 or DDK-204 (0, 25, 50, 100, 250, and 500 μg/mL) for 1 h. In the presence of the samples, 1 μg/mL lipopolysaccharide (LPS) was used as the stimulator, and the treated cells were placed in an incubator for one day. The nitrite levels in the cell media were determined using the Griess reagent: 100 μL of the stimulated supernatant was mixed with an equivalent volume of the Griess reagent. A microplate reader was used to compare the absorbance at 540 nm with a standard curve obtained using sodium nitrite (BioTek Instruments, Inc.). L-NMMA (50 μM), a standard inhibitor, was used as the positive control in this experiment. Each assay was repeated three times, and the results are expressed in terms of percentage of NO production.

TABLE 1 List of primers and their sequences used for mRNA gene expression validation by RT-PCR.

Gene	Primer sequence (5′-3′)
FOXO3	F: TCA AGG ATA AGG GCG ACA GC
	R: GGA CCC GCA TGA ATC GAC TA
TLR4	F: GAG GAC TGG GTG AGA AAC GA
	R: GAA ACT GCC ATG TCT GAG CA
Caspase 8	F: AGA GTC TGT GCC CAA ATC AAC
	R: GCT GCT TCT CTC TTT GCT GAA
MMP 9	F: CGT CGT GAT CCC CAC TTA CT
	R: AGA GTA CTG CTT GCC CAG GA
p38	F: CGA CTT GCT GCT GGA GAA GAT GC
	R: TCC ATC TCT TCT TGG TCA AGG
GAPDH	F: CAA GGT CAT CCA TGA CAA CTT TG
	R: GTC CAC CAC CCT GTT GCT GTA G

Reverse transcription polymerase chain reaction (RT-PCR)

The total RNA was extracted using QIAzol lysis reagents (QIAGEN, Germantown, MD, USA), and the reverse transcription reactions were performed using 1 μg of total RNA in 20 μL of the reaction buffer with an amfiRivert reverse transcription kit (GenDepot, Barker, TX, USA), according to manufacturer instructions. The obtained cDNA was amplified with primers, as shown in Table 1. The reaction was cycled 35 times: 30 s at 95 °C, 30 s at 60 °C, and 50 s at 72 °C. Using 1% agarose gels, the amplified RT-PCR products were analyzed, visualized using Safe-Pinky DNA Gel Staining (GenDepot, Barker, TX, USA), and imaged under ultraviolet light.

Statistical analysis

All experiments were performed at least in triplicate ($n = 3$) unless stated otherwise. The experimental data are reported as mean ± standard error (SEM). Statistical significances between the control and sample groups were evaluated by Student's t-test with a two-tailed distribution and two-sample equal variances. A greater extent of statistical significance is indicated by an increasing number of asterisks (*$p < 0.05$, **$p < 0.01$, and

TABLE 2 Ginsenoside profiles of DDK-401 and DDK-204 for *in vivo* pharmacokinetic assessments.

Samples	Rg1	Re	Rf	Rb1	Rg2	Rc	Rb2	Rb3	Rd	F2	Rg3	Rk1	Rg5	CK	Total (mg/g)
DDK-401 Fermented Ginseng Extract	1.66 ± 0.035	2.77 ± 0.025	0.38 ± 0.046	5.26 ± 0.123	2.35 ± 0.059	3.08 ± 0.061	3.6 ± 0.095	0.22 ± 0.010	1.05 ± 0.055	0.00 ± 0.000	0.78 ± 0.026	0.63 ± 0.080	0.5 ± 0.025	**10.69 ± 0.040**	32.98 ± 0.284
DDK-204 Red Ginseng Extract	0.96 ± 0.026	1.41 ± 0.031	0.39 ± 0.020	2.87 ± 0.051	0.22 ± 0.005	1.46 ± 0.026	1.17 ± 0.049	0.15 ± 0.040	0.57 ± 0.055	0.00 ± 0.000	0.22 ± 0.031	0.17 ± 0.021	0.15 ± 0.040	**0.00 ± 0.000**	9.72 ± 0.208

***$p < 0.001$) and hash markers (#$p < 0.05$, ##$p < 0.01$ and ###$p < 0.001$). The hash marker (#) indicates significance between the normal and stimulated controls, and the asterisk (*) indicates significant differences between the stimulation groups (DDK-204 or DDK-401).

Results and discussion

Ginsenoside absorption profiling after oral intake

Preparation of DDK-401 and DDK-204

Ginsenosides and ginseng extracts have been reported to have various pharmacological effects, and ginseng has been used as a medicinal herb in TCM for several centuries. However, ginsenosides are mainly absorbed in the gastrointestinal tract after the gut microbes hydrolyze the linear carbohydrates from their backbones. In addition, the minor ginsenosides, which have only one or no glycose moieties, generally reach the systemic circulation. Thus, the absorption and bioavailability of ginsenosides greatly depend on the gastrointestinal bioconversion ability of each individual, and the minor saponins must be enriched by various processing technologies. Bioconversion techniques such as puffing (Pu et al., 2021) and heat treatment (steaming) do not produce ginsenoside CK (Piao et al., 2020), which is one of the active metabolites that reaches systemic circulation and has various pharmacological activities (Sharma and Lee, 2020). Therefore, the pharmacologically active minor saponin CK must be enriched by the edible enzymes in the ginseng extract to maximize its biological activity irrespective of an individual's gut function. This study, we aimed to increase the total ginsenoside and CK content using pectinase and β-glucosidase enzymes to begin the glucose hydrolysis of major ginsenosides in red ginseng concentrate, such as Rb1, Rd, and Rg3. We performed additional fermentation with *Lactobacillus* species at 37 °C for 1 day to accelerate the hydrolysis of the glucose molecules from the major ginsenosides to increase CK production (Table 2). The synthesis of CK has been mainly reported from the hydrolysis of glycose molecules of the major ginsenosides, such as Rb1, Rb2, Rd, Rc, compound O, compound Y, compound Mc, Rg3, gypenoside XVII, and F2 (Sharma and Lee, 2020). As a result of the above processes, the fermented red ginseng extract (DDK-401) was enriched, with 10 mg/g of CK and 32.98 mg/g of total ginsenoside content, compared to the control red ginseng extract (DDK-204), which contained 9.72 mg/g of total ginsenosides and without CK. The CK was thus clearly produced by the fermentation process and not the steaming process (Piao et al., 2020). It was previously reported that the bioconversion and fermentation of red ginseng yields CK in Korean ginseng (Choi et al., 2016; Fukami et al., 2018).

Ginsenoside absorption profiling after oral intake of DDK-401

After oral intake, the human volunteers showed greater CK absorption from the fermented DDK-401 extract than from the control red ginseng extract (DDK-204) (Figure 2A). The T_{max} was 2.4 h, C_{max} was 184.8 ± 39.64 ng/mL, and AUC_{0-12h} was 920.3 ± 194.70 ng·h/mL for DDK-401, whereas the T_{max} was 12 h, C_{max} was 2.5 ± 1.09 ng/mL, and AUC_{0-12h} was 11.3 ± 4.66 ng·h/mL for DDK-204 (Table 3). These pharmacokinetic patterns are similar to those in other reports (Sharma and Lee, 2020). Although various studies have reported enhanced CK absorption after oral administration of fermented red ginseng extract, the concentration of CK in the blood plasma still varies by individual, as shown in Figure 2B (individuals with the highest CK absorption profiles).

Variations in the CK absorption profiles between male and female groups

Although high CK absorption has been reported previously (Sharma and Lee, 2020), differences in the absorption patterns between males and females following oral intake of fermented red ginseng extract have not been explored. Our results indicate that as a group, the female volunteers absorbed more CK (Figure 3B) than the male volunteers (Figure 3A), although this pattern also applied to individual female and male volunteers (Figure 3C). Similarly, the female volunteers were previously reported to absorb higher concentrations of CK than males after oral doses of a high concentration of CK (Chen et al., 2017).

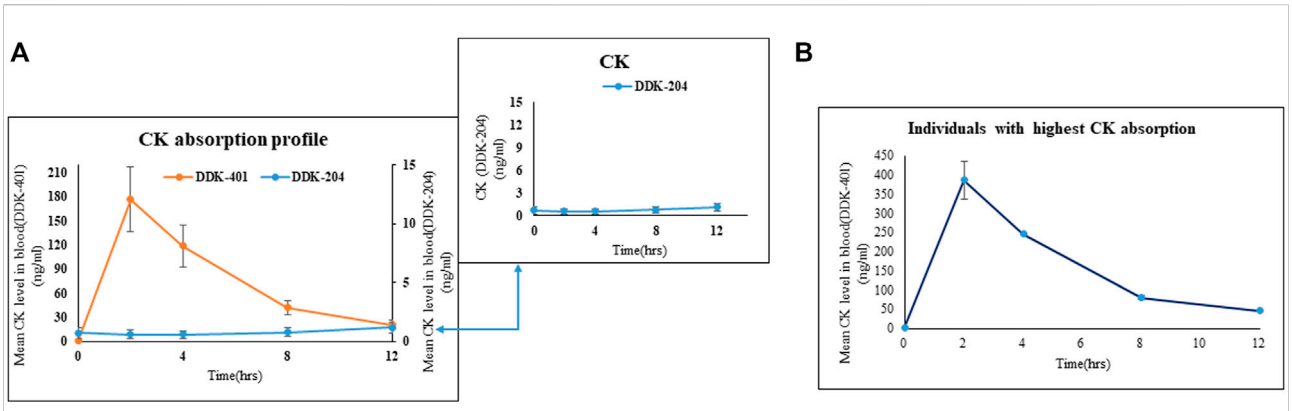

FIGURE 2
Absorption profiles of CK in human blood after oral intake of fermented red ginseng extract (DDK-401) and red ginseng extract (DDK-204). **(A)** Mean CK level. Inset shows the mean CK absorption profile after DDK-204 intake. **(B)** Mean CK level from individuals with highest CK absorption in this study.

TABLE 3 Pharmacokinetic parameters of CK in human blood after oral intake of fermented ginseng extract (DDK-401) and red ginseng extract (DDK-204).

Parameters	DDK-401	DDK-204
T_{max} (h)	2.4 ± 0.27	12.0 ± 0.00
C_{max} (ng/mL)	184.8 ± 39.64	2.5 ± 1.09
$AUC_{0\text{-}12h}$ (ng·h/mL)	920.3 ± 194.70	11.3 ± 4.66

RNA sequence analysis of blood plasma after oral intake of samples

Differential gene expression and KEGG pathway enrichment

As explained in the *Pharmacokinetic Assessment* section, whole mRNA transcripts were assessed against the human reference genome for genome-wide differential transcript expressions. The samples were grouped into four categories, namely DDK-401 (male and female) and DDK-204 (male and female). Overall, 701 transcripts were found to have differential expressions (Supplementary Table S3), and the transcripts overlapped among the groups, as illustrated in a Venn diagram (Supplementary Figure S1). The transcripts belonging to the tumor suppressor genes category are displayed in a heatmap (Figure 4). Overall, nine annotations were included in this study, as explained earlier. In addition, all differentially expressed genes were subjected to KEGG pathway enrichment in the David online webserver, which showed that the cell death pathways, such as apoptosis and necroptosis, were enriched by the extract treatments (Supplementary Table S4). Finally, we selected gene candidates (FOXO3, cysteine-aspartic protease 8 (caspase-8), toll-like receptor 4 (TLR4), and matrix metallopeptidase 9 (MMP-9)) for the RT-PCR expression analysis because these are known to be involved in the signaling and cell-death pathways as well as tumor suppression.

Effects of DDK-401 on the viabilities of HaCaT and lung cancer cells

The cytotoxicities of DDK-401 and DDK-204 to HaCaT cells was determined for safety purposes. The HaCaT cells represent normal cell conditions, and lung cancer cells (A549) were used to examine the apoptosis signaling pathway. Each sample was evaluated at various sample concentrations (62.5, 125, 250, and 500 μg/mL in HaCaT and 25, 50, 100, 250, and 500 μg/mL in A549 cells). As shown in Figure 5, at concentrations less than 500 μg/mL, both DDK-401 and DDK-204 were nontoxic to HaCaT cells. In the A549 cells, DDK-401 demonstrated minimal toxicity after 24 h at 250 μg/mL. At a concentration of 500 μg/mL after 24 h, DDK-401 showed significantly decreased cancer cell proliferation than DDK-204. Moreover, A549 cell viability was reduced by DDK-401 in a dose-dependent manner. The cytotoxicity results in this investigation match those in a previous report (Yu et al., 2018).

The results shown in Figure 5 indicate that at 500 μg/mL, DDK-401 and DDK-204 were only mildly toxic, from which it can be concluded that both substances are relatively safe when cell conditions are normal. On the other hand, in lung cancer A549 cells, which represent cell damage and imbalanced conditions, DDK-401 had a much higher toxicity than DDK-204, producing apoptosis of the cancer cells.

Antioxidant content shown by DPPH assay and ROS generation in HaCaT and cancer cells

Antioxidant capacity: DPPH and reducing power assays

The DPPH scavenging and potassium ferricyanide reducing power assays were used to evaluate the antioxidant capacities of DDK-401 and DDK-204, and the results are shown in Table 4.

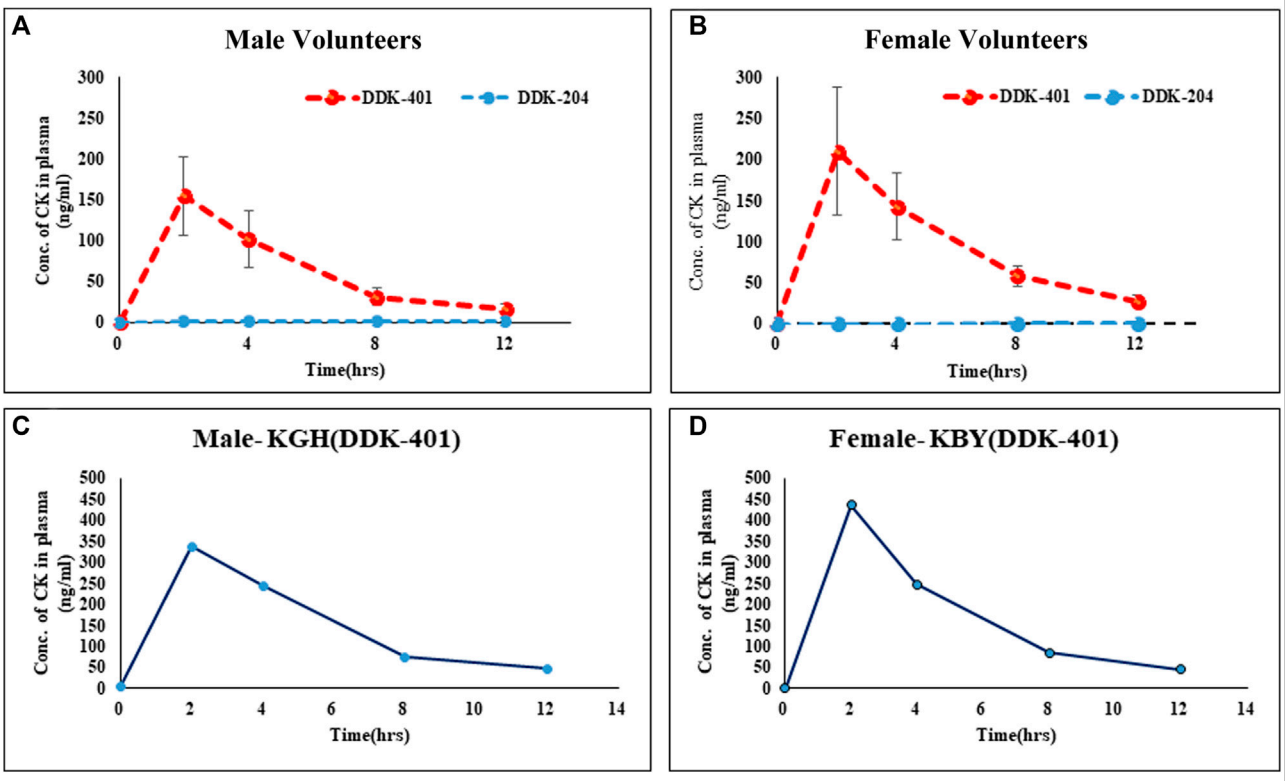

FIGURE 3
Absorption profiles of CK in human blood serum after oral intake of fermented red ginseng extract (DDK-401) and red ginseng extract (DDK-204): **(A)** male volunteers, **(B)** female volunteers; maximum CK absorption in individual **(C)** male and **(D)** female.

The most frequently used antioxidant standard for these assays is vitamin C; therefore, the results of the DPPH and potassium ferricyanide reducing power assays are expressed in terms of mg AAE/g of the extract. These assays are widely used to determine the antioxidant properties of compounds as free radical scavengers or hydrogen donors (Warinhomhoun et al., 2021) as well as the ability of the compounds to transform from Fe^{3+}/ferricyanide complex to Fe^{2+}/ferrous forms (Aryal et al., 2019). DDK-401 showed higher antioxidant abilities in both the DPPH and potassium ferricyanide reducing power assays, with values of 0.093 ± 0.02 and 0.340 ± 0.001 mg AAE/g of extract, respectively. In the DPPH assay, the antioxidant capacity of DDK-401 was generally 2 times higher than that of DDK-204, and in the potassium ferricyanide reducing power assay, it was 3 times higher than that of DDK-204. In agreement with a previous study (Jung et al., 2019; Park et al., 2021), we found that CK-enriched ginseng extract (DDK-401) exhibited greater antioxidant activity than the common red ginseng extract (DDK-204). This result could be attributed to CK's potential for radical scavenging activity in antioxidant assays (Baik et al., 2021). Antioxidants, whether endogenously produced or supplied by external sources, can scavenge ROS and reduce cellular oxidation, thereby alleviating oxidative stress (Liu et al., 2018).

Effect of DDK-401 on ROS production in HaCaT cells with H_2O_2-induced oxidative stress

We used the DCFH-DA assay to investigate the antioxidant properties of DDK-401 and determine whether it could reduce accumulated intracellular ROS in H_2O_2-induced HaCaT cells. Commonly, H_2O_2 is used to induce intracellular ROS and produce imbalance in the cellular oxidant–antioxidant levels. Because the mitochondria are the major sources of ROS, mitochondrial dysfunction caused by excess ROS can lead to apoptosis and DNA damage (Zhang et al., 2020). The mean value of the ROS levels measured in the group treated with 500 μM H_2O_2 was 260% higher than that in the control group. The trend of decreased cell viability after H_2O_2 exposure is shown in Figure 6A. Vitamin C was used as the positive control. For H_2O_2-induced oxidative stress in the HaCaT cells, DDK-401 was stronger than DDK-204 in a dose-dependent manner. At a concentration of 250 μg/mL, DDK-401 and DDK-204 reduced ROS levels by an average of 23% and 7%, respectively, compared with the group treated with only H_2O_2 (Figure 6A). These results may be attributed to the CK in DDK-401; previous studies have reported that CK activates the NF-κB and JNK pathways, which contribute to the

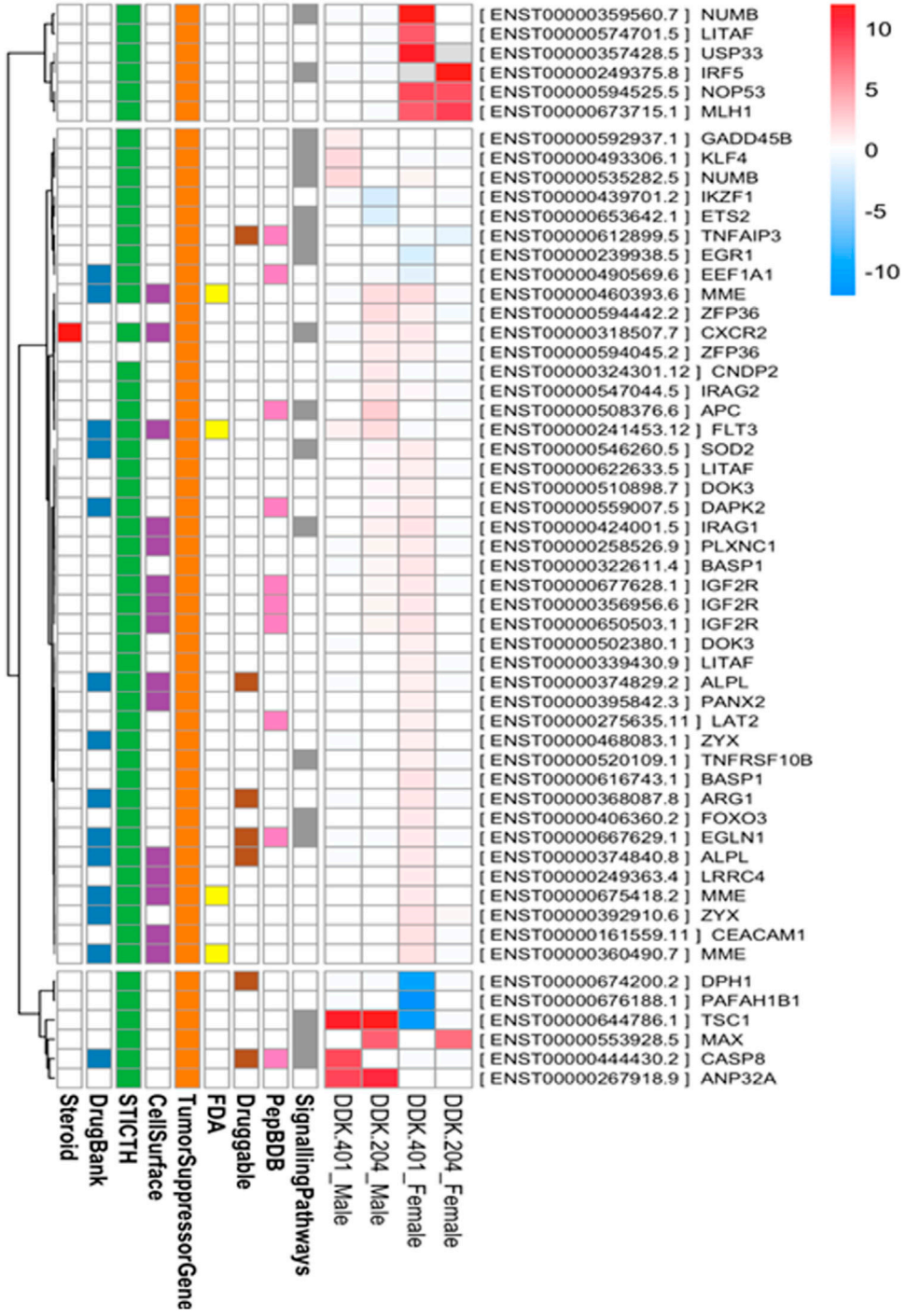

FIGURE 4
Transcripts belonging to the "tumor suppressor genes" category that were differentially expressed between the DDK-401 male and female groups and DDK-204 male and female groups displayed as a heatmap.

inhibition of TNF-α and anti-inflammatory activity related to ROS inhibition (Choi et al., 2007; Park et al., 2012). Oxidative stress usually activates certain signaling pathways, including the p38, MMP, and caspase pathways.

Effect of DDK-401 on ROS generation to induce apoptosis of cancer cells

In A549 cells, the DCFH-DA reagent was used to measure the intracellular ROS levels with DDK-401 and DDK-204 at

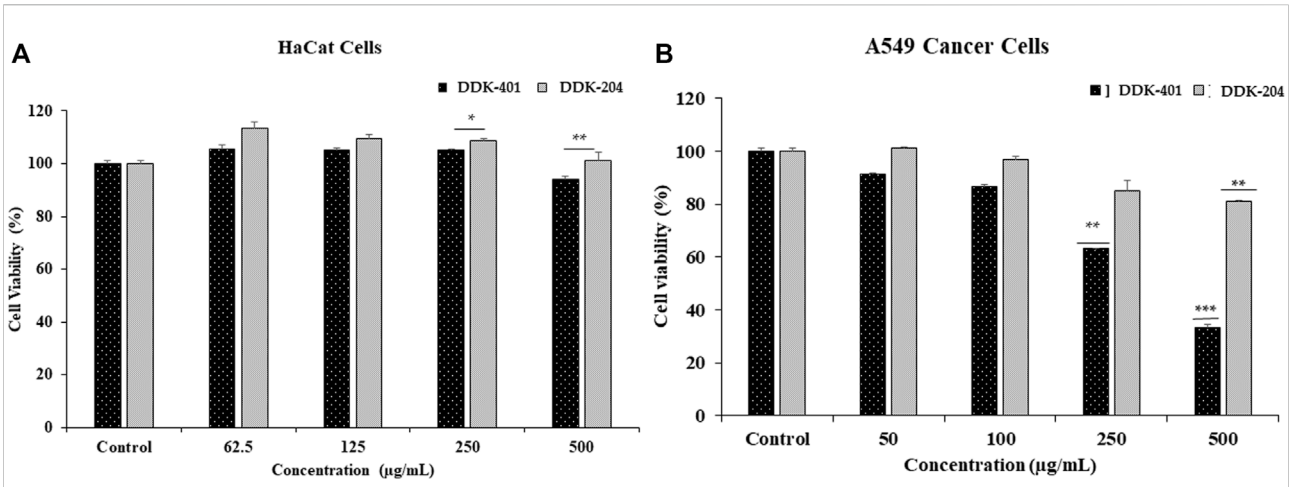

FIGURE 5
In vitro cytotoxicities of DDK-401 and DDK-204 samples in **(A)** HaCaT and **(B)** A549 lung cancer cells over 24 h. The graph shows the mean ± SD value of four repetitions. $^{**}p < 0.01$; $^{***}p < 0.001$ indicate significant differences from the control groups.

TABLE 4 Antioxidant capacity of DDK-401 and DDK-204.

Sample	DPPH	Reducing power
	(mg AAE[a]/g extract)	(mg AAE[a]/g extract)
DDK-401	0.093 ± 0.02	0.340 ± 0.001
DDK-204	0.049 ± 0.01	0.097 ± 0.002

[a]mg AAE/g extract: mg ascorbic acid equivalents/g extract; DPPH: 2,2-diphenyl-1-picrylhydrazyl radical scavenging assay.

various concentrations. Red ginseng extract has been shown to induce cancer cell death by causing DNA damage, stimulating ROS production, and activating numerous pro-apoptotic markers. Furthermore, mitochondrial damage can cause release of ROS because the mitochondria are the largest source of ROS (Brunelle and Chandel, 2002). At 500 g/mL, DDK-401 produced a higher level of ROS than DDK-204, as shown in Figure 6B. Thus, the antiproliferative action of DDK-401 could be assessed by measuring the ROS levels. Intracellular oxidative stress is known to cause cell death in a variety of cell lines; therefore, this assessment was crucial. The data show that DDK-401 could be a potential drug candidate in clinical trials for the treatment of lung cancer.

ROS have been identified as signaling molecules in various pathways that regulate both cell survival and cell death depending on the level (Azad et al., 2008; Chen et al., 2018). Apoptosis and autophagy are important molecular processes that maintain balance in organisms and cells. Apoptosis destroys damaged or unwanted cells, while autophagy maintains cellular homeostasis by recycling specific intracellular organelles and molecules, although autophagy can result in cell death in some cases (Thorburn, 2008; Fan and Zong, 2013). We conclude that DDK-401 reduced ROS production in normal cells (HaCaT) experiencing oxidative stress and also led to apoptosis of lung cancer (A549) cells, suggesting that DDK-401 could act as a molecular switch for these two cellular processes in response to cell damage signaling.

Effect of DDK-401 on gene expression affecting apoptotic and inflammatory responses

Living cells produce ROS as a normal metabolic byproduct. Under excessive stress, the cells generate excess ROS, so living organisms have evolved a series of response mechanisms to adapt to ROS exposure and use ROS as a signaling molecule. ROS molecules cause oxidative stress in a feedback mechanism involving numerous biological processes, including apoptosis, necrosis, and autophagy (He et al., 2017). Apoptosis is a normal process that occurs during development and aging as well as functions as a homeostatic mechanism to maintain cell populations in tissues. Apoptosis can even occur as a defense mechanism during immune responses or when cells are damaged by disease or toxins (Elmore, 2007). In this study, we investigated several gene markers that we selected through a whole-transcriptome search for differential expressions. We found differentially expressed genes related to apoptosis and immune responses to inflammation, such as FOXO3, TLR4, caspase-8, MMP-9, and p38 MAP kinase (p38) (Cuadrado and Nebreda, 2010; van der Vos and Coffer, 2011; Zheng et al., 2021). In addition, we investigated the effects of DDK-401 and DDK-204 without any stimulation (UV-B irradiation) in HaCaT cells to

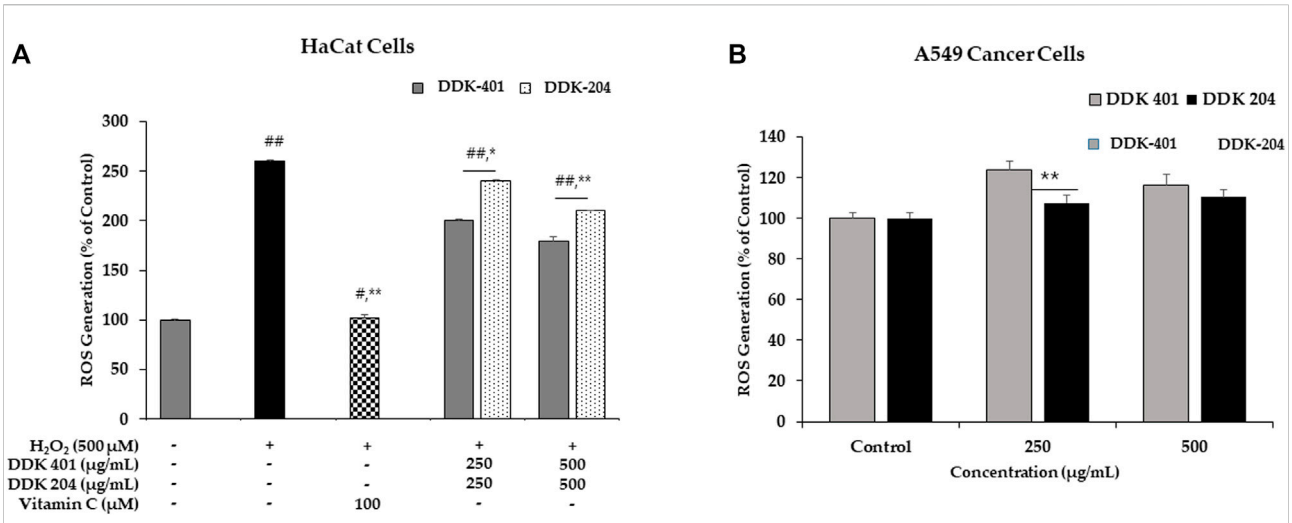

FIGURE 6
(A) Reactive oxygen species (ROS) inhibition by DDK-401 and DDK-204 in HaCaT cell lines treated with H_2O_2. The graph shows the mean ± SD value of three repetitions. *$p < 0.05$ and **$p < 0.01$ indicate significant differences from the control groups; #$p < 0.05$ and ##$p < 0.01$ indicate significant differences from the H_2O_2 stimulation groups. **(B)** ROS generation by DDK-401 and DDK-204 in A549 cancer cells. The graph shows the mean ± SD value of three repetitions. **$p < 0.01$ indicates significant difference from the control group.

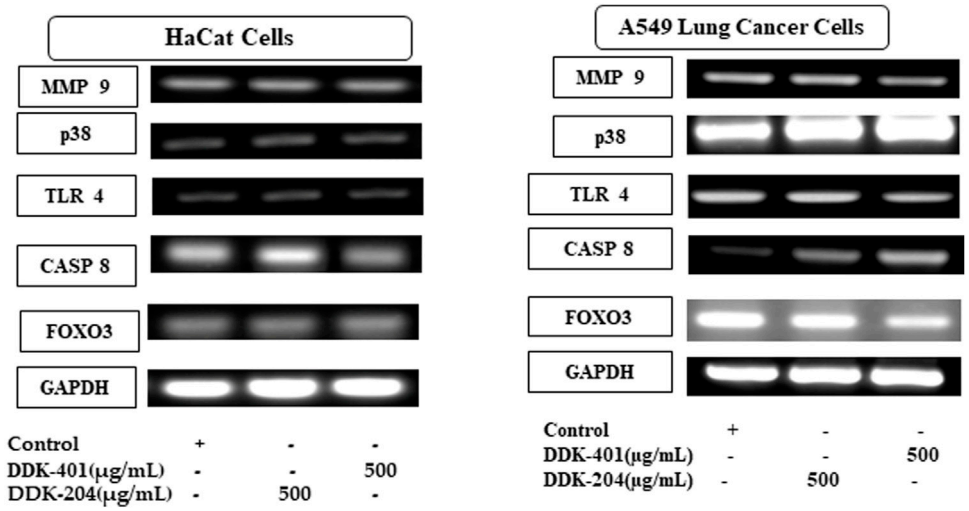

FIGURE 7
In vitro validation of the selected candidate gene expressions in normal (HaCaT) and lung cancer (A549) cell lines by RT-PCR.

observe whether our samples could trigger inappropriate apoptosis or inflammation under normal conditions showed in (Figure 7). The RT-PCR analysis (Supplementary Figure S3) showed that in HaCaT cells, neither compound regulated FOXO3, TLR4, MMP-9, or p38 expression, indicating that DDK-401 did not trigger inappropriate apoptosis or inflammation under normal conditions. The ability to control cellular living or death has enormous therapeutic potential. However, upregulation of caspase-8 was observed, which is similar to the RNA-seq data indicating differential expression (Figure 4). Although the activation of caspase-8 is mainly associated with death receptor signaling cascades, it is also activated downstream of the mitochondria. The roles of caspase-8 in the shift from autophagy to apoptosis in cisplatin-resistant MCF7 cells and in TRAIL-mediated autophagy in HCT 116 cells have already been studied (de Vries et al., 2006; Hou et al., 2010). In the lung cancer A549 cells, DDK-401 treatment downregulated the expressions of MMP9 and TLR4 while upregulating the expressions of

p38 and caspase-8 genes, compared with the cells treated with DDK-204. The MMPs are a group of zinc-dependent metalloenzymes that regulate various cellular processes, including tumor cell proliferation and metastasis (Guo et al., 2019). Several studies have noted that MMPs are overexpressed in malignant tissues than the adjacent normal tissues in a range of tumors, including lung, colon, breast, and pancreatic carcinomas (Radad et al., 2011; Nakhjavani et al., 2019). Previous research has shown that downregulating the expressions of intracellular MMP-9 can increase invasion and metastasis processes several cancers (Zhang et al., 2017, Liu et al., 2019). Furthermore, oxidative stress can induce receptor-dependent apoptosis and damage the mitochondria of normal cells. Mitochondrial dysfunction then further increases ROS accumulation and activates the p38 MAPK pathway. ROS can continuously activate p38 MAPK by activating MAPK kinase and inhibiting MAPK phosphatase. In A549 cells, ROS can regulate the expressions of Bax and Bcl-2 by activating p38 MAPK, which increases the level of cytochrome c in the cytoplasm and triggers the caspase cascade reaction leading to apoptosis (Jin et al., 2019; Nguyen and Nguyen, 2019). The caspases are a family of cysteine-containing proteolytic enzymes that play a central role in the execution phase of cell apoptosis. It has been reported that the effects of the caspase 8 pathway on cancer cells involve inducing apoptosis (Huang et al., 2019). The apoptosis induced by most anticancer drugs occur by the activation of caspases (González-Burgos et al., 2015; Kim and Kim, 2018). Caspase-8 is important in the death receptor-mediated extrinsic pathway, and DDK-401 promotes the activation of caspase-8 in A549 cells in this study, showing that it can cause apoptosis by activating the extrinsic caspase pathway (Wu et al., 2019; Yi, 2019). TLR4 is an important member of the type I transmembrane protein family. Recently, growing evidence has shown TLR4 in various tumors (Gao et al., 2017; Li and Ji, 2018; Zhou et al., 2019), including head and neck, lung, gastrointestinal, liver, pancreatic, skin, breast, ovarian, cervical, and prostate cancers. TLR4-mediated cancer growth is involved in breast tumor progression, and the downregulation of TLR4 prevented breast cancer progression and improved survival (Zhou et al., 2019c). According to our findings, DDK-401 could induce cell apoptosis by upregulating and downregulating various transcriptional factors under cancerous conditions.

Conclusion

Although ginseng and ginsenosides have been reported to have various pharmacological effects, the uptake of ginsenosides into systemic circulation, which is required for their effectiveness, depends on individual factors. Because CK was reported to be a minor saponin that reached systemic circulation, we enriched the total ginsenoside and CK content by fermenting red ginseng extract (DDK-401) via bioconversion and fermentation by edible enzymes. Because clinical trials are a prompt option for evaluating product efficacy, we evaluated DDK-401 in a clinical trial of healthy Korean volunteers. We found higher CK in blood plasma after oral intake of DDK-401 than after the consumption of the control red ginseng formula. Moreover, we identified differences in the CK absorption patterns between female and male volunteers, with higher concentrations of CK being detected in females than in males. We also observed differential expression patterns of various tumor suppressor genes between the female and male groups through RNA-seq analysis. DDK-401 exhibited no cytotoxicity in normal non-diseased HaCaT and RAW 264.7 cells, whereas it showed cytotoxicity in lung cancer cells (A549). Furthermore, DDK-401 inhibited H_20_2-induced ROS production in HaCaT cells and increased ROS production in cancer cells. Finally, the candidate genes responsible for apoptosis and inflammation were validated using RT-PCR (Figure 7). This is a pilot study reporting that fermented red ginseng extract (DDK-401) produces unique, differential absorption and gene regulation patterns compared with red ginseng extract (DDK-204). Thus, DDK-401 could be a potential candidate for further investigations in clinical trials for health promoting activities and anticancer agents; various nanoformulations could also be considered to boost its bioavailability and anticancer properties.

Data availability statement

The datasets presented in this study can be found in online repositories. The names of the repository/repositories and accession number(s) can be found below: ncbi.nlm.nih.gov, PRJNA873242.

Ethics statement

The study was approved by the Institutional Review Board of Kyung Hee University Hospital (KHGIRB-21-419). The patients/participants provided their written informed consent to participate in this study.

Author contributions

Conceptualization, S-KC and C-SL; methodology, S-KC, C-SL, and BK; software, JN, DUY, and VB; validation, DCY, SK, BK, S-KC, C-SL, and D-WL; formal analysis, RM, BK, and ZR; resources, S-KC, C-SL, BK, SK, and DCY; data curation, JA, RM, and VB; writing—original draft preparation, JN, ZR, and JA; writing—review and editing, JA, JN, ZR, S-KC, C-SL, and DUY;

supervision, HP, DCY, and SK; project administration, BK, D-WL, S-KC, C-SL, DUY, and SK; funding acquisition, DCY, SK, and BK. All authors have read and agreed to the published version of the manuscript.

Funding

This work was supported by the Korea Institute of Planning and Evaluation for Technology in Food, Agriculture and Forestry (IPET) through the Agri-Food Export Business Model Development Program funded by the Ministry of Agriculture, Food and Rural Affairs (MAFRA) (Project no: 320104-03). This research was also supported by the Basic Science Research Program through the National Research Foundation of Korea (NRF) funded by the Ministry of Education (grant no: NRF-2020R1I1A1A01070867) and Daedong Korea Ginseng Co., Ltd., South Korea.

Acknowledgments

The samples was provided by Daedong Korea Ginseng Co., Ltd., South Korea.

Conflict of interest

D-WL is employed by Hanbangbio Inc. and S-KC is employed by Daedong Korea Ginseng Co., Ltd.

The remaining authors declare that the research was conducted in the absence of any commercial or financial relationships that could be construed as a potential conflict of interest.

Publisher's note

Supplementary material

The Supplementary Material for this article can be found online at: https://www.frontiersin.org/articles/10.3389/fphar.2022.999192/full#supplementary-material

References

Akter, R., Kwak, G.-Y., Ahn, J. C., Mathiyalagan, R., Ramadhania, Z. M., Yang, D. C., et al. (2021). Protective effect and potential antioxidant role of kakadu plum extracts on alcohol-induced oxidative damage in HepG2 cells. *Appl. Sci.* 12, 236. doi:10.3390/app12010236

Aryal, S., Baniya, M. K., Danekhu, K., Kunwar, P., Gurung, R., and Koirala, N. (2019). Total phenolic content, flavonoid content and antioxidant potential of wild vegetables from Western Nepal. *Plants* 8, 96. doi:10.3390/plants8040096

Azad, M. B., Chen, Y., and Gibson, S. B. (2008). Regulation of autophagy by reactive oxygen species (ROS): Implications for cancer progression and treatment. *Antioxid. Redox Signal.* 11, 777–790. doi:10.1089/ars.2008.2270

Baik, I.-H., Kim, K.-H., and Lee, K. (2021). Antioxidant, anti-inflammatory and antithrombotic effects of ginsenoside compound K enriched extract derived from ginseng sprouts. *Molecules* 26, 4102. doi:10.3390/molecules26134102

Ban, M. S., Kim, Y., Lee, S., Han, B., Yu, K.-S., Jang, I.-J., et al. (2021). Pharmacokinetics of ginsenoside compound K from a compound K fermentation product, CK-30, and from red ginseng extract in healthy Korean subjects. *Clin. Pharmacol. Drug Dev.* 10, 1358–1364. doi:10.1002/cpdd.949

Bausch-Fluck, D., Goldmann, U., Müller, S., Oostrum, M. V., Müller, M., Schubert, O. T., et al. (2018). The *in silico* human surfaceome. *Proc. Natl. Acad. Sci. U. S. A.* 115, E10988-E10997–E10997. doi:10.1073/pnas.1808790115

Bolger, A. M., Lohse, M., and Usadel, B. (2014). Trimmomatic: A flexible trimmer for illumina sequence data. *Bioinformatics* 30, 2114–2120. doi:10.1093/bioinformatics/btu170

Boopathi, V., Subramaniyam, S., Mathiyalagan, R., and Yang, D.-C. (2020). Till 2018: A survey of biomolecular sequences in genus Panax. *J. Ginseng Res.* 44, 33–43. doi:10.1016/j.jgr.2019.06.004

Borman, N., and Kim, C.-H. J. Y. M. J. (1966). The history of ancient Korean medicine. *Yonsei Med. J.* 7, 103–118. doi:10.3349/ymj.1966.7.1.103

Brunelle, J., and Chandel, N. J. A. (2002). Oxygen deprivation induced cell death: An update. *Apoptosis* 7, 475–482. doi:10.1023/a:1020668923852

Chen, L., Zhou, L., Wang, Y., Yang, G., Huang, J., Tan, Z., et al. (2017). Food and sex-related impacts on the pharmacokinetics of a single-dose of ginsenoside compound K in healthy subjects. *Front. Pharmacol.* 8, 636. doi:10.3389/fphar.2017.00636

Chen, Q., Kang, J., and Fu, C. (2018). The independence of and associations among apoptosis, autophagy, and necrosis. *Signal Transduct. Target. Ther.* 3, 18. doi:10.1038/s41392-018-0018-5

Choi, I.-D., Ryu, J.-H., Lee, D.-E., Lee, M.-H., Shim, J.-J., Ahn, Y.-T., et al. (2016). Enhanced absorption study of ginsenoside compound K (20-*O*-*β*-(D-Glucopyranosyl)-20(S)-protopanaxadiol) after oral administration of fermented red ginseng extract (HYFRG™) in healthy Korean volunteers and rats. *Evid. Based. Complement. Altern. Med.* 2016, 3908142. doi:10.1155/2016/3908142

Choi, J. H., Jang, M., Nah, S.-Y., Oh, S., and Cho, I.-H. J. J. O. G. R. (2018). Multitarget effects of Korean red ginseng in animal model of Parkinson's disease: Antiapoptosis, antioxidant, antiinflammation, and maintenance of blood–brain barrier integrity. *J. Ginseng Res.* 42, 379–388. doi:10.1016/j.jgr.2018.01.002

Choi, K., Kim, M., Ryu, J., and Choi, C. (2007). Ginsenosides compound K and Rh(2) inhibit tumor necrosis factor-alpha-induced activation of the NF-kappaB and JNK pathways in human astroglial cells. *Neurosci. Lett.* 421, 37–41. doi:10.1016/j.neulet.2007.05.017

Christensen, L. P. (2008). Chapter 1 ginsenosides: Chemistry, biosynthesis, analysis, and potential health effects, *Advances in food and nutrition research*. Cambridge, MA, USA, Academic Press.

Court, W. E. (2000). *Ginseng, the genus Panax*. London, UK: CRC Press.

Cuadrado, A., and Nebreda, A. R. (2010). Mechanisms and functions of p38 MAPK signalling. *Biochem. J.* 429, 403–417. doi:10.1042/BJ20100323

De Vries, J. F., Wammes, L. J., Jedema, I., Van Dreunen, L., Nijmeijer, B. A., Heemskerk, M. H. M., et al. (2006). Involvement of caspase-8 in chemotherapy-induced apoptosis of patient derived leukemia cell lines independent of the death receptor pathway and downstream from mitochondria. *Apoptosis* 12, 181–193. doi:10.1007/s10495-006-0526-6

Dharmananda, S. (2002). The nature of ginseng: Traditional use, modern research, and the question of dosage. *HerbalGram* 1, 17.

Elmore, S. (2007). Apoptosis: A review of programmed cell death. *Toxicol. Pathol.* 35, 495–516. doi:10.1080/01926230701320337

Fan, Y. J., and Zong, W. X. (2013). The cellular decision between apoptosis and autophagy. *Chin. J. Cancer* 32, 121–129. doi:10.5732/cjc.012.10106

Fukami, H., Ueda, T., and Matsuoka, N. (2018). Pharmacokinetic study of compound K in Japanese subjects after ingestion of Panax ginseng fermented by Lactobacillus paracasei A221 reveals significant increase of absorption into blood. *J. Med. Food* 22, 257–263. doi:10.1089/jmf.2018.4271

Gao, Y., Chu, S., Zhang, Z., and Chen, N. (2017). Hepataprotective effects of ginsenoside Rg1 – a review. *J. Ethnopharmacol.* 206, 178–183. doi:10.1016/j.jep.2017.04.012

González-Burgos, E., Fernandez-Moriano, C., and Gómez-Serranillos, M. P. (2015). Potential neuroprotective activity of ginseng in Parkinson's disease: A review. *J. Neuroimmune Pharmacol.* 10, 14–29. doi:10.1007/s11481-014-9569-6

Grondin, C. J., Davis, A. P., Wiegers, J. A., Wiegers, T. C., Sciaky, D., Johnson, R. J., et al. (2021). Predicting molecular mechanisms, pathways, and health outcomes induced by Juul e-cigarette aerosol chemicals using the Comparative Toxicogenomics Database. *Curr. Res. Toxicol.* 2, 272–281. doi:10.1016/j.crtox.2021.08.001

Guo, Y.-H., Kuruganti, R., and Gao, Y. (2019). Recent advances in ginsenosides as potential therapeutics against breast cancer. *Curr. Top. Med. Chem.* 19, 2334–2347. doi:10.2174/1568026619666191018100848

He, L., He, T., Farrar, S., Ji, L., Liu, T., and Ma, X. (2017). Antioxidants maintain cellular redox homeostasis by elimination of reactive oxygen species. *Cell. Physiol. biochem.* 44, 532–553. doi:10.1159/000485089

Hou, W., Han, J., Lu, C., Goldstein, L. A., and Rabinowich, H. (2010). Autophagic degradation of active caspase-8: A crosstalk mechanism between autophagy and apoptosis. *Autophagy* 6, 891–900. doi:10.4161/auto.6.7.13038

Hu, S. Y. (1976). The genusPanax (Ginseng) in Chinese medicine. *Econ. Bot.* 30, 11–28. doi:10.1007/bf02866780

Huang, X., Li, N., Pu, Y., Zhang, T., and Wang, B. (2019). Neuroprotective effects of ginseng phytochemicals: Recent perspectives. *Molecules* 24, E2939. doi:10.3390/molecules24162939

Jin, Y., Cui, R., Zhao, L., Fan, J., and Li, B. (2019). Mechanisms of Panax ginseng action as an antidepressant. *Cell Prolif.* 52, e12696. doi:10.1111/cpr.12696

Jin, Y., Kim, Y.-J., Jeon, J.-N., Wang, C., Min, J.-W., Noh, H.-Y., et al. (2015). Effect of white, red and black ginseng on physicochemical properties and ginsenosides. *Plant Foods Hum. Nutr.* 70, 141–145. doi:10.1007/s11130-015-0470-0

Jung, J. H., Kang, I. G., Kim, D. Y., Hwang, Y. J., and Kim, S. T. J. J. O. G. R. (2013). The effect of Korean red ginseng on allergic inflammation in a murine model of allergic rhinitis. *J. Ginseng Res.* 37, 167–175. doi:10.5142/jgr.2013.37.167

Jung, J., Jang, H. J., Eom, S. J., Choi, N. S., Lee, N.-K., and Paik, H.-D. (2019). Fermentation of red ginseng extract by the probiotic Lactobacillus plantarum KCCM 11613P: Ginsenoside conversion and antioxidant effects. *J. Ginseng Res.* 43, 20–26. doi:10.1016/j.jgr.2017.07.004

Kachur, K., and Suntres, Z. E. (2016). The antimicrobial properties of ginseng and ginseng extracts. *Expert Rev. anti. Infect. Ther.* 14, 81–94. doi:10.1586/14787210.2016.1118345

Kang, S., and Min, H. (2012). Ginseng, the 'immunity boost': The effects of Panax ginseng on immune system. *J. Ginseng Res.* 36, 354–368. doi:10.5142/jgr.2012.36.4.354

Kim, E. H., and Kim, W. (2018). An insight into ginsenoside metabolite compound K as a potential tool for skin disorder. *Evid. Based. Complement. Altern. Med.* 2018, 8075870. eCAM. doi:10.1155/2018/8075870

Kim, H. K. (2013). Pharmacokinetics of ginsenoside Rb1 and its metabolite compound K after oral administration of Korean Red Ginseng extract. *J. Ginseng Res.* 37, 451–456. doi:10.5142/jgr.2013.37.451

Lee, H.-S., Kim, M.-R., Park, Y., Park, H. J., Chang, U. J., Kim, S. Y., et al. (2012). Fermenting red ginseng enhances its safety and efficacy as a novel skin care anti-aging ingredient: *In vitro* and animal study. *J. Med. Food* 15, 1015–1023. doi:10.1089/jmf.2012.2187

Lee, S. M., Bae, B.-S., Park, H.-W., Ahn, N.-G., Cho, B.-G., Cho, Y.-L., et al. (2015). Characterization of Korean red ginseng (Panax ginseng meyer): History, preparation method, and chemical composition. *J. Ginseng Res.* 39, 384–391. doi:10.1016/j.jgr.2015.04.009

Li, Z., and Ji, G. E. (2018). Ginseng and obesity. *J. Ginseng Res.* 42, 1–8. doi:10.1016/j.jgr.2016.12.005

Liu, H., Zhang, W., Zou, B., Wang, J., Deng, Y., and Deng, L. (2020). DrugCombDB: A comprehensive database of drug combinations toward the discovery of combinatorial therapy. *Nucleic Acids Res.* 48, D871-D881–D881. doi:10.1093/nar/gkz1007

Liu, L., Anderson, G. A., Fernandez, T. G., and Doré, S. (2019). Efficacy and mechanism of Panax ginseng in experimental stroke. *Front. Neurosci.* 13, 294. doi:10.3389/fnins.2019.00294

Liu, Z.-Q. (2012). Chemical insights into ginseng as a resource for natural antioxidants. *Chem. Rev.* 112, 3329–3355. doi:10.1021/cr100174k

Liu, Z., Ren, Z., Zhang, J., Chuang, C.-C., Kandaswamy, E., Zhou, T., et al. (2018). Role of ROS and nutritional antioxidants in human diseases. *Front. Physiol.* 9, 477. doi:10.3389/fphys.2018.00477

Majeed, F., Malik, F. Z., Ahmed, Z., Afreen, A., Afzal, M. N., and Khalid, N. (2018). Ginseng phytochemicals as therapeutics in oncology: Recent perspectives. *Biomed. Pharmacother.* 100, 52–63. doi:10.1016/j.biopha.2018.01.155

Mathiyalagan, R., Wang, C., Kim, Y. J., Castro-Aceituno, V., Ahn, S., Subramaniyam, S., et al. (2019). Preparation of polyethylene glycol-ginsenoside Rh1 and Rh2 conjugates and their efficacy against lung cancer and inflammation. *Molecules* 24, 4367. doi:10.3390/molecules24234367

Mccarthy, D. J., Chen, Y., and Smyth, G. K. (2012). Differential expression analysis of multifactor RNA-Seq experiments with respect to biological variation. *Nucleic Acids Res.* 40, 4288–4297. doi:10.1093/nar/gks042

Mohanan, P., Subramaniyam, S., Mathiyalagan, R., and Yang, D.-C. (2018). Molecular signaling of ginsenosides Rb1, Rg1, and Rg3 and their mode of actions. *J. Ginseng Res.* 42, 123–132. doi:10.1016/j.jgr.2017.01.008

Murugesan, M., Mathiyalagan, R., Boopathi, V., Kong, B. M., Choi, S.-K., Lee, C.-S., et al. (2022). Production of minor ginsenoside CK from major ginsenosides by biotransformation and its advances in targeted delivery to tumor tissues using nanoformulations. *Nanomaterials* 12, 3427. doi:10.3390/nano12193427

Nakhjavani, M., Hardingham, E. J., Palethorpe, M. H., Tomita, Y., Smith, E., Price, J. T., et al. (2019). Ginsenoside Rg3: Potential molecular targets and therapeutic indication in metastatic breast cancer. *Medicines* 6, E17. doi:10.3390/medicines6010017

Nguyen, N. H., and Nguyen, C. T. (2019). Pharmacological effects of ginseng on infectious diseases. *Inflammopharmacology* 27, 871–883. doi:10.1007/s10787-019-00630-4

Panossian, A., Abdelfatah, S., and Efferth, T. (2021). Network Pharmacology of ginseng (Part II): The differential effects of red ginseng and ginsenoside Rg5 in cancer and heart diseases as determined by transcriptomics. *Pharmaceuticals* 14, 1010. doi:10.3390/ph14101010

Park, J.-S., Shin, J. A., Jung, J.-S., Hyun, J.-W., Van Le, T. K., Kim, D.-H., et al. (2012). Anti-inflammatory mechanism of compound K in activated microglia and its neuroprotective effect on experimental stroke in mice. *J. Pharmacol. Exp. Ther.* 341, 59–67. doi:10.1124/jpet.111.189035

Park, S. K., Hyun, S. H., In, G., Park, C.-K., Kwak, Y.-S., Jang, Y.-J., et al. (2021). The antioxidant activities of Korean red ginseng (Panax ginseng) and ginsenosides: A systemic review through *in vivo* and clinical trials. *J. Ginseng Res.* 45, 41–47. doi:10.1016/j.jgr.2020.09.006

Patro, R., Duggal, G., Love, M. I., Irizarry, R. A., and Kingsford, C. (2017). Salmon provides fast and bias-aware quantification of transcript expression. *Nat. Methods* 14, 417–419. doi:10.1038/nmeth.4197

Piao, X. M., Huo, Y., Kang, J. P., Mathiyalagan, R., Zhang, H., Yang, D. U., et al. (2020). Diversity of ginsenoside profiles produced by various processing Technologies. *Molecules* 25, E4390. doi:10.3390/molecules25194390

Posadzki, P., Watson, L. K., and Ernst, E. (2013). Adverse effects of herbal medicines: An overview of systematic reviews. *Clin. Med.* 13, 7–12. doi:10.7861/clinmedicine.13-1-7

Pu, J. Y., Ramadhania, Z. M., Mathiyalagan, R., Huo, Y., Han, Y., Li, J. F., et al. (2021). Ginsenosides conversion and anti-oxidant activities in puffed cultured roots of mountain ginseng. *Processes* 9, 2271. doi:10.3390/pr9122271

Radad, K., Moldzio, R., and Rausch, W.-D. (2011). Ginsenosides and their CNS targets. *CNS Neurosci. Ther.* 17, 761–768. doi:10.1111/j.1755-5949.2010.00208.x

Ramadhania, Z. M., Nahar, J., Ahn, J. C., Yang, D. U., Kim, J. H., Lee, D. W., et al. (2022). Terminalia ferdinandiana (kakadu plum)-mediated bio-synthesized ZnO nanoparticles for enhancement of anti-lung cancer and anti-inflammatory activities. *Appl. Sci.* 12, 3081. doi:10.3390/app12063081

Riaz, M., Rahman, N. U., Zia-Ul-Haq, M., Jaffar, H. Z. E., and Manea, R. (2019). Ginseng: A dietary supplement as immune-modulator in various diseases. *Trends Food Sci. Technol.* 83, 12–30. doi:10.1016/j.tifs.2018.11.008

Sharma, A., and Lee, H.-J. (2020). Ginsenoside compound K: Insights into recent studies on pharmacokinetics and health-promoting activities. *Biomolecules* 10, E1028. doi:10.3390/biom10071028

Shin, J. H., Park, Y. J., Kim, W., Kim, D. O., Kim, B. Y., Lee, H., et al. (2019). Change of ginsenoside profiles in processed ginseng by drying, steaming, and puffing. *J. Microbiol. Biotechnol.* 29, 222–229. doi:10.4014/jmb.1809.09056

Shin, Y., Subramaniyam, S., Chun, J.-M., Jeon, J.-H., Hong, J.-M., Jung, H., et al. (2021). Genome-wide differential methylation profiles from two terpene-rich medicinal plant extracts administered in osteoarthritis rats. *Plants* 10, 1132. doi:10.3390/plants10061132

Sohn, S.-H., Kim, S.-K., Kim, Y.-O., Kim, H.-D., Shin, Y.-S., Yang, S.-O., et al. (2013). A comparison of antioxidant activity of Korean White and Red Ginsengs on H 2 O 2-induced oxidative stress in HepG2 hepatoma cells. *J. Ginseng Res.* 37, 442–450. doi:10.5142/jgr.2013.37.442

Subbiah, V., Zhong, B., Nawaz, M. A., Barrow, C. J., Dunshea, F. R., and Suleria, H. A. (2020). Screening of phenolic compounds in Australian grown berries by lc-esi-qtof-ms/ms and determination of their antioxidant potential. *Antioxidants* 10, 26. doi:10.3390/antiox10010026

Szklarczyk, D., Santos, A., Von Mering, C., Jensen, L. J., Bork, P., and Kuhn, M. (2016). Stitch 5: Augmenting protein-chemical interaction networks with tissue and affinity data. *Nucleic Acids Res.* 44, D380–D384. doi:10.1093/nar/gkv1277

Thorburn, A. (2008). Apoptosis and autophagy: Regulatory connections between two supposedly different processes. *Apoptosis* 13, 1–9. doi:10.1007/s10495-007-0154-9

Uhlén, M., Fagerberg, L., Hallström, B. M., Lindskog, C., Oksvold, P., Mardinoglu, A., et al. (2015). Proteomics. Tissue-based map of the human proteome. *Science* 347, 1260419. doi:10.1126/science.1260419

Van Der Vos, K. E., and Coffer, P. J. (2011). The extending network of FOXO transcriptional target genes. *Antioxid. Redox Signal.* 14, 579–592. doi:10.1089/ars.2010.3419

Warinhomhoun, S., Muangnoi, C., Buranasudja, V., Mekboonsonglarp, W., Rojsitthisak, P., Likhitwitayawuid, K., et al. (2021). Antioxidant activities and protective effects of dendropachol, a new bisbibenzyl compound from Dendrobium pachyglossum, on hydrogen peroxide-induced oxidative stress in HaCaT keratinocytes. *Antioxidants* 10, 252. doi:10.3390/antiox10020252

Wen, Z., He, J., Tao, H., and Huang, S. Y. (2019). PepBDB: A comprehensive structural database of biological peptide-protein interactions. *Bioinformatics* 35, 175–177. doi:10.1093/bioinformatics/bty579

Wishart, D. S., Feunang, Y. D., Guo, A. C., Lo, E. J., Marcu, A., Grant, J. R., et al. (2018). DrugBank 5.0: A major update to the DrugBank database for 2018. *Nucleic Acids Res.* 46, D1074-D1082–d1082. doi:10.1093/nar/gkx1037

Wu, T., Kwaku, O. R., Li, H.-Z., Yang, C.-R., Ge, L.-J., and Xu, M. (2019). Sense ginsenosides from ginsengs: Structure-activity relationship in autophagy. *Nat. Product. Commun.* 14, 1934578X1985822. doi:10.1177/1934578x19858223

Yi, Y.-S. (2019). Roles of ginsenosides in inflammasome activation. *J. Ginseng Res.* 43, 172–178. doi:10.1016/j.jgr.2017.11.005

Yu, J. S., Roh, H.-S., Baek, K.-H., Lee, S., Kim, S., So, H. M., et al. (2018). Bioactivity-guided isolation of ginsenosides from Korean Red Ginseng with cytotoxic activity against human lung adenocarcinoma cells. *J. Ginseng Res.* 42, 562–570. doi:10.1016/j.jgr.2018.02.004

Yu-Hang, G., Revathimadhubala, K., and Ying, G. (2019). Recent advances in ginsenosides as potential therapeutics against breast cancer. *Curr. Top. Med. Chem.* 19, 2334–2347. doi:10.2174/1568026619666191018100848

Zhang, H., Wang, D., Ru, W., Qin, Y., and Zhou, X. (2017). "13 - an overview on ginseng and energy metabolism," in *Sustained energy for enhanced human functions and activity*. Editor D. BAGCHI (Academic Press).

Zhang, J., Wang, W., and Mao, X. (2020). Chitopentaose protects HaCaT cells against H2O2-induced oxidative damage through modulating MAPKs and Nrf2/ARE signaling pathways. *J. Funct. Foods* 72, 104086. doi:10.1016/j.jff.2020.104086

Zhao, M., Kim, P., Mitra, R., Zhao, J., and Zhao, Z. (2016). TSGene 2.0: An updated literature-based knowledgebase for tumor suppressor genes. *Nucleic Acids Res.* 44, D1023–D1031. doi:10.1093/nar/gkv1268

Zheng, S.-D., Wu, H.-J., and Wu, D.-L. (2012). Roles and mechanisms of ginseng in protecting heart. *Chin. J. Integr. Med.* 18, 548–555. doi:10.1007/s11655-012-1148-1

Zheng, Z., Xiao, Z., He, Y.-L., Tang, Y., Li, L., Zhou, C., et al. (2021). Heptapeptide isolated from isochrysiszhanjiangensis exhibited anti-photoaging potential via MAPK/AP-1/MMP pathway and anti-apoptosis in UVB-irradiated HaCaT cells. *Mar. Drugs* 19, 626. doi:10.3390/md19110626

Zhou, P., Xie, W., He, S., Sun, Y., Meng, X., Sun, G., et al. (2019). Ginsenoside Rb1 as an anti-diabetic agent and its underlying mechanism analysis. *Cells* 8, 204. doi:10.3390/cells8030204

Zhou, P., Xie, W., Sun, Y., Dai, Z., Li, G., Sun, G., et al. (2019c). Corrigendum to "ginsenoside Rb1 and mitochondria: A short review of the literature". *Mol. Cell. Probes* 43, 1–5. doi:10.1016/j.mcp.2020.101626

Zhu, L., Luan, X., Dou, D., and Huang, L. (2019). Comparative analysis of ginsenosides and oligosaccharides in white ginseng (WG), red ginseng (RG) and black ginseng (BG). *J. Chromatogr. Sci.* 57, 403–410. doi:10.1093/chromsci/bmz004

Frontiers in Pharmacology

Explores the interactions between chemicals and living beings

The most cited journal in its field, which advances access to pharmacological discoveries to prevent and treat human disease.

Discover the latest Research Topics

See more →

Frontiers

Avenue du Tribunal-Fédéral 34
1005 Lausanne, Switzerland
frontiersin.org

Contact us

+41 (0)21 510 17 00
frontiersin.org/about/contact